Numerical Simulation of Aerofoil and Bluff Body Flows by Vortex Dynamics

NUMERICAL SIMULATION OF AEROFOIL AND BLUFF BODY FLOWS BY VORTEX DYNAMICS

D.T.C. Porthouse

Ph.D. Thesis

December 1983

SUMMARY

The computer simulation of flow separation from bluff bodies is achieved by a method which solves the two-dimensional incompressible Navier-Stokes equations using clouds of point vortices. The vortices convect each other, and have an additional random motion to represent viscosity, as originally proposed by A.J. Chorin. Some justifications for the introduction of randomness as the agent of entropy production are presented.

The method is applied to some simple boundary layer simulations, and then in combination with an integral equation method due to E. Martensen, the flow around bluff bodies of arbitrary shape is simulated in order to predict lift and drag. The stalling characteristics of aerofoil NACA 0012 are reproduced from first principles by computer simulation, and the results compared to experiment. The dependency of the Strouhal number against Reynolds number for the von Karman vortex street behind a circular cylinder is also investigated by simulation. An attempt is made to simulate the phenomenon of rotating stall which appears in compressors as the first sign of aerodynamic overloading.

NUMERICAL SIMULATION OF AEROFOIL AND BLUFF BODY FLOWS BY VORTEX DYNAMICS

D.T.C. Porthouse

Ph.D. Thesis

December 1983

This Thesis describes work carried out by the author in the Department of Mechanical Engineering at the University of Newcastle upon Tyne. No part of this work has been previously submitted for a degree either at this University, or at any other University or Institution,

DTC Porthouse

D.T.C. Porthouse.

For Georges Seurat

CONTENTS

NOMENCLATURE

a	Height of vortex above surface; constant relating cascade inlet and outlet angles; length of flat plate.
b	Constant relating cascade inlet and outlet angles.
c	Specific heat at constant volume.
C_D	Drag coefficient, 2 Drag force/(ρU^2)
C_L	Lift coefficient, 2 Lift force/(ρU^2)
d	Displacement thickness coefficient, or constant of proportionality; Height of wind tunnel.
H	Boundary layer form factor, d/θ.
i	Index.
j	Index.
k	Constant of proportionality; thermal conductivity.
K	The Weinig lattice effect coefficient.
$K_{i,j}$	Influence or coupling coefficient.
$\underset{\sim}{l}_i$	Unit vector parallel to surface.
L	Characteristic length.
$L_{i,j}$	Operator matrix from Martensen Method, the inverse of $K_{i,j}$.

M_i Component of flow speed, parallel to surface, induced by free vortex.

N_i Component of flow speed, normal to surface, induced by free vortex.

m(i) The kernel function obtained as part of the solution of a Fredholm integral equation.

n Number of vortices; number of pivotal points on contour.

p Pressure; probability.

p_o Stagnation pressure, $p + \frac{\rho U^2}{2}$

P Cumulative probability.

Q Heat transferred across system boundary.

r Radial co-ordinate.

r_c Radius of vortex core.

r_{rms} Root mean square distance of recession of a point vortex in random motion.

Re Reynolds number, LU/ν.

s Distance around aerofoil perimeter (intrinsic co-ordinate).

t Time, pitch/chord ratio.

T_w Boundary layer shear stress at surface.

u x component of velocity.

U Internal energy; characteristic or mainstream velocity.

U_1 Flow speed below vortex sheet.

U_2 Flow speed above vortex sheet.

$\underset{\sim}{U}$ Velocity vector; velocity of moving vortex.

v y component of velocity

V_i Column vector upon which $L_{i,j}$ operates to give the flow speed distribution around a contour.

V Velocity induced by moving vortex.

W Work transferred across system boundary.

x Cartesian co-ordinate.

y Cartesian co-ordinate.

z $x + i\,y$

α Thermal diffusivity, $k/\rho c$.

α_0 The zero lift angle, or effective stagger of a cascade.

α_1 The flow inlet angle to a cascade.

α_2 The flow outlet angle from a cascade.

α_m The vector mean angle, $\tan^{-1}(\tan\alpha_1 + \tan\alpha_2)/2$.

ϵ Energy thickness coefficient, or constant of proportionality.

γ Strength of vortex.

Γ	The 'bound' circulation on a contour.
Γ_x	The bound circulation which maintains a Kutta condition for unit flow parallel to the x-axis.
Γ_y	The bound circulation which maintains a Kutta condition for unit flow parallel to the y-axis.
θ	Angular co-ordinate; momentum thickness coefficient; intrinsic co-ordinate of angle around contour.
ν	Kinematic viscosity.
ρ	Density.
ϕ	Complex velocity potential.
$\underset{\sim}{\omega}$	Vorticity, curl $\underset{\sim}{U}$.
Ω	Step change in vorticity across surface in boundary layer flow.

CHAPTER 1. INTRODUCTION

The outstanding feature of fluid mechanics is its non-linearity. Of course, many other physical problems are also non-linear, but it is usually the case that one can achieve a good understanding by simple linear approximations. This is rarely so in fluid mechanics. The consequence is that one is forced to divide the subject into different areas, each with its own list of assumptions. Aerodynamics divides into compressible flows and incompressible flows. Incompressible flows divide into potential flows and boundary layer flows. Boundary layer flows divide into laminar flows and turbulent flows. Compressible flows divide into isentropic flows and shock flows. Anyone studying all of these topics for the first time will have the feeling that there is no one subject called fluid mechanics, but rather a series of very particular analyses borrowing techniques from many different systems of mathematical calculus. Consequently, one may be well versed in both boundary layer flows and shock flows taken separately, but incapable of producing a theory of the interaction between shock waves and boundary layers.

This Thesis presents an attempt to reinstate fluid mechanics as a single subject. Only two-dimensional incompressible flows will be dealt with here, which is enough to begin with, since the principal effects of convection

and viscosity will be encountered even with this restriction. However, the methods to be developed are not restricted, and the analysis of three-dimensional compressible flows will rely upon insights obtained from the study of two-dimensional incompressible flow. Inevitably, one is forced to use computers to perform flow simulations. It will be seen, though, that the requirement to produce computer programs of the quality necessary to simulate realistically high Reynolds numbers means that there is no attenuation of the demands made upon traditional mathematical analysis.

The aim of this Thesis is to use computer simulation to reproduce the characteristics of real flows, such as the complicated swirling flows in the wake of an unstreamlined body. From about the year 1987, it will be commonplace to use the new generation of 32-bit desktop microcomputers to do this, and for a relatively small cost, one will be able to predict, say, the flow around engineering structures such as bridges and cooling towers before erecting them in peril of the wind. This cost will be even less than the cost of putting models in wind tunnels, and certainly it will be much more convenient to use 'numerical wind tunnels'. It is therefore timely to develop the theory necessary to program these computers, and to do preliminary comparisons with experiment of the results of these computer programs.

By Galileo's Principle of Relativity, one has no way of knowing if one is moving or stationary. One does however know if one is rotating, due to the apparent existence of centrifugal and Coriolis forces. It follows that the natural variable that one should use to describe a fluid is its state of rotation, or vorticity, since the velocity of the fluid at any point can always be made equal to zero by a Galilean transformation, while this is not true of vorticity. The computer simulation will therefore be based upon vortex dynamics. Any solid bodies in the flow will be analysed by an integral equation method due to Martensen[1]. Viscosity will be interpreted as diffusion of vorticity, and modelled by the Brownian motion of vortex elements.

1.1 GENERAL CONSIDERATIONS

The most general consideration of a fluid flow is based upon its thermodynamics, but it would be best to leave this to the concluding chapter when we shall have a clearer idea of the type of system being considered. It will suffice to say for the moment that fluid mechanics is a branch of dynamics. The most general description of a dynamical system is due to Hamilton, and consequently one talks of a Hamiltonian system much as one would recognise the existence of a machine without knowing the precise

details of that machine's operation. The many-body gravitational problem is an example of a Hamiltonian system, and two-dimensional vortex dynamics is another.

The key property of a Hamiltonian system in which we are interested is its reversibility, and this will not always be easy to guarantee in computer simulation. Reversibility also means that there is no friction or viscosity in the system, and any failure to respect reversibility introduces a phantom viscosity which can often be much larger than the viscosity which we add explicitly. Thus we must consider methods of computer simulation which overcome this problem if we wish to simulate realistically high Reynolds numbers.

The diffusion of vorticity is the irreversible part of the process, which will be simulated by adding randomness to the Hamiltonian system on an appropriate scale. The idea that adding randomness converts a reversible system into an irreversible system will be returned to in Chapter 9. Any errors in the computer program itself are an additional type of randomness which may well be much larger than the randomness we add, and this must now be considered.

1.2 THE RULES OF COMPUTER SIMULATION OF DYNAMICS

The use of electronic computers to simulate large dynamical systems was conceived during the Second World War when novel military requirements caused a demand for a fresh attack on traditionally unsolvable problems. After the War, in 1950, Charney, Fjortoft and von Neumann[2] proposed the use of computers for weather prediction. It is strange that in all the time since then, the commonsense idea of reversibility in the computer simulation of any dynamic system has had such little publicity. There are many textbooks explaining how to do numerical solutions of ordinary differential equations, but to the author's knowledge, not one of these even mentions reversibility, despite the fact that as long ago as 1967, Buneman[3] stated of computer programs used for simulation:

> Indeed, such programs ought to allow, by a change of sign of the time variable, for the exact tracing of a system back from the final state to the initial conditions.

In practice this is too idealistic, but until matters are put right in principle, one is in no position to go on to consider irreversible systems.

The basic idea of this Thesis is not restricted to fluid mechanics. It is that one takes a Hamiltonian system, and shows firstly that at least in

principle one can perform a computer simulation which is reversible i time. Any computer simulation of a dynamical system which does not mee this criterion of reversibility can be rejected as substandard. The effec of running a substandard computer program is to cause the system to hav internal friction, quantified by the viscosity, which is unknown. Well, i one cannot quantify the viscosity effectively present in a compute simulation, one is not doing science!

Well-known methods of numerical integration, such as the standard Runge-Kutta and Adams-Moulton methods, are not reversible when used with finit time steps. Thus such methods are of no use in the simulation o Hamiltonian systems of non-trivial size. One must instead use methods suc as the Central Difference or Improved Euler methods, which treat information obtained at different times symmetrically. Higher order method are also available.

If one thinks of a few simple Hamiltonian systems one will see the rationality of insisting upon a reversible method. A satellite which i supposed to be moving in a circular orbit around a planet will move in a spiral when simulated with a non-reversible method applied in Cartesian co-ordinates. It can be shown that with a reversible method the path of the satellite must be strictly circular, though numerical errors will result ir

an error in the orbital period. With a reversible method, one is at least able to say what the 'orbit' means.

Likewise, it should be possible to simulate a pendulum swinging with constant amplitude, an electron moving in a magnetic field with constant speed, a gyroscope precessing and nutating with constant amplitude and frequency, and in fact any Hamiltonian system where although one is forced to use one co-ordinate system, one knows that in principle there is another co-ordinate system in which some of the co-ordinates are ignorable. All of these examples of perpetual motion may be readily simulated by a reversible method. The application of an irreversible method would have some strange consequences.

In practice, a reversible method of integration would seem to require many iterations to convergence, except on a computer with arithmetic of finite precision. Given this finite precision, the effect of errors is the same as that of viscosity, so a quick rule of thumb is that if a computer represents numbers to 1 part in 10,000,000 say, then the maximum Reynolds Number achievable on that computer is the square of 10,000,000. There would of course be other limitations in terms of computer memory, speed and so on. When the system being simulated is stable, the consequence of a computer simulation at finite Reynolds number is not serious. In

considering the motion of a small number of point vortices, Aref[15] shows that any Hamiltonian system with more than just a few degrees of freedom is likely to be unstable in the sense that small variations in the initial conditions produce large variations in the state of the system at a later time. In the case of two-dimensional point vortices, Aref states that the motion of three vortices is stable, but the motion of four vortices is not. Thus computer simulation of large-scale Hamiltonian systems may well be impossible, but this does not matter to us since such systems are not likely to be encountered in engineering applications.

Once there is no doubt about the reversible nature of a simulation, one can then go on to consider irreversible processes. To simulate Reynolds numbers less than the maximum possible, one can use whatever random number generator is present on a particular computer to introduce randomness into the system under consideration. Initially, this randomness has the effect of making the system prone to its characteristic instabilities, so that one expects to encounter turbulence in fluid flows. Such turbulence is always a transient phenomenon, since eventually the system 'thermalises', that is, it achieves a Maxwellian distribution. The added randomness overwhelms the errors due to finite precision in the computer representation of a real number, while having the same ultimate effect.

This is the point of a method originally due to Chorin[4], whose development will now be described.

1.3 THE DEVELOPMENT OF VORTEX DYNAMICS

The subject of vortex interactions has been recently comprehensively reviewed by Saffman and Baker[5]. This section describes only those contributions which have had a direct impact upon the author's work, or are likely to modify it in the future. Criticism is expressed where appropriate, but it should be said that now that it is known that one should never confuse reversible and irreversible processes, such criticism is intended purely for the clarification of matters in practical computer simulation.

Newtonian mechanics has forces, which cause accelerations, modifying the velocity and position of a body, which in turn is likely to modify the force acting upon the body. In describing the behaviour of the body, one must use two systems of analysis. These are kinematics, or moving geometry, and dynamics, which may be called kinematics plus forces. This dualism has been historically rejected by those with a philosophical preference for monism. The Newtonian viewpoint eventually won in classical mechanics at least, and today the monist viewpoint is rarely encountered except in one

subject: vortex dynamics. The Newtonian dualism is transformed to one system of analysis which studies vortex motions, and another system of analysis which merely says that there is conservation of vorticity. Thus there is still dualism in vortex dynamics, but the principle of conservation of vorticity is so self-evident that all one's effort is concentrated upon the vortex motions, and vortex dynamics is effectively monist.

This has led some people to extrapolate from incompressible fluid mechanics to everything else, and to propose that in the solar system, or galaxy, there is a cosmic vortex at work. At the other end of the scale, it would be nice if atoms were miniature ring vortices, and molecules consisted of interlocking rings...

The idea of vorticity is thus very old, but it was first given serious expression by Kelvin, who formulated the principle of invariance of circulation, and Helmholtz, who gave a description of vortex motions. The first serious work which has an impact upon this Thesis is Rosenhead's[6] attempt in 1931 to simulate the Kelvin-Helmholtz instability using point vortices and a mechanical computer. Abernathy and Kronauer[7] published their study of vortex instabilities in 1962, using the same methods as Rosenhead, but with an electronic computer.

Fromm[8] considered a stream-function/vorticity approach. This uses a mesh in which the value of vorticity is known only at points on the mesh. Fromm was able to reproduce the von Karman vortex street, but there is a major objection to his approach. The consequences of a fluid flow diagonal to the mesh are shown in figure [1.1]. A vortex initially at a point on the mesh has components of velocity in two directions, and thus after a logical time step it is split between two new mesh points. After another time step, the distribution of the vortex between mesh points is beginning to take on the form of a normalised Pascal's triangle, and after many time steps the vortex has been dramatically diffused over the mesh. If one had not made the logical choice of time step, the diffusion would also take place in the streamwise direction. This diffusion, which is both anisotropic and not relativistically invariant, rules out any form of finite difference method or finite element method for the simulation of unsteady flow. Salmon[9] points out that such methods are not Hamiltonian in inspiration, and this is accordingly the price that one must pay. It is of course possible to produce a reversible finite difference method, but such a method, in which there is both reversibility and apparent diffusion, can only be regarded as an absurdity (such behaviour is correctly known as dispersion).

The finite element method is not working properly in simulating

convection, and figure [1.1] could be redrawn for the convective transport of any quantity, whether active or passive (active quantities, such as vorticity or internal energy, modify the flow after some convection has occured, while passive quantities, such as a dyestuff or a radioactive isotope used as a tracer, do not). As long as one part of a fluid is indistinguishable from another, there is nothing to convect in the sense that one cannot use the fluid as a medium of communication, and the finite element method can then be used. When one part of the fluid is distinguishable from another by properties such as vorticity or entropy, there is then a convection equation that one can write down for such properties, and the use of a finite element method becomes dubious even in steady flow unless one always ensures that the grid used in the method is aligned with the flow. It might be thought that some sort of 'undiffusion' could be introduced to correct the finite difference method's tendency to diffuse information. Whatever method of undiffusion one invented could then be applied to construct a computer simulation of a perpetual motion machine of the second kind. One can only feel sceptical. It would be best not to allow information to diffuse in the first place.

Gerrard[10] produced the first display of a vortex street using the method of Rosenhead. With plenty of hindsight, the objection that can be made to

his 1967 paper is that there may be an effective viscosity due to numerical errors which is not quantified. Initially, the flow behind a circular cylinder is symmetric. Only later does an asymmetry appear leading to the vortex street. A Hamiltonian system would never evolve into a vortex street from an initial condition of symmetry, so one is left with the question: if it is not a Hamiltonian system, then what is it?

In 1973, Christiansen[11] proposed to represent vorticity by particles, but to sample this vorticity with a grid. From the vorticity distribution on the grid, the velocity distribution may be rapidly obtained, and then the velocity of each point vortex is derived by interpolation. Christiansen's method would behave sensibly with flow diagonal to the grid, and it is much faster than the original Rosenhead method. An apparently deterring feature of Christiansen's method is his reporting of a 'diochotron instability' in a two-dimensional ring of vorticity, causing it to evolve into a configuration resembling a swastika. In fact, an examination of Christiansen's boundary condition reveals that there is no such instability, but that this is the proper stable deterministic evolution of the ring vortex. The ring vortex has in effect a host of mirror images reflected in the boundaries of the flow field, and these cause the observed behaviour. Again, Christiansen's simulations may be described as

simulations at unknown Reynolds number.

In the same year, Chorin[4] proposed a modification of Rosenhead's method in which random motion is added to represent viscosity. He presented a simulation of the von Karman vortex street. This method was re-invented by the author some years later as a Monte-Carlo method. Monte-Carlo methods are often regarded as methods of desperation, when one is unable to find any other method. However, the use of this method can be rationalised by the proposition that only random motion can cause a sensible increase in entropy, since the deterministic evolution of a system is merely a series of transformations which do not alter its information content. Though one may not accept this proposition on philosophical grounds, it will be seen that there is certainly good reason for accepting it with respect to the computer simulation of large dynamic systems.

In 1978, Chorin[12] described the application of the method to boundary layer simulations. It is strange that Chorin did not present a simulation of a separating boundary layer, thus effectively explaining flow separation, even though this would have been but a short step given the existence of a boundary layer computer program. This simulation will be done by the author.

In 1980, Lewis[13] extended Rosenhead's method to bodies of arbitrary shape,

but without viscosity. This marked the commencement of an engineering interest in vortex dynamics. In 1983, Stansby and Dixon[14] combined the methods of Christiansen[11] and Chorin[4], which is obviously a direction to pursue in the future, since one can take many more vortices and thus reduce the errors due to randomness alone. One can also think about compressibility and three-dimensional flows. However, there is one point on which one can criticise Stansby and Dixon's work. They have conscientiously reported that their method of calculating the pressure distribution on the surface of a solid body cannot guarantee its 'closure', analogous to walking in a closed path around a mountain range and not arriving back at the same height. It is on such points of detail that the author feels justified in not adopting Christiansen's method until other matters have been resolved.

Apart from this main line of development, vortex methods have been used to simulate the Rayleigh-Taylor instability (Baker,Meiron and Orszag[16]) and Leonard[17] has reported on the simulation of three-dimensional vortex dynamics. There remains much to do in two dimensions, and the relevant mathematics will now be developed.

1.4 THE PLAN OF THIS THESIS

In Chapter 2, we will begin with the continuous Navier-Stokes equations, and show how to represent them using discrete vortices. Every aspect of the correspondence between a particulate model and the continuum model will be considered. The mechanism responsible for turbulence, the Kelvin-Helmholtz instability, will also be introduced. Chapter 3 then applies this model to some simple boundary layer flows, such as a reconstruction of the standard Blasius profile, and Chapter 4 then uses the same boundary layer model to give an explanation of flow separation in terms of vorticity. These three chapters cover preliminary topics, and Chapter 3 in particular is a detour from the main topic of the flow around bluff bodies and stalling aerofoils.

Chapter 5 presents the method of analysing two-dimensional bodies of arbitrary shape by an integral equation method due to Martensen. The computer program developed is applied to the aerofoil NACA 0012, and the results for surface pressure distributions and the streamlines of the flow are compared to experiment.

Having separately tested the integral equation method as a component of the computer program being developed, we then proceed to Chapter 6. The method of computer simulation of the separated flow around bluff bodies is described. This will involve abandonment of several familiar concepts of

aerofoil flows, such as bound circulation and the Kutta condition. There is no special method of predicting flow separation, which is left to evolve spontaneously. The Blasius theorem for the calculation of the surface pressure distribution will also be replaced by another method based upon vortex fluxes.

Chapter 7 then gives two cases. An attempt is made to reconstruct the stalling characteristics of the aerofoil NACA 0012 at angles of attack from 0^{o} to 90^{o}. The flow around a circular cylinder as a function of Reynolds number is then presented. Both of these cases are compared to experiment. Chapter 8 introduces the flow around multiple bodies, for which no experimental comparisons have been made, but an attempt is made to simulate the phenomenon of rotating stall in compressors.

Chapter 9 is the conclusion. Since this work can be extended to compressible flow, its thermodynamic implications are as least as interesting as the work itself. It will be essential to consider these implications whenever one resorts to computer simulation to tackle complex dynamic problems.

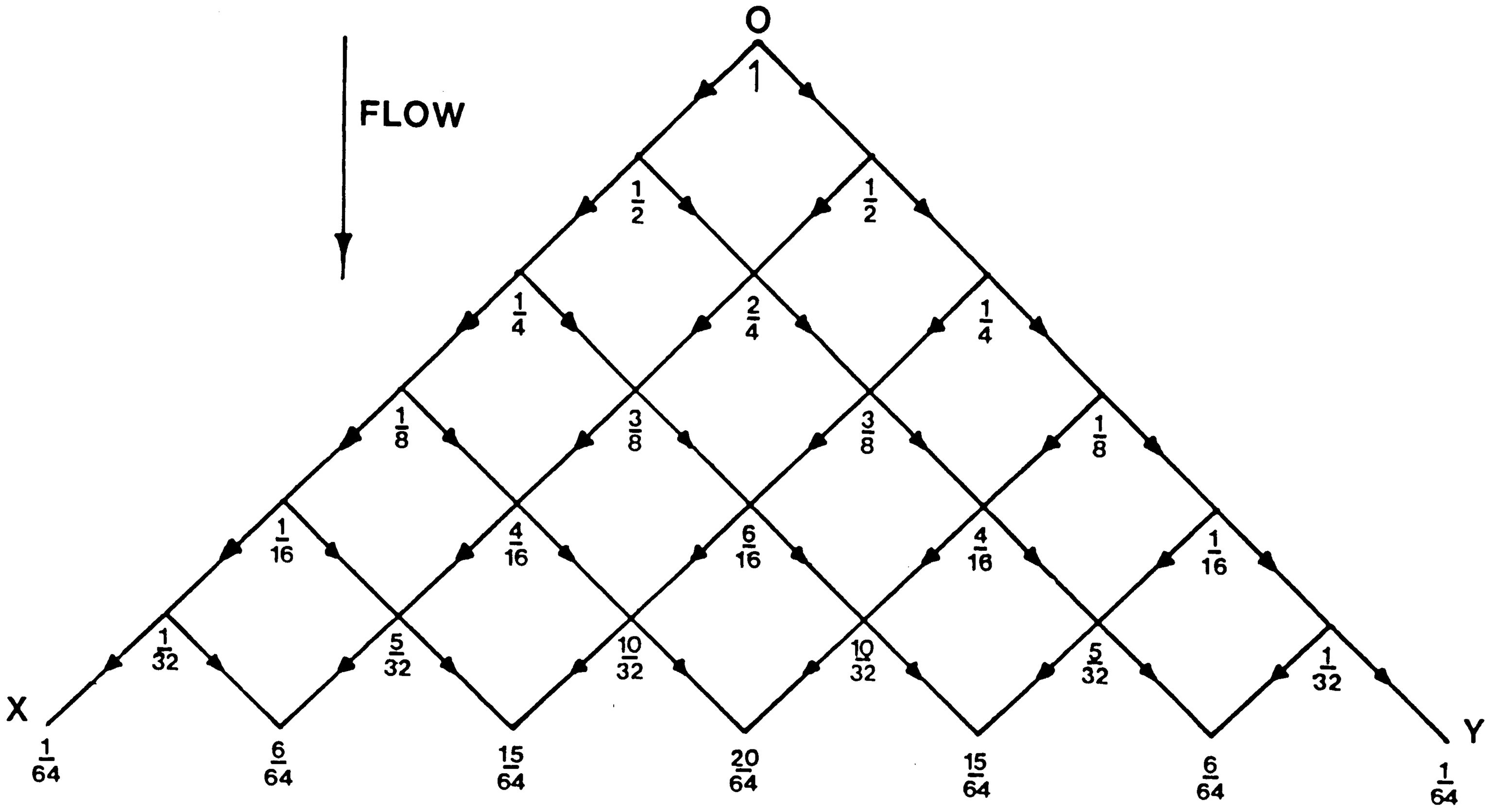

Figure 1.1 The 'convection' of a point vortex by a finite-difference method.

CHAPTER 2. DERIVATION OF THE FLOW MODEL

This chapter shows the relation between the Navier-Stokes equation of the flow field and the model presented here, which describes the flow using point vortices exerting an action at a distance. We begin with some standard analysis of the Navier-Stokes equation, which may be expressed as

$$\frac{\partial \underset{\sim}{U}}{\partial t} + \underset{\sim}{U}.\nabla \underset{\sim}{U} = -\frac{\nabla p}{\rho} + \nu \nabla^2 \underset{\sim}{U} \qquad (2.1)$$

Vorticity may be introduced into equation (2.1) through the vector identity

$$\underset{\sim}{U}.\nabla \underset{\sim}{U} = \nabla\left(\frac{U^2}{2}\right) - \underset{\sim}{U} \times (\nabla \times \underset{\sim}{U})$$

$$= \nabla\left(\frac{U^2}{2}\right) - \underset{\sim}{U} \times \underset{\sim}{\omega} \qquad (2.2)$$

Equation (2.1) may then be written in the form

$$\frac{\nabla p}{\rho} + \nabla\left(\frac{U^2}{2}\right) = \underset{\sim}{U} \times \underset{\sim}{\omega} - \frac{\partial \underset{\sim}{U}}{\partial t} + \nu \nabla^2 \underset{\sim}{U} \qquad (2.3)$$

With the restriction to incompressible flow, we have

$$\frac{\nabla p_o}{\rho} = \underset{\sim}{U} \times \underset{\sim}{\omega} - \frac{\partial \underset{\sim}{U}}{\partial t} + \nu \nabla^2 \underset{\sim}{U} \qquad (2.4)$$

In equation (2.4), the contribution of moving vorticity appears explicitly, and for this reason it is frequently a more useful form of the Navier-Stokes equation.

The stagnation pressure term may be eliminated from equation (2.4) by taking the curl, using the identity

$$\text{curl}(\text{grad}(\text{any scalar})) = 0$$

This gives

$$0 = \nabla \times (\underset{\sim}{U} \times \underset{\sim}{\omega}) - \frac{\partial \underset{\sim}{\omega}}{\partial t} + \nu \nabla^2 \underset{\sim}{\omega}$$

or

$$\frac{\partial \underset{\sim}{\omega}}{\partial t} + \underset{\sim}{U}.\nabla \underset{\sim}{\omega} = \underset{\sim}{\omega}.\nabla \underset{\sim}{U} + \nu \nabla^2 \underset{\sim}{\omega} \qquad (2.5)$$

The first term on the R.H.S. represents the concentration of vorticity that is achieved when a vortex filament is stretched. This causes neighbouring vortex filaments to crowd together, so that although the strength of any one filament stays constant, the vortex density increases. This cannot happen in two-dimensional flow, so the first term on the R.H.S. of equation (2.5) is then zero. $\underset{\sim}{\omega}$ is a vector which is always directed normal to the (x,y) plane, so that it can be treated as a scalar. Thus we shall be concerned with the equation

$$\frac{\partial \underset{\sim}{\omega}}{\partial t} + \underset{\sim}{U}.\nabla \underset{\sim}{\omega} = \nu \nabla^2 \underset{\sim}{\omega} \qquad (2.6)$$

In section 2.1 the convection of vorticity will be dealt with, according to the equation

$$\frac{\partial \underset{\sim}{\omega}}{\partial t} + \underset{\sim}{U}.\nabla \underset{\sim}{\omega} = 0 \qquad (2.7)$$

In section 2.2 the influence of diffusion of vorticity will be considered. Finally in section 2.3 the method of integrating equation (2.4) will be described.

2.1 CONVECTION OF VORTICITY

Since equation (2.7) may be written as

$$\frac{D \underset{\sim}{\omega}}{Dt} = 0 \qquad (2.8)$$

it follows that elements of vorticity may be regarded as moving with the fluid. This form of the equation is known as the 'substantive derivative' or the 'comoving' form depending upon the terminology preferred. The vortex strength of each element does not change, so there is conservation of vorticity (this is Kelvin's circulation theorem in another terminology). The element of vorticity will be represented by a point vortex of strength

γ which induces a flow

$$\frac{\gamma}{2\pi r}$$

in concentric circles around itself.

For this vortex a complex potential

$$\phi = \frac{i\gamma \ln(z)}{2\pi} \tag{2.9}$$

may be specified, where

$$u - iv = \frac{d\phi}{dz} \tag{2.10}$$

For several vortices the complex potentials may be added

$$\phi = \sum_{j=1}^{n} \frac{i\gamma_j}{2\pi} \ln(z - z_j) \tag{2.11}$$

Two of the questions which arise in describing the flow as a collection of singularities are answered in subsection 2.1(a). The motion of vorticity is described in subsection 2.1(b).

2.1(a) Vortex Statics

By vortex statics is meant a flow in which there is no moving vorticity, or a flow in which moving vorticity is temporarily frozen. We shall only be concerned with two aspects of vortex statics, namely resolution effects and

the unbounded speed of the flow at a vortex core.

An observer is defined here as a person who can measure the fluid velocity at any point with some instrument which does not disturb the flow, and which has a limited accuracy (experimental measurements are normally accurate to within 1%). In real fluid flows, the vorticity is usually distributed in the flow. If this vorticity can be represented by a cloud of point vortices, then it is of interest to examine whether an observer distant from the cloud is able to tell the difference between point vortices and distributed vorticity by measuring the fluid velocity distribution in his vicinity.

For example, a vortex sheet can be represented by an array of point vortices. Such an array along the Y-axis (figure [2.1]) has a complex potential

$$\phi = \sum_{j=-\infty}^{\infty} \frac{i\,\gamma}{2\pi} \ln(z - i\,j\,t) \qquad (2.12)$$

It may be shown by a conformal transformation (Wilkinson[18]) that the components of velocity of the flow are

$$u = \frac{\gamma}{2\,t} \frac{\sin(2\pi\ y/t)}{\cosh(2\pi\ x/t) - \cos(2\pi\ y/t)}$$

$$v = -\frac{\gamma}{2t}\,\frac{\sinh(2\pi x/t)}{\cosh(2\pi x/t) - \cos(2\pi y/t)} \qquad (2.13)$$

Suppose the observer is a distance t from the sheet, and can move parallel to it. It can be calculated from equation (2.13) that he will attempt to measure a variation of about 0.4% in v and u/v (u is small compared to v). At a distance of 2t from the array, the variation in velocity will drop to 0.0006%, which the observer is unlikely to detect. The variation at other distances is shown in figure [2.1], from which we conclude that the average observer cannot resolve the difference between a continuous vortex sheet and an array of point vortices until he is as close to the array as the distance between successive vortices. A similar result will hold for any other configuration of vorticity. This is an extremely rapid falling off of resolving power with distance from the sheet and it is favourable for the flow model.

It will nevertheless be necessary to go much nearer to the array, and then to deal with the problem that, depending upon the observer's precise position, the flow speed could be very small or very large due to the degree of proximity to any one point vortex. One rather obvious way to deal with this is to let each vortex have a core similar to a Rankine vortex. An appropriate radius for the array of point vortices would be t/2. This

method will be adopted for free vorticity.

When a contour is present, we have some additional information. The total flux and circulation induced on the contour by an external point vortex are both zero, and this becomes significant when the contour is represented by discrete points. This extra condition is applied to modify the influence of the vortex on the nearest point on the contour (figure [2.2]) so that the total induced flux and circulation are always exactly zero, irrespective of the distance between vortex and contour. For simple contours, it is ensured that sensible velocities are induced everywhere on the contour. This method of 'taming' the vortex will be described in greater detail in a later chapter. The fact that it can be done will allow us to draw smooth streamlines extremely near to contours which are represented by rows of point vortices, where the streamlines would otherwise be zigzag lines.

It has been shown in this subsection that point vortices are a good representation of distant regions of vorticity. For nearby regions of vorticity, techniques are available to make the discrete vortices look like continuously distributed vorticity. Since we can add complex potentials, two-dimensional vortex statics is a linear subject. The usual non-linearity of fluid flows appears when the vortices are moving.

2.1(b) Vortex Dynamics

In a cloud of free point vortices, it follows from equation (2.8) that to be consistent one must assume that every vortex is moving with the local flow velocity. One can always do a Galilean transformation to bring the flow at any point to rest, and if there is a point vortex there then it must also be at rest, or some strange new principle must be devised to explain why it is moving. This local flow velocity is attributable to every other point vortex, and perhaps to a mainstream flow (Rosenhead[6]). Thus the velocity of the ith vortex is given by

$$u_i = U + \sum_{\substack{j=1 \\ j\neq i}}^{n} \frac{\gamma_j}{2\pi} \frac{(y_i - y_j)}{(x_i - x_j)^2 + (y_i - y_j)^2}$$

and

$$v_i = V - \sum_{\substack{j=1 \\ j\neq i}}^{n} \frac{\gamma_j}{2\pi} \frac{(x_i - x_j)}{(x_i - x_j)^2 + (y_i - y_j)^2} \qquad (2.14)$$

(Note that the summations exclude any influence of a vortex upon itself)

Equation (2.14) tells us that every vortex tends to orbit every other vortex, reminding us perhaps of clusters of stars which move around each

under the influence of their mutual gravitational attraction.

A single vortex in a stationary flow will not move at all. Two vortices will orbit each other if they have the same sign. The centre of vorticity will remain fixed, and so will the variance of the vorticity distribution around this centre. To a distant observer, due to the resolution effects described in subsection 2.1(a), the two vortices will appear as a single vortex (figure [2.3]). Thus for a computer program to describe the vortex motion, it often does not matter if the period of rotation of two nearby vortices is computed incorrectly, since there will be negligible effect on the rest of the flow. It is therefore possible to give each vortex a core, which disposes of the difficulty of the vortex being a singularity. Equation (2.14) has been modified so that when then velocity is required outside some selected core radius r_c, the flow speed is given by

$$\frac{\Gamma}{2\pi r^2}\,\underset{\sim}{r}$$

Inside the core, the flow speed is given by

$$\frac{\Gamma}{2\pi r_c^2}\left(2 - \frac{r^2}{r_c^2}\right)\underset{\sim}{r}$$

The core velocity distribution is shown in figure [2.4]. The quantity r_c

should be chosen as the minimum length scale of a particular problem, but it must be admitted that at high Reynolds numbers, this minimum length scale would be too small be practical to adopt on existing computers. Thus the larger length scale actually chosen is arbitrary.

One could of course use the simpler distribution

$$\frac{\Gamma}{2\pi r_c}\,\frac{r}{r_c}$$

which is also shown in figure [2.4], and there would be little difference to the numerical simulation. The velocity distribution actually chosen is more aesthetic.

For a flow with many vortices, equation (2.14) must be integrated numerically in time. The velocity at any point in the flow may calculated from equation (2.11), so we have a complete kinematic description of the flow. It is also necessary to show that the description is dynamically consistent. Though we started with the Navier-Stokes equations, which are dynamic equations, the fact that the fluid is incompressible allows us to remove pressure from the equations by taking the curl, and thus derive a kinematic equation of vortex motion. We should now go back and show that the vortex motions are associated with sensible pressure distributions.

This will be done in section 2.3. First we consider the other principal type of vortex motion - diffusion.

2.2 DIFFUSION

Diffusion of vorticity without convection will be considered first. Then two examples of diffusion with convection will be given. These are the point vortex in subsection 2.2(a), and the Kelvin-Helmholtz instability of the vortex sheet in subsection 2.2(b).

Equation (2.6) reduces to the diffusion equation

$$\frac{\partial \omega}{\partial t} = \nu \nabla^2 \omega \tag{2.15}$$

which may be applied to many processes, such as heat conduction or suspended particles in Brownian motion (Einstein[19], Smoluchowski[20], Perrin[21]).

There is an analogy between the macroscopic diffusion of a substance and the microscopic random motion of real or hypothetical particles of that substance. In the previous section the point vortex was considered as if it were the fundamental particle of two-dimensional incompressible flow. It is logical to represent diffusion of vorticity by the random motion of individual members of a cloud of point vortices (no other method is known to the author). This model of diffusion was applied by Chorin[4] to the

circular cylinder and to a laminar boundary layer. It was separately re-invented by the author as a variant of the 'Monte-Carlo' method.

The use of this method immediately introduces a new feature. Whereas the Navier-Stokes equations appear to be deterministic, the simulation proposed here is probabilistic, bringing an uncertainty into the method which is discussed in subsection 2.2(a). A second new feature is that the random motion of point vortices continually injects disturbances into the flow. For many flow simulations this is a desirable feature which can be exploited to provoke instabilities such as the Kelvin-Helmholtz instability of a vortex sheet (subsection 2.2(b)), or the instabilities which lead to the Von Karman vortex street or rotating stall in compressors. In fact, in the applications of the 'random vortex' method given here, our motives are not primarily to simulate diffusion, but rather to search for instabilities by a method with a known and quantifiable side effect (i.e. diffusion). As a rule, at Reynolds numbers below 10,000 we will aim to simulate diffusion. Above Re = 10,000 we will be looking for instabilities.

The method of displacing each point vortex is obtained from the diffusion equation written in polar co-ordinates

$$\frac{\partial \omega}{\partial t} = \frac{\nu}{r} \frac{\partial}{\partial r}\left[r \frac{\partial \omega}{\partial r} \right] \qquad (2.16)$$

For an initial point vortex, this has the solution (Batchelor[22])

$$\omega = \frac{\gamma}{4\pi\nu t} \exp\left[-\frac{r^2}{4\nu t}\right] \qquad (2.17)$$

This solution is shown in figure [2.5]. Equation (2.17) is re-interpreted as the probability of finding the point vortex in a certain region of space at a later time, given that its initial position is known. That is, the probability of finding the vortex in the interval (r,r+dr) and (θ,θ+dθ) is

$$p = \frac{1}{4\pi\nu t} \exp\left[-\frac{r^2}{4\nu t}\right] dr\ r\ d\theta \qquad (2.18)$$

The total probability of finding the point vortex anywhere in the plane is of course equal to one. A particle moving at random in this way is said to undergo a 'Wiener' process after the mathematician Norbert Wiener[23], who first stated formal rules for the process. The most important rule is that there is no correlation between successive displacements of the particle.

For a computer simulation, there is available a random number generator which produces random numbers equally likely to be anywhere in the interval (0,1). To turn this distribution into the distribution required by equation (2.18) we equate the cumulative probability distributions. Thus integrating equation (2.18)

$$P = \int_0^{2\pi} \int_0^{r} \frac{\exp\left[-\frac{r^2}{4\nu t}\right]}{4\pi\nu t} \, dr \, r \, d\theta$$

$$= \exp\left[-\frac{r^2}{4\nu t}\right] \qquad (2.19)$$

If this equation is inverted

$$r = \sqrt{4\nu t \ln\frac{1}{P}} \qquad (2.20)$$

We generate a value of P from the interval (0,1] and use equation (2.20) to obtain the corresponding value of r, the displacement. A random direction θ must also be chosen for the displacement from the interval $[0,2\pi)$. This pair of quantities (r,θ) gives a displacement whose probability density is that of equation (2.18). For many vortices, many pairs of random numbers, all independent of each other, must be generated. If the ith vortex has a velocity (u_i,v_i) due to convection, then

$$dx_i = u_i dt + \sqrt{4\nu\, dt \ln\frac{1}{P_i}} \cos(\theta_i)$$

$$dy_i = v_i\,dt + \sqrt{4\nu\,dt\,\ln\frac{1}{P_i}}\quad \sin(\theta_i) \qquad (2.21)$$

gives a prediction of the new position of the vortex after time dt.

In practice, within a time step dt, the processes of diffusion and convection are taken separately. The new position of each vortex due to convection alone is predicted. The new position is then corrected according to the improved Euler method (see Table 2.1), the point being that this numerical method is time-reversible, and so it keeps variance of vorticity and entropy constant, as they should be with convection alone. This does depend upon iterating the improved Euler method until it converges. In fact only one iteration is performed, but the residual error will be much less than the error of the random displacement applied at the end of the time step. This random displacement is expected to increase both entropy and variance of vorticity. When this process is repeated many times, the interaction between convection and diffusion is obtained.

It may be commented that instead of equation (2.21), one could use the simpler equation

$$dx_i = u_i\,dt + \sqrt{4\nu\,dt}\quad \cos\theta_i$$

$$dy_i = v_i\,dt + \sqrt{4\nu\,dt}\quad \sin\theta_i \qquad (2.22)$$

By the Central Limit Theorem, repeated application of this simpler formula would have the same effect as formula (2.21). In both formulae there is no correlation between successive displacements of a point vortex, and the expected variance of the displacement is the same. The expression (2.21) was used for the boundary layer work, and for early work on flow separation, but later, when simplifications to the bluff body computer program were sought, expression (2.22) was used.

2.2(a) The Diffusion of a Point Vortex

A computer simulation has been performed to show the diffusion of a pointlike vortex according to the 'random vortex' method. The vortex was divided into one hundred parts. Each of these was given an independent random displacement on every time step, and was also convected by the other ninety-nine vortices. Parameter values chosen were ν=0.01 and dt=0.02. The process of diffusion is shown in figure [2.6]. A convention is used throughout this Thesis that clockwise vortices are drawn as vertical lines, and anti-clockwise vortices as horizontal lines. The length of the line is proportional to the strength of the vortex. The midpoint of the line is the

exact position of the vortex, not that this matters, for the position of any one vortex is uncertain and the vortices have no individual identity. This convention gives an overall impression of clouds of vorticity which is cheap to draw on a computer and which survives reduction by photographic techniques. The vortices in figure [2.6] are all clockwise.

From figure [2.6], it is apparent that the diffusion is isotropic. The variance of the vorticity distribution, $E(r^2)$ for any one vortex, can be obtained from equation (2.20) as

$$E(r^2) = \int_0^1 4\nu t \ln \frac{1}{P} \, dP$$

$$= 4\nu t \tag{2.23}$$

Four numerical simulations have been performed with four different sets of random numbers. The actual variance of the vorticity distribution

$$\frac{1}{100} \sum_{i=1}^{100} (x_i^2 + y_i^2)$$

as a function of time is shown in figure [2.7] for batches of fifty time steps, with the theoretical variance for comparison. It can be seen that there is an error of up to 17%, with a typical error of 10%.

Milinazzo and Saffman[24] have treated the diffusing point vortex by the same method, and they observe a comparable error. They performed a

theoretical analysis of the possible variation in the observed variance, which may be formulated as the inverse problem of deducing the viscosity by watching the vortex cloud diffusing and by measuring the slope of the lines in figure [2.7]. An independent observer knows that the increase in variance on each time step, divided by 4dt, should give the viscosity. There will be an error in the value of viscosity derived from observation which will become larger as the fractional change in variance decreases at later times. This can be seen from figure [2.7], where initially, the variance increases regularly. Later in time, the increase is not so regular, and at one point on one run, there is even a decrease (the observer would conclude from this that the viscosity was temporarily negative!). The results are given in figure [2.7] in batches of fifty timesteps. If the results were plotted at shorter intervals of time, they would appear more 'noisy', since the fractional change in variance is then smaller in each time interval. This behaviour illustrates an uncertainty principle in the 'Brownian' motion. As we attempt to look at the results in more detail, so the results obtained become noisier and less certain. The noise is reduced by integrating the data in some way to give an overall result, such as the lift and drag on a bluff body.

It is possible to give the uncertainty principle a formulation which

leads to an alternative interpretation of the Reynolds number. If the variance increases as

$$r_{rms} = \sqrt{4 \nu t}$$

a definition of the variance in velocity is given by

$$\frac{dr_{rms}}{dt} \equiv \frac{r_{rms}}{t} = \sqrt{\frac{4 \nu}{t}}$$

and

$$r_{rms} \frac{dr_{rms}}{dt} = 4 \nu \qquad (2.24)$$

which is an uncertainty principle for the Wiener process originally proposed by Fürth[25]. For a point vortex it may be expressed as

uncertainty in position x uncertainty in velocity = 4 x kinematic viscosity

On the L.H.S., the first term may be compared to a characteristic length, and the second term to a characteristic velocity

$$\frac{r_{rms}}{L} \frac{\frac{dr_{rms}}{dt}}{U} = \frac{4 \nu}{LU} = \frac{4}{Re} \qquad (2.25)$$

from which the Reynolds number arises naturally as a measure of the rate of diffusion.

The distribution of vorticity from the centre may be examined by associating with each vortex a quantity

$$P = \exp\left[- \frac{r^2}{4 \nu t} \right] \qquad (2.26)$$

(Note how the analysis of the last section is now being done in reverse)

It has been established that P will have a uniform probability of taking a value anywhere in the interval (0,1). The one hundred values of P obtained are sorted into order, and plotted in figure [2.8]. The expected value of the first P is 0.01, the second P is 0.02, the third P is 0.03, and so on. Each graph of figure [2.8] is expected to be a straight line running from (0,0) to (1,1). Most of the graphs show this quite well, with the graph at t=3 being the worst case.

It has been seen that there are errors associated with this method, which for the order of one hundred vortices, are typically about 10%. This is to be expected, since for n vortices the order of magnitude of the error is given by statistical theory as

$$\frac{1}{\sqrt{n}}$$

There is also 'noise' produced by the random movement of the vortices. This noise can be filtered by using sampling methods which obtain integrals, of

which figures [2.7] and [2.8] are examples. Other integrals which will be met are boundary layer momentum thickness, and the lift and drag forces on a body.

2.2(b) The Kelvin-Helmholtz Instability

A vortex sheet may be represented as a row of point vortices (Rosenhead[6], Abernathy and Kronauer[7]). Again one hundred such vortices have been used, and they are repeated periodically so that the velocity induced by one vortex is given by an expression of the form (2.13) (this arrangement could also be regarded as the flow in a narrow gap between two concentric circular cylinders). Rosenhead showed that if one of the point vortices were given a small displacement, then the displacement would continue to grow, so that the vortex sheet exhibits the Kelvin-Helmholtz instability. There is an imbalance between the convective velocities induced by neighbouring vortices on the displaced vortex, which acts in the direction which tends to increase the displacement. Rosenhead's computation is repeated in figure [2.9] for comparison, with two length periods shown. Abernathy and Kronauer showed that transverse waves in the sheet could have the same effect, causing it to 'snap' into discrete vortices. An explanation of the instability in terms of Bernoulli's Theorem is given by

sheet. It may be commented that this explanation predicts that there will be an instability, but it does not predict the subsequent development of the instability so well as the method based upon vorticity.

If every vortex in the sheet is moving at random, then we have an ample source of perturbations to destabilise the sheet, but first, it is of interest to look at diffusion alone. In figure [2.10], there is no convection, that is, the relevant part of the computer program has been temporarily removed. Under the influence of pure 'diffusion' the vortex sheet spreads out transversely. The vortices show the amount of clustering which would be expected from probability theory. In figure [2.11], with the same viscosity (and the same sequence of random numbers), convection of vortices has been restored to the computer program. The behaviour of the sheet is now very different. The perturbations in the sheet produced by the 'random vortex' method cause it to snap into discrete vortices. Initially, there appear to be four or five discrete vortices per length of sheet. As these develop they amalgamate into two vortices per length, and then into one large vortex. Since this large vortex must go on diffusing, we may expect that ultimately it will be dispersed to restore the continuous vortex sheet. Nevertheless, for the time being, the different behaviour of the sheet indicates that we are observing two-dimensional turbulence.

A Reynolds number may be defined, based upon the length period of the vortex sheet, the velocity jump across it, and the viscosity associated with the random motion. In figure [2.11], we have seen a transition to turbulence for Re=5000.

In figure [2.12] the behaviour for Re=2000 (and the same sequence of random numbers) is shown. Again the development of two-dimensional turbulence is observed. The vortex sheet seems to break up into fewer discrete vortices per length at the beginning, which we might expect.

In figure [2.13], for Re=1000 (and the same sequence of random numbers) a vortex cluster is briefly formed, but then it disperses.

At Re=500 (figure [2.14]) (with the same random numbers yet again) there is probabilistic clustering of vorticity, but no apparent transition to turbulence. The mean flow is laminar, despite the random motion of the individual vortices.

Note the apparent paradox that as the viscosity is increased, and the random motion of vorticity is increased, the overall flow changes from turbulent to laminar flow. This is not a paradox if we think of the vortex clusters 'boiling' at high viscosity. On the other hand, with the 'random vortex' method, no matter how small we make the viscosity, the resulting flow will often be quite different from flow with no viscosity at all, due

to the perturbations. This makes the method attractive for simulating real fluid flows. The difference between an ideal fluid and a fluid with infinitesimal viscosity is the story of fluid mechanics!

However, real turbulence is three-dimensional, and may be fundamentally different from two-dimensional 'turbulence' because of the stretching of vortex filaments, which can never be simulated by a two-dimensional model. It would be better to say that we have simulated transition to turbulence rather than turbulence itself. The transition is a two-dimensional phenomenon due to the Kelvin-Helmholtz instability. Once it has begun, but not before, three-dimensional effects appear. In the examples given later, two-dimensional turbulence will often be encountered. Indeed, it is arguable that phenomena such as the Von Karman vortex street represent a special case of two-dimensional turbulence with just one frequency present. Leonard[27] has made a preliminary study of the vortex sheet instability in three dimensions, using an artificial perturbation as in figure [2.9].

Now that we have a kinematic model which is expected to be good at reproducing the behaviour of the real flow, it is possible to go back to the Navier-Stokes equation and look at the derivation of the pressure distribution from the vortex motion.

2.3 THE PRESSURE DISTRIBUTION

Given the distribution of vorticity in the flow, we may obtain the velocity at any point. Thus our problem is to obtain the pressure distribution of an incompressible flow, given the velocity distribution. The solution to this means solving the Navier-Stokes equation for specified velocity distribution, which we will now proceed to do.

Recall the Navier-Stokes equation

$$\frac{\partial \underset{\sim}{U}}{\partial t} + \underset{\sim}{U}.\nabla \underset{\sim}{U} = -\frac{\nabla p}{\rho} + \nu \nabla^2 \underset{\sim}{U} \qquad (2.1)$$

As well as the vector identity (2.2) there is another useful identity. Both identities may be expressed as

$$\underset{\sim}{U}.\nabla \underset{\sim}{U} = \nabla\left(\frac{U^2}{2}\right) - \underset{\sim}{U} \times \underset{\sim}{\omega} \qquad (2.2)$$

$$\nabla^2 \underset{\sim}{U} = \nabla(\nabla.\underset{\sim}{U}) - \nabla \times (\nabla \times \underset{\sim}{U})$$

$$= - \nabla \times \underset{\sim}{\omega} \qquad (2.27)$$

where the flow is incompressible. This allows equation (2.4) to be written in the form

$$\frac{\nabla p_o}{\rho} = (\underset{\sim}{U} - \nu \nabla) \times \underset{\sim}{\omega} - \frac{\partial \underset{\sim}{U}}{\partial t} \qquad (2.28)$$

The operator

$$(\underset{\sim}{U} - \nu \nabla)$$

is reminiscent of the problem of heat conduction in moving media (for an example familiar to the author, the quenching of a very hot surface, see Duffey and Porthouse[28]). In heat conduction

$$\rho c \, (\underset{\sim}{U} - \alpha \nabla) \, T$$

is the heat flux in a moving medium. When this operator acts upon a vector rather than a scalar, it is a formality by the way in which the vector is defined that we must insert a vector product to give a flux vector. Thus

$$(\underset{\sim}{U} - \nu \nabla) \times \underset{\sim}{\omega}$$

may be interpreted as a vortex flux. Equation (2.28) says that the stagnation pressure gradient along a contour is related to the vortex flux across the contour. Now, in the computer programs described above, this vortex flux is an observable quantity. We can see how many vortices cross a contour in a given time, and whether this crossing is due to diffusion or convection is beside the point.

From the observation a generalised transport velocity may be obtained, which represents the effects of both diffusion and convection (by analogy, a 'random thermion' method in heat conduction would yield an observable heat flux which could be related to an average velocity of the thermions).

This permits the first simplification of equation (2.28)

$$\frac{\nabla p_o}{\rho} = E(\underset{\sim}{U}) \times \underset{\sim}{\omega} - \frac{\partial \underset{\sim}{U}}{\partial t} \qquad (2.29)$$

where the velocity is now to be understood as a generalised velocity. It is appropriate to use the statistical notation for expected value in equation (2.29) when the vortices are moving with a random component. The vortices must not be thought of as having an individual identity since this will lead to a paradox: there is no reason why an individual vortex should drift down a gradient of vortex density.

Note that this generalised velocity is the velocity of the vortex motion, which could be quite different from the local velocity of the fluid. If we inserted an infinite number of rotating cylinders into the flow, we could determine the local vortex density at any point in the flow, subject of course to the condition

$$\nabla . \underset{\sim}{\omega} = 0$$

If these cylinders then moved under our control, it would be the value of $E(\underset{\sim}{U})$ that we chose that should appear in equation (2.29), not the value of the local velocity $\underset{\sim}{U}$. It is on this principle that turbines and compressors exchange useful work with their fluid. The blades of turbines and compressors are arrays of moving vortices, and the value of $E(\underset{\sim}{U})$ is the

rotational velocity of the rotor. Equation (2.29) can then be viewed as a differential form of the Euler pump equation.

Because of the change in our view of the flow from a dynamic to a kinematic description, it is legitimate to talk of vortices 'inducing' a velocity and a pressure distribution in the flow. The remaining dynamic condition is the conservation of vorticity, which is a simple thing to ensure.

The stagnation pressure distribution induced by a single moving point vortex can be readily derived by writing equation (2.29) in component form and finding a solution. This solution, since it applies to a moving vortex, may then be checked against the solution in a moving framework in which the vortex is stationary. For a single point vortex, moving with velocity $E(\underset{\sim}{U})$ and inducing a velocity $\underset{\sim}{V}$ at some other point, this solution is the simple expression

$$p_o = \rho\, E(\underset{\sim}{U}).\underset{\sim}{V} \qquad (2.30)$$

for the stagnation pressure induced at that other point. The isobars of stagnation pressure are circles which touch the vortex, as shown in figure [2.15]. Since in equation (2.29), $\underset{\sim}{\omega}=0$ except at the singularity, we have in fact a linear equation. It follows from this that for several moving point

vortices we may add the contribution due to each vortex to give the total stagnation pressure. If the ith vortex is moving with velocity $E(\underset{\sim}{U}_i)$ and induces a velocity $\underset{\sim}{V}_i$ at a point, then the stagnation pressure at that point is

$$p_o = \rho \sum_{i=1}^{n} E(\underset{\sim}{U}_i) \cdot \underset{\sim}{V}_i \qquad (2.31)$$

or

Stagnation Pressure = Eulerian acceleration potential

By the reasoning given here we suppose that equation (2.31) is a general solution to

$$\frac{\nabla p_o}{\rho} = -\frac{\partial \underset{\sim}{U}}{\partial t} \qquad (2.32)$$

representing the influence of distant moving vorticity. It turns out serendipitously that the effect of local moving vorticity

$$\frac{\nabla p_o}{\rho} = E(\underset{\sim}{U}) \times \underset{\sim}{\omega} \qquad (2.33)$$

is also included in equation (2.31). To show this, consider a horizontal vortex sheet. Let the sheet have a velocity jump from U_1 to U_2 (figure [2.16]). Although there is no acceleration anywhere in the flow, there is

still an acceleration potential, so equation (2.31) may still be integrated for each elementary vortex in the sheet. This gives a stagnation pressure above the sheet of

$$p_{o_{\text{above}}} = \frac{(U_1 + U_2)}{2} \quad \frac{(U_2 - U_1)}{2} \tag{2.34}$$

where the sheet is moving with speed

$$E(\underset{\sim}{U}) = \frac{(U_1 + U_2)}{2}$$

and inducing a flow velocity

$$\underset{\sim}{V} = \frac{(U_2 - U_1)}{2}$$

The stagnation pressure below the sheet is similarly obtained from equation (2.31)

$$p_{o_{\text{below}}} = \frac{(U_1 + U_2)}{2} \quad \frac{(U_1 - U_2)}{2} \tag{2.35}$$

The difference in stagnation pressure across the sheet is

$$\frac{(U_1 + U_2)}{2} (U_2 - U_1) = \frac{U_2^2}{2} - \frac{U_1^2}{2} \tag{2.36}$$

This stagnation pressure difference could also be obtained by integrating equation (2.33) through the sheet!

The result has been established that equation (2.31) is a full solution to equation (2.29). Equation (2.31) is in fact the simple general solution to the Navier-Stokes equation which has been sought (note that it is assumed that all accelerations are due to moving vorticity, and not, for example, due to an accelerating body in the flow). A list of continuous and discrete vortex equivalents is given in Table 2.2.

It has been shown in this subsection that the discrete vortex simulation of the Navier-Stokes equation is consistent with the dynamics. Incompressible flow can be described by vortex kinematics, with conservation of vorticity as the dynamical principle. The several terms of the Navier-Stokes equation are shown to have a common origin in moving vorticity, and for a specified distribution of vorticity, the Navier-Stokes equations may be integrated to give the stagnation pressure distribution. Since stagnation pressure changes are the only useful (or detrimental) changes, and in aerodynamic devices they are provided by moving vorticity, it follows that the moving vortex is our principal interest. We have found a way to write the Navier-Stokes equation which emphasises the moving vortex, and which leads to a solution based upon it. This solution turns

out to be simple. All one has to do now is to determine the transport velocity of the vortices in the flow...

Finally, it should be commented that the way in which a moving vortex modifies the pressure distribution means that we cannot use Blasius' Theorem to calculate the force on a body in separated flow. This is the practical point of this section.

TABLE 2.1 THE NUMERICAL METHOD

(1) Compute the convective velocities of each vortex, that is, the values of (x_i,y_i) give (u_i,v_i).

(2) Predict the new position of each vortex:

$$(x_i'',y_i'') := (x_i,y_i) + (u_i,v_i)\,dt$$

(3) Correct the new position of each vortex by one application of the improved Euler method.

$$(x_i',y_i') := [(x_i,y_i) + (x_i'',y_i'')]/2$$

The values of (x_i',y_i') give (u_i',v_i').

$$(x_i'',y_i'') := (x_i,y_i) + (u_i',v_i')\,dt$$

(4) Give every vortex a random displacement.

Generate (P_i,θ_i).

$$(x_i'',y_i'') := (x_i'',y_i'') + (\cos\theta_i,\sin\theta_i)\sqrt{4\,\nu\,dt\,\ln\frac{1}{P_i}}$$

(5) Put $(x_i,y_i) := (x_i'',y_i'')$ and go back to step (1) for a new time step.

TABLE 2.2 DISCRETE-VORTEX ANALOGUES OF THE FLOW FIELD EQUATIONS

Complete set for two-dimensional incompressible flow

Vorticity $\underset{\sim}{\omega} = \nabla \times \underset{\sim}{U}$

All the vorticity is concentrated at a number of singularities with position (x_i, y_i) and strength γ_i, inducing a velocity at (x,y) equal to

$$\sum_{i=1}^{n} \frac{\gamma_i}{2\pi} \frac{(y - y_i, x_i - x)}{(x - x_i)^2 + (y - y_i)^2}$$

Continuity $\nabla . \underset{\sim}{U} = 0$

This is automatically satisfied by any one singularity, and thus by any group of singularities.

Convection $\frac{\partial \underset{\sim}{\omega}}{\partial t} + \underset{\sim}{U} . \nabla \underset{\sim}{\omega} = 0$

Every vortex singularity 'orbits' every other singularity:

$$(u_i, v_i) = \sum_{\substack{j=1 \\ j \neq i}}^{n} \frac{\Gamma_j}{2\pi} \frac{(y_i - y_j, x_j - x_i)}{(x_i - x_j)^2 + (y_i - y_j)^2}$$

Diffusion $\frac{\partial \underset{\sim}{\omega}}{\partial t} = \nu \nabla^2 \underset{\sim}{\omega}$

In addition to its convective velocity, every vortex is given a random motion, so every vortex is expected to recede from every other vortex. This is equivalent to diffusion. Vorticity is expected to drift down a gradient of vortex density according to Fick's Law (do not think of the vortices as having an individual identity since this can lead to a paradox). The drift velocity can be added to the convective velocity to give a generalised transport velocity, E(U), which is used to compute the pressure distribution.

Pressure $\frac{\nabla p_o}{\rho} = E(\underset{\sim}{U}) \times \underset{\sim}{\omega} - \frac{\partial \underset{\sim}{U}}{\partial t}$

Add the acceleration potentials due to each moving vortex to obtain the total stagnation pressure at (x,y):

$$p_o = \rho \sum_{i=1}^{n} \frac{\gamma_i}{2\pi} \frac{(y - y_i)\, u_i + (x_i - x)\, v_i}{(x - x_i)^2 + (y - y_i)^2}$$

One can add the velocity due to each vortex (which is independent of the vortex velocity) to obtain the flow velocity elsewhere, and thus the dynamic pressure. By subtracting this dynamic pressure from the stagnation pressure, one obtains the local static pressure, or the 'real' pressure.

Note that the principle of superposition can be used to obtain flow velocity and stagnation pressure, but not directly to obtain static pressure.

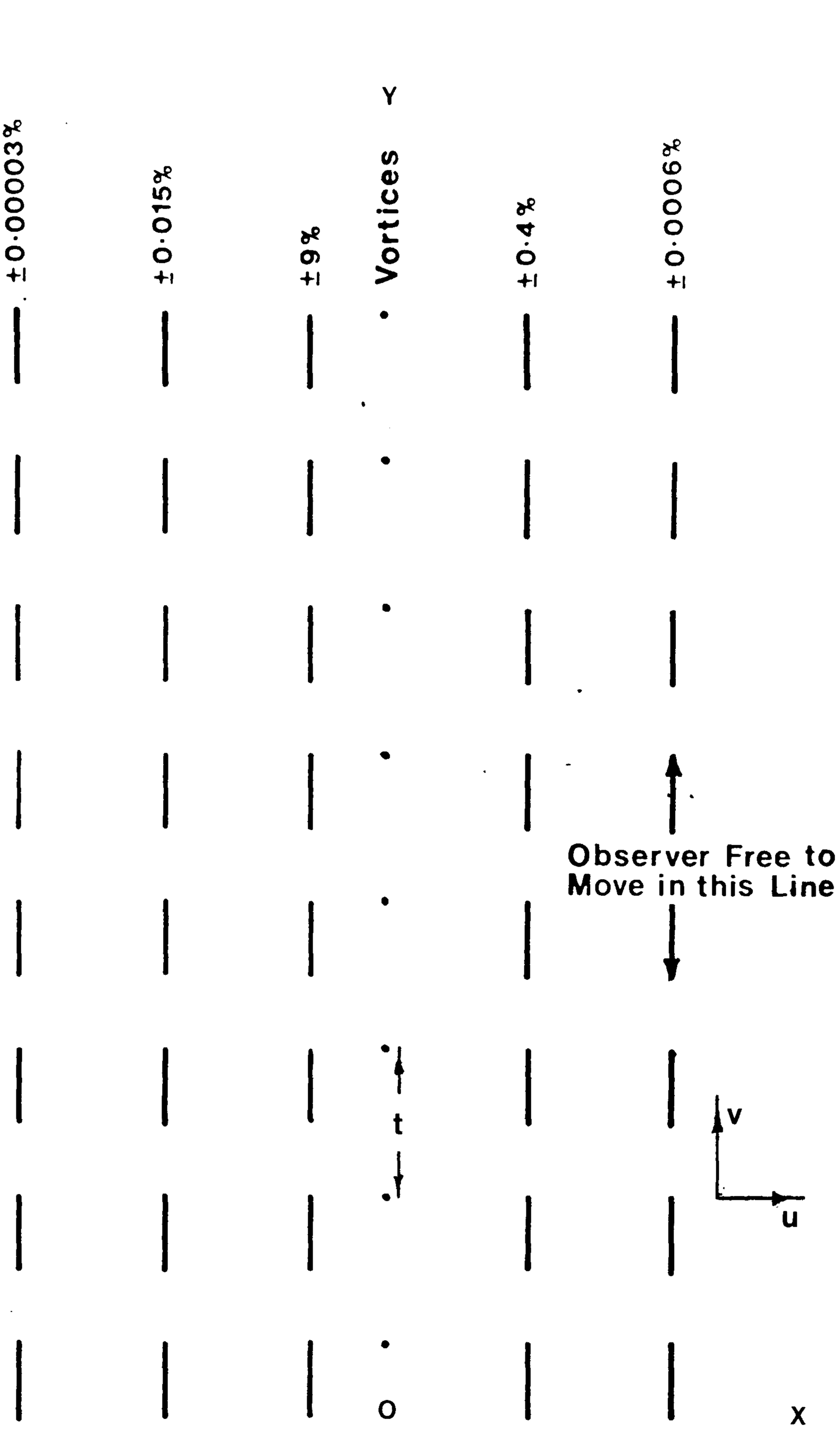

Figure 2.1 The Variation in Flow Velocity due to an Array of Point Vortices

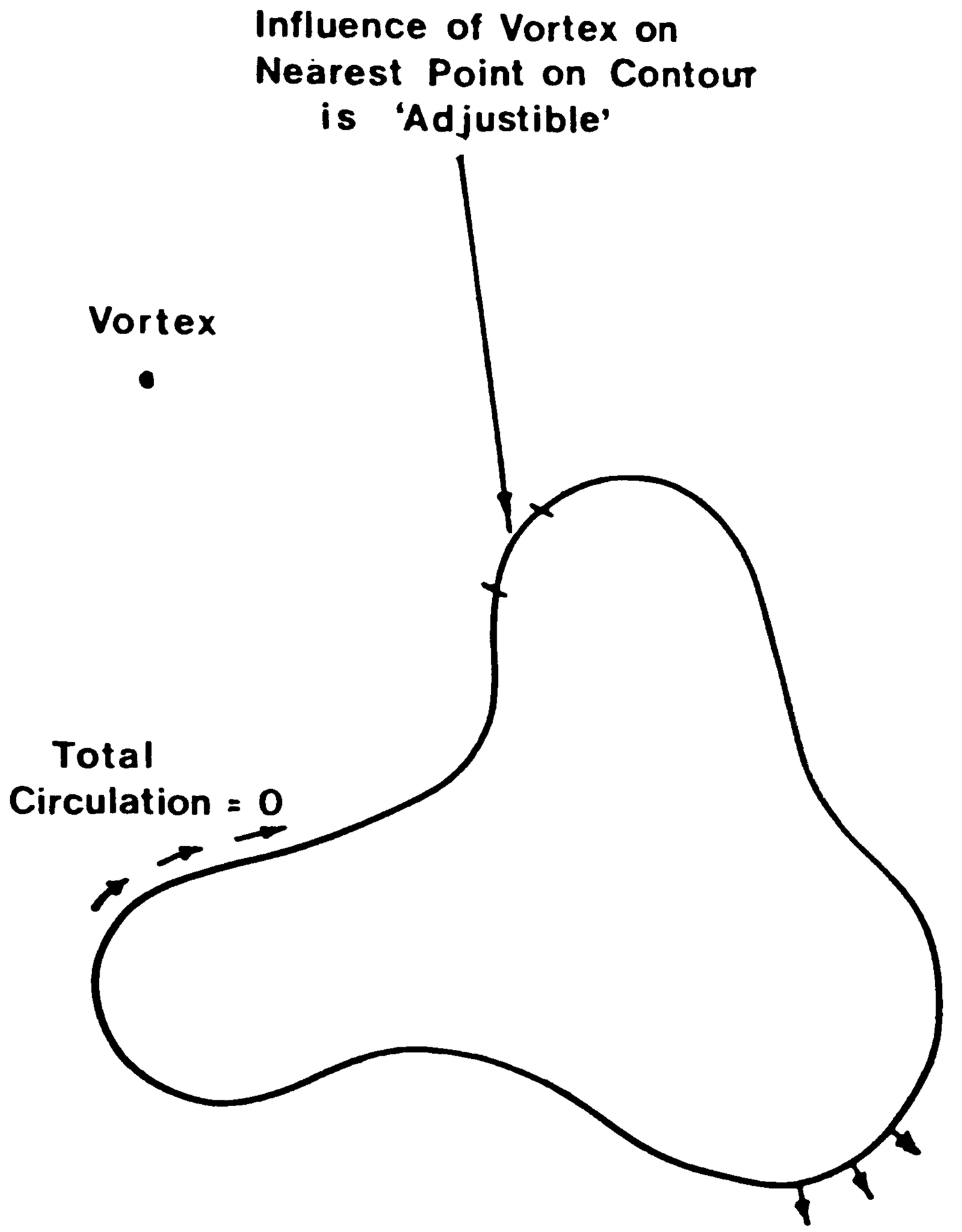

Figure 2.2 The Influence upon a Contour of an External Vortex

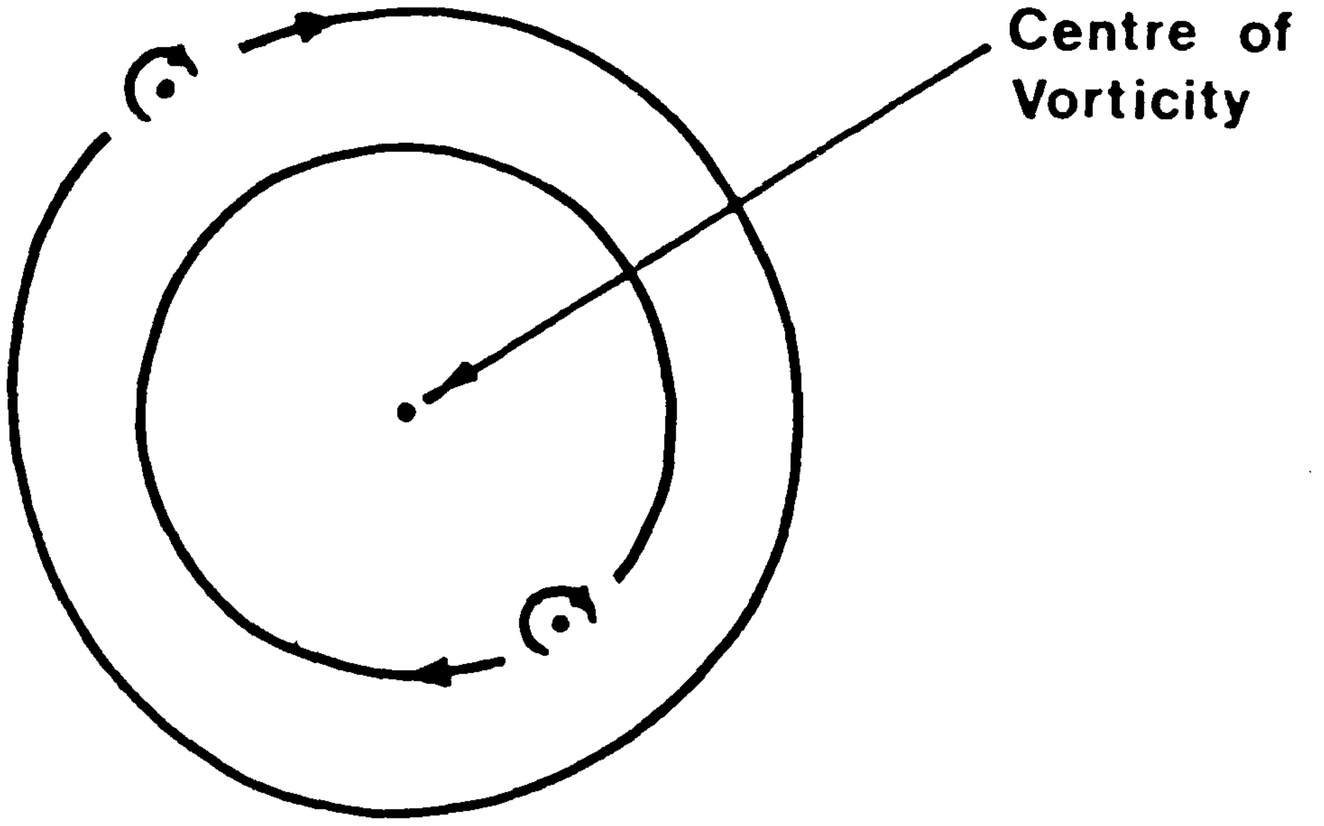

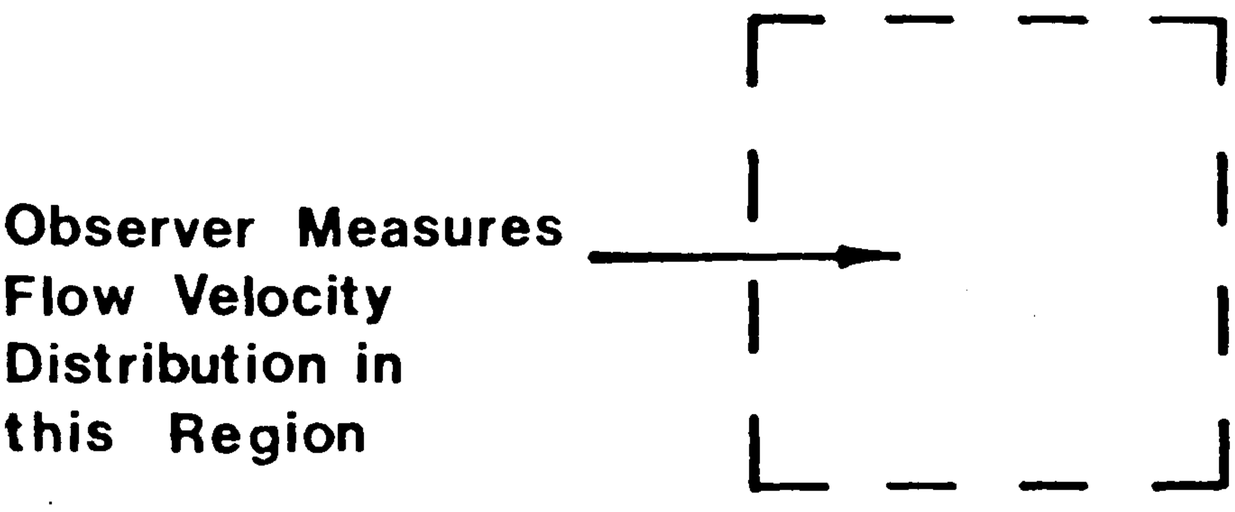

Figure 2.3 The Motion of a Pair of Vortices

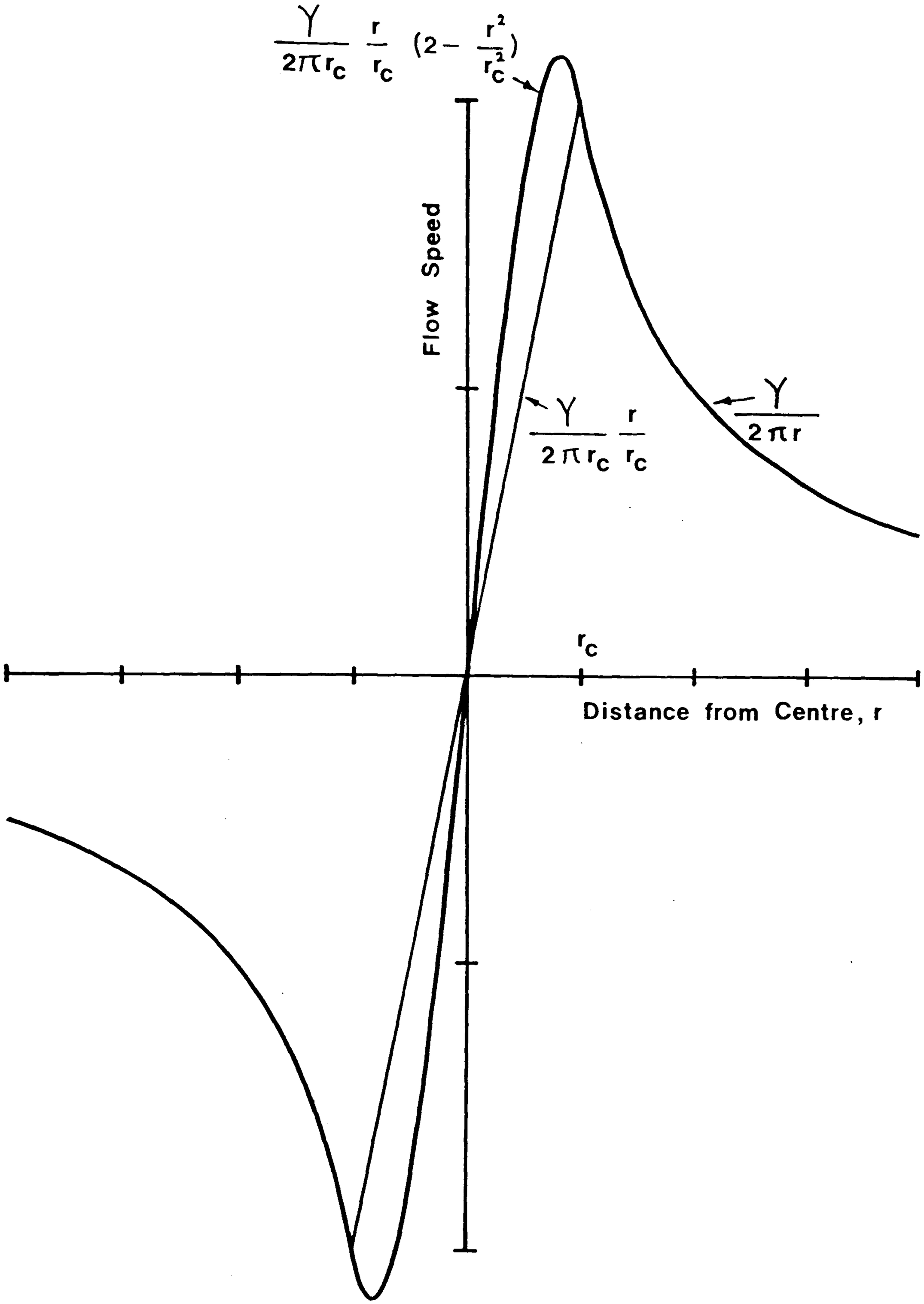

Figure 2.4 The Flow Speed near a Vortex Core

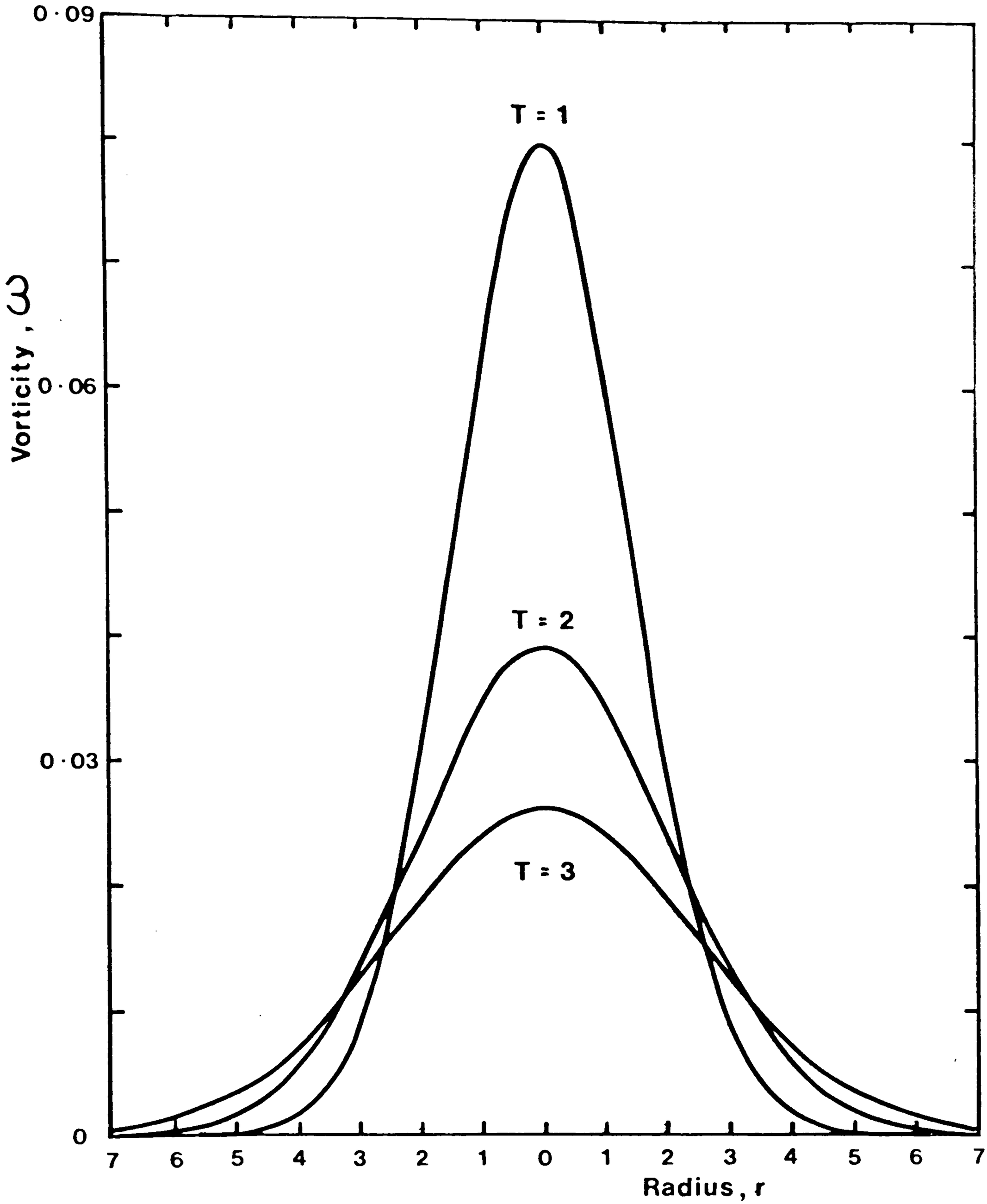

Figure 2.5 The Diffusion of a Point Vortex by Analysis

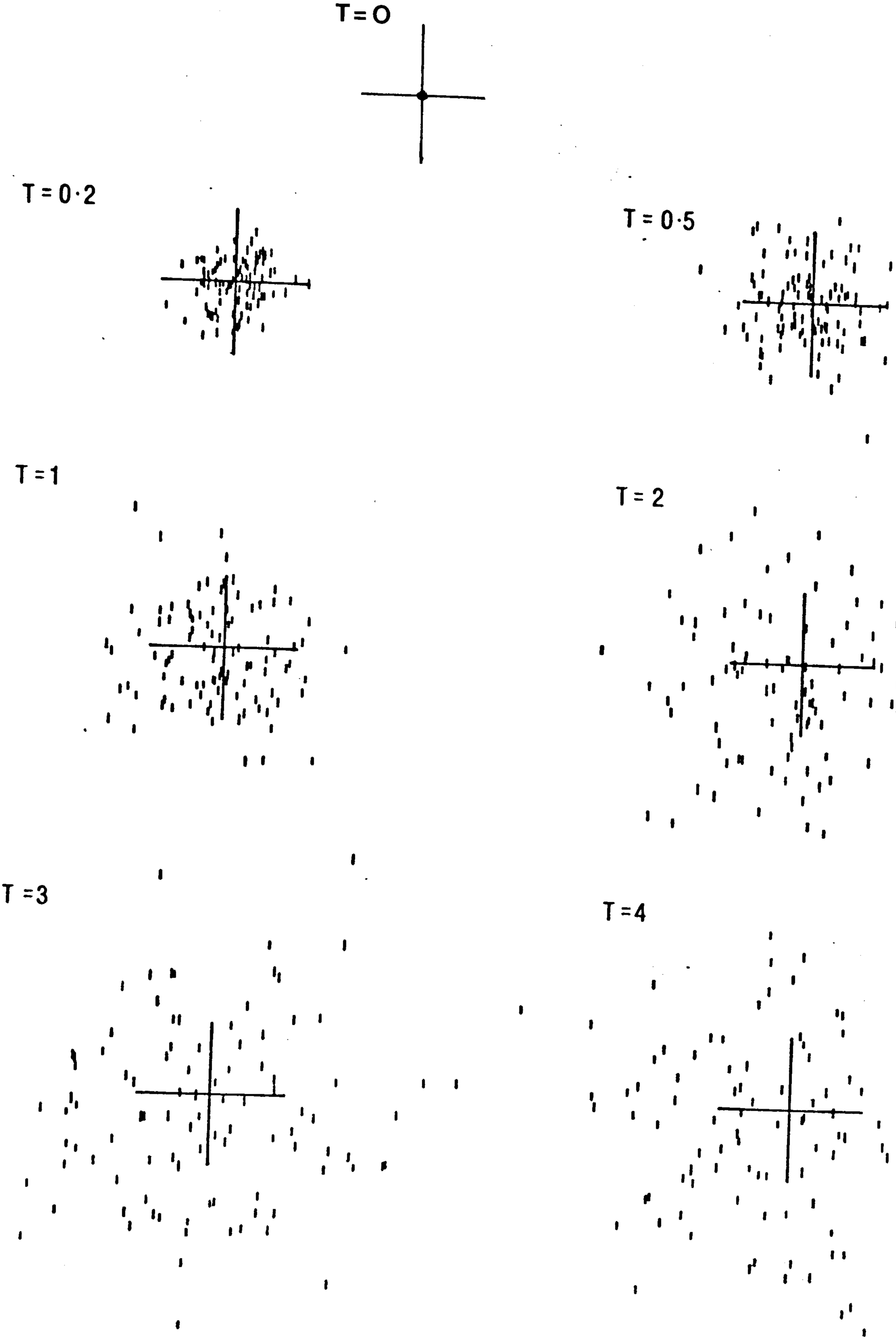

Figure 2.6 The Diffusion of a Point Vortex

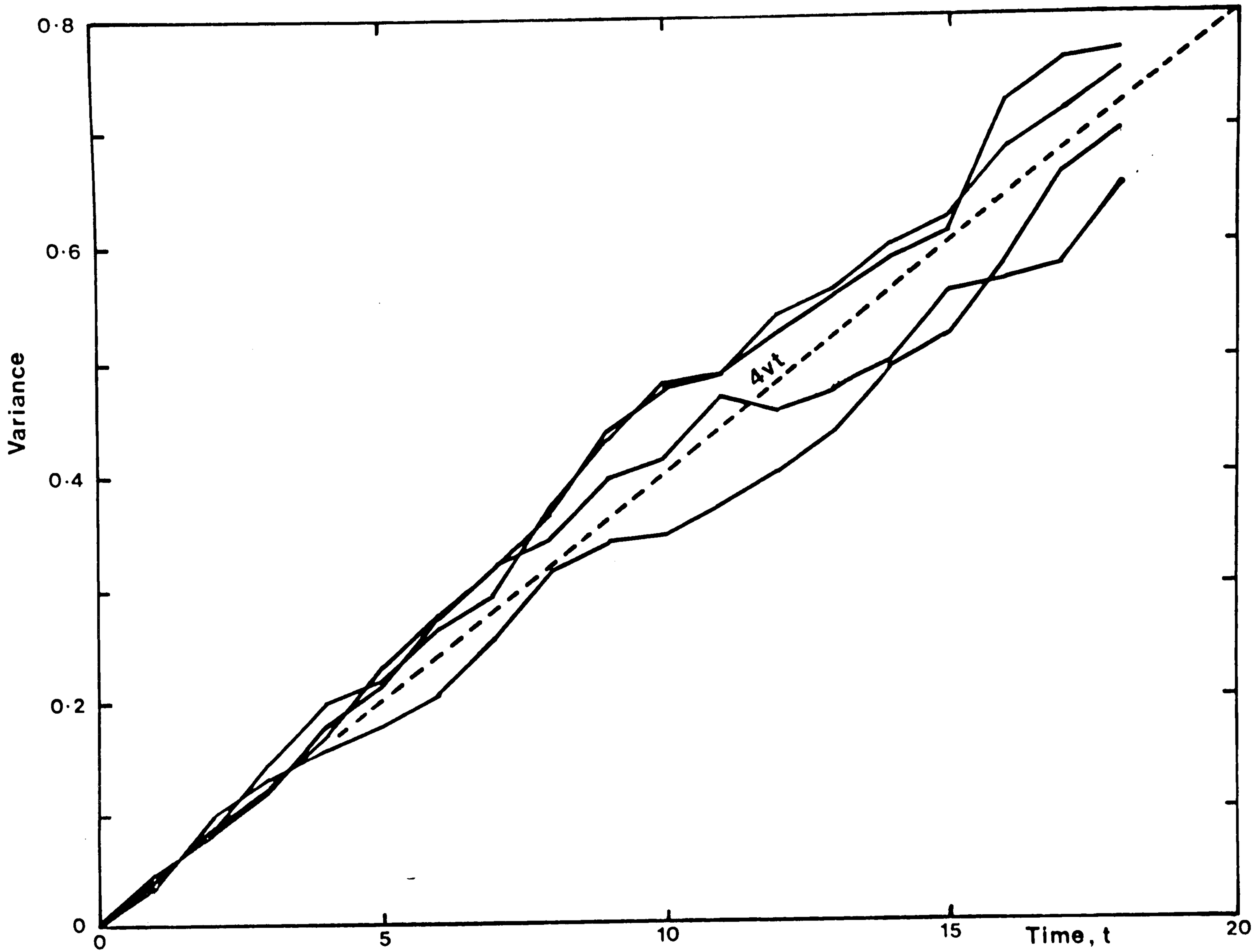

Figure 2.7 The Variance of the Vortex Distribution with Time

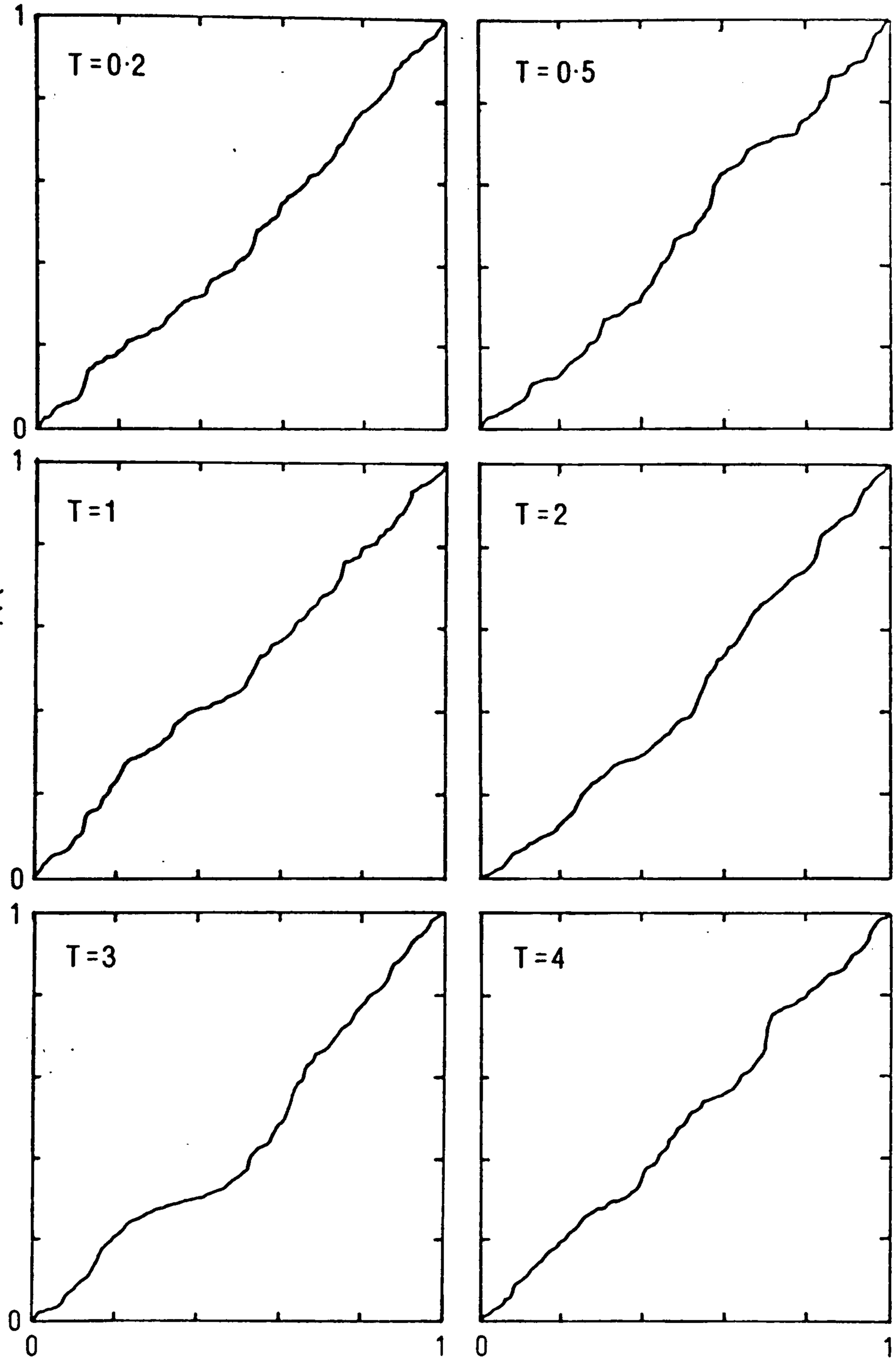

Figure 2.8 Radial Distribution of the Vortices

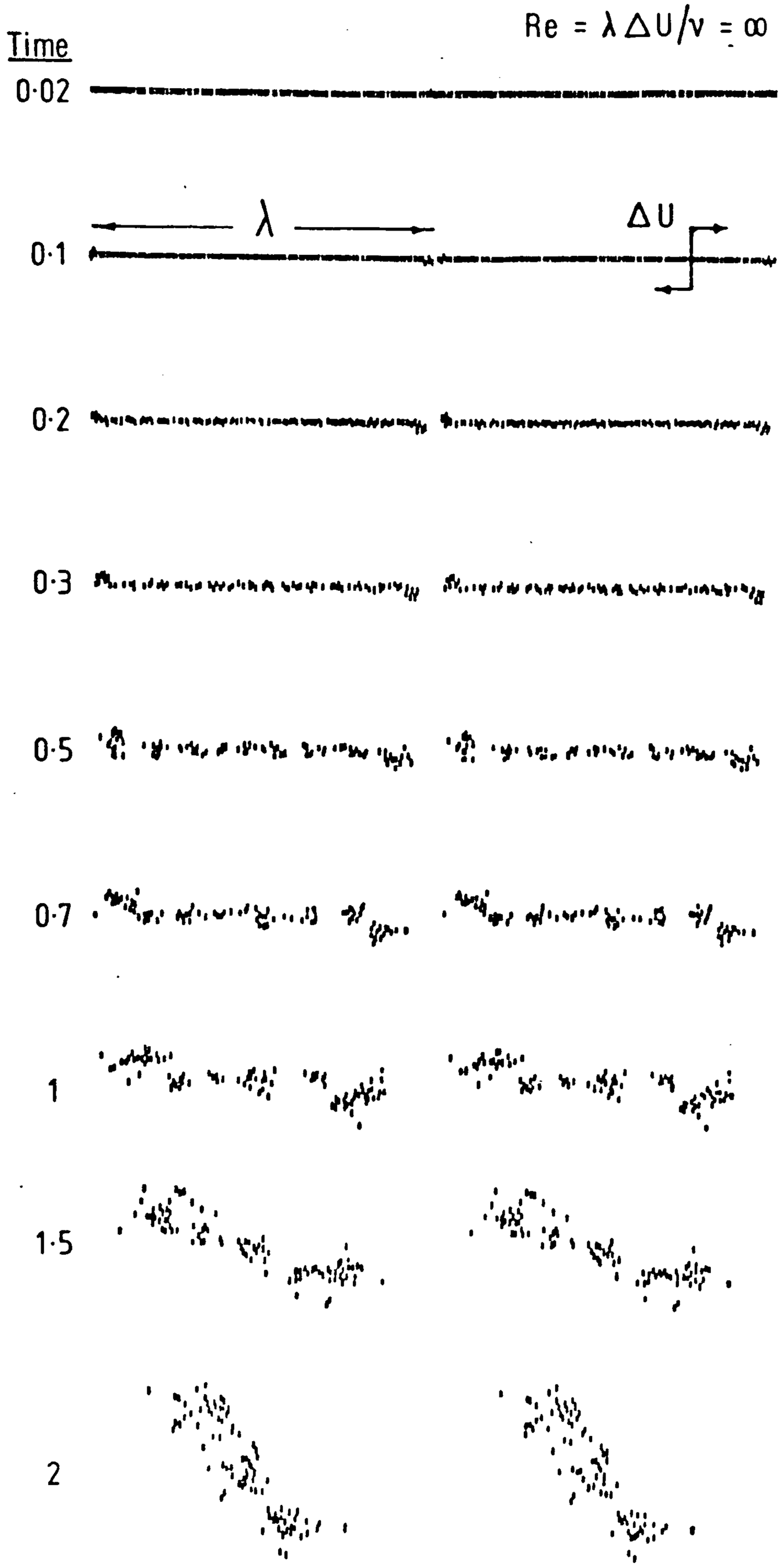

Figure 2.9 Demonstration of the Kelvin-Helmholtz Instability by an Artificial Perturbation

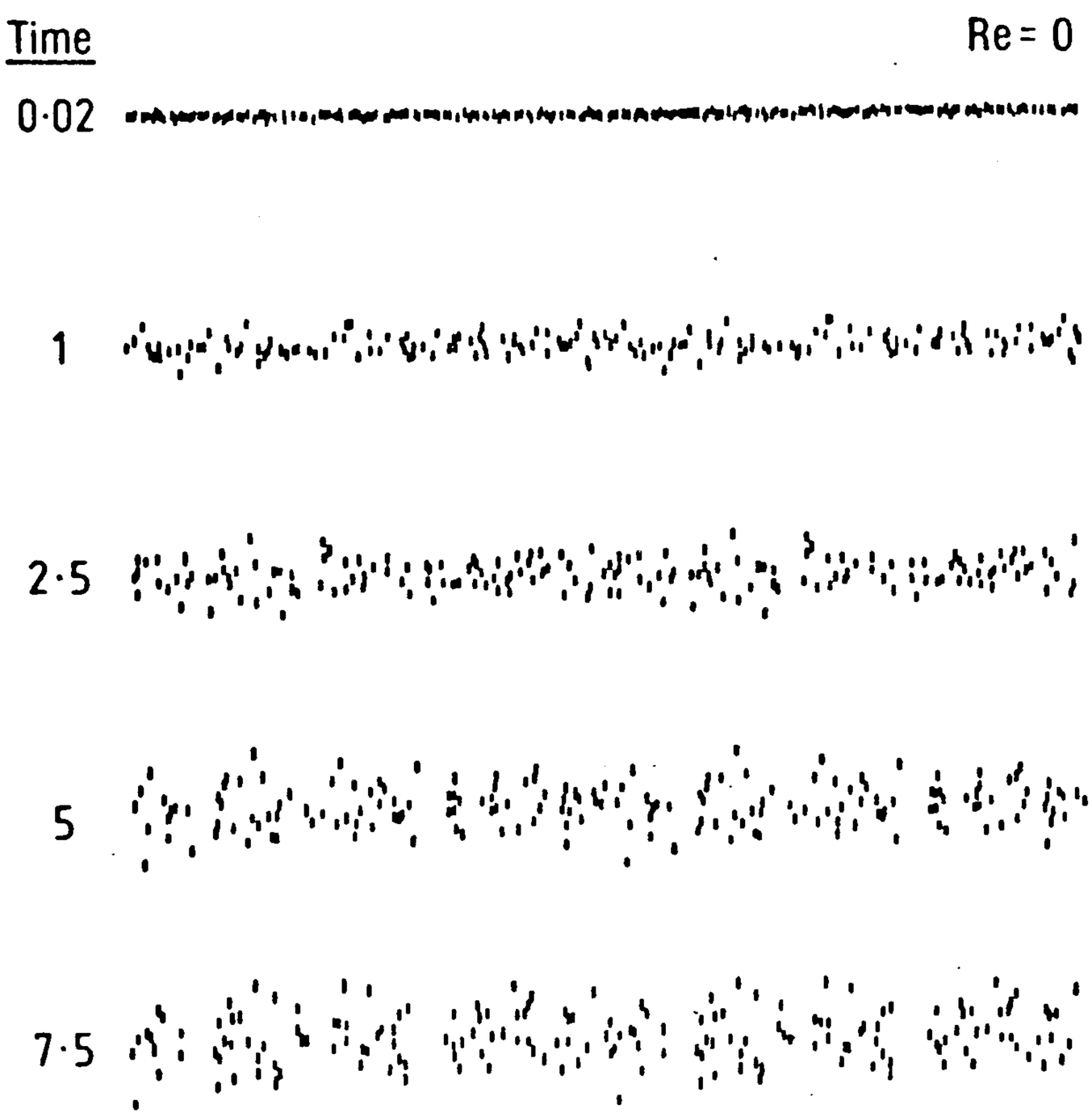

Figure 2.10 The Vortex Sheet with Diffusion but no Convection

Time

Re = 5000

0·02

0·2

0·5

1

1·5

2·5

3·5

5·5

7·5

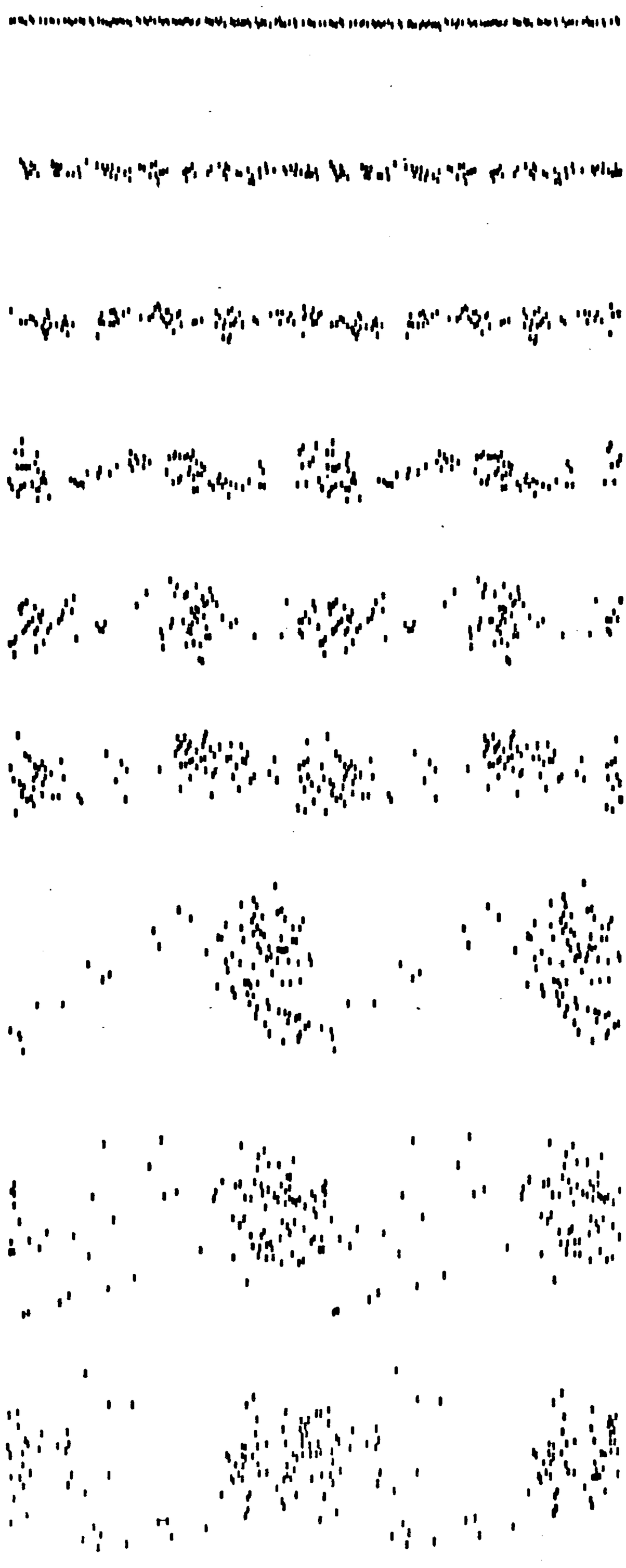

Figure 2.11 The Vortex Sheet at Re = 5000

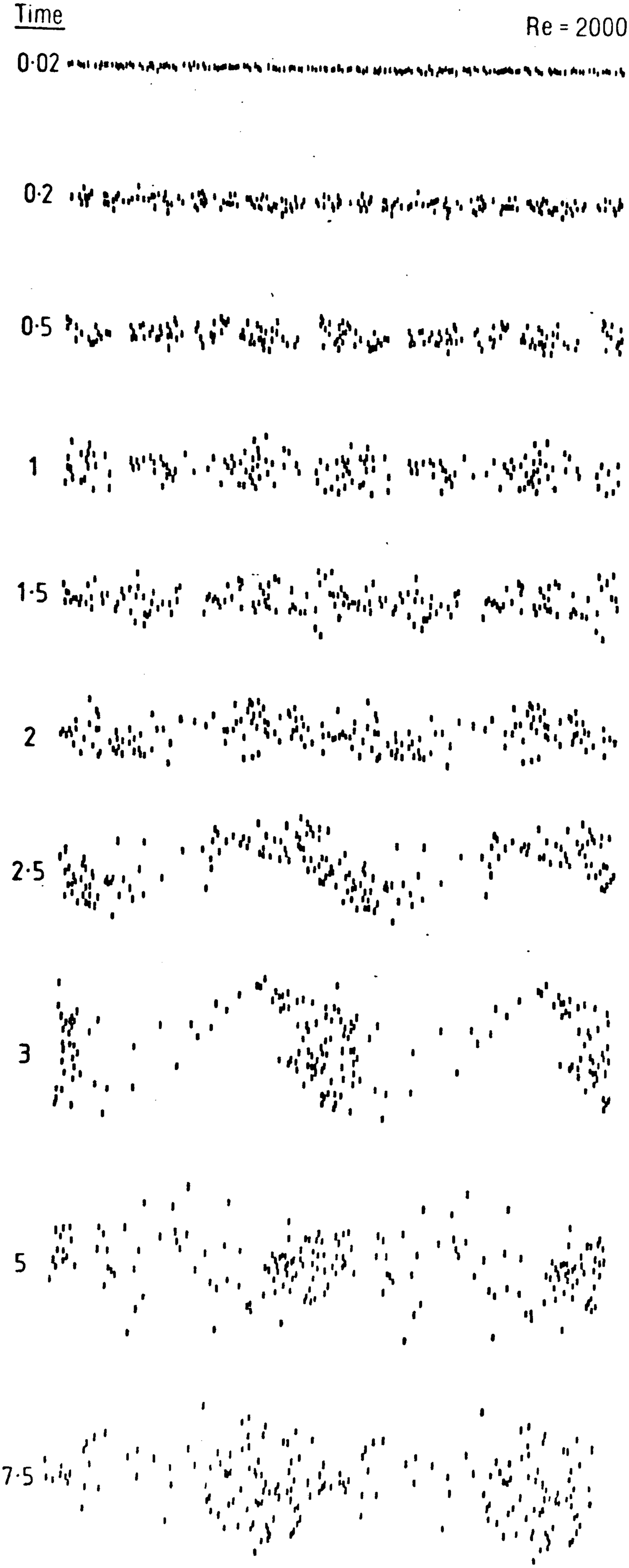

Figure 2.12 The Vortex Sheet at Re = 2000

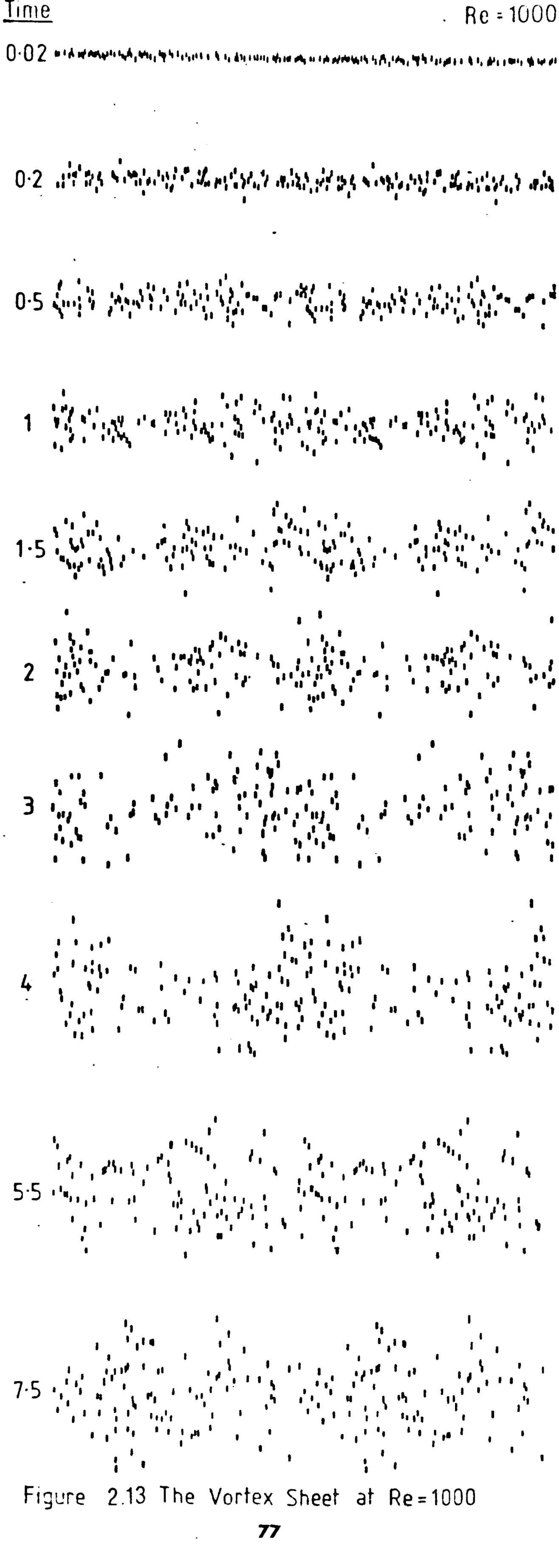

Figure 2.13 The Vortex Sheet at Re=1000

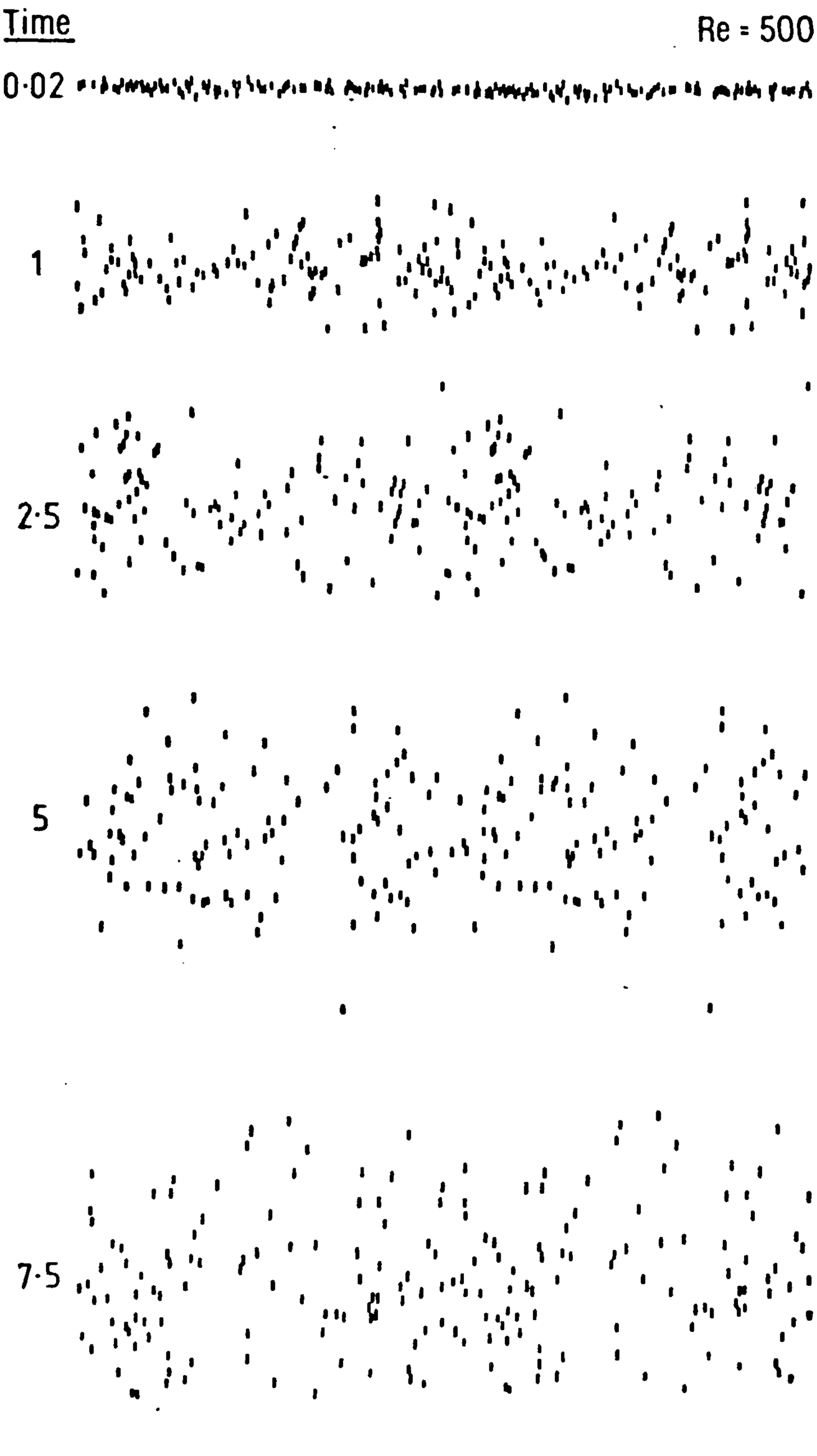

Figure 2.14 The Vortex Sheet at Re = 500

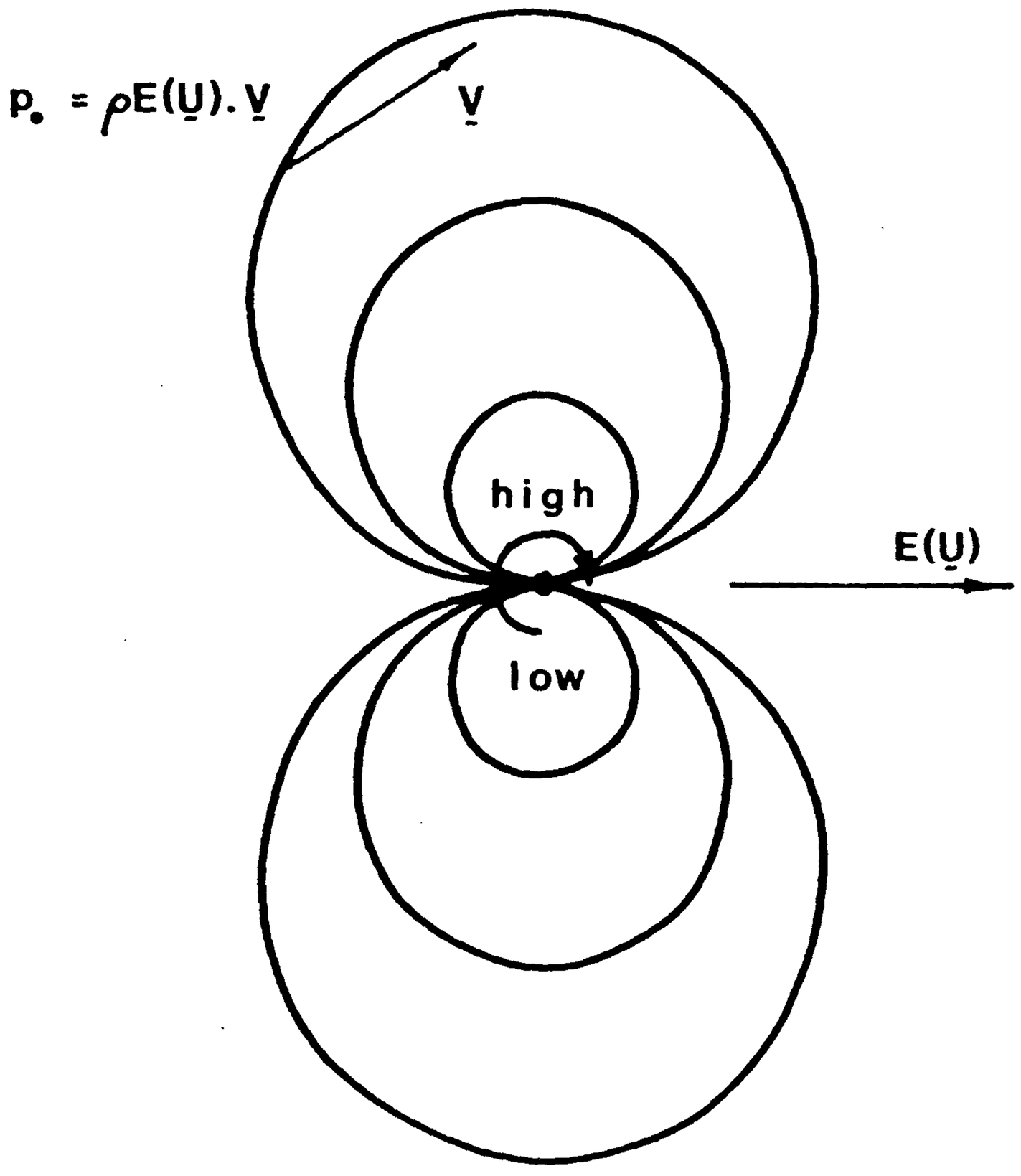

Figure 2.15 The Isobars of Stagnation Pressure Corresponding to a Moving Vortex

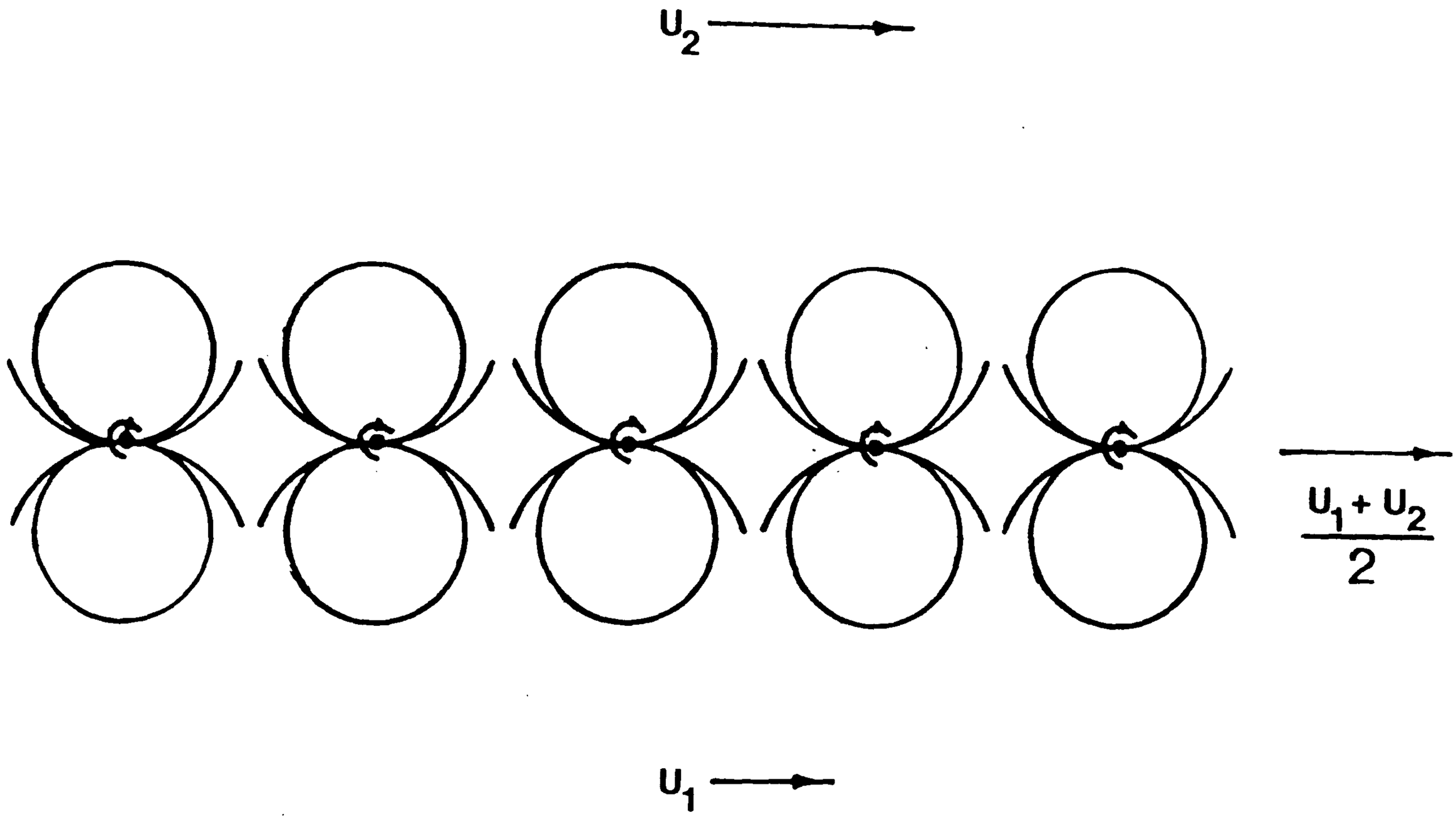

Figure 2.16 An Array of Moving Vortices

CHAPTER 3. THE BOUNDARY LAYER COMPUTER PROGRAM.

The methods developed in Chapter 2 will now be applied to the boundary layer. The purpose of the computer program described here is to give an understanding of boundary layer behaviour, and also to test the random vortex method on known solutions of the Navier-Stokes equations. The computer program is not intended to compete in speed and accuracy with programs using conventional methods, but from it we may gain a 'feel' for flow separation which will aid in interpreting the results of the bluff body computer program described in later chapters. Indeed, the development of the bluff body computer program was closely guided and inspired by the insights provided by the boundary layer program.

This chapter describes the program. Section 3.1 gives an introductory description, and section 3.2 gives a more detailed description (this may be omitted at a first reading). In section 3.3 three laminar similarity profiles are simulated as a test of the program, and in section 3.4 a discussion of boundary layer turbulence with two-dimensional flow is presented. The next chapter will attempt to answer the question of why the flow separates in an adverse pressure gradient.

3.1 INTRODUCTORY DESCRIPTION

Vorticity in the boundary layer is undergoing four processes - creation, diffusion, convection and annihilation, and the computer program must simulate each of these in turn. These processes are, in a very thin boundary layer, independent of the curvature of the surface. Thus, as an acceptable approximation, the surface may be treated as if unwrapped onto a flat plate with a specified external velocity distribution.

Each element of vorticity in the boundary layer may be assumed to be accompanied by a reflected vortex of opposite rotation below the surface. This arrangement automatically satisfies the condition that there is no flow normal to the surface. When a vortex is created, the reflected vortex is created with it, so vorticity is always conserved if it is only created or destroyed in pairs of elements of opposite rotation. Whatever happens to a vortex element also happens to its mirror image.

The vortices are created to satisfy the no-slip boundary condition of zero flow parallel to the surface. They diffuse by a random motion as described in Chapter 2. Their convective velocity is that due to the mainstream flow velocity at that point, to their mirror image, and to every other vortex and reflected vortex in the layer.

Should a vortex be very near to another vortex at any time, it is

convenient to combine them, unless the combined vortex strength would be greater than some upper limit to prevent very strong vortices accumulating. If the two vortices are of opposite rotation when they meet, there will be annihilation of vorticity due to the recombination. Should a vortex move below the surface, it is considered to have met its mirror image on the way through the surface, and to have been annihilated. It is therefore removed from the flow. Note that on the next time step, it may be necessary to replace this vortex with another to satisfy the no-slip condition.

These processes are summarised in figure [3.1]. As the computer program is run for time step after time step, there is a drift of vorticity away from the surface and the establishment of a boundary layer (figure [3.2]). If this boundary layer reaches a steady state, with a balance between diffusion and convection, then it is possible to derive quantities such as the momentum thickness, and to compare these with existing theory for known cases such as the Blasius profile.

3.2 DETAILED DESCRIPTION

A flowchart of the computer program is given in Table 3.1. The computer simulation of each process is here described in detail.

3.2(a) Creation

Vortices are created in pairs of opposite rotation to ensure that the boundary condition of no flow normal to the surface is automatically satisfied. Wherever the vortex moves, by diffusion or convection, the mirror vortex moves with it. If the vortex is recombined or annihilated, the mirror vortex shares the same fate. Thus the no normal flow condition is always satisfied exactly.

By contrast, the boundary condition of no flow parallel to the surface is only satisfied approximately, or on average. The plate, which lies along the X-axis from x=0 to x=1, is divided into one hundred sections. The velocity U_i at the midpoint of each of these sections is calculated as the velocity due to the mainstream flow and to all existing vortex pairs, according to the equation

$$U_i = U_{mainstream} + 2 \sum_{j=1}^{n} K_{i,j} \gamma_j \qquad (3.1)$$

where

$$K_{i,j} = - \frac{y_j}{2\pi \left((x_i - x_j)^2 + (y_i - y_j)^2 \right)} \qquad (3.2)$$

The use of equation (3.2) might allow a vortex pair very near to the

surface to induce an absurdly large velocity there. A correction is applied to the influence coefficient of the point on the surface immediately below the point vortex to prevent this. It is known that for a point distant from the surface the circulation integral along the surface may be related to the angle subtended by the surface with respect to the point (figure [3.3])

$$\sum_{i=1}^{100} K_{i,j} /100 = \tan^{-1}\left[\frac{1 - x_j}{y_j}\right] - \tan^{-1}\left[\frac{x_j}{y_j}\right] \qquad (3.3)$$

The influence coefficient of the vortex pair upon the nearest point on the surface is obtained from equation (3.3) after obtaining all the other influence coefficients from equation (3.2). This ensures that no matter how near the point vortex goes to the surface, it always induces a sensible speed everywhere along the surface.

Having calculated the flow speed along the surface, vorticity is created according to

$$\gamma_i = U_i /100 \qquad (3.4)$$

along with mirror vorticity. Each vortex pair represents the vortex sheet which, laid along the surface at an infinitesimal height above it, would produce a speed sufficient to cancel U_i, and thus to satisfy the no-slip

the moment. The new vortices are placed above the surface at a position

$$(x_i, \sqrt{4 \nu \, dt/3})$$

The reasoning behind the choice of height is based upon an assumption that newly created vorticity must have been created to replace vorticity which was annihilated upon crossing the surface on the previous time step. Local to the surface, the boundary layer may be considered as a region of constant vorticity. Such a region would be depleted by diffusion of vorticity across the surface (figure [3.4]). In time t, the variance of the depleted vorticity is

$$\frac{\int_0^\infty y^2 \, (\Omega - \omega) \, dy}{\int_0^\infty (\Omega - \omega) \, dy}$$

$$\left[\frac{y^3}{3} \, (\Omega - \omega)\right]_0^\infty + \int_0^\infty \frac{y^3}{3} \frac{d\omega}{dy} \, dy$$

$$= \frac{}{\left[y \, (\Omega - \omega)\right]_0^\infty + \int_0^\infty y \, \frac{d\omega}{dy} \, dy}$$

by the formula for integration by parts. The first term in both numerator

and denominator is equal to zero, which leaves the ratio of two integrals containing the term

$$\frac{d\omega}{dy} = \frac{\Omega}{\sqrt{4\pi\nu t}} \exp\left[-\frac{y^2}{4\nu t}\right]$$

where it may be noted that there is a solution for $d\omega/dx$, but no solution for ω. With the cancellation of similar terms in numerator and denominator, the lost variance becomes equal to

$$= \frac{\int_0^\infty \frac{y^3}{3} \exp\left[-\frac{y^2}{4\nu t}\right] dy}{\int_0^\infty y \exp\left[-\frac{y^2}{4\nu t}\right] dy}$$

$$= \frac{\left[-\frac{2\nu t}{3} y \exp\left[-\frac{y^2}{4\nu t}\right]\right]_0^\infty + \int_0^\infty \frac{4\nu t}{3} y \exp\left[-\frac{y^2}{4\nu t}\right] dy}{\int_0^\infty y \exp\left[-\frac{y^2}{4\nu t}\right] dy}$$

$$= 4\nu t/3$$

To replace this depleted vorticity, the conservation of variance of

vorticity above the surface is appropriate, since this region of vorticity should be in equilibrium, with no net diffusion, which means the same thing as no net change in variance. This is a heuristic argument.

This newly created vorticity may then be taken away by convection and diffusion, so that on the next time step, the no-slip condition is no longer satisfied exactly, and another hundred vortices must be created. These new vortices can usually be expected to have small magnitude, and they are likely to be combined with other vortices in the flow.

When there is insufficient vorticity above some part of the surface, extra vorticity is created and diffuses outwards to remedy the deficiency. If there is excessive vorticity in the layer, though some of the excess vorticity will be removed by diffusion back to the surface, there will be a tendency for oppositely rotating vorticity to be created and to diffuse outwards. It will combine with the vorticity in the flow to reduce its strength. Thus the computer program is self-governing, and on average the no-slip condition will be observed.

3.2(b) Diffusion

Diffusion is produced by a series of random displacements of every vortex, as described in Chapter 2 (equation (2.21)). A vortex is equally

likely to go in any direction, so it is the Navier-Stokes equation, rather than Prandtl's equation, which is being solved. If a vortex diffuses across the surface, it is removed from the flow. This introduces a directional bias to an otherwise isotropic process, which ensures that vorticity tends on average to diffuse away from the surface. The mirror-vortex moves in response to its partner.

Various devices have been tried to reduce the error of the 'random vortex' method by controlling the diffusion of the vortices to attempt to make it more regular. For example, the displacements given to a cloud of vortices could be adjusted to preserve the invariance of the centre of vorticity of the cloud, and to force the correct increase in variance. Such devices are known to statisticians and practitioners of the Monte Carlo method as 'variance reduction'. They were unsuccessful, and so the computer program presented here remains unaltered. This is just as well, since if one is to use a random method honestly, one should be wary of attempting to pre-determine the outcome.

3.2(c) Convection

The velocity of any one vortex is computed as a two-dimensional vector, so again it is the full Navier-Stokes equation which is being solved,

rather than Prandtl's approximate equation. The velocity of the vortex is the sum of the mainstream flow velocity at the point, the velocity induced by its mirror vortex, and the velocity induced by every other vortex pair. It was shown in Chapter 2 that it is difficult to resolve a row of point vortices from some distance away by a measurement of local velocity variation. When each vortex is accompanied by a mirror image the resolving power is even less, since the flow induced at a distance is effectively that due to rows of vortex doublets, where induced speed falls off with the square of distance. Each part of the boundary layer is affected by its neighbouring parts upstream and downstream, but there is little direct effect any further upstream or downstream. The boundary layer or wake far downstream of the surface can be crudely represented by just a few vortices without much effect on the part of the layer in which we are interested.

As described in Chapter 2, the vortices have been given a core of radius 1/200, and the improved Euler method of time marching has been used.

3.2(d) Annihilation

Vortices can be removed by two mechanisms. They may drift below the surface, or they may encounter vorticity of opposite rotation. Vortices which drift below the surface are just removed and forgotten. This may

leave a deficiency of vorticity in the flow. The vortex creation technique described above will put the appropriate amount of vorticity back in the flow, at a distance above the surface of

$$\sqrt{4\,\nu\,dt/3}$$

which represents an estimate, based on variance, of where the annihilated vortex came from before it crossed the surface. In a decelerating boundary layer, vortices should be moving back to the surface to be destroyed. It is when this process breaks down, as we shall see, that flow separation occurs.

A practical upper limit to the number of vortices is 500, and computing time is proportional to the square of the number of vortices. With 100 vortices being added at every time step, the computer program would not run for long unless vortices in the flow are recombined. A search is made for pairs of nearby vortices. When such a pair is found, some logic is performed, which is summarised in Table 3.2. If the two vortices are of opposite sign, they are always recombined, and placed at a position (x,y) recommended by Deffenbaugh and Marshall[29] as

$$x = \frac{x_1 |\gamma_1| + x_2 |\gamma_2|}{|\gamma_1| + |\gamma_2|}$$

$$y = \frac{y_1 |\gamma_1| + y_2 |\gamma_2|}{|\gamma_1| + |\gamma_2|} \qquad (3.5)$$

This is not the centre of vorticity when the two vortices are of opposite rotation, but it still represents the best place to put the new vortex. It is justified heuristically that when clouds of vortices diffuse into each other, equation (3.5) is true on average.

This recombination algorithm resembles negative viscosity. There is no negative viscosity apparent in the computer simulations to be presented, and the very idea may be dismissed as absurd, since it implies that, by analogy, one could take a blurred photograph and unblur it by some form of image processing despite the absolute loss of information in the process of blurring. This is a good example of the Entropy Principle: a copy of an out-of-focus photograph cannot be any less out-of-focus, and attempts to remedy this by any method whatsoever will fail. It would nevertheless be preferrable to avoid explicit arguments against negative viscosity altogether, since a virtue of the 'random vortex' theory is its implicit

inclusion of the Entropy Principle. If a vortex-in-cell method is ever adopted, it would be worth thinking carefully about this point.

By this recombination, vorticity can also be annihilated. In the decelerating boundary layer, both types of annihilation are likely to be working at the same time.

3.3 THE LAMINAR BOUNDARY LAYER

An obvious first test of the computer program is to attempt to reconstruct the Blasius profile. This has been done by Chorin[12] previously, and is repeated here both for the sake of confirmation, and to derive the shear stress distribution. Another good test is the 'stagnation point' flow at the front of a body, given by $U=kx$, where the boundary layer thickness is known to be constant. One other similarity profile to be attempt is the 'critical deceleration' profile where the flow is just about to separate. Many other similarity profiles could be attempted, but these three are the three definitive cases.

3.3(a) The Blasius Profile

The program is executed with constant external velocity. It is necessary to wait for some time before a steady state is reached to the approximation

permitted by the method. Now we have a distribution of point vortices (figure [3.5]) from which a velocity profile must be obtained. It will be assumed for the moment that the boundary layer thickness grows in proportion to the square root of distance down the plate, this being the standard result for the Blasius profile. If a vortex has co-ordinates (x,y), then its position may be normalised to

$$\left[\frac{1,\ y}{\sqrt{x}} \right]$$

for sampling (figure [3.6]). Sampling was restricted to the region from x=0.4 to x=0.8. This is to exclude the initial region x<0.4, where there are too few vortices in the boundary layer, and a great amount of 'noise' could be expected. The region near the end, x>0.8, is also excluded since it is influenced by the wake, where the boundary layer is not the same.

Given a number of vortices in one vertical line, it is known that the flow velocity increases from zero to one (in some appropriate system of absolute units) and so the total strength of all the vorticity must be equal to one. The strength of each vortex is scaled to ensure this. Thus both position and vortex stength are normalised. The velocity distribution is given by

$$u(y) = \int_0^y \gamma(\eta)\ d\eta \qquad (3.6)$$

The actual method of obtaining velocity distribution is shown in figure [3.6]. Between any two successive vortices a midpoint is selected, so between any two successive midpoints there is just one vortex, which need not be halfway between the midpoints. The velocity increment from one midpoint to the next is equal to the normalised strength of this vortex, so that a velocity profile can be derived. In figure [3.7], for ten successive time steps selected at random, the velocity profiles are shown. They do indeed correspond to the Blasius profile within the expected error of the method.

From the velocity profile it is possible to obtain values for displacement thickness coefficient

$$d = \int_0^\infty \left[1 - \frac{u}{U}\right] dy \Big/ \sqrt{Re} \qquad (3.7)$$

momentum thickness coefficient

$$\theta = \int_0^\infty \frac{u}{U}\left[1 - \frac{u}{U}\right] dy \Big/ \sqrt{Re} \qquad (3.8)$$

and energy thickness coefficient

$$\epsilon = \int_0^\infty \frac{u}{U}\left[1 - \frac{u^2}{U^2}\right] dy \Big/ \sqrt{Re} \qquad (3.9)$$

for comparison with the known results for the Blasius profile. Figure [3.8] shows the dependency upon time of these quantities as calculated from x=0.4 to x=0.8. There is an initial growth period which lasts up to three units of time (the unit of time is the transit time of the mainstream flow along the plate). Due to the random vortex method, there is considerable fluctuation in the result, but the average values of $d = 1.87 \pm 0.29$, $\theta = 0.69 \pm 0.09$ and $\epsilon = 1.02 \pm 0.21$ agree with known results ($d = 1.72$, $\theta = 0.664$, $\epsilon = 1.046$) within the accuracy that can be expected from this method.

The distribution of shear stress along the plate can also be calculated. The shear stress is given by

$$T_w = \nu \frac{du}{dy} = \nu \omega \qquad (3.10)$$

At the surface, the shear stress is exactly equal to viscosity multiplied by the vorticity just outside the surface. The problem becomes one of determining the density of the vortices near the surface. One way is just to count how many vortices lie within a certain distance of the plate. This distance would need to be significantly less than the boundary layer thickness, and it is not obvious how to ensure this near the leading edge. An alternative method is to integrate equation (3.10), incidently removing

the initial singularity in T_w, to give

$$\int T_w \, dx = \gamma \int \omega \, dx \qquad (3.11)$$

For the Blasius profile, this integral happens to be equal to the momentum thickness, since by the momentum integral equation (Schlichting[30])

$$\frac{d\theta}{dx} = \frac{T_w}{\rho U^2} - (H + 2) \frac{\theta}{U} \frac{dU}{dx} \qquad (3.12)$$

where, in absolute units

$$\rho U^2 = 1$$

and

$$\frac{dU}{dx} = 0$$

so it can at the same time be shown how the momentum thickness grows along the plate. The vortex density can now be sampled by watching the quantity of vorticity which crosses the plate in one time step (as in figure [3.4]). This is equal to

$$= \int_0^\infty (\Omega - \omega) \, dy$$

$$= \int_0^\infty y \frac{d\omega}{dy} \, dy$$

$$= \int_0^{\infty} \frac{y\,\Omega}{\sqrt{4\pi\nu\,dt}} \exp\left[-\frac{y^2}{4\,\nu\,dt}\right] dy$$

$$= \Omega\sqrt{\nu\,dt/\pi}$$

We observe the quantity of vorticity which actually crosses the surface, from which

$$T_w = \Omega_{\text{actual}} \sqrt{\frac{\pi\nu}{dt}} \qquad (3.13)$$

Since the boundary layer should be in equilibrium, the same amount of vorticity should be created on the surface to be put back into the flow, except at the singularity at the leading edge. There are thus two currents of vorticity in opposite directions, and a mean current is obtained as the average of these. This is then integrated along the X-axis in a manner analogous to the derivation of the Blasius profile to give the shear stress distribution. Note that equation (3.13) represents a new type of differentiation in the limit as

$$dt \longrightarrow 0 \qquad \text{and} \qquad \Omega_{\text{actual}} \longrightarrow 0$$

The distributions are shown in figure [3.9]. There is considerable fluctuation in these distributions, which is to be expected since fewer vortices are being sampled than in the derivation of the velocity profile.

Twenty successive distributions have been shown, with the theoretical distribution for comparison. In figure [3.10] these twenty distributions have been averaged. The average distribution is in fair agreement with theory, and justifies the assumption made in deriving the velocity profile that the boundary layer grows parabolically.

3.3(b) The Stagnation Point Profile

A stagnation point flow is given by the external velocity distribution

$$U=kx$$

(so of course $U>0$ when $x>0$, and $U<0$ when $x<0$)

This type of flow is present in the local region around the forward stagnation point of any body in a flow. Viscous diffusion tends to thicken up a boundary layer, while acceleration of the flow tends to make it thinner. For $U=kx$ thes two tendencies balance each other, so that the boundary layer is of constant thickness. There is a known solution for this flow which is the solution to the full Navier-Stokes equation.

In the computer simulation a plate was lain along the x-axis from $x=-0.5$ to $x=0.5$. The program was run from the initial condition (figure [3.11]) until the steady state was reached (figure [3.12]). The position of each vortex need not be normalised for sampling, since the boundary layer

thickness appears to be constant. The strength of each vortex is normalised as y/x, and then normalised again to give unit external flow. The velocity profile and boundary layer thickness are derived as for the Blasius profile. The velocity profiles are shown in figure [3.13]. The agreement with theory is not so good as in the case of the Blasius profile. The various boundary layer thicknesses are overpredicted by about 40% (the computer program has been carefully checked, but no error, such as a factor of the square root of two, has been detected). The shear stress distributions are shown in figure [3.14], for which the agreement with theory is better. It is strange that the boundary layer is significantly too thick, but the shear stress is not too low.

3.3(c) The Critically Decelerating Boundary Layer

The external velocity distribution in this case is given by

$$U = k\,x^{-0.0904}$$

The singularity at the leading edge is not a problem since with the plate divided into one hundred elements, the first value of x at the midpoint of the first element is 1/200, and U takes an acceptable value. The boundary layer growth is shown in figure [3.15], and the steady state in figure

[3.16]. Velocity profiles are shown in figure [3.17]. These profiles are expected to be re-entrant. In fact, they are indistinguishable from the Blasius profile. The shear stress distributions (figure [3.18]) have an initial singularity which could not be predicted theoretically. Thereafter, they should be flat, since T_w=0 with 'critical deceleration'. There is in fact a progressive increase in most cases.

On the whole, the results obtained for critical deceleration look the same as the Blasius profile. The computer program has been good at simulating the Blasius profile, only moderate at simulating the stagnation point profile, and poor at simulating the critical deceleration profile. This is in increasing order of sensitivity to the interaction between diffusion and convection, so the implication is that the latter boundary layers are not being simulated in enough detail. It is still instructive to attempt these different cases to assess the limitations of the method, which can be overcome by using more vortices and a shorter time step. This is beyond the capacity of the existing generation of computers. The vortex-in-cell method of Christiansen[11] could also be used. The ability of Christiansen's method to use some 10,000 vortices would reduce the error due to their random motion to about 1%, so this is a direction for future work. The present method can still be used in the next chapter to look at

the mechanism of flow separation, since it is only the trend which is sought, and not accurate numerical results.

3.4 THE TURBULENT BOUNDARY LAYER

Since the random vortex method is a simulation of the Navier-Stokes equation, it should be able to represent turbulence. Real turbulence is three-dimensional, while the method given here is two-dimensional, but it is still worth running the computer program to see how turbulence could develop. At high Reynolds numbers, the turbulent boundary layer has a detailed fine structure and not enough point vortices could be used for a practical simulation on existing computers. Nevertheless, the coarse structure of turbulence, or the lower end of its frequency spectrum, can still be shown.

A constant velocity turbulent boundary layer is shown in figure [3.19]. Over the first 40% of the plate, the kinematic viscosity ν has the value 0.002, and after this it has the value 0.00002. This is a contrived way of obtaining turbulence, but for the random vortex model, the initial laminar boundary layer is extremely long and impossible to simulate all the way to the instability.

In Chapter 2, turbulence was attributed to the Kelvin-Helmholtz

instability represented by the 'snapping' of a vortex sheet. The boundary layer may be viewed as a stack of vortex sheets which are all liable to snap anywhere (figure [3.20]). Due to molecular motion of the fluid or to surface roughness, snaps are initiated at random. Vorticity collects into clusters, which are themselves vulnerable to further random snaps, so that sometimes these clusters break up again, and sometimes they amalgamate into clusters as large as the boundary layer itself.

Vorticity can be seen in clusters in simulations of the laminar boundary layer as well (figure [3.5]). Anything with a random component will appear to be clustered at some time, but in the case of the laminar layer, these clusters will be dispersed by viscosity within a few time steps. In the turbulent layer, the clusters persist over many time steps. This can be seen in figure [3.19].

This brief look at a turbulent boundary layer concludes our interest in the subject of boundary layers as such. With the aim of simulating the flow around bluff bodies, it is necessary to do a close examination of the boundary layer to deduce a mechanism for flow separation, so it is inevitable that a boundary layer computer program must be written and tested. Now we can return to our real interest - flow separation.

TABLE 3.1 THE BOUNDARY LAYER COMPUTER PROGRAM

(1) Evaluate the flow velocity $(U_i, 0)$ at the aerofoil surface at 100 equally spaced points.

(2) Create 100 new vortices with strengths

$$\gamma_i = U_i / 100$$

Place them at a height

$$\sqrt{\frac{4 \nu \, dt}{3}}$$

above the surface.

(3) Give every vortex a random displacement to represent diffusion.

(4) Compute the convection of each vortex by the Improved Euler Method.

(5) Combine nearby vortices by rules given in Table 3.2.

(6) Remove any vortices below the surface.

(7) Sample the vorticity distribution as desired.

(8) Go back to step (1) for another time-step.

TABLE 3.2 THE VORTEX COMBINATION RULES

Measure the distance from every vortex to every other vortex. Upon finding two vortices nearer together than some limit:

(1) Let the vortices be denoted by 1 and 2.

Put

$$\Gamma = \Gamma_1 + \Gamma_2$$

If Γ is less than a specified limit

then (a) Replace the two vortices by a single vortex of strength and position

$$x\ |\Gamma_1| + x\ |\Gamma_2|,\ y\ |\Gamma_1| + y\ |\Gamma_2|$$

$$\frac{}{|\Gamma_1| + |\Gamma_2|}$$

otherwise (b) Replace the two old vortices by two new vortices of strength $\Gamma/2$. Place these vortices so that the mean and variance of the vortex distribution are conserved.

(2) Tag any new vortices just created so that they cannot be combined again on the same time step.

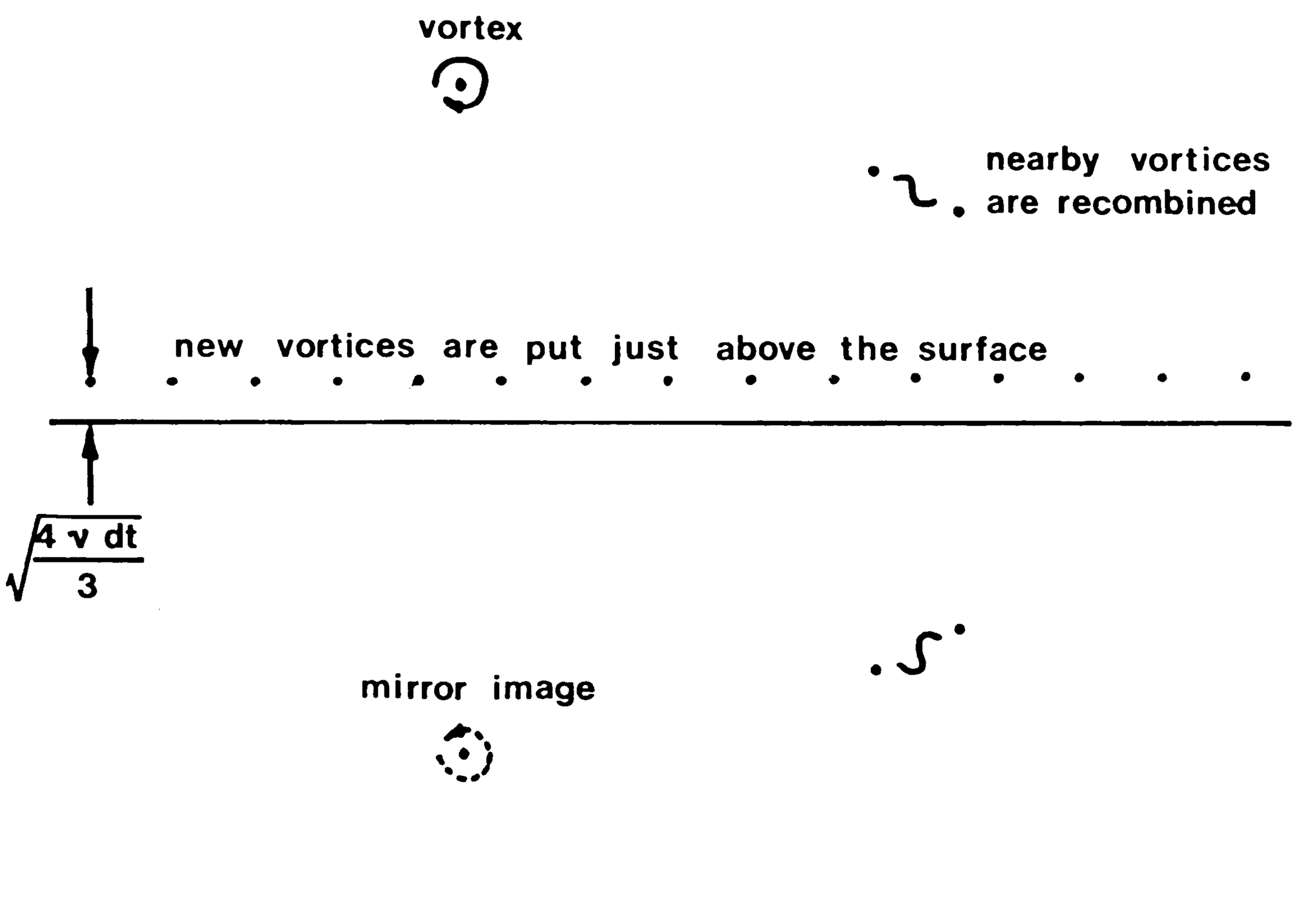

Figure 3.1 The Boundary Layer Computer Program

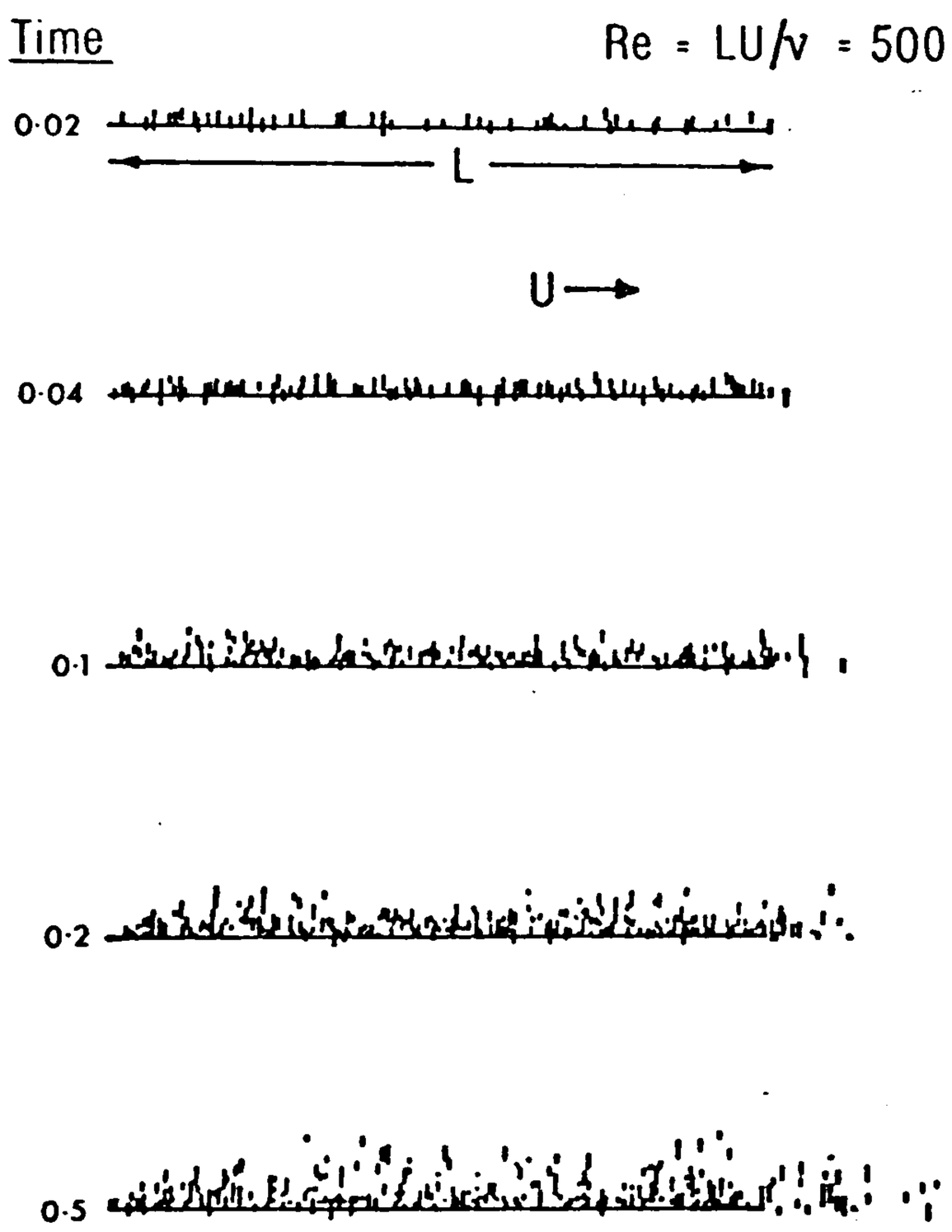

Figure 3.2 Initial Development of the Boundary Layer

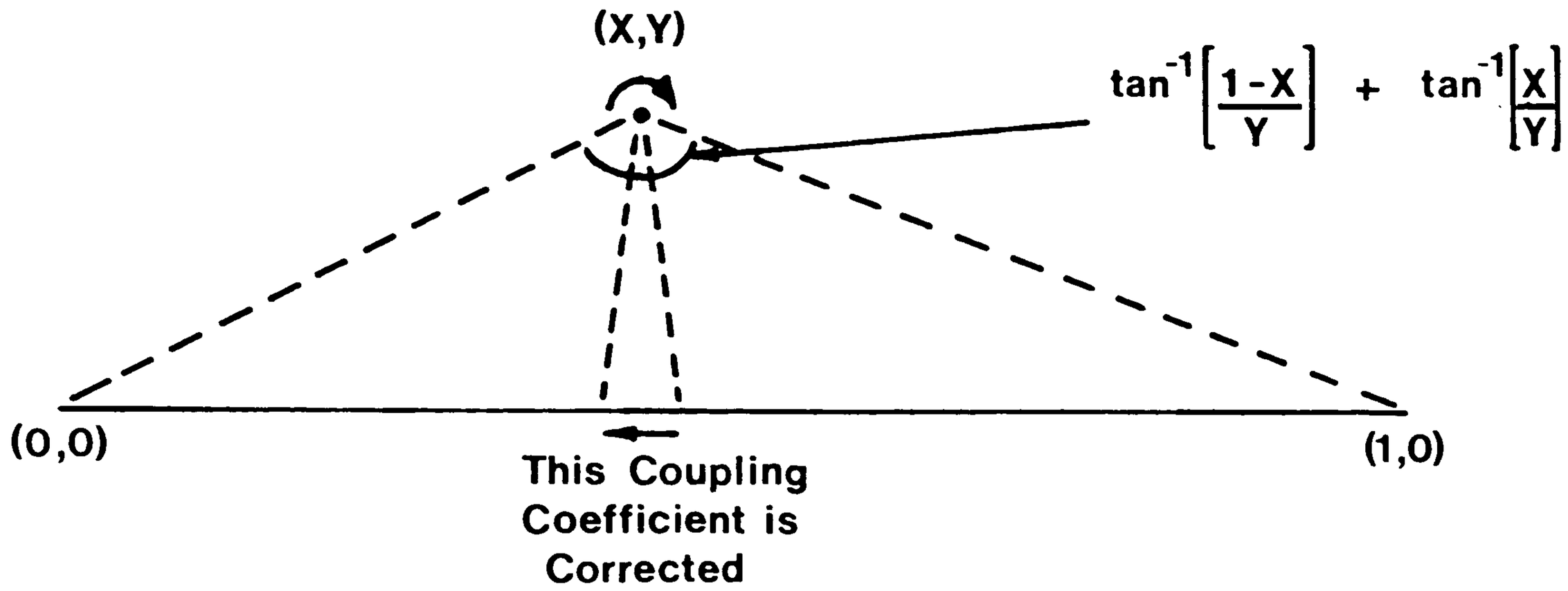

Figure 3.3 The Correction of the Influence of a Vortex upon the Nearest Point on the Surface

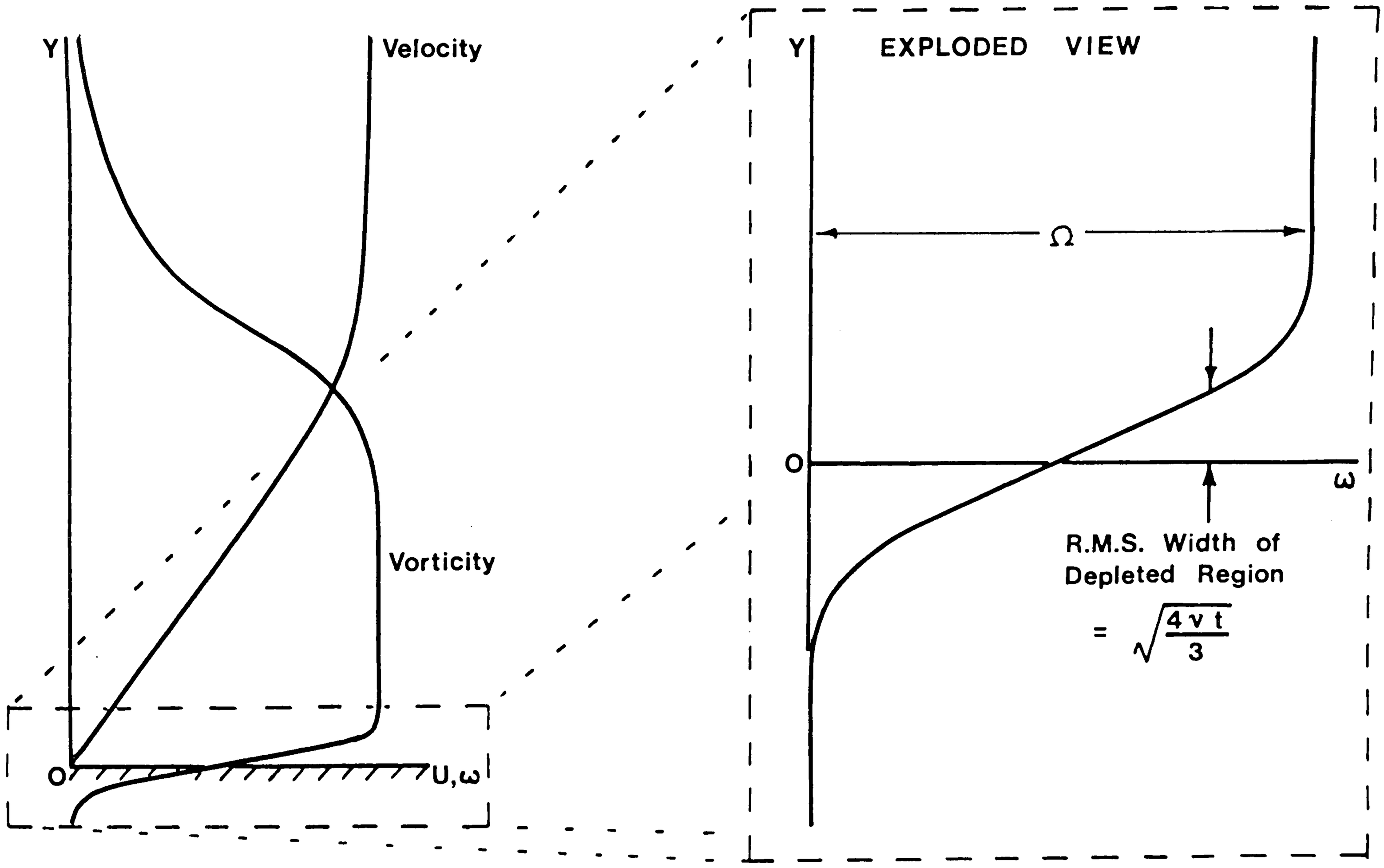

Figure 3.4 The Depletion of Vorticity in Time, t, by Diffusion back through the Surface

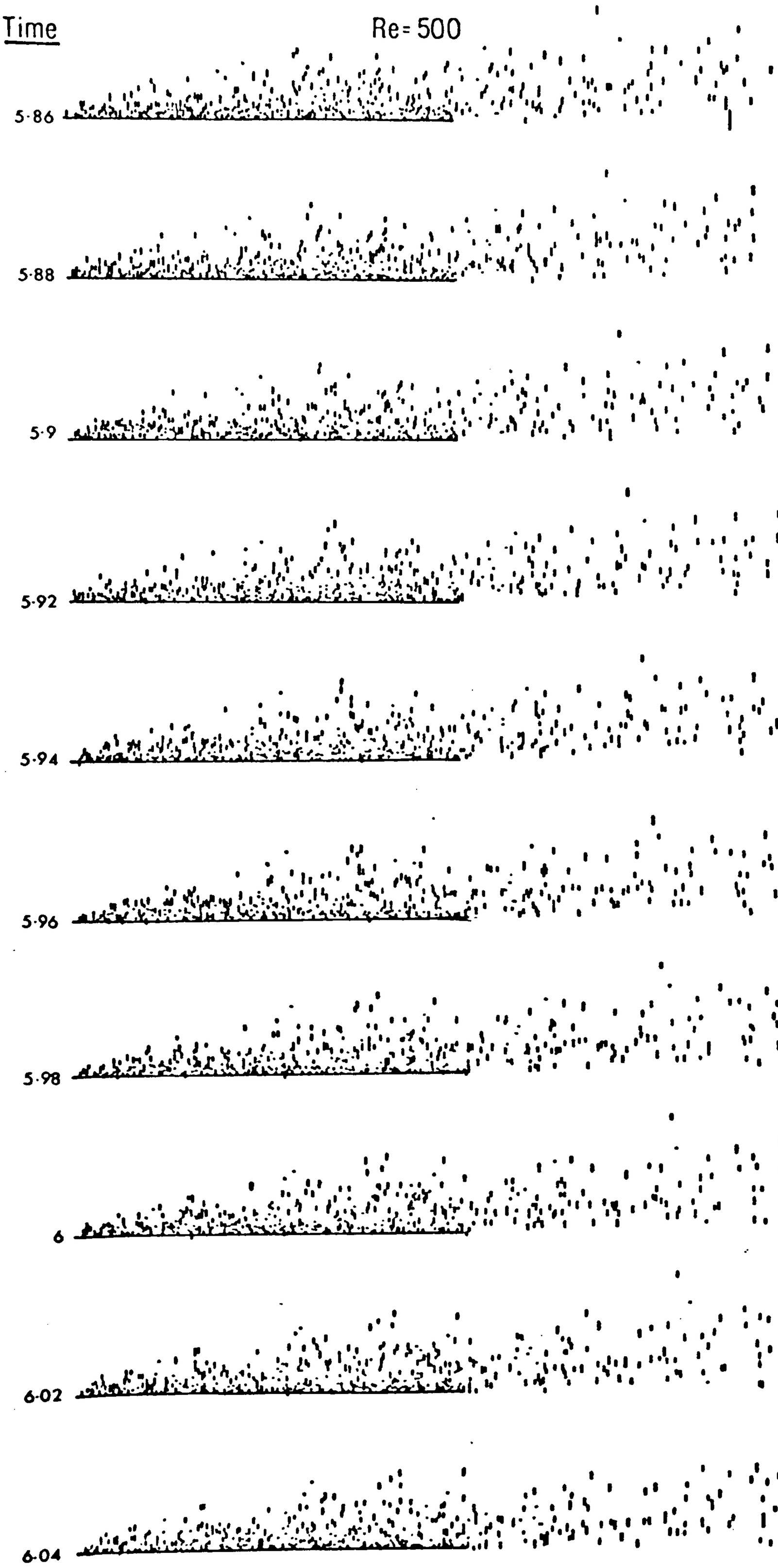

Figure 3.5 The Laminar Boundary Layer with Constant Mainstream Flow

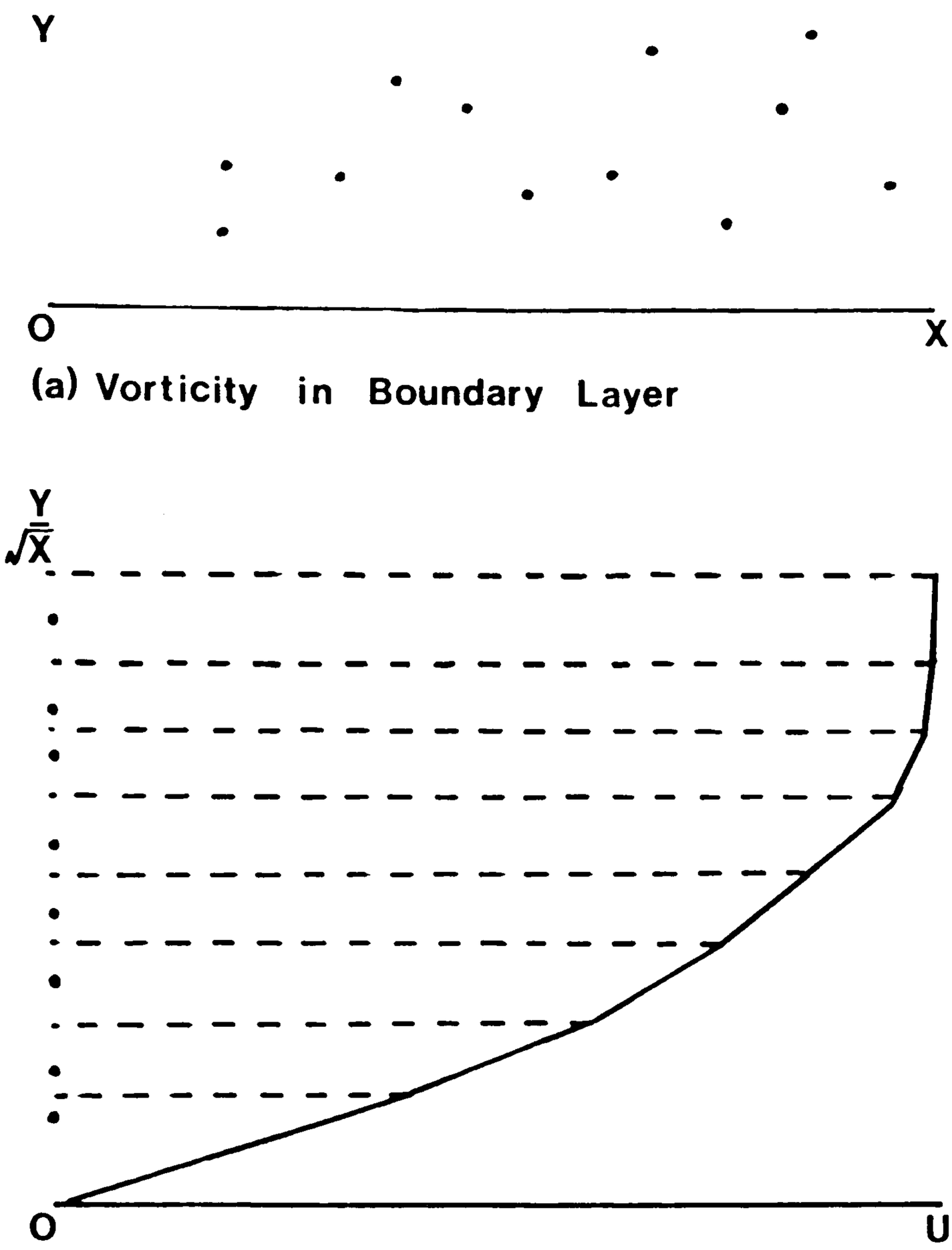

(a) Vorticity in Boundary Layer

(b) Normalised Positions of Vortices Integrated to give the Velocity Profile

Figure 3.6 The Derivation of the Velocity

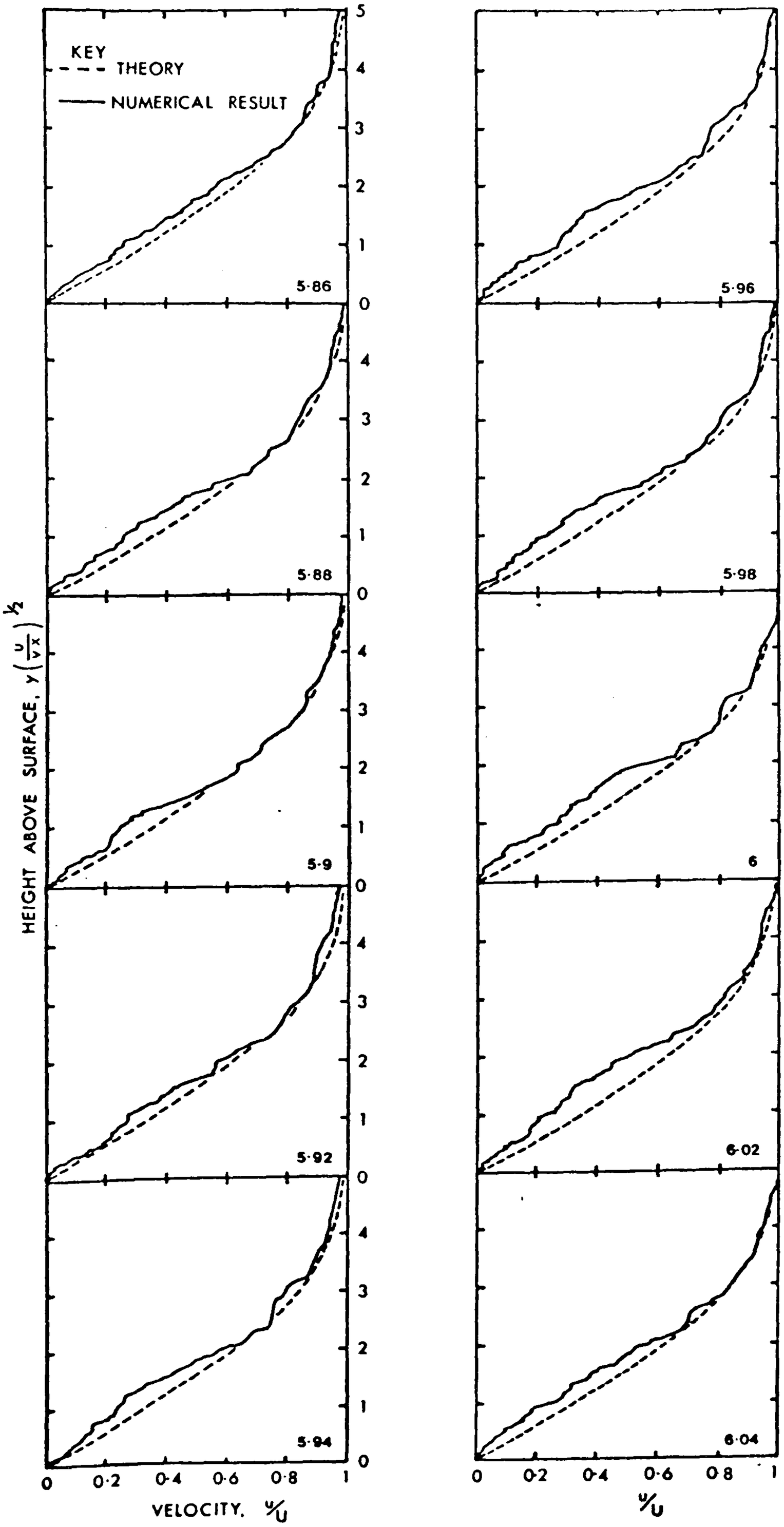

Figure 3.7 The Blasius Profile

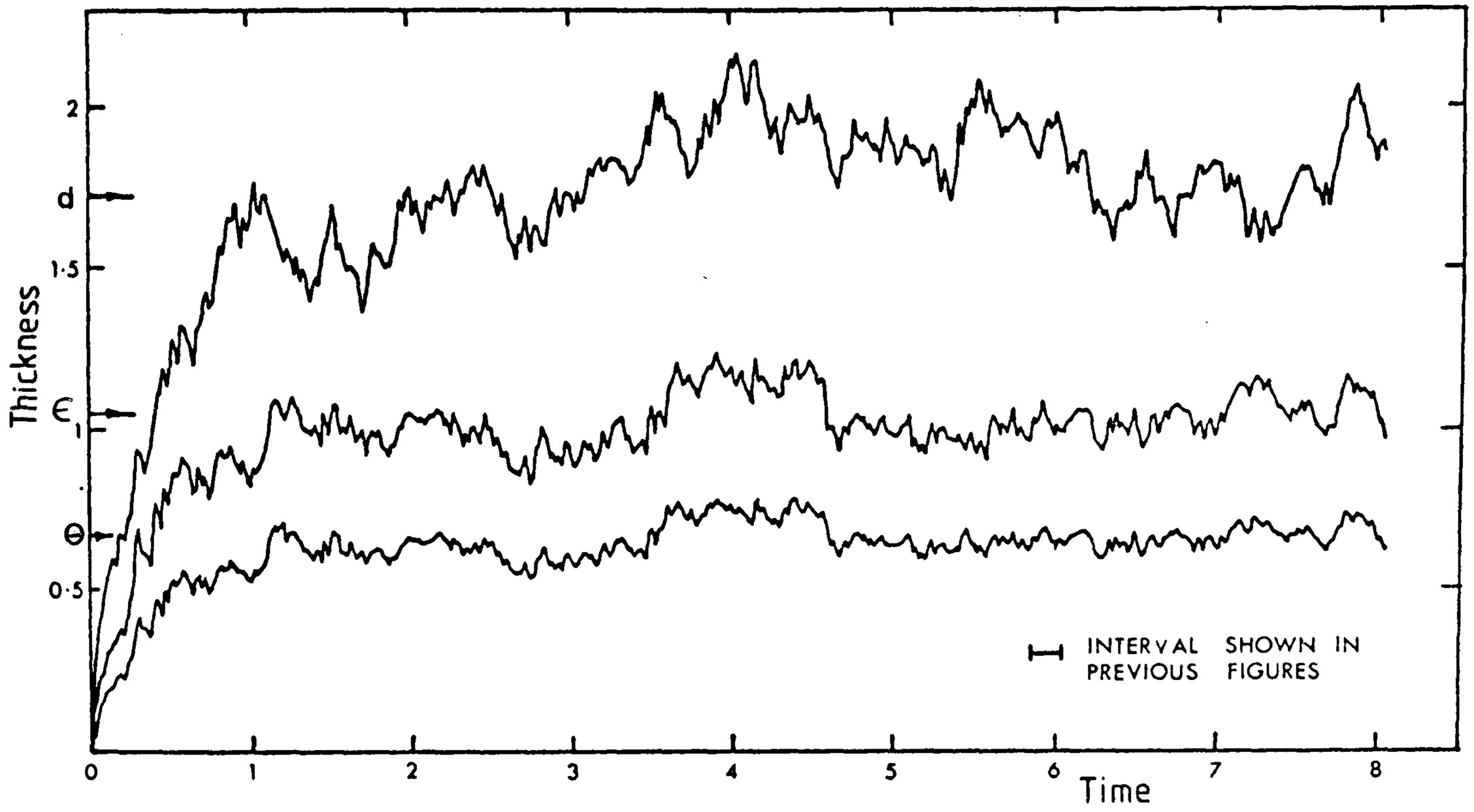

Figure 3.8 The Variation of the Thickness Parameters with Time

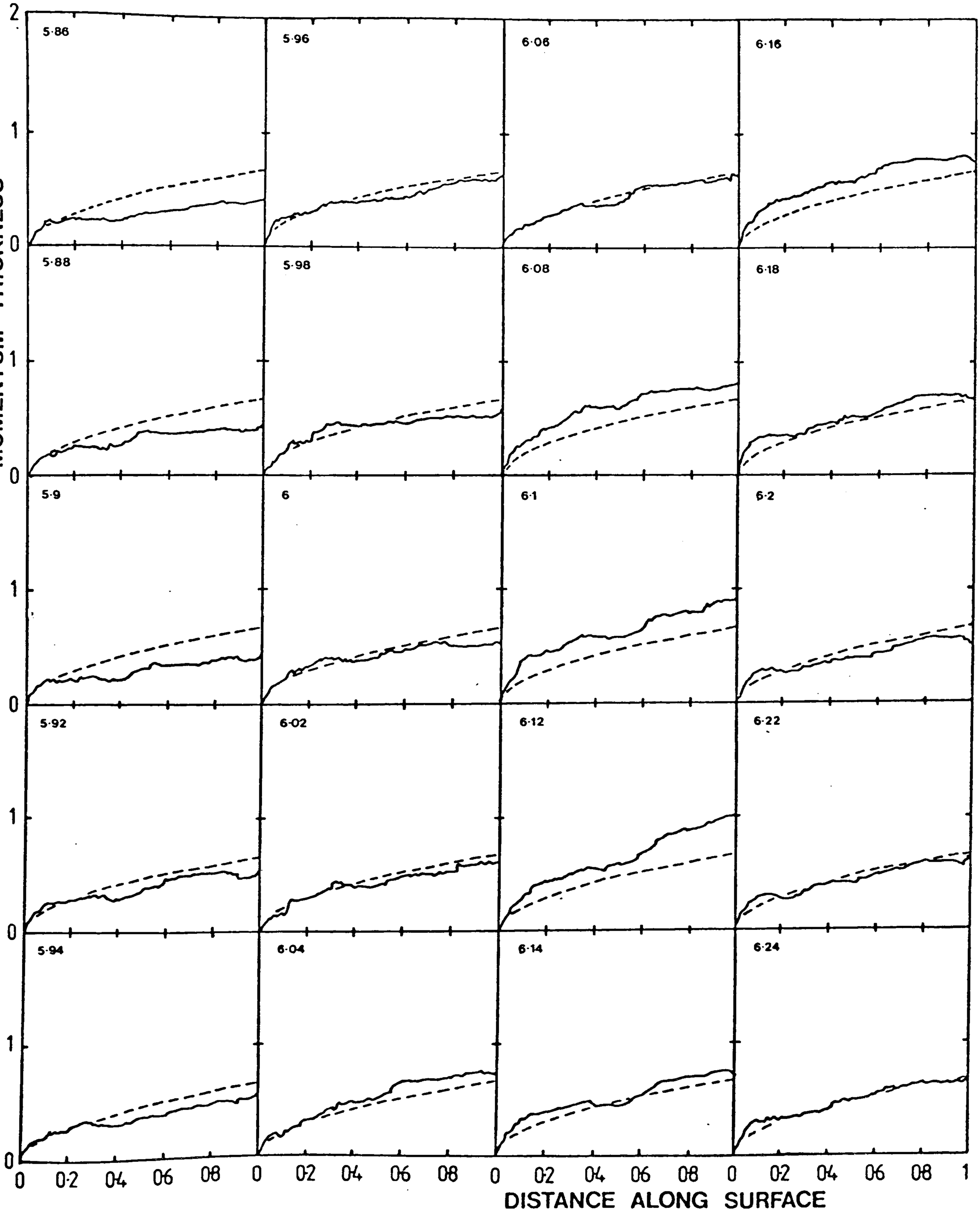

Figure 3.9 The Growth of the Boundary Layer

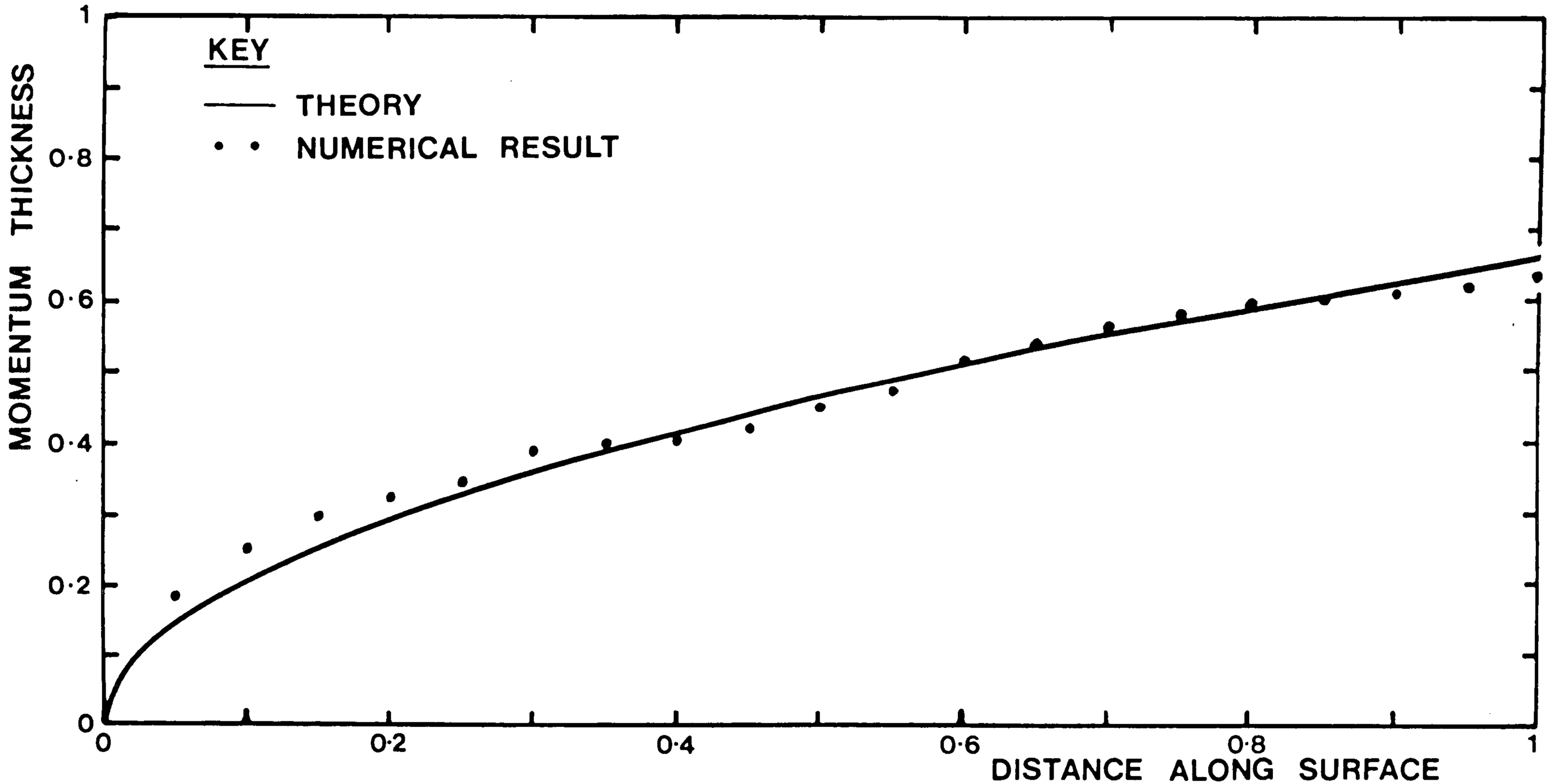

Figure 3.10 The Growth of the Boundary Layer

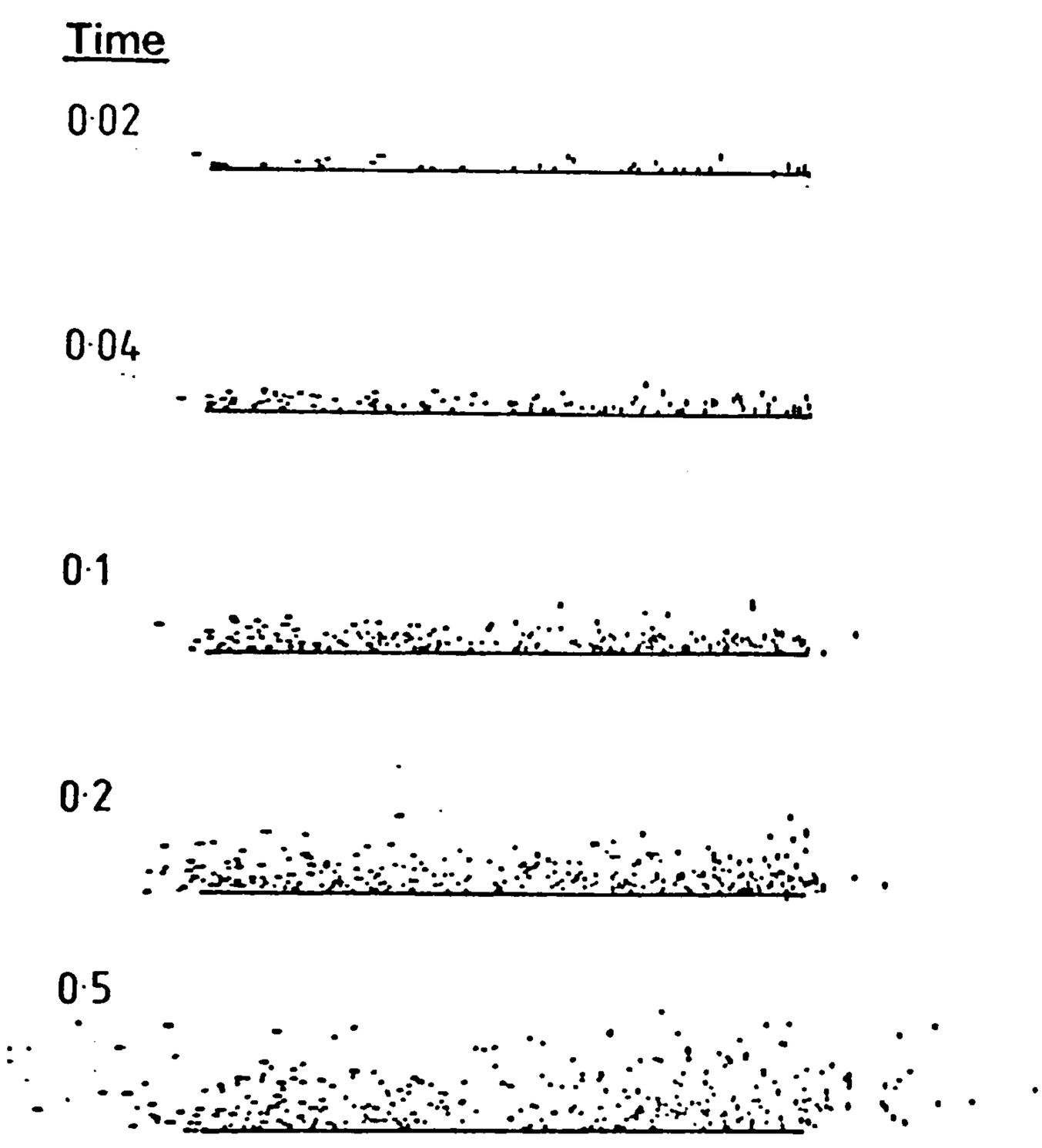

Figure 3.11 Initial Development of the Stagnation Point Boundary Layer

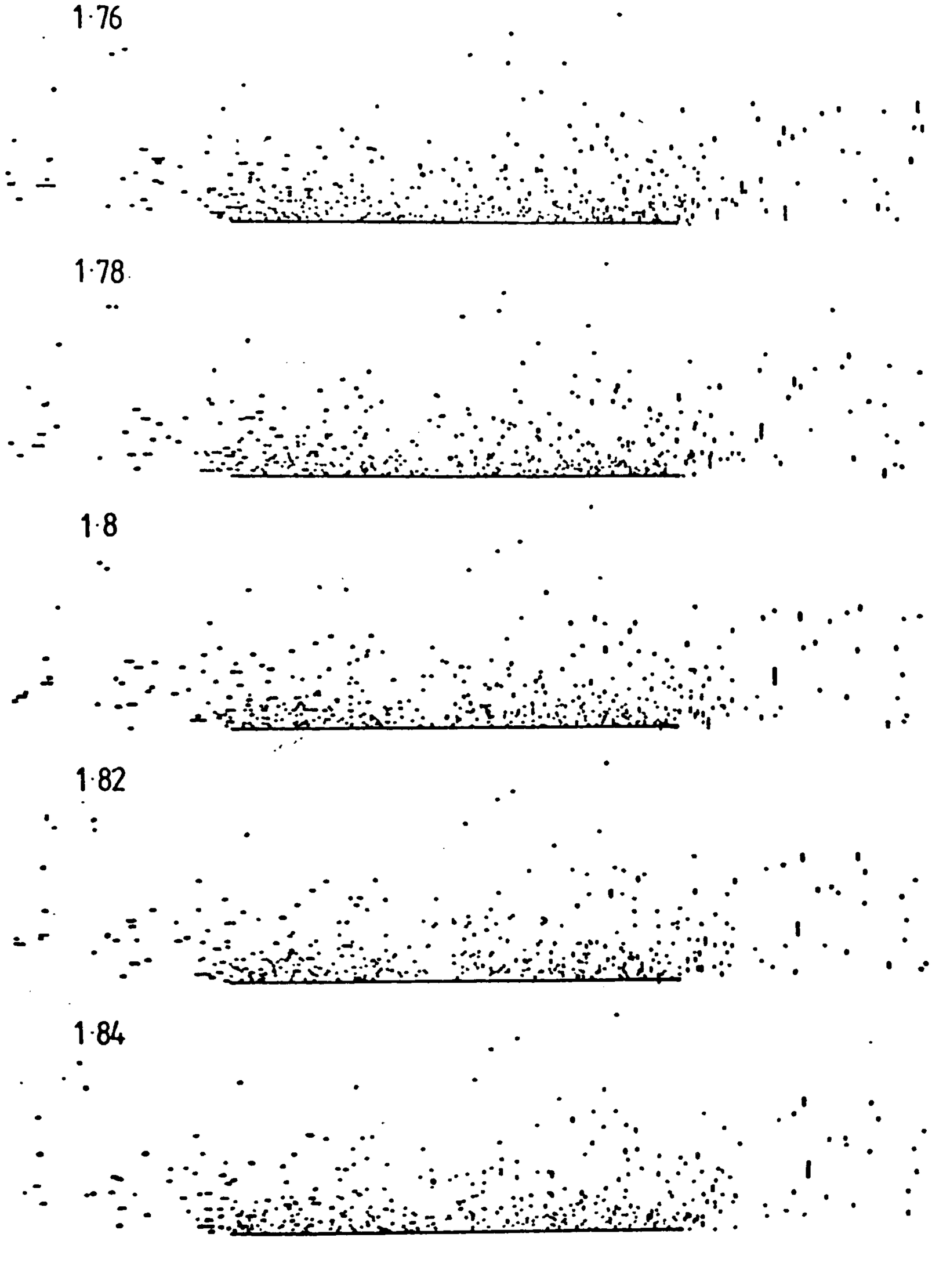

Figure 3.12 The Stagnation Point Boundary Layer

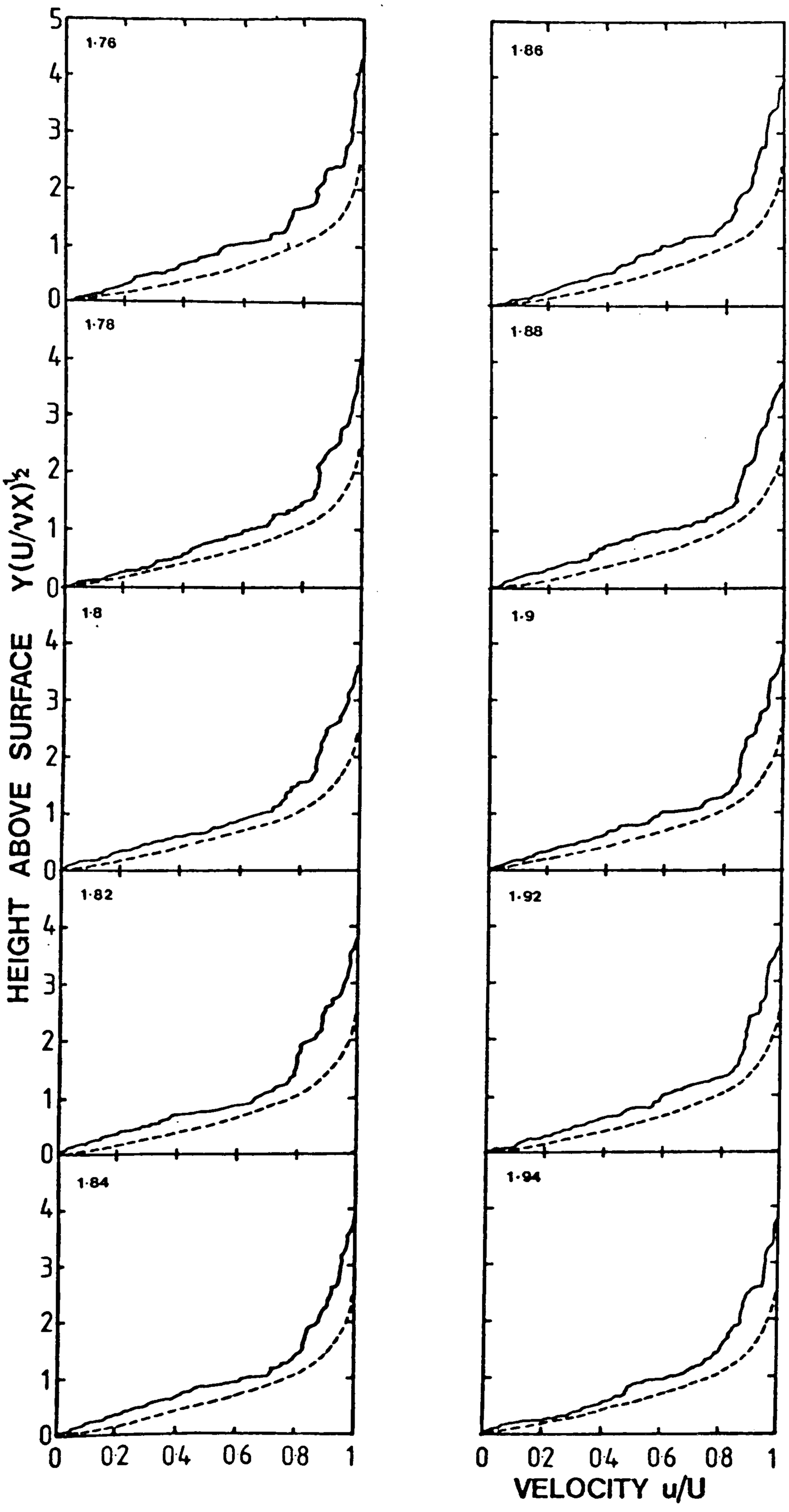

Figure 3.13 The Stagnation Point Profile

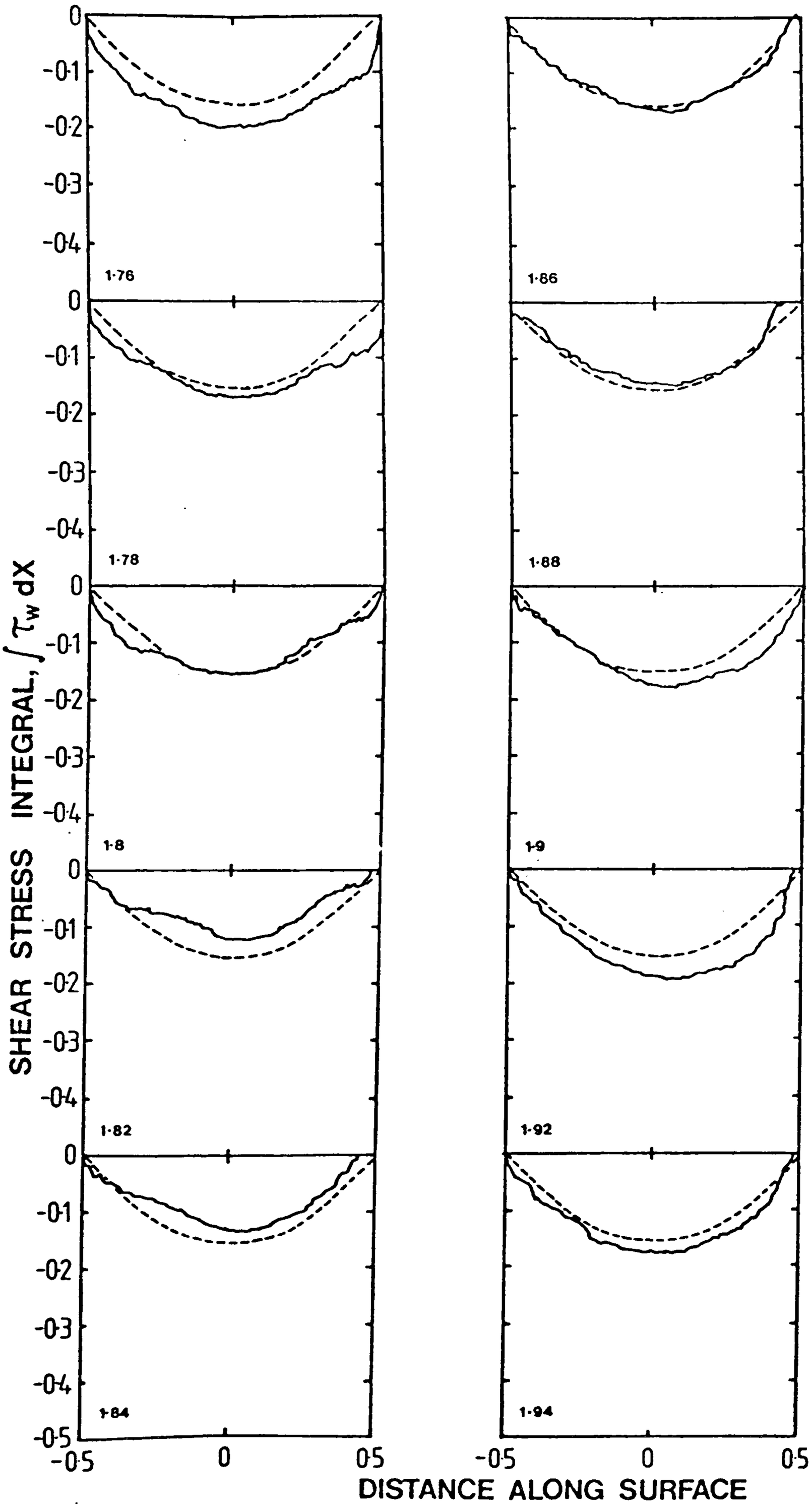

Figure 3.14 The Shear Stress near the Stagnation Point

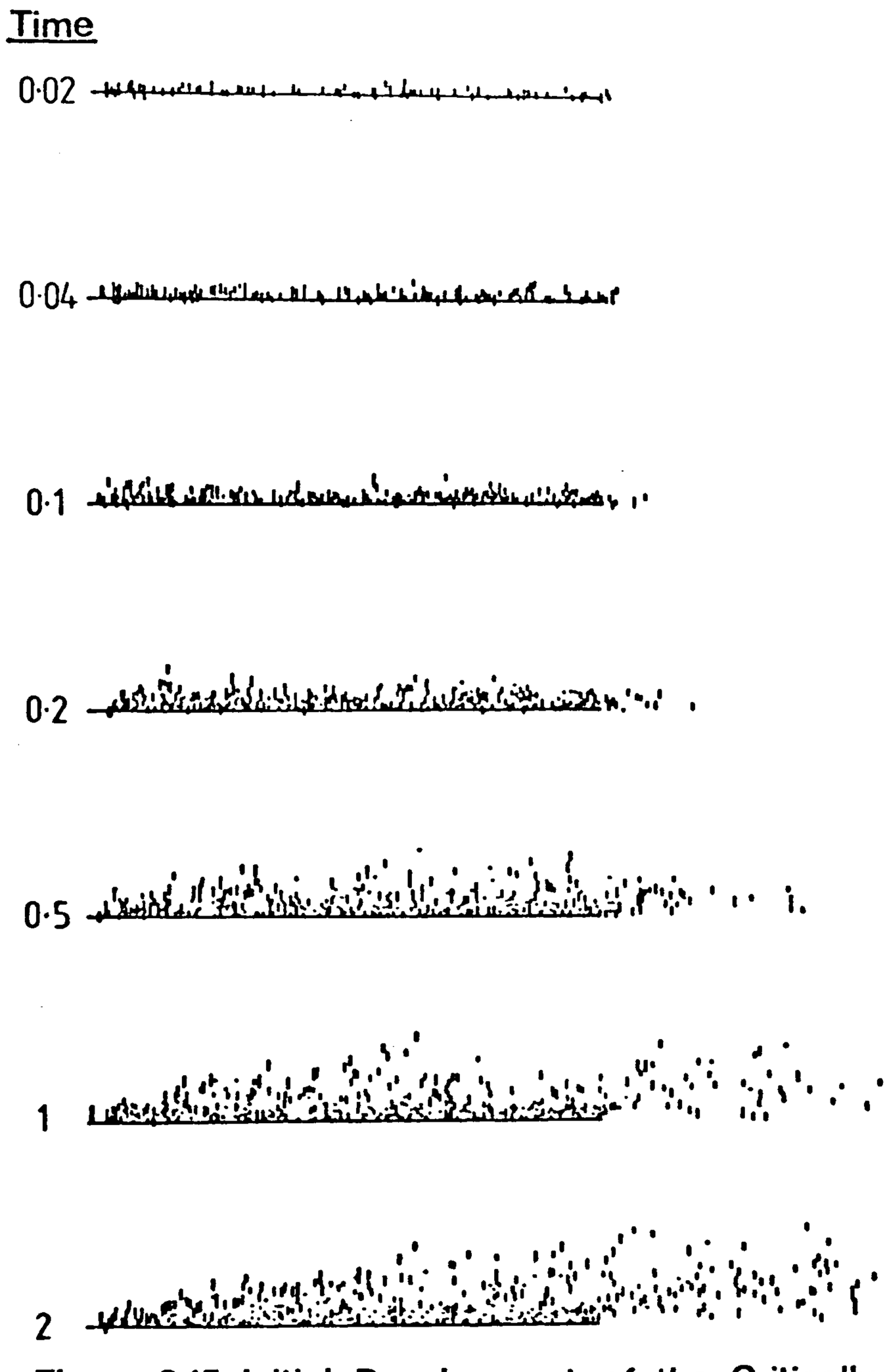

Figure 3.15 Initial Development of the Critically Decelerated Boundary Layer

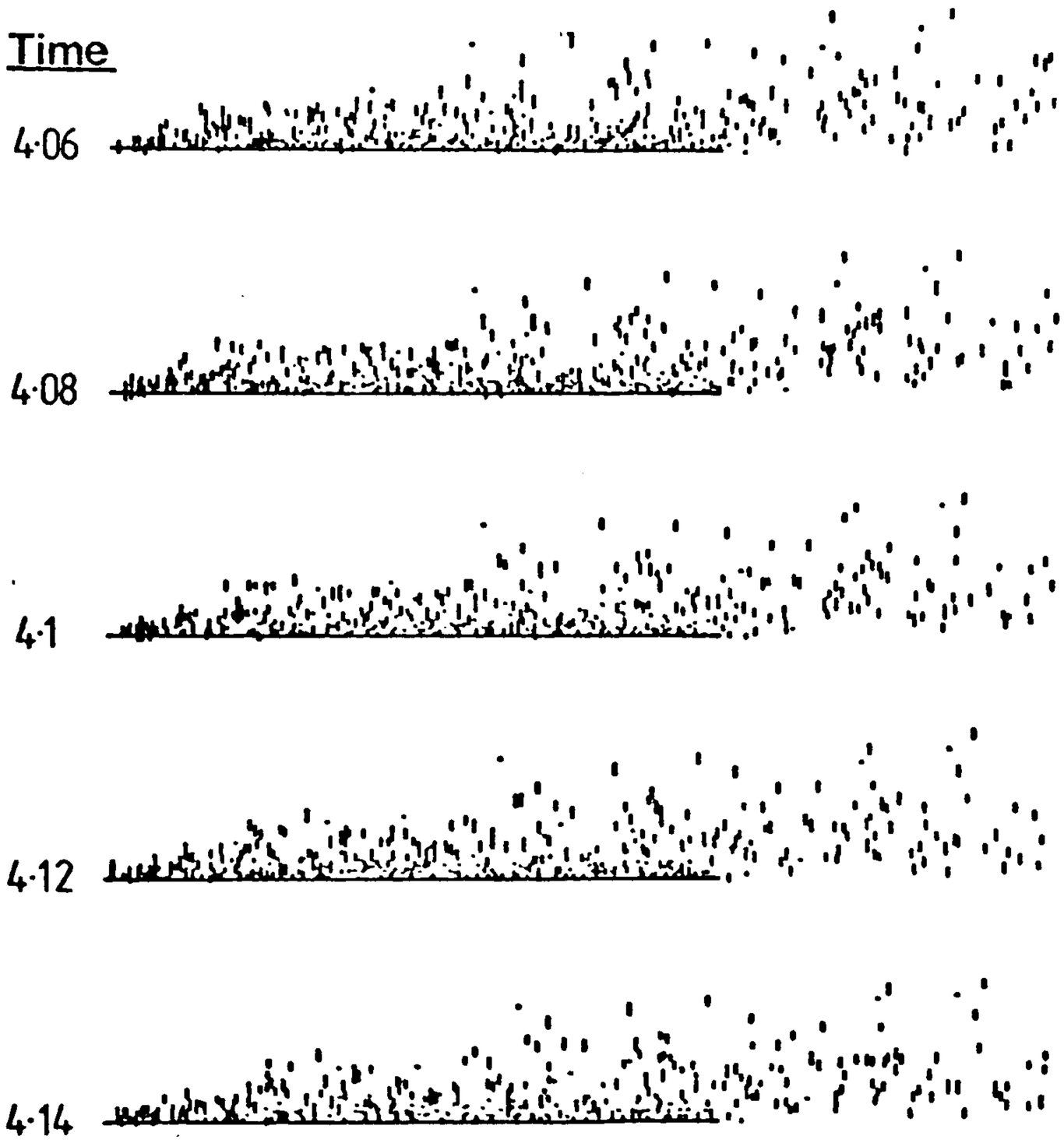

Figure 3.16 The Critically Decelerated Boundary Layer

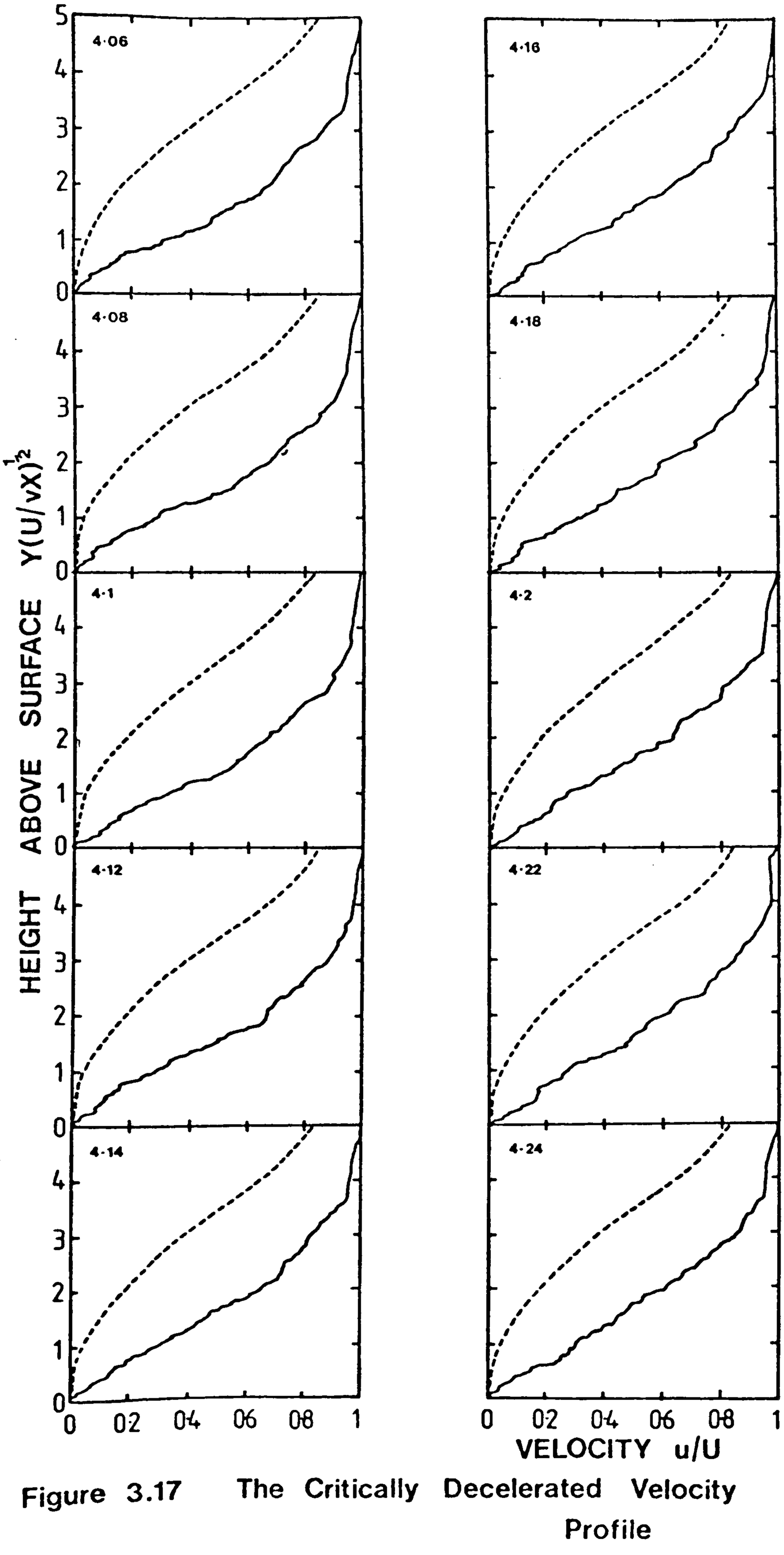

Figure 3.17 The Critically Decelerated Velocity Profile

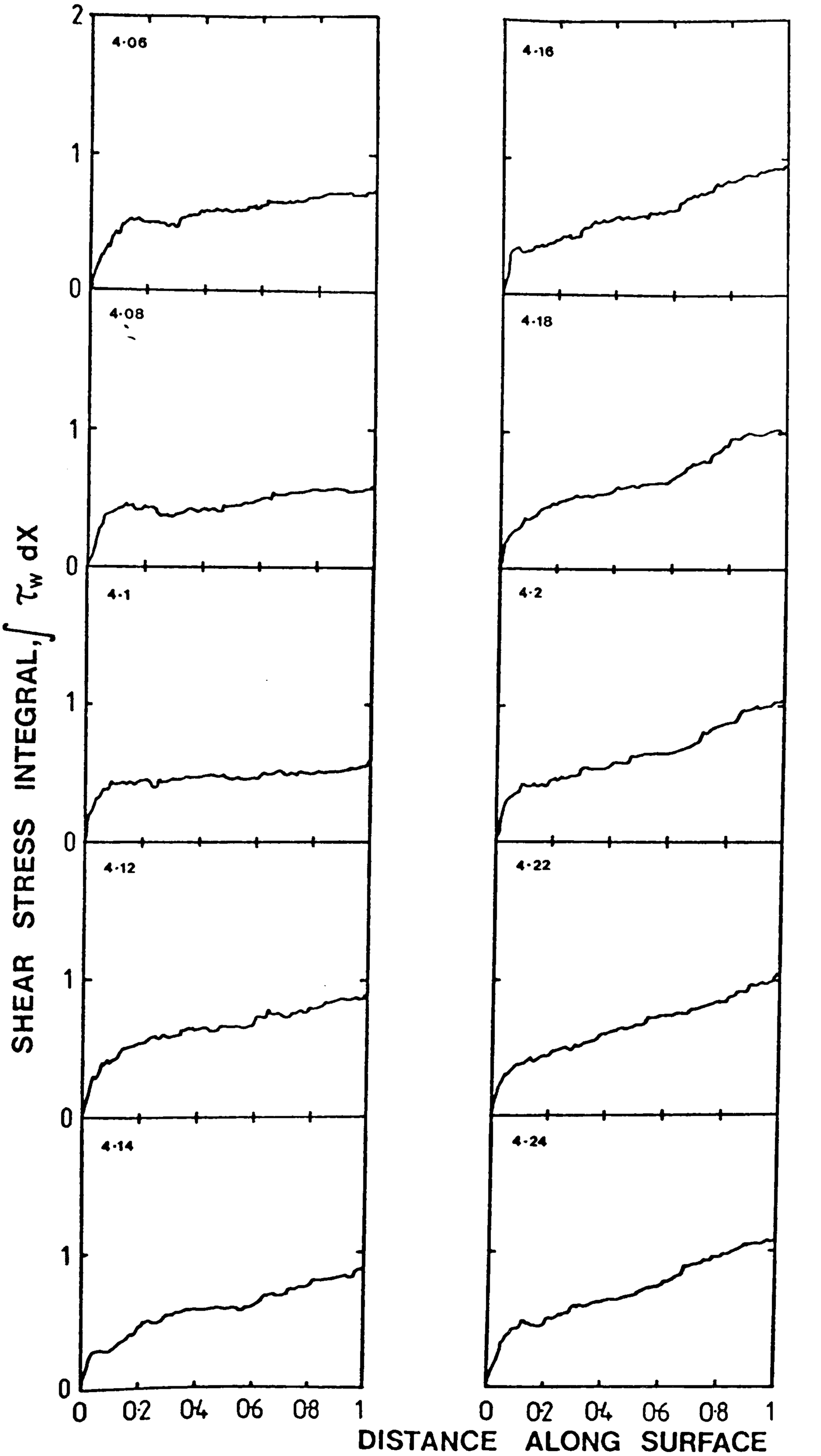

Figure 3.18 The Shear Stress at Critical Deceleration

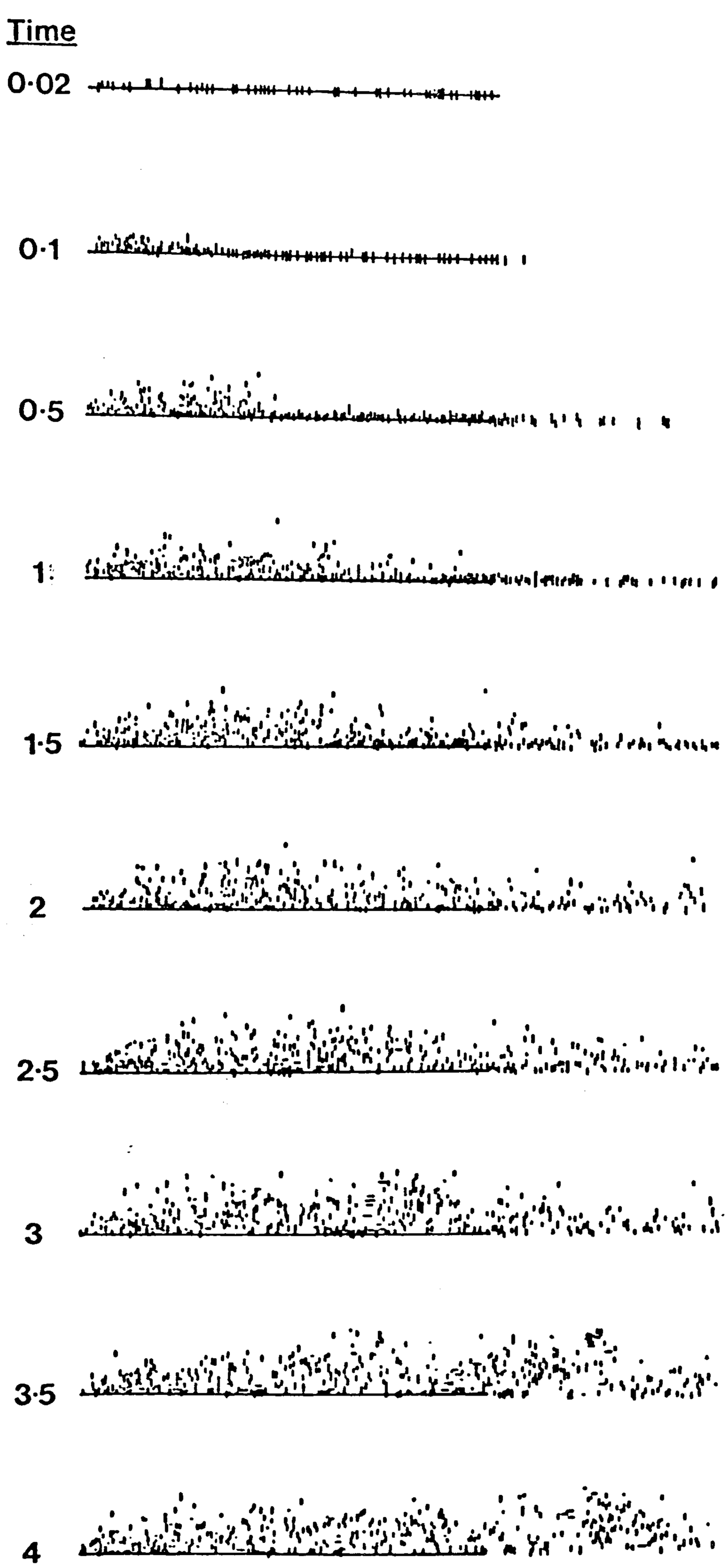

Figure 3.19 A 'Turbulent' Boundary Layer

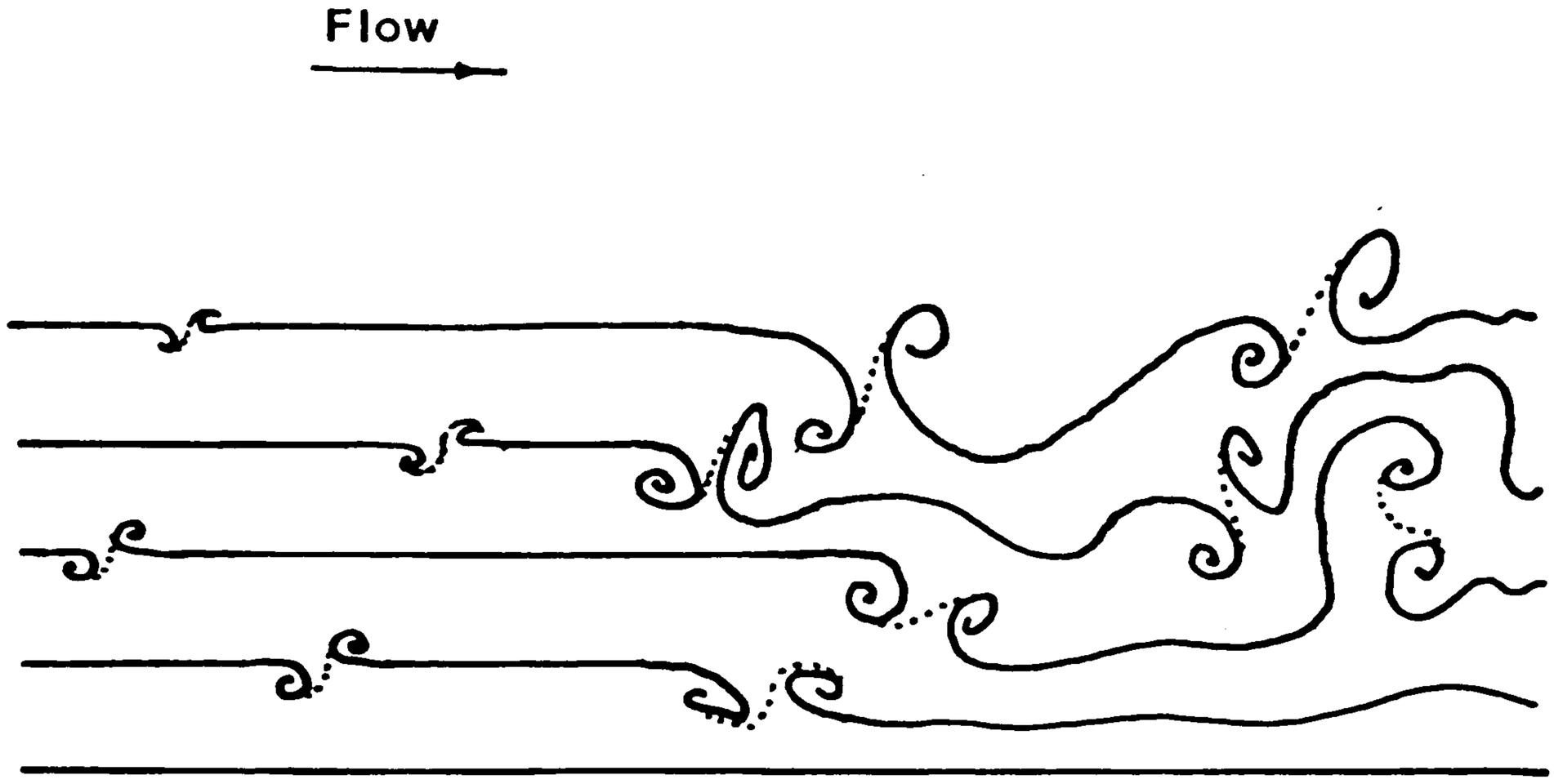

Figure 3.20 The Transition to Turbulence

CHAPTER 4. THE MECHANISM OF FLOW SEPARATION

This topic deserves a short chapter to itself since it is a central part of this Thesis. The wish to simulate the flow around bluff bodies means that, although there may be little interest in the subject of boundary layers for its own sake, a knowledge of the mechanism of flow separation is essential to determine the most suitable model for flow separation in the bluff body computer program. The customary explanation of flow separation in terms of fluid in the boundary layer being unable to negotiate an unfavourable pressure gradient in its 'tired' state does not provide much guidance, since it is not quite obvious with this explanation that there should be any backflow or recirculation of the fluid. This chapter aims to show that a clearer explanation may be given in terms of the vortex dynamics.

The boundary layer computer program has been executed with a strongly decelerating external velocity profile. The development of the vortex dynamics is described in section 4.1. From this development, it is possible to interpret the well-known Thwaites' parameter. Section 4.2 presents this interpretation.

4.1 THE DECELERATING BOUNDARY LAYER

In figure [4.1], the boundary layer is shown with a strongly decelerating external velocity. Over the first half of the plate, the external velocity is constant and equal to unity (in absolute units). Over the second half of the plate, the velocity drops linearly to a value of 0.3, and remains at this value downstream. As the boundary layer grows, a region of backflow appears, which is apparent in figure [4.2] by the counter-clockwise vorticity in the flow.

Suppose the deceleration was such that the flow would just separate. Over the latter half of the surface, vorticity should be diffusing from the flow back towards the surface. Diffusion is the only mechanism which can remove vorticity from the flow, and it is inadequate when there is a strong deceleration and a great amount of vorticity has to be removed quickly. Then some excess vorticity remains in the flow. New vorticity coming from upstream, under the influence of this excess vorticity, will be convected outwards (figure [4.3]). The new vorticity is then even less able to be removed from the flow, since it is further from the surface. Another wave of vorticity coming from upstream will be convected outwards even further by this accumulation of vorticity. The boundary layer has now lost its ability to be self-governing, and so it explodes until its thickness is

comparable with the body dimensions. It is then of course no longer appropriate to talk of a boundary layer. This is the mechanism of flow separation in terms of vortex dynamics.

The flow induced at the surface by the accumulation of excess vorticity is now in the upstream direction. This causes vorticity of opposite rotation to diffuse from the surface, and to establish a region of recirculating flow. Between the recirculating region and the region of forward flow there is a frontier at which vorticity of opposite rotation is mixing and being annihilated. Though it is not observed in this case, it is possible for the backflow to separate, and to contain within it a region of forward flow. It is conceivable that this very small forward flow region also separates, causing yet another region of backflow, and so on (figure [4.4]). Such separations may be termed secondary separations, and they can be observed in photographs of flow separation, as in Prandtl and Tietjens.[32]

For strong deceleration of the mainstream flow, vorticity piles up due to the kinematic effect of deceleration (figure [4.5]), and then explodes outwards by convection, with diffusion being unable to prevent this happening. This behaviour, observed here in the boundary layer, will also be seen with the bluff body computer program. In fact, it will still occur even when very few vortices are used to represent the boundary layer, which

shows that the phenomenology of the 'random vortex' method is close to the physical flow. This means that in going to a bluff body flow, there is no need for a vast number of vortices to simulate flow separation, although there would be such a need if it were desired to analyse the body's boundary layers. It is necessary to test, however, that an aerofoil still stalls at about the correct angle of attack.

4.2 AN INTERPRETATION OF THWAITES' PARAMETER

Thwaites[33] showed that for many boundary layers, there is a parameter

$$\frac{\theta^2}{\nu}\left(-\frac{dU}{dx}\right)$$

which measures the liability of a boundary layer to separate. When this parameter exceeds a relatively small critical value (of about 0.082 in a laminar boundary layer), the flow separates. An interpretation of Thwaites' parameter will now be given. This is not a derivation, but an explanation of how the parameter represents the influences at work during flow separation.

As the flow decelerates, vorticity piles up as a kinematic effect. This is represented through the term

$$-\frac{dU}{dx}$$

The vorticity then induces itself to move away from the surface. Now, each vortex has a mirror image below the surface. Therefore, the velocity induced is that due to a vortex doublet, for which the induced flow is, in the complex plane

$$u - i v = \frac{i\gamma}{2\pi}\left(\frac{1}{z - i a} - \frac{1}{z + i a}\right)$$

$$= -\frac{a\gamma}{\pi}\,\frac{x^2 + a^2 - y^2 - 2 i x y}{x^4 + y^4 + a^4 + 2 x^2 y^2 + 2 x^2 a^2 - 2 a^2 y^2}$$

When x>>y and x>>a the vertical component of the flow, v, is proportional to the height, a, of the vortex above the surface, or the separation of the vortex doublet. This is on average proportional to the boundary layer momentum thickness, θ (figure [4.6]). The velocity induced at some other point by the doublet is proportional to the height, y, of that other point above the surface, which is also proportional to the momentum thickness.

That is

$$v = -\frac{2\gamma}{\pi}\frac{ay}{x^3} \quad \propto \quad -\frac{2\gamma}{\pi}\frac{\theta^2}{x^3}$$

As the boundary layer convects itself, then, we would expect the induced vertical velocity to be proportional to the square of boundary layer thickness. This is represented through the term

$$\theta^2$$

Opposing separation is the action of viscosity, which tends to remove excess vorticity from the flow. In the Thwaites expression, this is just represented by ν. Thus the Thwaites' parameter may be interpreted as

$$\frac{\text{vortex convection}}{\text{vortex removal}} \quad \text{vortex pileup}$$

and when this exceeds a critical value, then there will be flow separation.

We have now extracted everything useful from boundary layer theory, and are able to consider the separation of the flow from bluff bodies, but first, it is necessary to have a method of analysing the shape of a bluff body. This is provided by the Martensen Method.

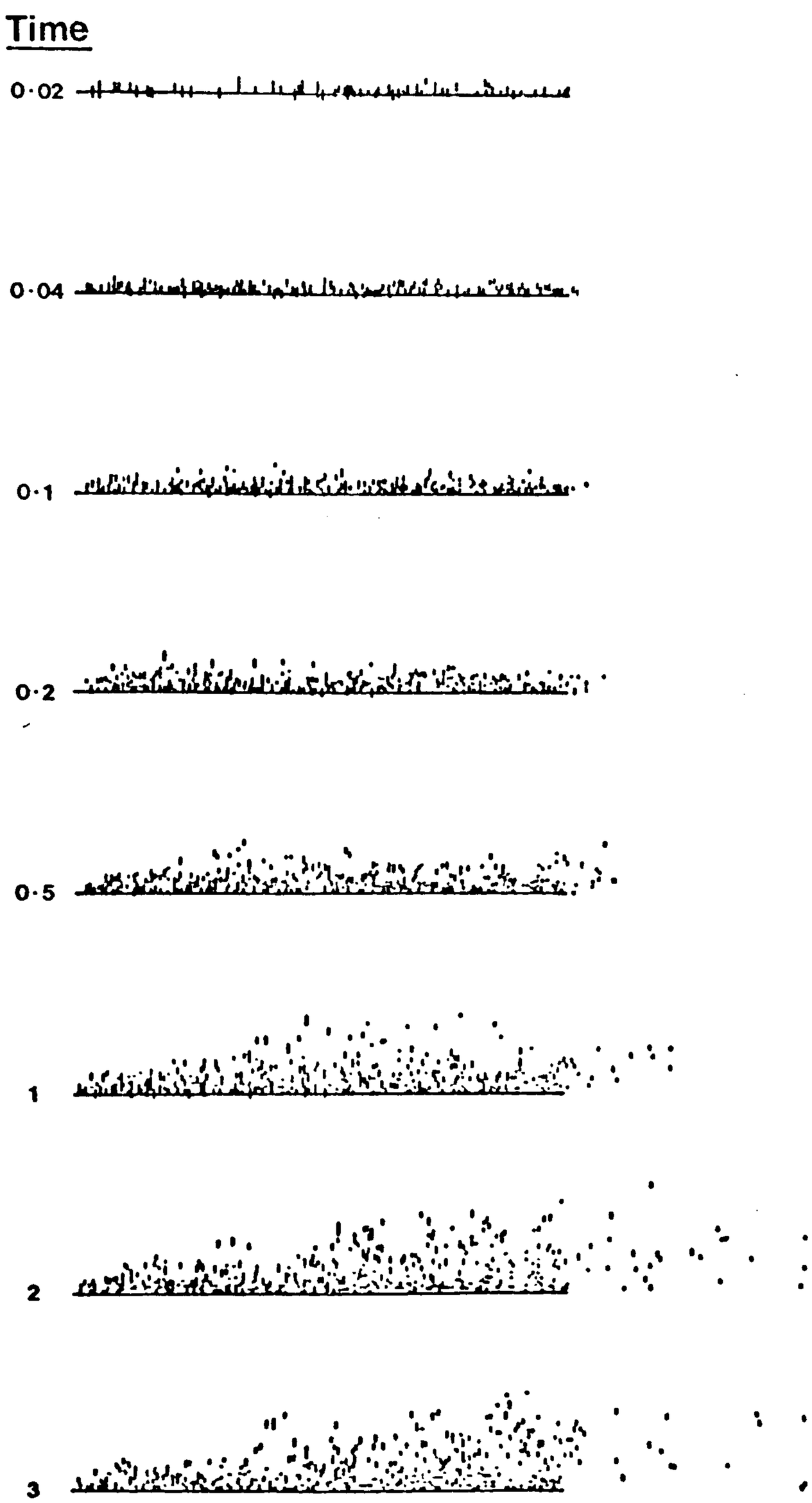

Figure 4.1 Initial Development of Flow Separation

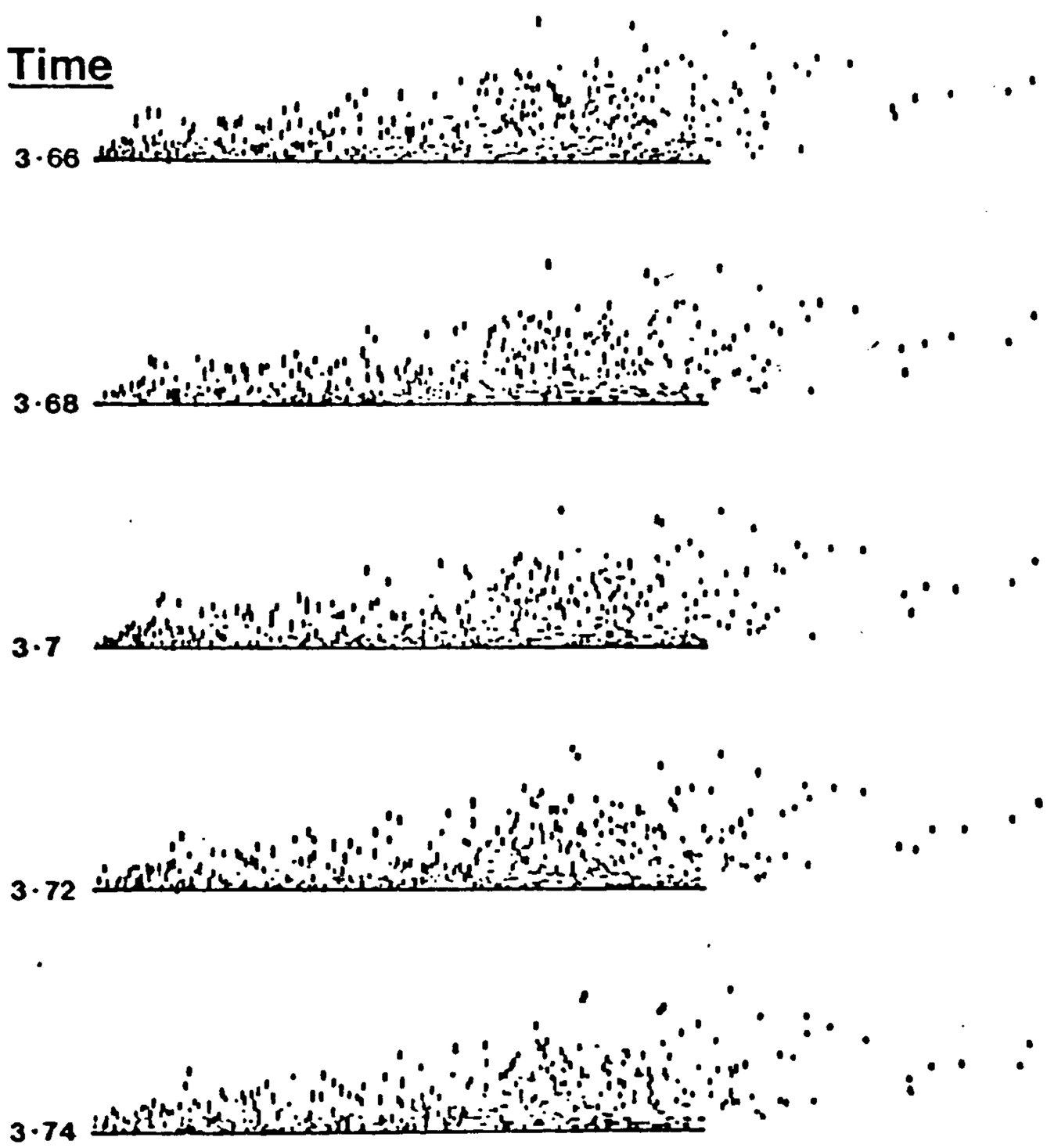

Figure 4.2 Flow Separation

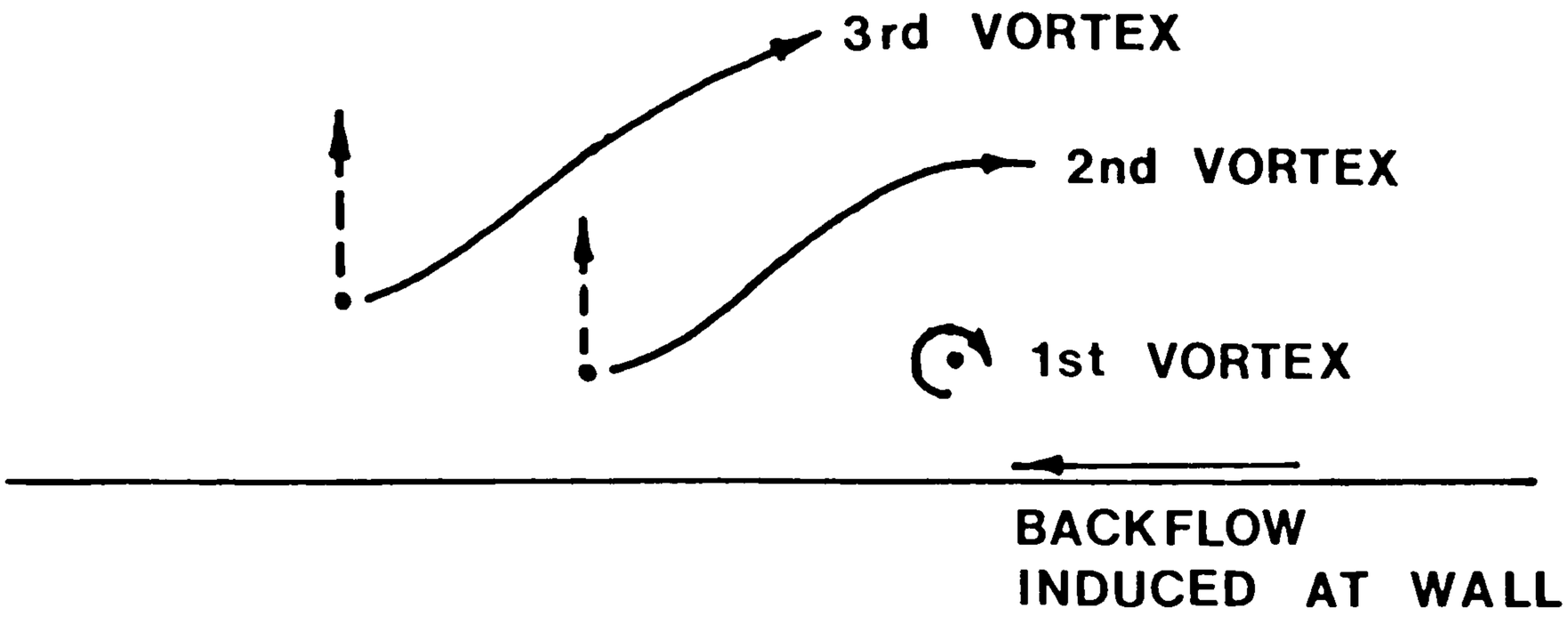

Figure 4.3 The 'Explosion' of the Boundary Layer

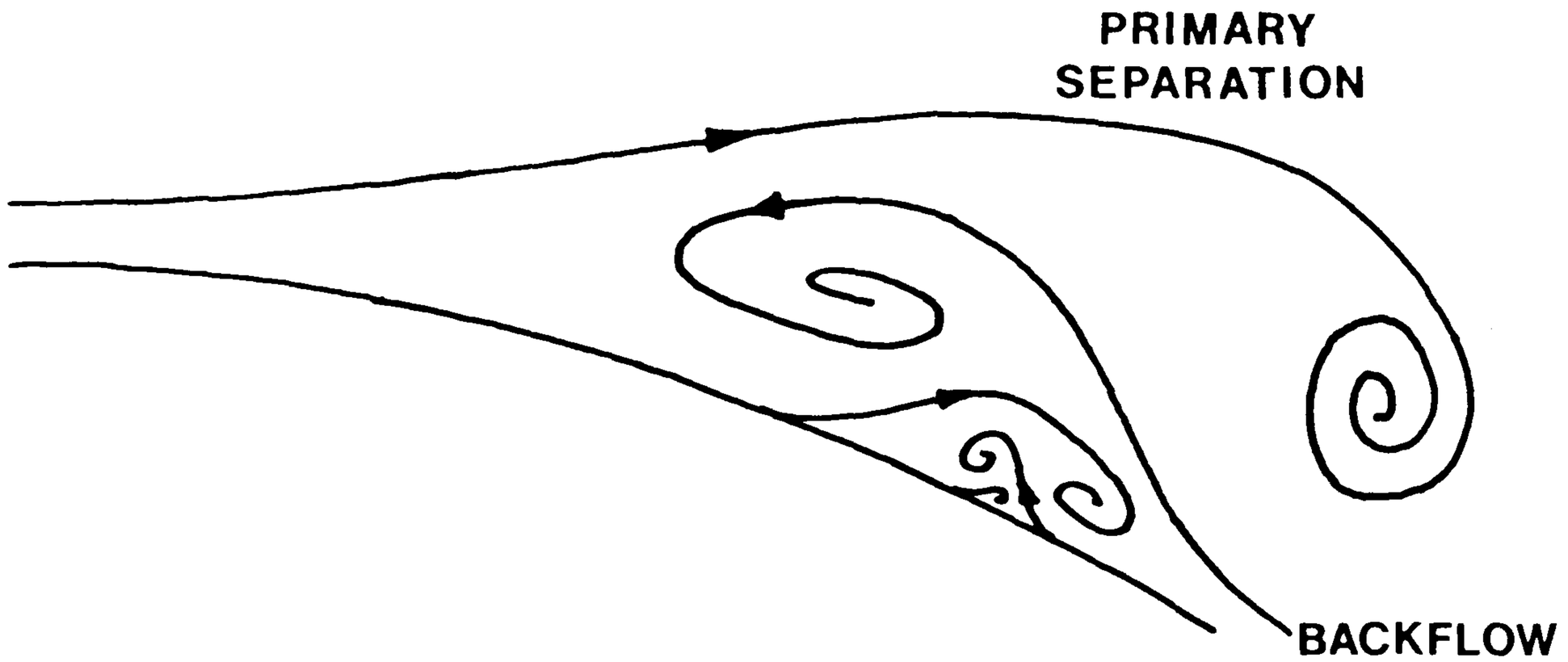

Figure 4.4 Secondary Separations

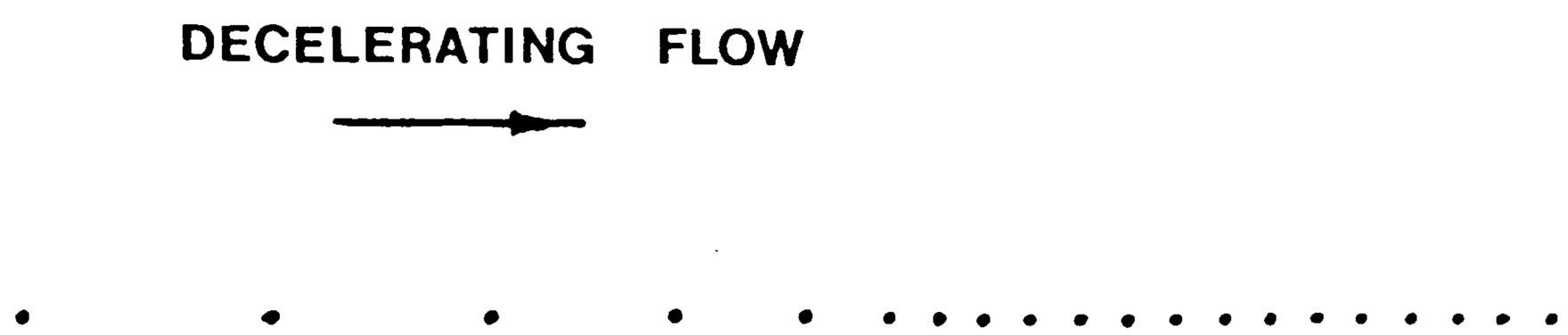

Figure 4.5 Vortex Pileup as a Kinematic Effect

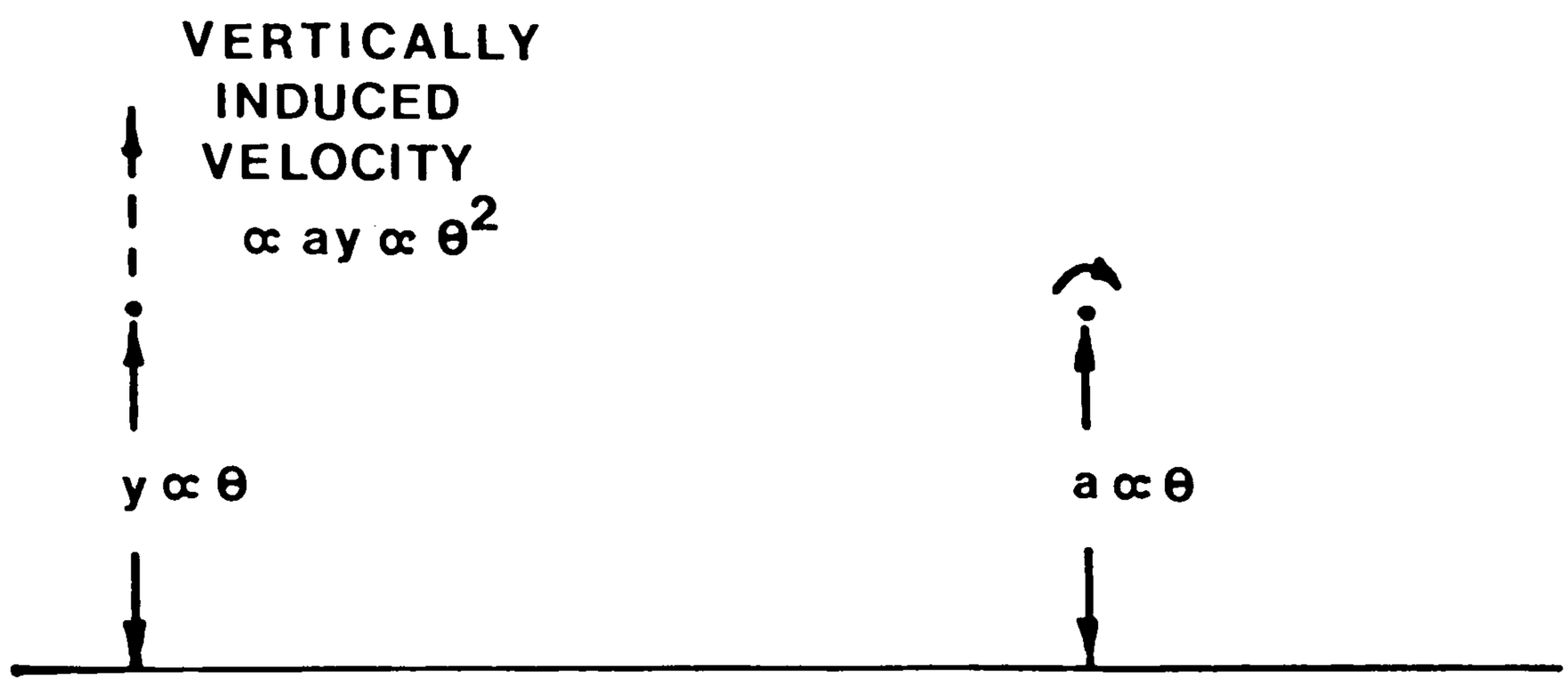

Figure 4.6 The Velocity Induced by a Vortex and its Image

CHAPTER 5. THE MARTENSEN METHOD

A method to calculate the flow around two-dimensional bodies of arbitrary shape has been specified by Martensen[1] and developed further by Wilkinson[18]. This chapter describes the application of the method to the calculation of unseparated flows, and the next chapter will describe separated flows. The unseparated flow around a body is the initial state of the flow around that body after it has been impulsively started from rest, before vorticity has had time to diffuse away and perhaps to separate. Thus the unseparated flow calculation is the logical starting point for the separated flow calculation.

Section 5.1 describes the Martensen method, with comments on improvements or simplifications made by the author. The intention has been to develop a suite of reliable program modules from which a selection is made for any particular flow separation problem. Section 5.2 gives theoretical methods for plotting the streamlines around an unstalled aerofoil in a wind tunnel as a test of the method. Section 5.3 describes the comparison of the theoretical predictions with experiment for aerofoil NACA 0012 in a wind tunnel.

5.1 DESCRIPTION OF THE METHOD

If we have a vortex sheet of strength γ (dimensions L/T), then the speed induced by this sheet on one side of it is $\gamma/2$, and on the other side it is $-\gamma/2$. Other vortices may be added to the flow elsewhere until the speed on one side of the sheet is γ, and on the other side the speed is zero. The vortex sheet may then be regarded as the boundary layer around a solid body. The vorticity in the layer is equal to the flow speed just outside the layer.

For a closed contour, the speed just inside any point on the contour (figure [5.1]) is given by

$$0 = \frac{-\gamma(i)}{2} + \oint K(i,j)\gamma(j)\, ds(i) + \text{external influences} \qquad (5.1)$$

For a uniform flow, the external influence is

$$\underset{\sim}{U}.\underset{\sim}{l}(i)$$

where $\underset{\sim}{l}(i)$ is a unit vector parallel to the surface. Equation (5.1), which is known as a Fredholm integral equation of the second kind, has a solution of the general form

$$\gamma(i) = \oint L(i,j)\, \underset{\sim}{U}(j).d\underset{\sim}{s}(j) + \Gamma m(i) \qquad (5.2)$$

where Γ is an arbitrary constant. This constant may be defined as the total

bound circulation on the contour, and this determines the function m(i).

To solve equation (5.1), a suite of computer programs has been written, which is shown in figure [5.2]. The profile generation program generates a set of (x,y) co-ordinates to describe the contour. Different programs may be used to generate aerofoils, circles or polygons. In the case of an aerofoil, the pivotal points are generated by a formula of the form

$$1 + \cos\left[\frac{i}{2\pi n}\right]$$

which puts more pivotal points near the leading and trailing edges (figure [5.3]). For other bodies, something similar may be used. For example, a polygon should have pivotal points packed near the vertices. In addition to the pivotal points, intermediary points are generated by the same formula. The value of Δs for a pivotal point is taken as the distance between the intermediary points on either side of it, and the value of θ is the slope of the line joining these intermediate points. Care must be taken over the quadrant when θ is defined, and also over whether the contour is specified in clockwise or anti-clockwise order, or the computer program will confuse the inside with the outside of the contour, with bizarre results.

In the case of a NACA aerofoil, there is a generating equation which could be differentiated to give the value of θ. This was tested with the

Martensen method, but for some reason the results obtained when θ was defined by differentiation gave an unrealistic behaviour at the trailing edge, while definition of θ by the slope between intermediate points gave sensible results. This shows that the Martensen method is sensitive to the way in which it is programmed. The method chosen here works satisfactorily in the sense that it converges quickly with an increasing number of pivotal points.

The matrix operator program contains the core of the Martensen Method. Equation (5.1) may be written in a discrete element form suitable for numerical computation

$$\frac{\gamma_i}{2} = \underset{\sim}{U}_i \cdot \underset{\sim}{l}_i + \sum_j K_{i,j} \gamma_j \Delta s_j \qquad (5.3)$$

where the vorticity (or velocity) will be evaluated at n pivotal points.

The vector $\underset{\sim}{l}_i$ has components

$$(\cos \theta_i, \sin \theta_i)$$

and for an isolated object, the coupling or influence coefficient is

$$K_{i,j} = \frac{(y_i - y_j) \cos \theta_i + (x_i - x_j) \sin \theta_i}{2\pi \left((x_i - x_j)^2 + (y_i - y_j)^2\right)} \qquad (5.4)$$

It is interesting to note that a circle has the property that $K_{i,j}$ is a constant between any two points (this is related to the classical geometric property that the angle subtended by a chord at any other point on the circle is a constant, the chord in this case being infinitesimal). This leads to a quick analytical solution of the Martensen Method, and indicates that the circle is the best type of contour for the method. Since any contour is locally the same as a circle, the influence of a pivotal point on adjacent pivotal points is almost the same as the influence of the pivotal point on itself due to local radius of curvature. This assists us in constructing a picture of the matrix which is being formed (figure [5.4]).

For an object which is cascaded, or repeated at intervals of t along the y-axis, the coupling coefficient may be derived from a conformal transformation in the complex plane, and written in the form

$$K_{i,j} = \frac{s(y)\ c(y)\ \cos\theta_i \ + \ sh(x)\ ch(x)\ \sin\theta_i}{2\pi\ \left((sh(x))^2 + (s(y))^2\right)} \qquad (5.5)$$

where

$$x = x_i - x_j \qquad y = y_i - y_j$$

$$s(y) = \frac{t}{\pi} \sin\frac{\pi y}{t} \qquad c(y) = \cos\frac{\pi y}{t}$$

$$sh(x) = \frac{t}{\pi} \sinh \frac{\pi x}{t} \qquad ch(x) = \cosh \frac{\pi x}{t} \tag{5.6}$$

As t becomes large, equation (5.5) becomes equation (5.4). To guarantee that this happens numerically, the functions (5.6) are best computed from their expansions. For example

$$sh(x) = x + \frac{\pi^2}{t^2}\frac{x^3}{3!} + \frac{\pi^4}{t^4}\frac{x^5}{5!} + \frac{\pi^6}{t^6}\frac{x^7}{7!} + \ldots\ldots$$

A point vortex placed upon any contour should induce a total circulation around that contour equal to half the strength of the vortex (except for the special case where the vortex is placed at a vertex of the contour). So for the coupling coefficients, it should be the case that

$$\sum_i K_{i,j} \Delta s_i = 1/2 \tag{5.7}$$

The largest coupling coefficient other than $K_{i,i}$ is obtained from equation (5.7) instead of (5.4) or (5.5) in order to ensure that the condition (5.7) is always observed. For a single aerofoil, the largest coefficient is usually on the trailing diagonal as shown in figure [5.4]. This correction is due to Wilkinson[18].

The circulation is introduced by 'throwing away' any equation of the

system (5.3) (preferably the last equation) and replacing it by

$$\Gamma = \sum_j \gamma_j \Delta s_j \qquad (5.8)$$

It is sensible to redefine $K_{i,j}$ as

$$K_{i,j} = K_{i,j} \Delta s_j \qquad \text{when } i \neq j \text{ and } i \neq n$$

$$K_{i,j} = K_{i,j} \Delta s_j - 1/2 \qquad \text{when } i = j \text{ and } i \neq n$$

$$K_{n,j} = \Delta s_j$$

and if

$$V_i = \underset{\sim}{U}_i . \underset{\sim}{l}_i \qquad \text{when } i \neq n$$

$$V_i = \Gamma \qquad \text{when } i = n$$

then

$$K_{i,j} \gamma_j = V_i \qquad (5.9)$$

The matrix $K_{i,j}$ is shown as a picture in figure [5.4]. It is acceptable to throw away an equation because, given the first (n-1) equations, no new information is conveyed by the nth equation, and so we must find another source of information to make up n equations. This will be either a Kutta condition or a circulation condition.

A computer can invert this matrix to give another matrix L. This inversion is actually quite simple since K is a 'good' matrix with a

dominant leading diagonal, except for the last row if that is where equation (5.8) has been placed, but then the matrix is still well-behaved providing that it is only the last row which does not have the largest term on the leading diagonal. A simple method has been used for the matrix inversion, but there is no deterioration in the quality of the computer programming as stressed in Chapter 1.

Then

$$Y_j = \qquad L_{j,i} V_i \qquad (5.10)$$

is analogous to equation (5.2). The matrix L is the 'operator matrix' from which the program takes its name. This matrix acts upon the velocity distribution around the contour with the body absent to give the velocity distribution with the body present.

Once the operator matrix has been computed, it is stored on magnetic disc within the computer, and effectively we are finished with the Martensen method. This matrix contains all the information about the body which is needed to compute its behaviour in a variety of flows, and flow separation is not the only computer project which could be undertaken using the operator matrix. For unseparated flows, the next program, which applies the Kutta-Joukowksi condition, yields results on the surface velocity and

pressure distribution around an aerofoil which may be compared with experiment, and possibly with the theoretical predictions of other workers.

The Kutta condition program first obtains three solutions by using the matrix operator just calculated. These are

(i) Unit uniform flow along the X-axis, with no net bound vorticity.

(ii) Unit uniform flow along the Y-axis, with no net bound vorticity.

(iii) No flow, with unit bound vorticity.

Any other uniform flow can be synthesised by a linear combination of solutions (i), (ii) and (iii). For any one flow angle, there is a unique combination with solution (iii) which, for an aerofoil, gives a stagnation point at the trailing edge (the Kutta-Joukowksi condition). This reduces the above three solutions to two of practical interest

(i) Unit flow along the X-axis, with Kutta condition.

(ii) Unit flow along the Y-axis, with Kutta condition.

The program computes these solutions, and puts them onto a magnetic disc for the streamline tracer program, or for various programs which the user may write to give pressure distributions at different angles of attack.

Because there are really just two solutions of interest, it follows that the characteristics of an aerofoil or cascade may be represented by just two constants obtainable from the Martensen method. This pair of constants may be expressed in a number of forms. The first form is the circulation Γ_y for a flow along the Y-axis and Γ_x for flow along the X-axis. For flow in a direction α, the Kutta condition is maintained if

$$\Gamma = \Gamma_x \cos\alpha + \Gamma_y \sin\alpha \qquad (5.11)$$

where

$$\tan\alpha = (\tan\alpha_1 + \tan\alpha_2)/2$$

The second form is illustrated by writing the lift coefficient as

$$C_L = 2\pi K \sin(\alpha - \alpha_o) \qquad (5.12)$$

For a cascade, K is termed the Weinig lattice coefficient. For an isolated flat plate K=1, and for ordinary aerofoils, in theory K>1. The angle α_o is the angle of zero lift or zero circulation. For a symmetric aerofoil this is just the angle of the camber line. For a cascade, α_o is the effective stagger angle, which may differ from the nominal stagger angle by a few degrees. It follows that

$$K = \sqrt{\Gamma_x^2 + \Gamma_y^2} \quad /2 \tag{5.13}$$

$$\alpha = - \tan^{-1} (\Gamma_x / \Gamma_y) \tag{5.14}$$

The third form exists for cascades as an inlet-outlet angle relation

$$\tan \alpha_2 = a \tan \alpha_1 + b \tag{5.15}$$

where

$$a = \frac{2t + \Gamma_y}{2t - \Gamma_y}$$

$$b = \frac{2\Gamma_x}{2t - \Gamma_y} \tag{5.16}$$

Thus knowledge of t and any one of the three pairs (Γ_x, Γ_y), (K, α_o) and

(a,b) gives a rule for predicting the behaviour of a cascade.

5.2 STREAMLINE TRACING

The distribution of vorticity around the aerofoil may be used to obtain the flow velocity at any point away from the aerofoil, with each vortex

element on the contour inducing part of the velocity at that point. Far from the contour, it is impossible, by a measurement of local velocity which has some small error, to resolve the contribution of each vortex element to the induced velocity. When an observer approaches close to the aerofoil, though, the individual vortices can induce very large or very small velocities in any direction depending upon the precise position of the observer. Thus, near the aerofoil, the streamlines would not be parallel to the surface of the aerofoil. This difficulty can be overcome by a method with the same idea as Wilkinson's[18] correction (5.7) which will be described in detail because it is also essential to the flow separation program to ensure that nearby free vorticity does not induce absurdly large velocities on the surface.

Regarding the aerofoil as an abstract contour, a vortex placed at some distance will induce flow through the contour. The induced circulation around the contour, and total induced flow through it, must both be zero. When the contour is replaced by discrete elements, there is now an additional condition on the coupling coefficients (or 'coupling vector'). For the circulation

$$\sum_i M_i \Delta s_i = 0 \qquad (5.17)$$

and for the flux

$$\sum_{i} N_i \Delta s_i = 0 \tag{5.18}$$

where

$$M_i = \frac{y_i \cos\theta_i + x_i \sin\theta_i}{2\pi (x_i^2 + y_i^2)}$$

$$N_i = \frac{y_i \sin\theta_i - x_i \cos\theta_i}{2\pi (x_i^2 + y_i^2)} \tag{5.19}$$

A search is made for the element on the contour nearest to the vortex. For all of the other coupling coefficients, equation (5.19) is employed. The coupling coefficients of the nearest element are then obtained from equations (5.17) and (5.18). With this technique, it is guaranteed that the vortex induces no circulation or flux around the contour. As the vortex approaches the contour, the velocity distribution induced on the contour always remains sensible.

Now, the coupling vector which describes the influence of a vortex at A on a point B is equal to minus the coupling vector of B on A (figure [5.5])

(This is a variation on Newton's Third Law). Thus the coefficients M_i and N_i which have been calculated and corrected going from a fictitious unit vortex to the contour may be used in reverse to calculate the influence of the contour on the exterior point (with a simple rotation of axes when necessary). The corrected coupling coeffients are obviously valid for a distant point. When the point is very close to the contour, calculating the velocity this way will actually ensure that the flow speed is almost the same as the speed at the nearest point on the aerofoil obtained from the Martensen method, and the flow direction is parallel to the surface. It could be said that by this method, point vortices have been made 'tame' when they are normally 'wild' due to the infinite speed at their core.

It is thus possible to determine the flow velocity (u,v) reliably at any point (x,y). In steady flow, a particle moving with this velocity follows a streamline, so that after a numerical time step dt, the new position of the particle may be estimated as

$$(x + u\,dt,\ y + v\,dt)$$

This value is supplied to the improved Euler method to give a revised and more accurate estimate. By repeating this process many times, the streamlines of the flow may be constructed, which can be plotted by a

computer graph plotter. Without the correction to the coupling coefficients described above, streamlines plotted near the body turn out to be zigzag lines. With the correction, smooth streamlines are obtained. The use of a reversible time stepping method ensures that having traced a streamline from A to B, we can trace it back to A exactly if we put

$$dt_{new} = - dt_{old}$$

and it is self-evident that this is a desirable property. The height of a streamline from far upstream to far downstream is another example of a conserved quantity for which a reversible method is mandatory.

When an aerofoil is placed in a wind tunnel (figure [5.6]), it can be analysed as a cascade of aerofoils and mirror images. The Martensen method has been extended to deal with more than one body, as a later chapter will describe. A pair of aerofoils was repeated in a cascade, using equation (5.5) to obtain the coupling coefficients, and each aerofoil was given a Kutta condition. The streamlines must be traced under the influence of the body and of all its images. For flow parallel to the tunnel walls, the streamlines at the notional position of the walls have been proved to be straight lines within the accuracy of the computer (1 part in 10,000,000), which is a good test of the computer program. The flow elsewhere is modified by the effective presence of the walls, so with this arrangement,

we can do a direct comparison with experiment without doubts about the influence of the wind tunnel walls.

5.3 COMPARISON WITH EXPERIMENT

The aerofoil NACA 0012 is shown in its wind tunnel in figure [5.7]. The tunnel was of octagonal cross section, but the diagonal faces were sufficiently small for us to assume it to be rectangular and for the two-dimensional theory to be applicable. The width and height of the tunnel were both eighteen inches, and the aerofoil chord was six inches, giving a value t=6 (including the mirror image). The aerofoil spanned the tunnel. It could be rotated and clamped at any angle, which means unfortunately that the Martensen method must be repeated for every flow angle since the aerofoil-mirror-image geometry was changing. For an isolated aerofoil, one application of the Martensen method produces an operator matrix which remains the same at any flow angle, and one can then use the principle of superposition. For the aerofoil in the wind tunnel, the operator matrix itself is a function of flow angle, and must be computed each time a new flow angle is required.

There was no way of presetting the zero angle of attack of the aerofoil, so it was necessary to repeat each test with the aerofoil at both positive

and negative incidence. This was in fact desirable, because the pressure tappings on the aerofoil were placed alternately (figure [5.8]) so that by including the opposite incidence, twice as much useful information on the pressure distribution around the aerofoil was obtained. By connecting alternate pressure tappings to successive tubes of a multi-tube manometer, a picture of the pressure distribution around the aerofoil was obtained, in which the lift was roughly equal to the enclosed area. When the aerofoil was inverted, this picture should have appeared to be the same. This served to check the setting of the angle of attack. The zero angle of attack could then be determined by rotating the aerofoil until the pressure distributions on both sides of the aerofoil are visually matched, a method which was repeatable to within one tenth of a degree.

There were pressure tappings on the tunnel walls, which were used to determine the flow speed at the working section. It was found that the readings from the wall tappings showed small fluctuations with time which would be tolerable enough in the reading from any one tapping on the aerofoil, but since the wall tapping measurements were relatively more important, their fluctuations were damped by the insertion of capillary tubes and bottles into the tube to the manometer (whose electrical analogue is also shown in figure [5.9]. This removed the fluctuations, but made it

necessary to be especially careful in testing for leaks, since the flow resistance in the tunnel-manometer line was made large, and thus it was comparable to the flow resistance of potential leaks. The tunnel was then calibrated against a known National Physical Laboratory pitot tube placed in the working section. A check was also made for the uniformity of flow across the tunnel in the working section, which turned out to be better than ±1%. Once the probe was removed, the aerofoil was placed in position and its pressure tappings were connected directly to the manometer.

Figure [5.10] shows the pressure distribution measured at zero angle of attack, with the results of the Martensen method for comparison. The aerofoil surface is shown unwrapped, since this method of display is the most appropriate when dealing with bluff bodies. The aerofoil used is symmetric about the chord line, but it can be seen from figure [5.10] that there is an apparent asymmetry in the pressure distribution measured. Small variations in the shape of the aerofoil near the leading edge can be expected to have this effect.

Figures [5.11] and [5.12] show the pressure distributions at 5 and 10 degrees angle of attack. Also shown are the theoretical predictions for the aerofoil with its system of mirror images, and for the simpler case of the aerofoil alone. It is obvious that the difference between the two theories

is much less than the difference between either theory and experiment, so with hindsight we hardly need to have bothered with the mirror images. It has been worthwhile finding this out nevertheless, so we may eliminate the influence of the walls as a reason for any discrepancy between theory and experiment. It might be suspected that, looking at the suction surface results alone, there was an error in calibration, but such an error could not account for the results from the pressure surface, so it may be taken as a genuine observation that the pressure distributions obtained correspond to a lift which is less than the theoretical value. This has been observed before, and a possible reason will be given after the description of streamline tracing.

The technique used to trace streamlines relied upon the detection by a thermocouple of the thermal wake downstream of an electrically heated wire (figure [5.13]). Preliminary trials showed that a wake temperature could be detected to a temperature resolution of about 0.1K. The wake temperature used in the experiments was 1-2K, giving 10-20 levels of resolution by a digital voltmeter. The wake width was about 1/2 inch at the distance downstream examined. The temperature in the wake was read every 1/20 inch, giving a temperature profile through the wake, of which a typical example is shown in figure [5.14]. The distribution of temperature is obviously

Gaussian, so it is simple to make an unbiassed estimate of the centre of the wake, and this estimate can be repeated to within 1/40 inch. The number of readings taken through the wake compensated for the low resolution of the digital voltmeter, and the shape of the temperature distribution makes it amenable to statistical analysis.

For the heater wire in four standard positions, wake traverses were performed at a number of positions downstream. Then each temperature profile was analysed to give its mid position, which is assumed to be the trace of the streamline which coincides with the heater wire. Results at zero angle of attack show that the method is working as expected (figure [5.15]). Care must be taken in finding the position of the thermocouple probe within the tunnel. In the stream of air the probe tends to bend downwind. Its position was determined by lowering it until it just touched the aerofoil (its reflection in the polished surface of the aerofoil helps). The distance of the probe from the trailing edge can be measured, and a straight line from the position on the tunnel wall to the position of contact with the aerofoil indicates the lean of the probe. The points plotted in figure [5.15] lie along this line. An error in the horizontal position of the probe is not so serious as an error in the vertical position. Figure [5.15] gives an indication of overall positioning errors.

Results at both 5 and -5 degrees are shown in figure [5.16], and at 10 and -10 degrees in figure [5.17]. Theoretical streamlines are shown for comparison. Though the general trend is the same, there is an obvious discrepancy between theory and experiment. The observed streamlines are less curved or deflected than the predicted streamlines. This discrepancy is presumably associated with smaller circulation on the aerofoil than would be expected theoretically. Thus the lift on the aerofoil is smaller, and this is corroborated by the discrepancy in the pressure distribution referred to above. As described by Goldstein[34], these effects were also observed by Tanner[35] and by Bryant and Williams[36]. It is implied that since the observed lift is smaller, the Kutta condition is not present on the aerofoil.

The theoretical model is inviscid, so the discrepancy could be attributed to the effect of the boundary layer. However, at this Reynolds number (200,000), the boundary layer will be so thin that it is difficult to believe that it could have any direct effect upon the lift. Instead, there may be an indirect effect, where the boundary layers may affect the Kutta condition so as to 'weaken' it. When an aerofoil is started from rest, there is no initial circulation. This means that the rear stagnation point does not correspond to the trailing edge (figure [5.18]). A starting

vortex is shed, and after a long time the rear stagnation point has moved back to the trailing edge. This is of course a well-known piece of theory, but it is of interest to quantify the actual motion of the stagnation point near the trailing edge. The Martensen method has been performed with aerofoil NACA 0012 at ten degrees angle of attack (without the mirror images). Instead of the Kutta condition computer program, another short program was used, which applied a condition of known circulation (so repeatedly running this program would, by trial and error, yield the circulation giving the Kutta condition). With zero circulation, it was found that the rear stagnation point was at a distance of 1% of the chord from the trailing edge, which is much smaller than the way in which figure [5.18] is usually drawn in textbooks. The position of the stagnation point for other values of circulation is shown in figure [5.19]. A quick estimate of boundary layer thickness for a laminar boundary layer is just

$$\frac{1}{\sqrt{Re}} \lesssim 0.002 \quad \text{(Chord lengths)}$$

As an order of magnitude, this is comparable to the motion of the trailing edge stagnation point, so it is credible that the boundary layer could affect the Kutta condition, and the observed reduction in lift compared to

the theoretical value can be understood. A method of predicting the interaction between boundary layer and trailing edge has yet to be developed. The computer program described in the next chapter is a beginning, though it would need either a much bigger computer than any existing at the moment, or the application of a vortex-in-cell method (Christiansen[11]) which can describe the aerofoil boundary layers in greater detail.

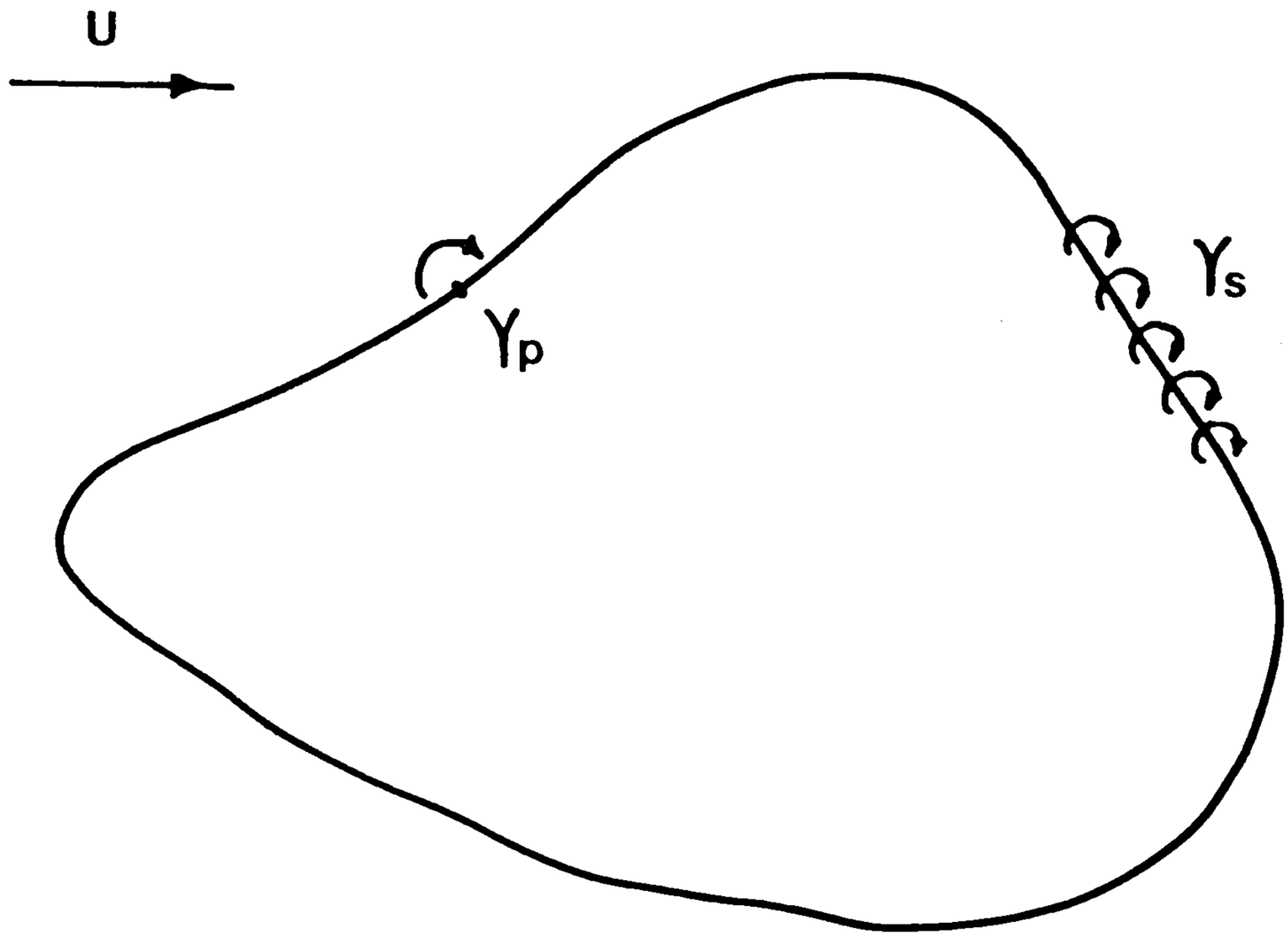

Figure 5.1 The Martensen Method

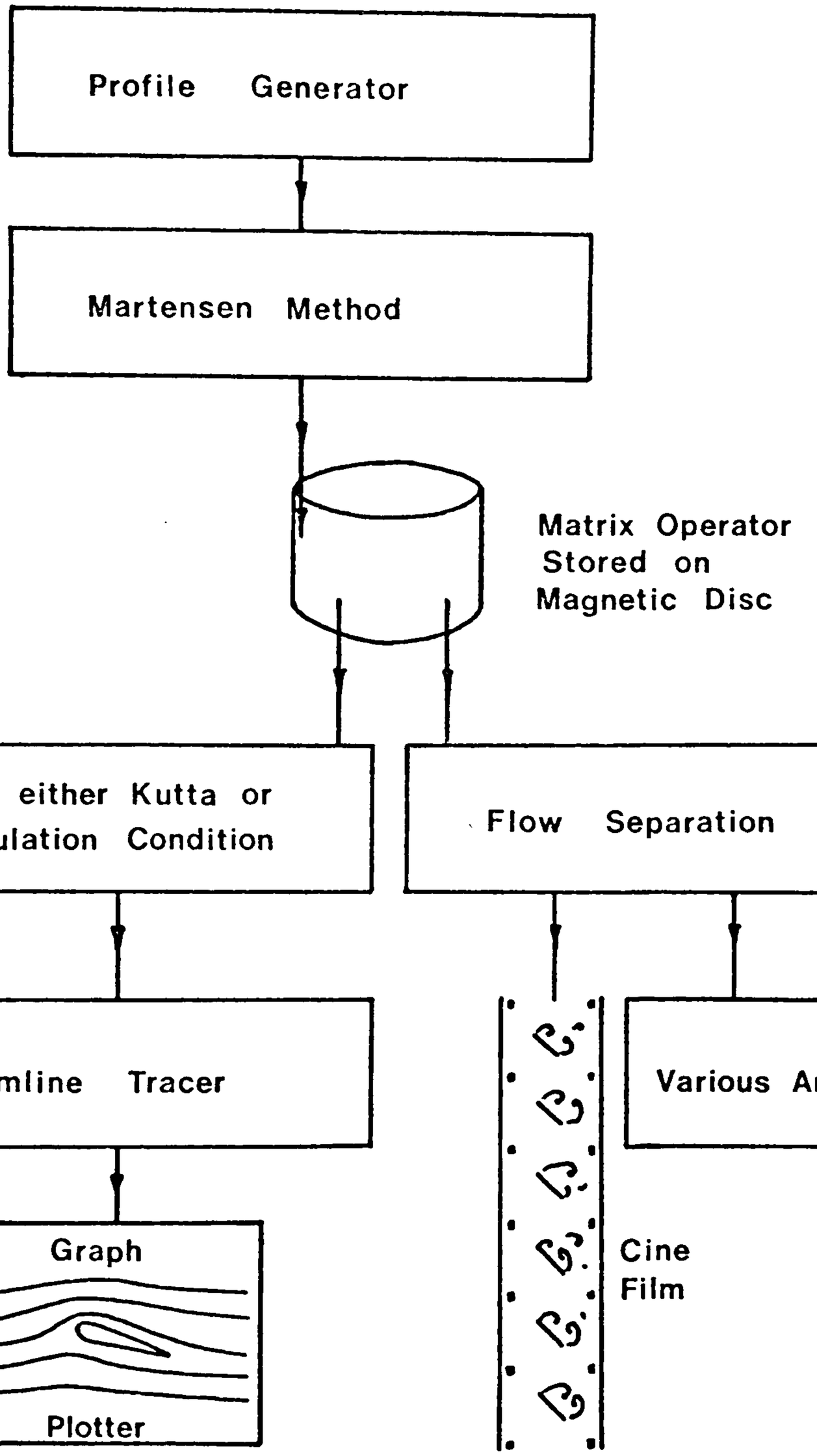

Figure 5.2 The Computational System

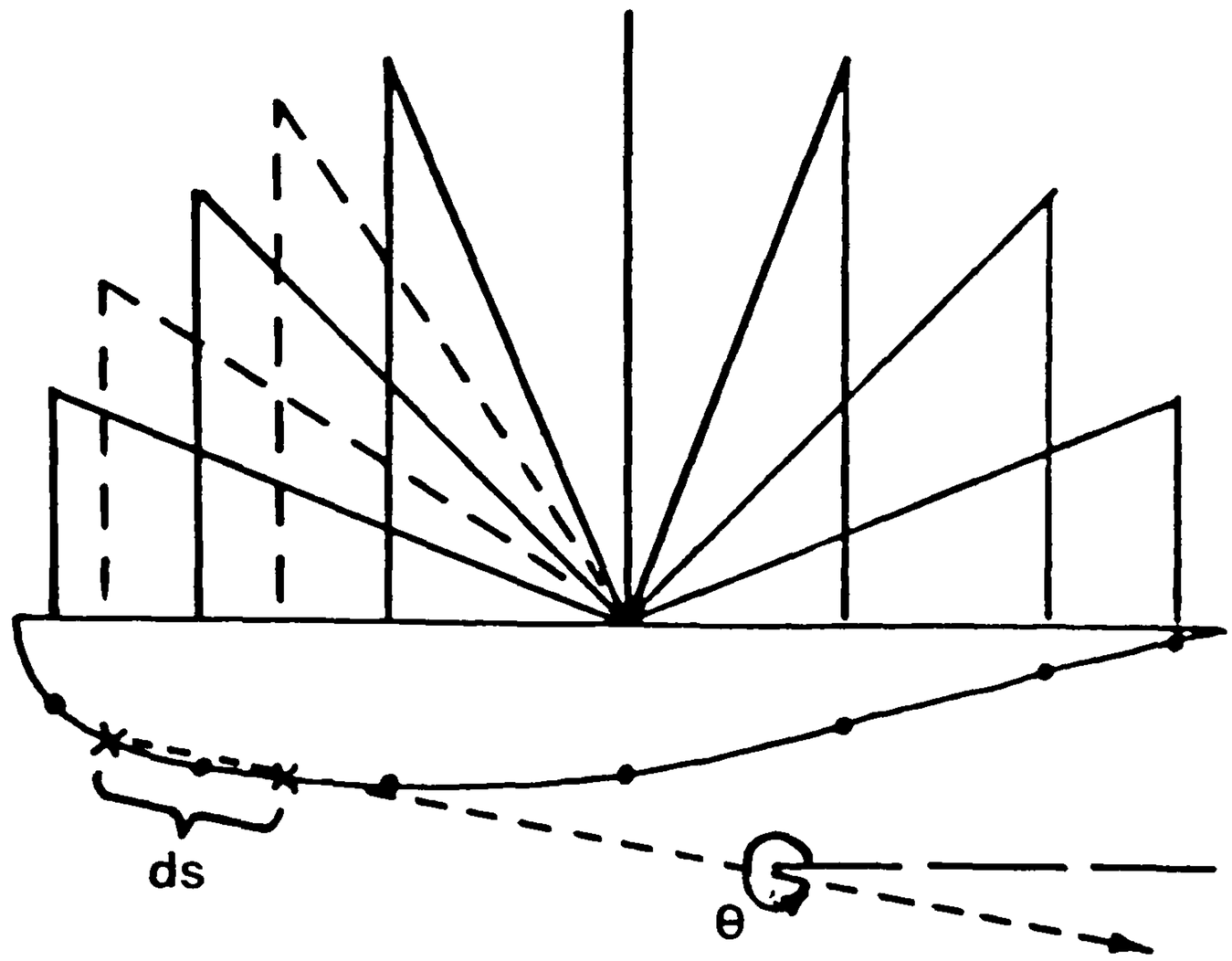

(a) An Aerofoil

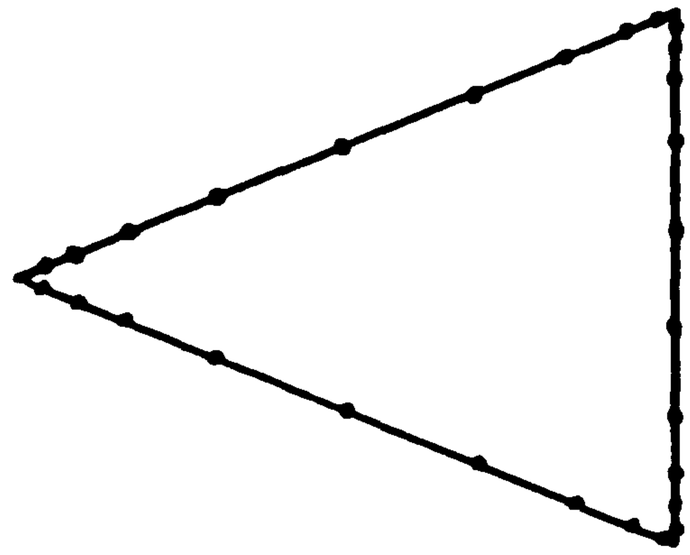

(b) A Wedge

Figure 5.3 Generation of a Profile with Pivotal Points packed in Sensitive Positions

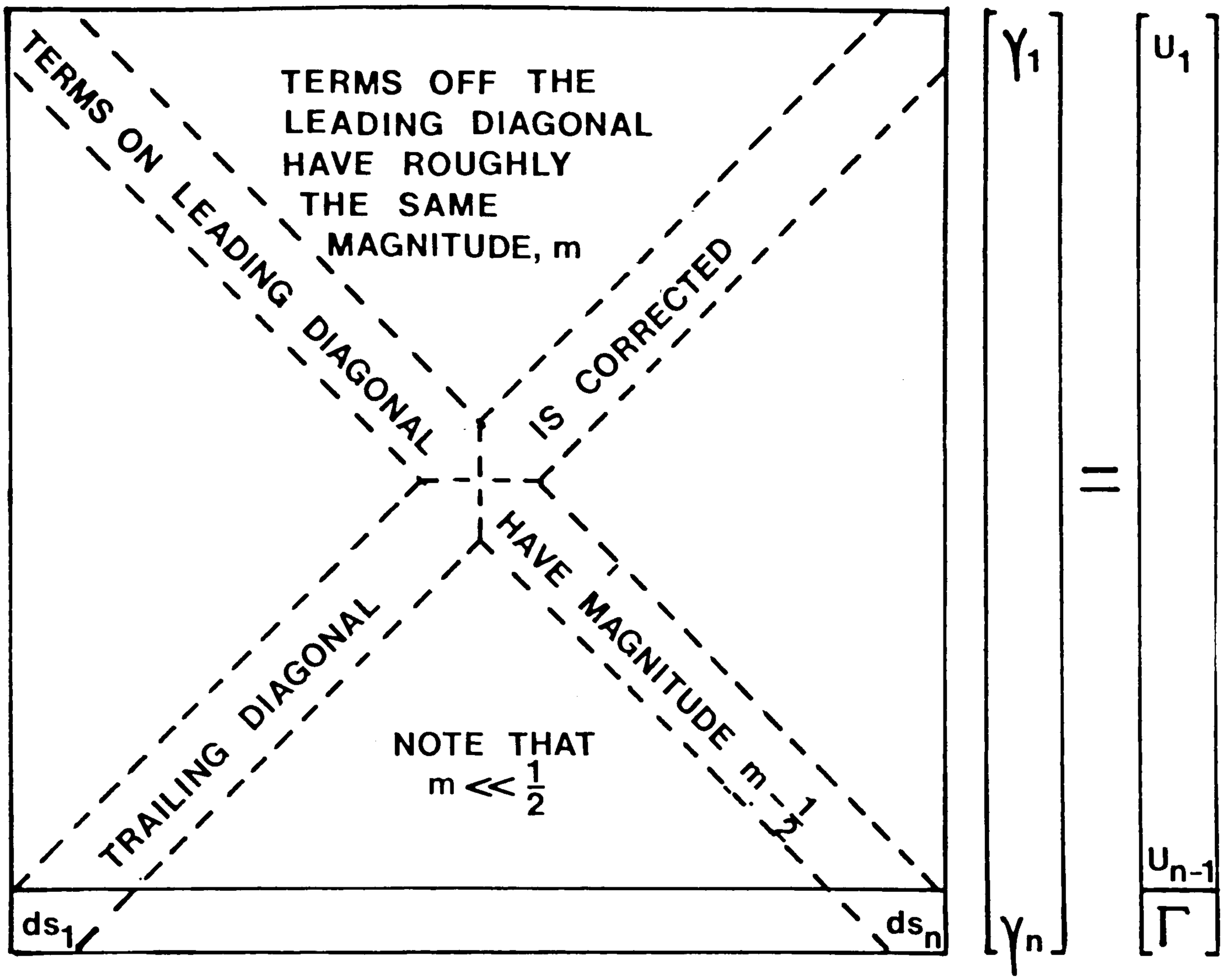

Figure 5.4 The Matrix before Inversion

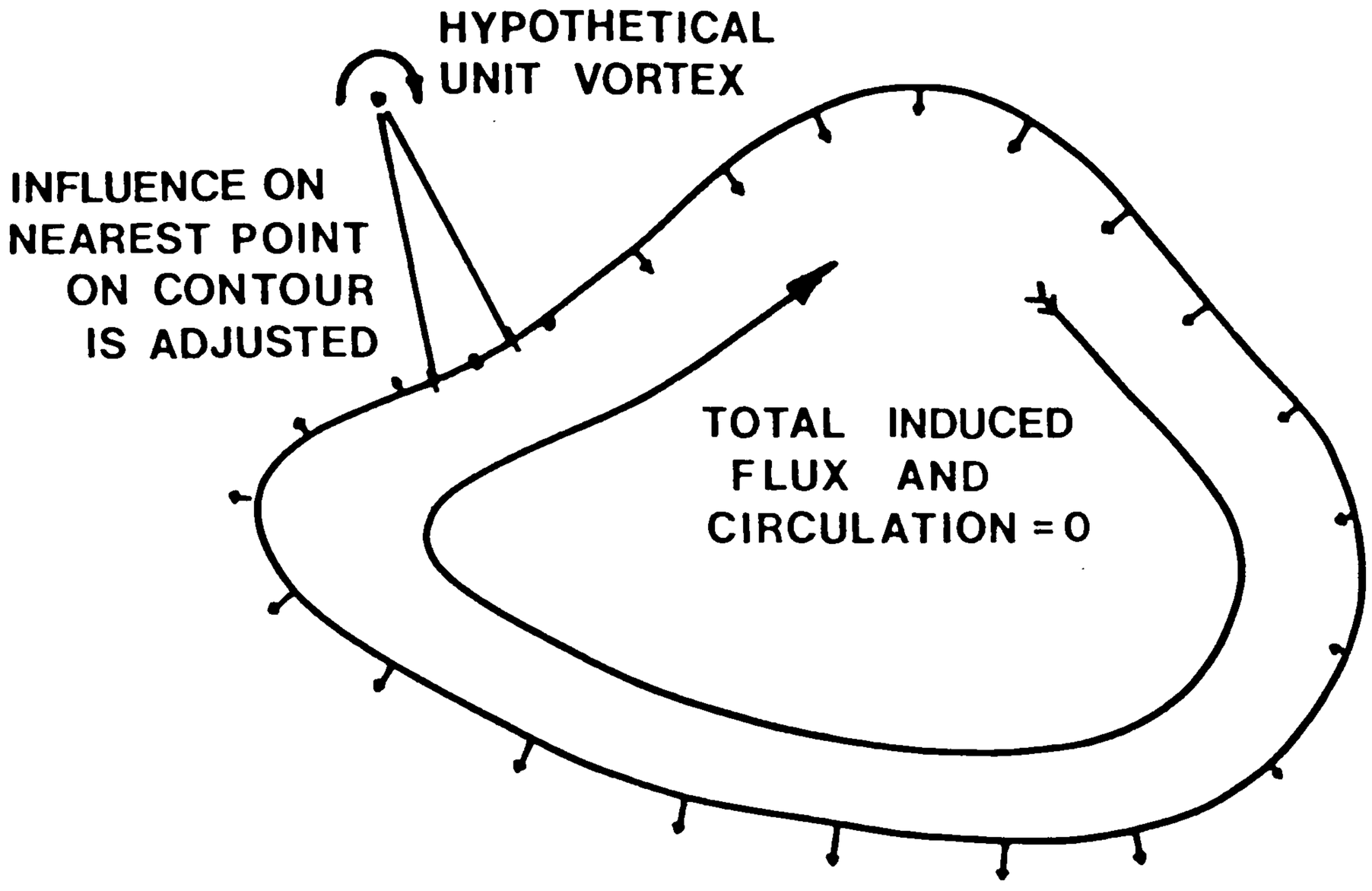

(a) Correction of the Coupling Vector

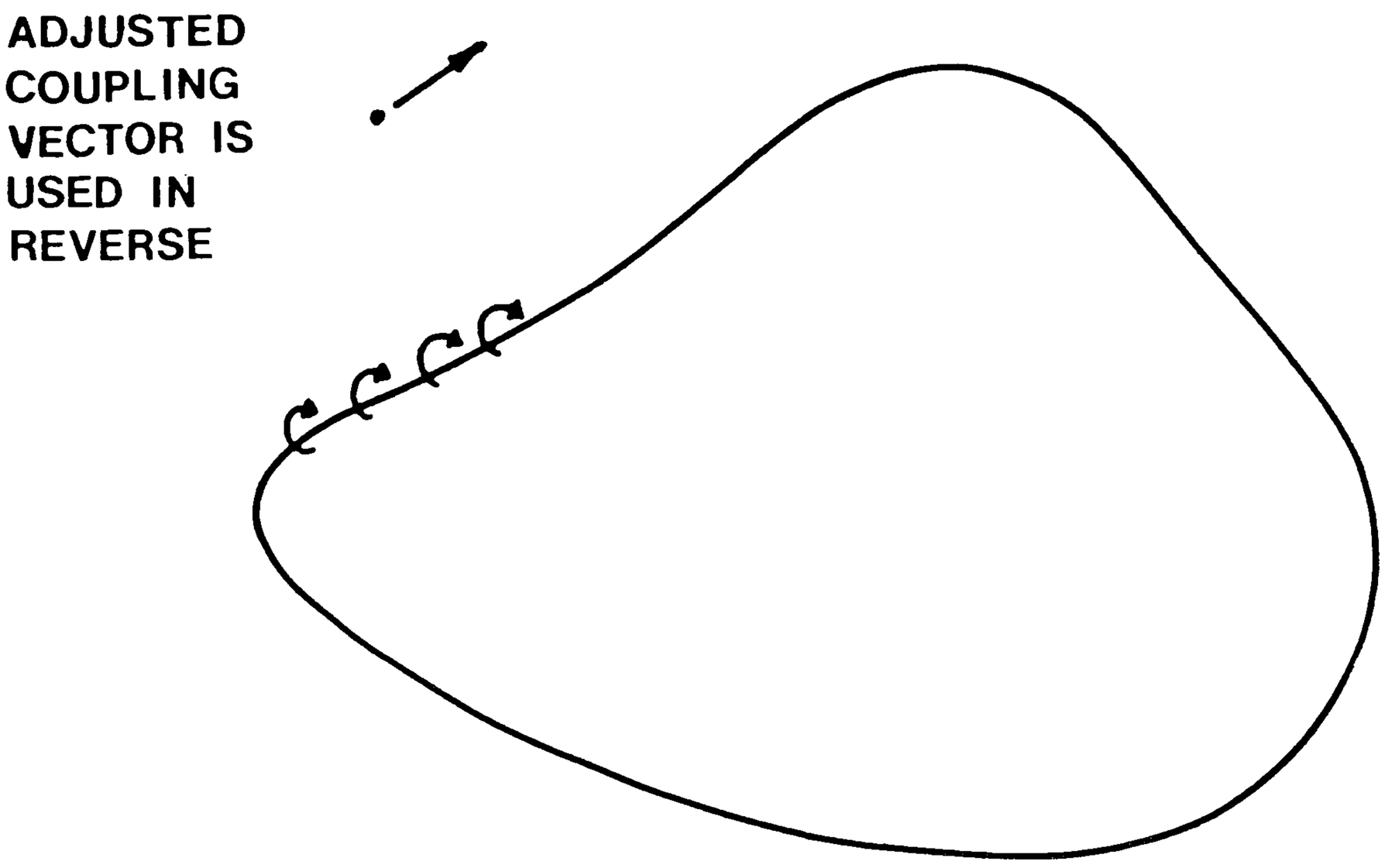

(b) 'Action and Reaction are Equal and Opposite'

Figure 5.5 The Method of Obtaining Sensible Flow Velocities near a Contour

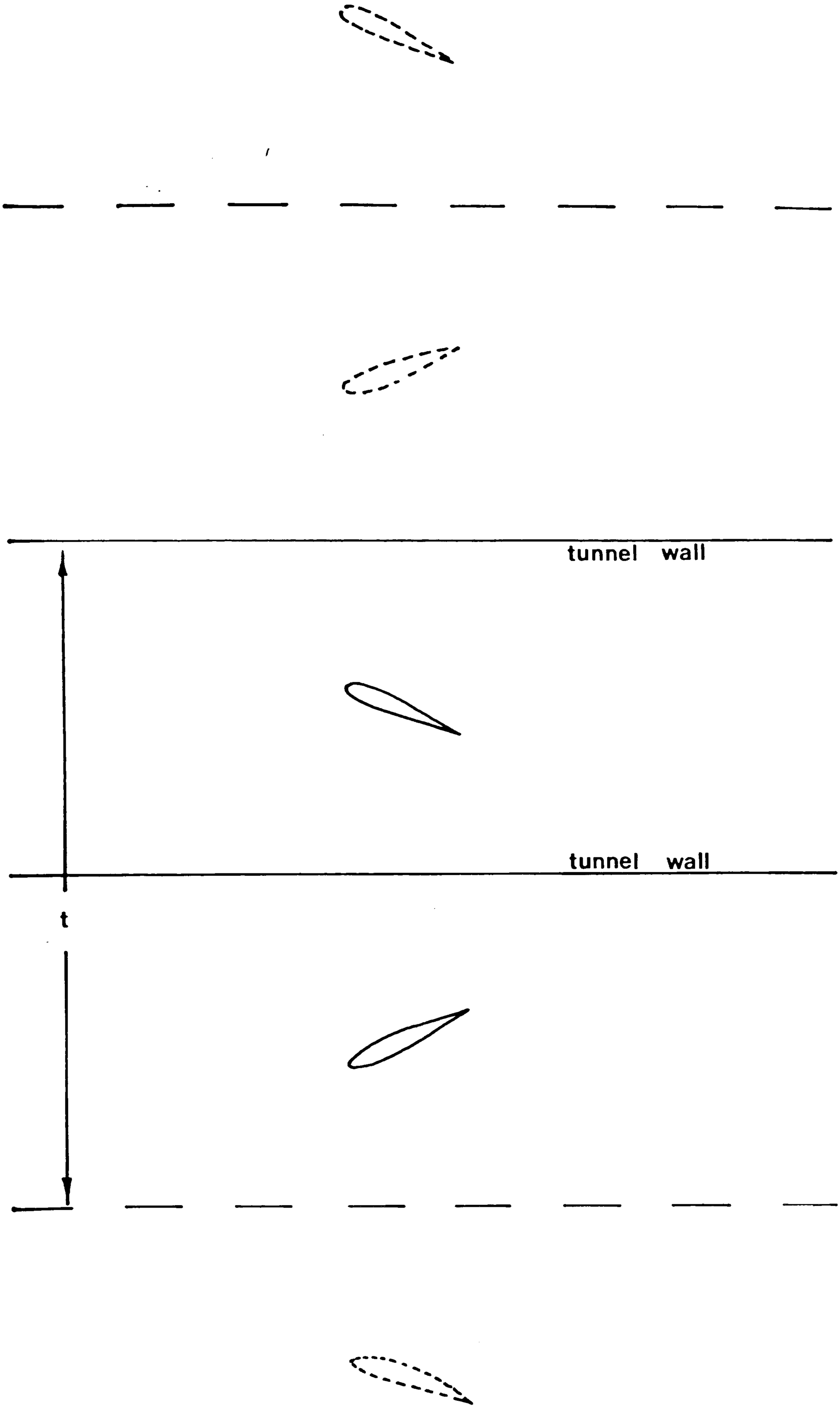

Figure 5.6 The Aerofoil and its Image System

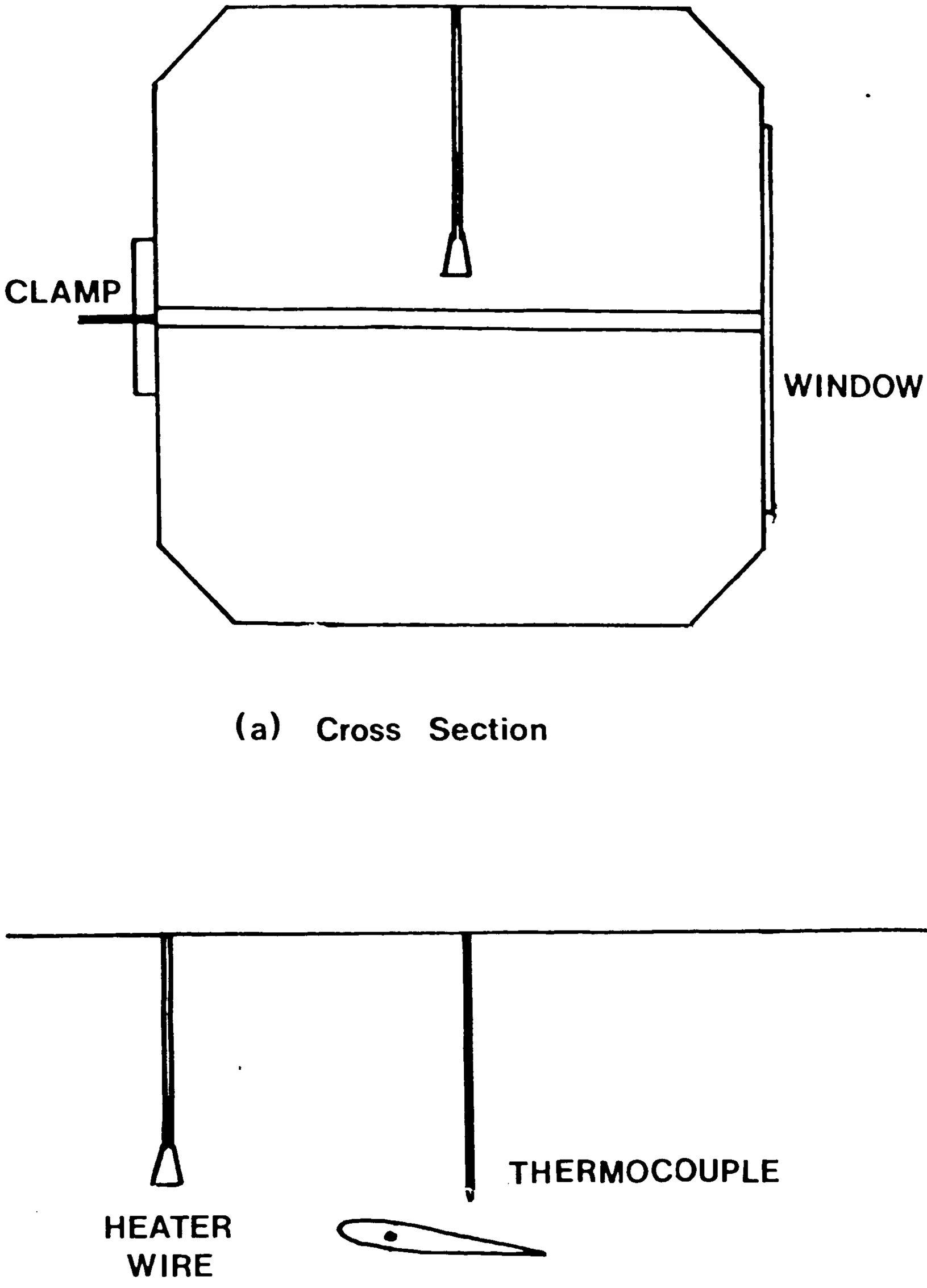

(a) Cross Section

(b) Side View

Figure 5.7 The Aerofoil in the Wind Tunnel

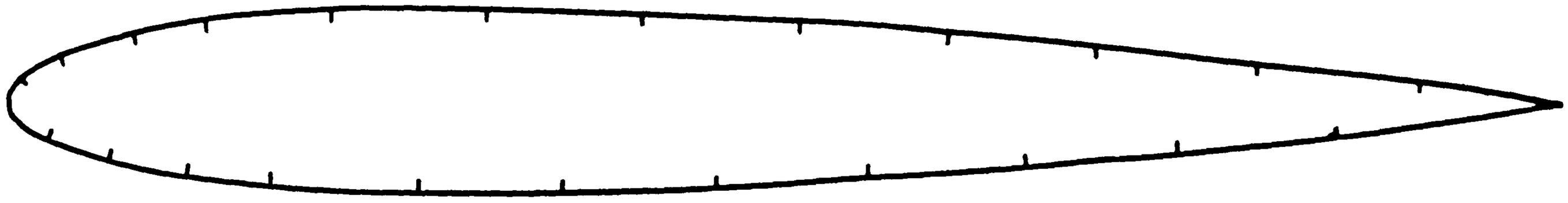

Figure 5.8 The Pressure Tappings on Aerofoil NACA 0012

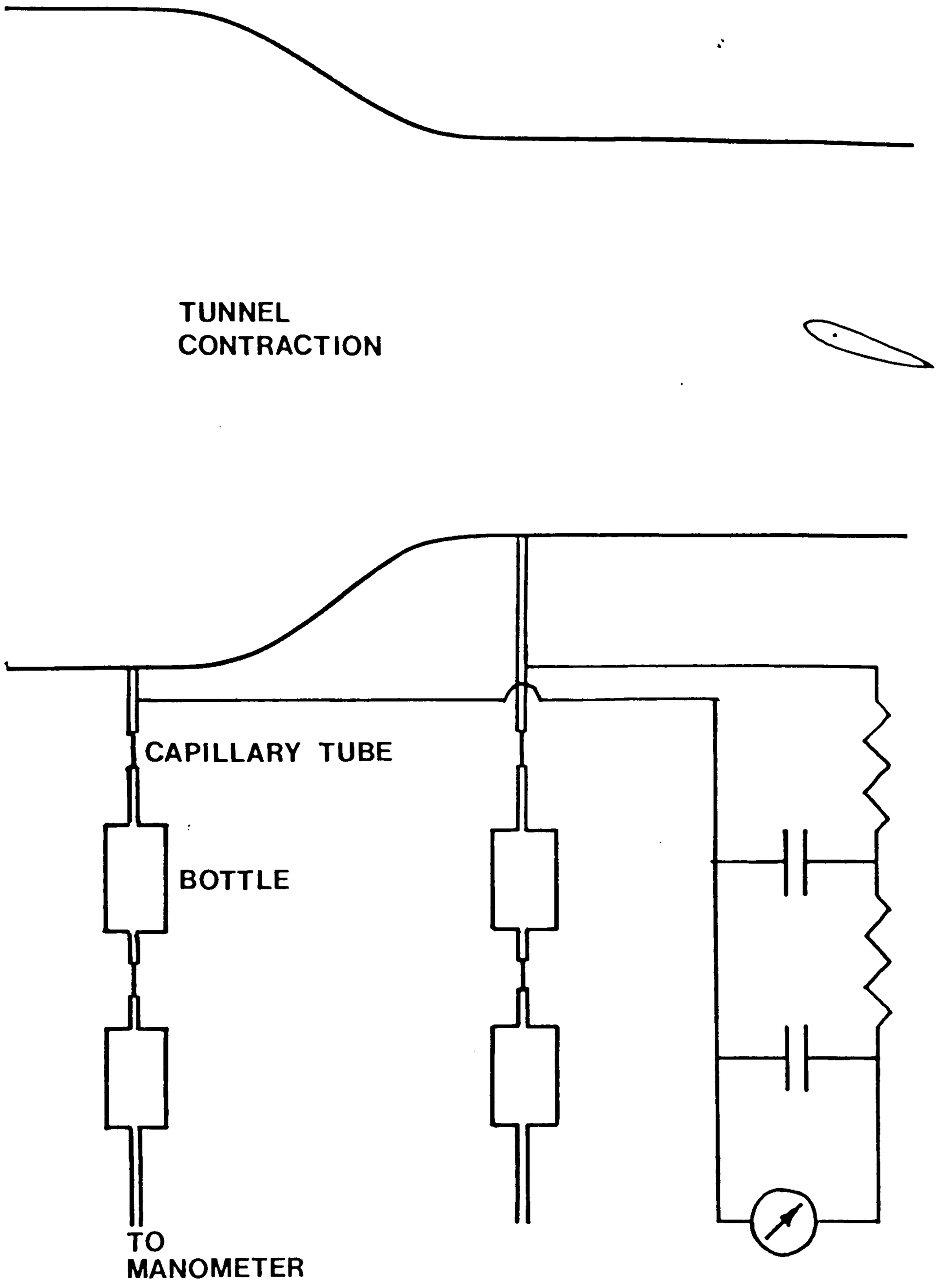

Figure 5.9 The Damping of the Pressure Signal, with an Electrical Analogy

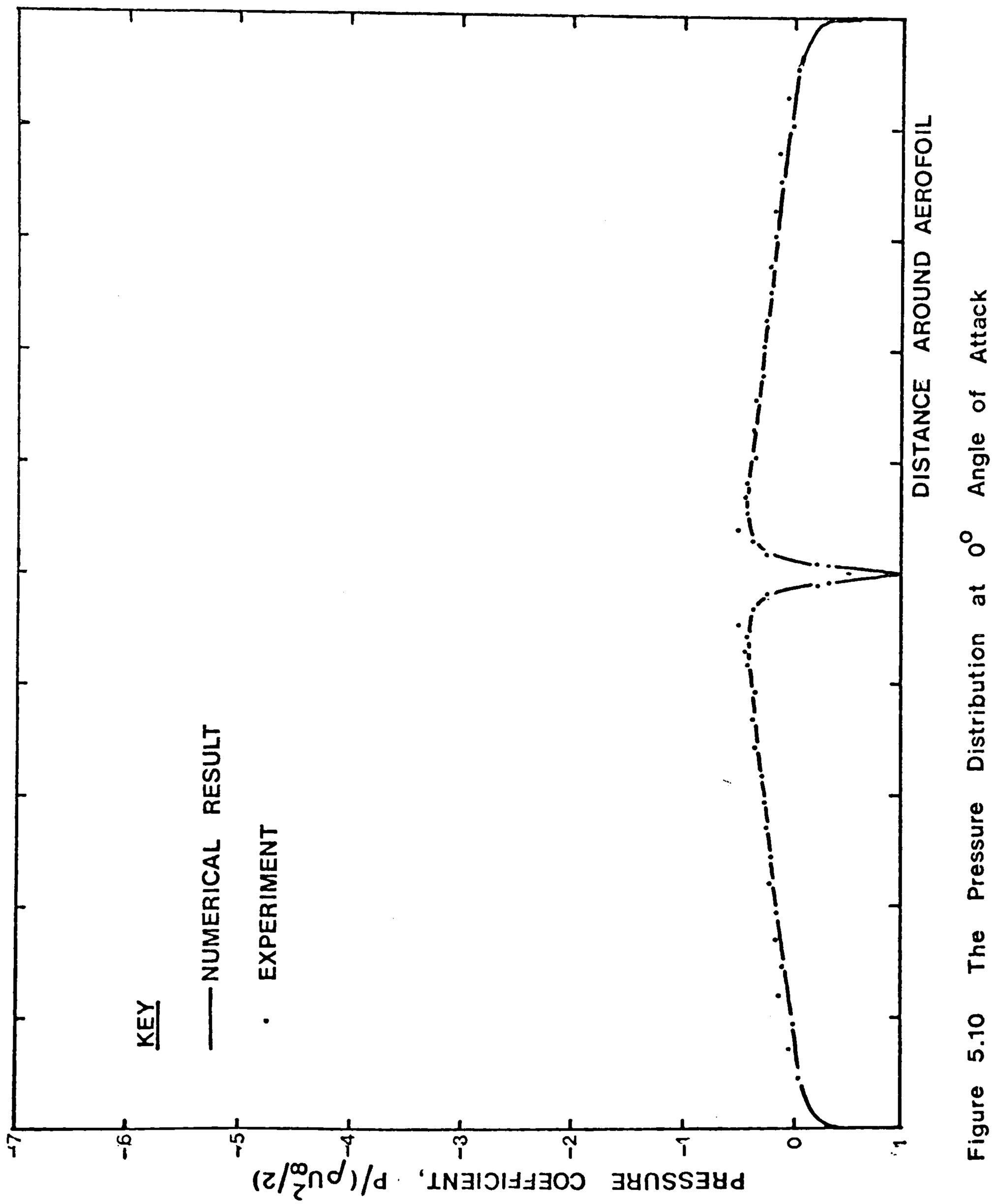

Figure 5.10 The Pressure Distribution at 0^o Angle of Attack

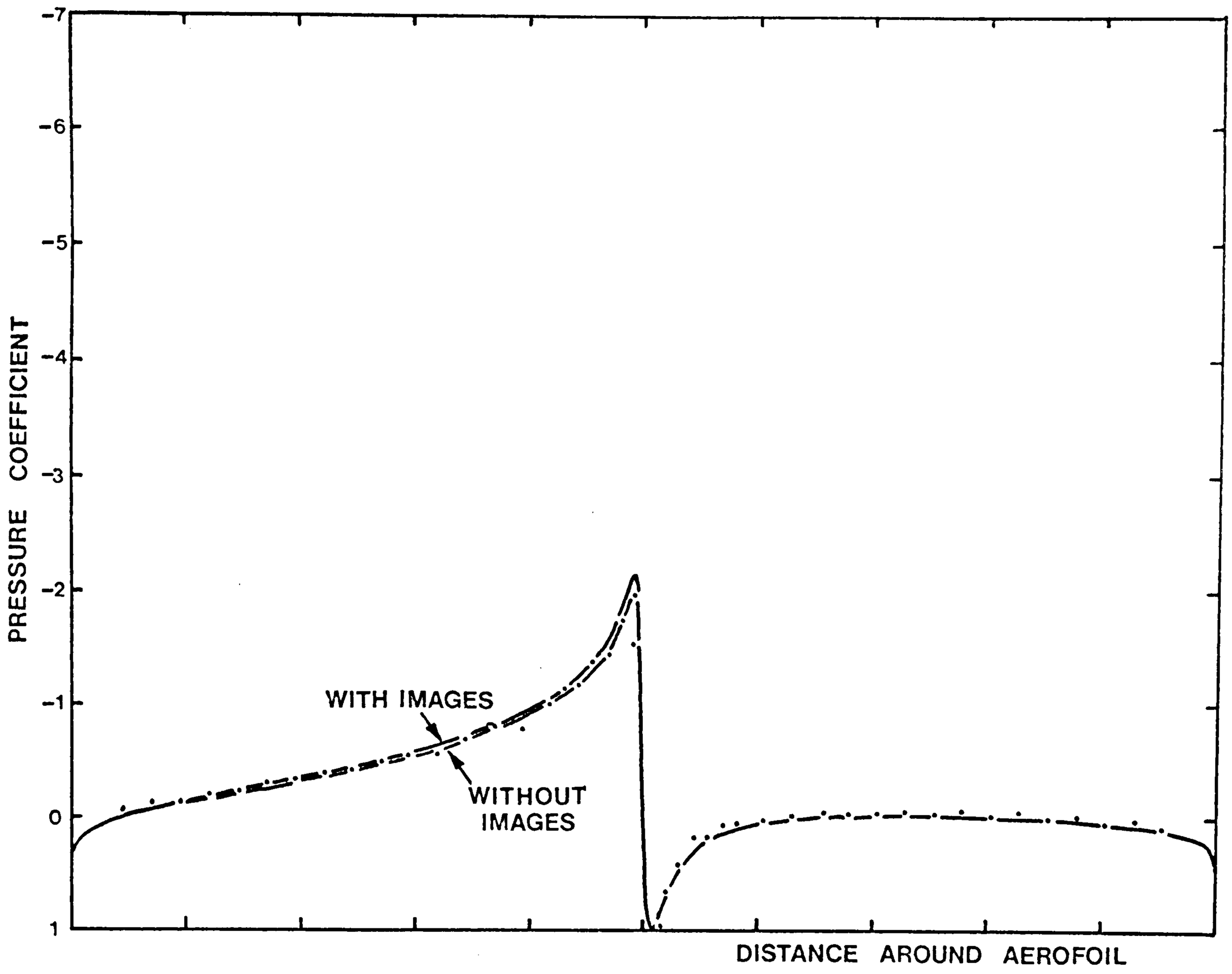

Figure 5.11 The Pressure Distribution at 5^{o} Angle of Attack

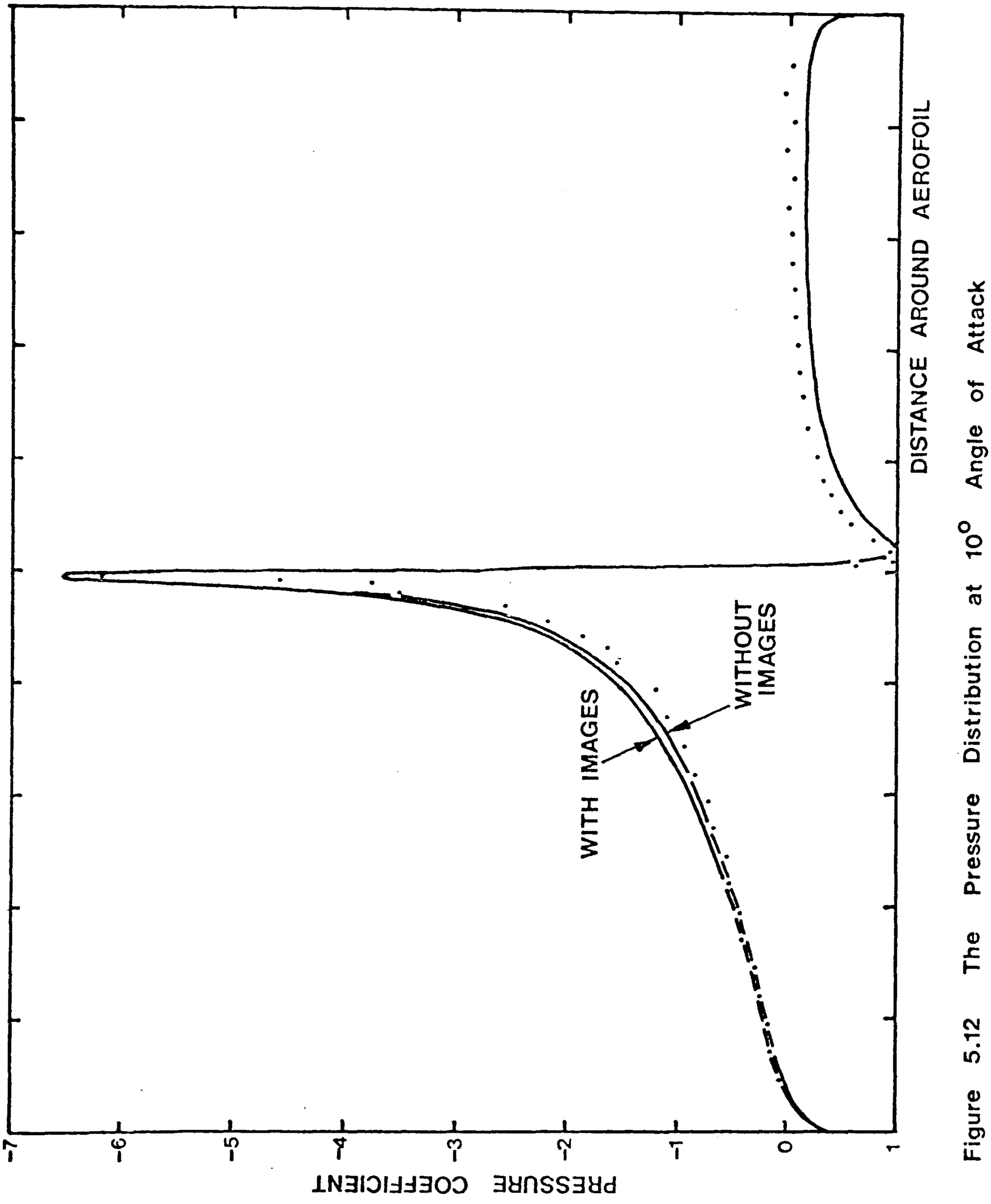
The Pressure Distribution at 10° Angle of Attack
DISTANCE AROUND AEROFOIL
WITH IMAGES
WITHOUT IMAGES
PRESSURE COEFFICIENT
-7
-6
-5
-4
-3
-2
-1
0
1

Figure 5.12

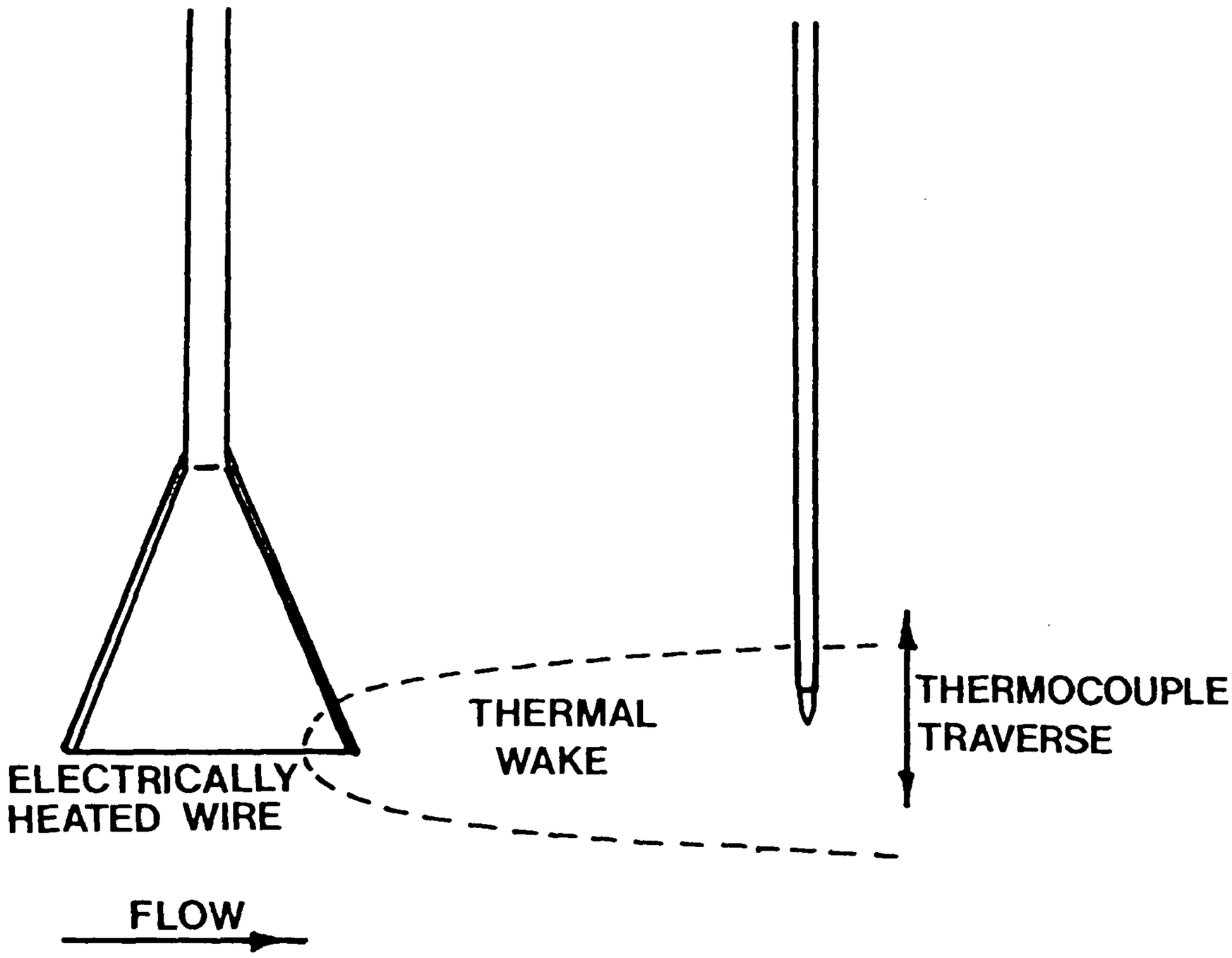

Figure 5.13 The Detection of the Wake downstream of a Heated Wire

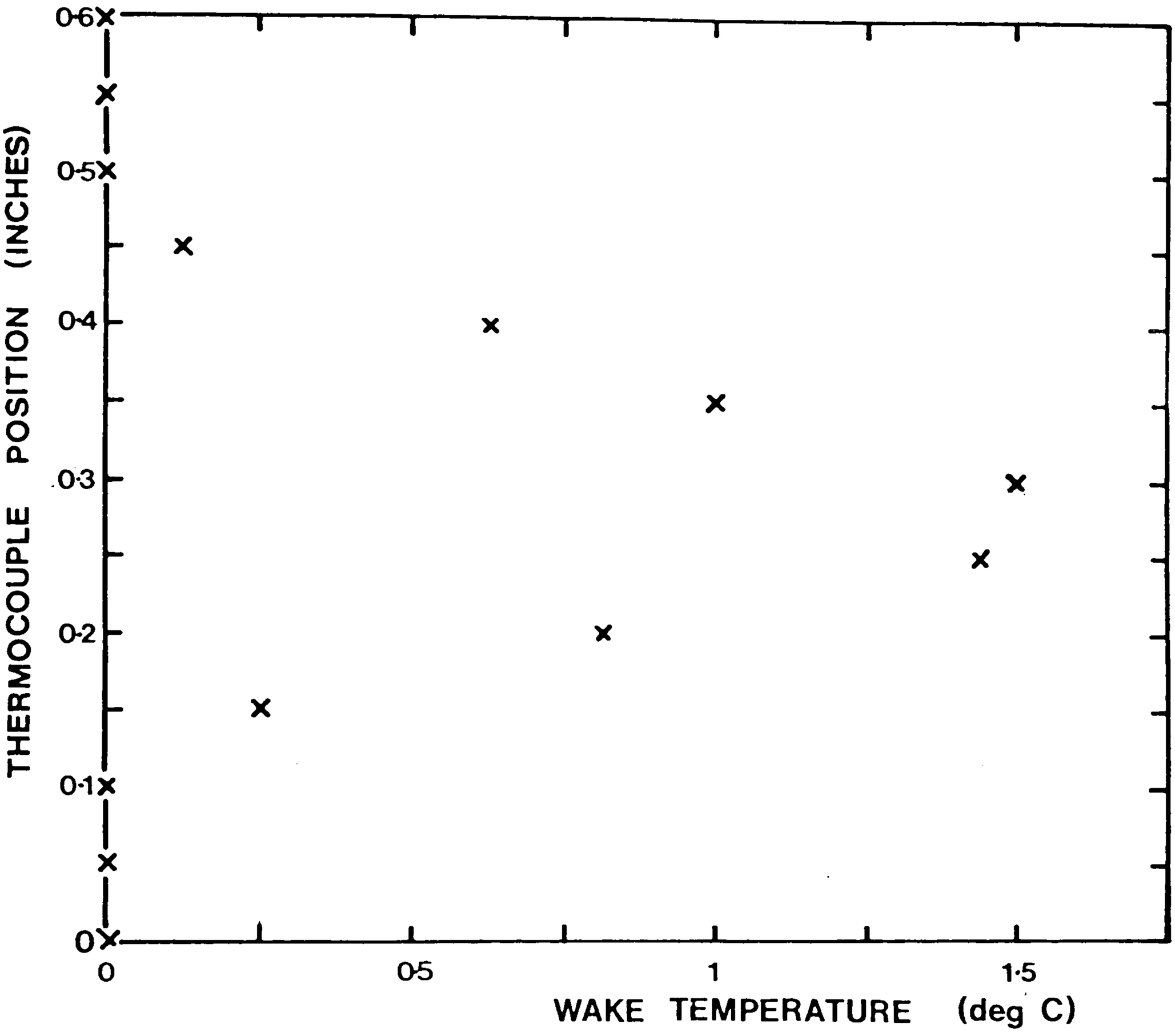

Figure 5.14 A Typical Wake Temperature Profile

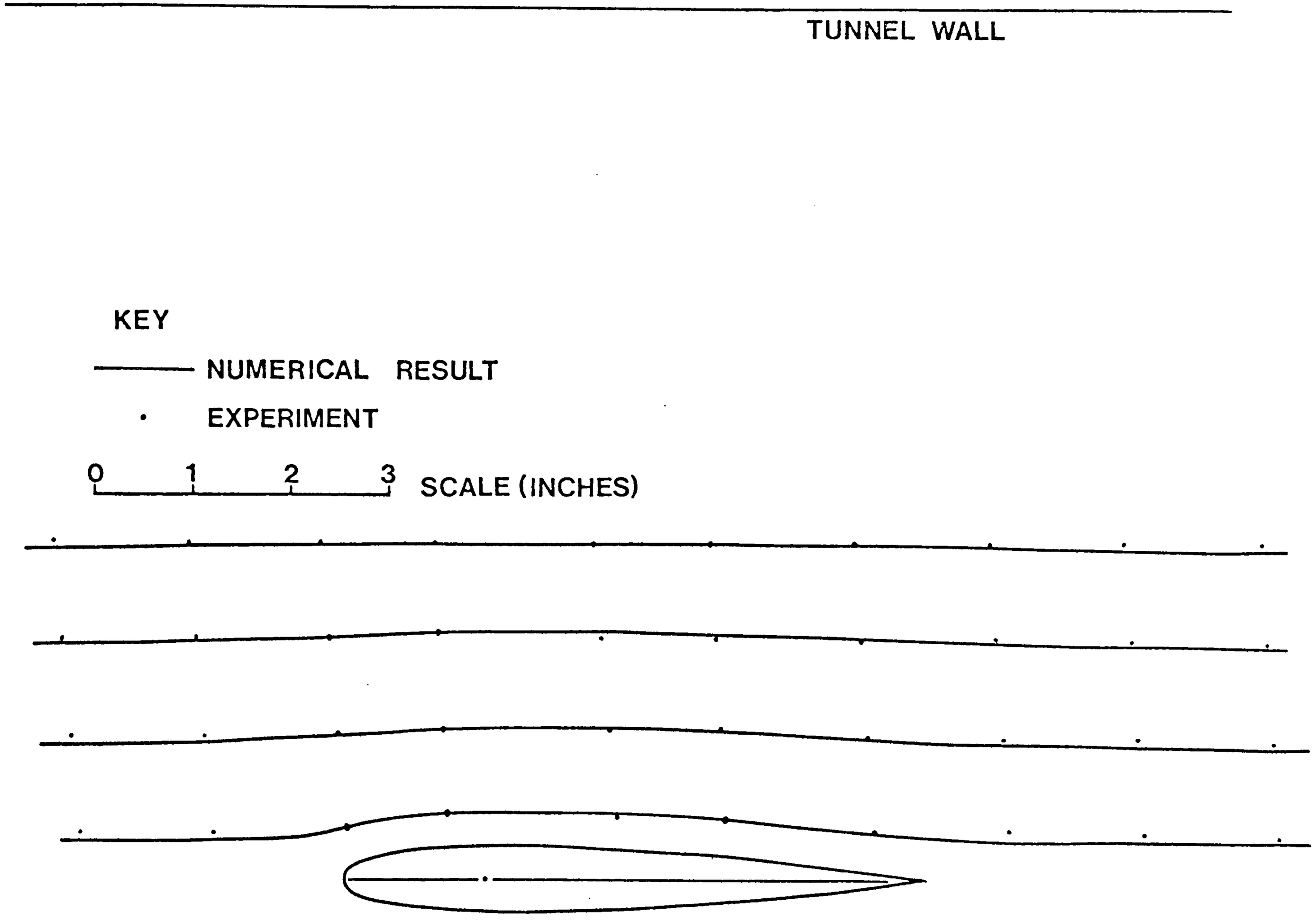

Figure 5.15 Streamline Tracing at 0^{o} Angle of Attack

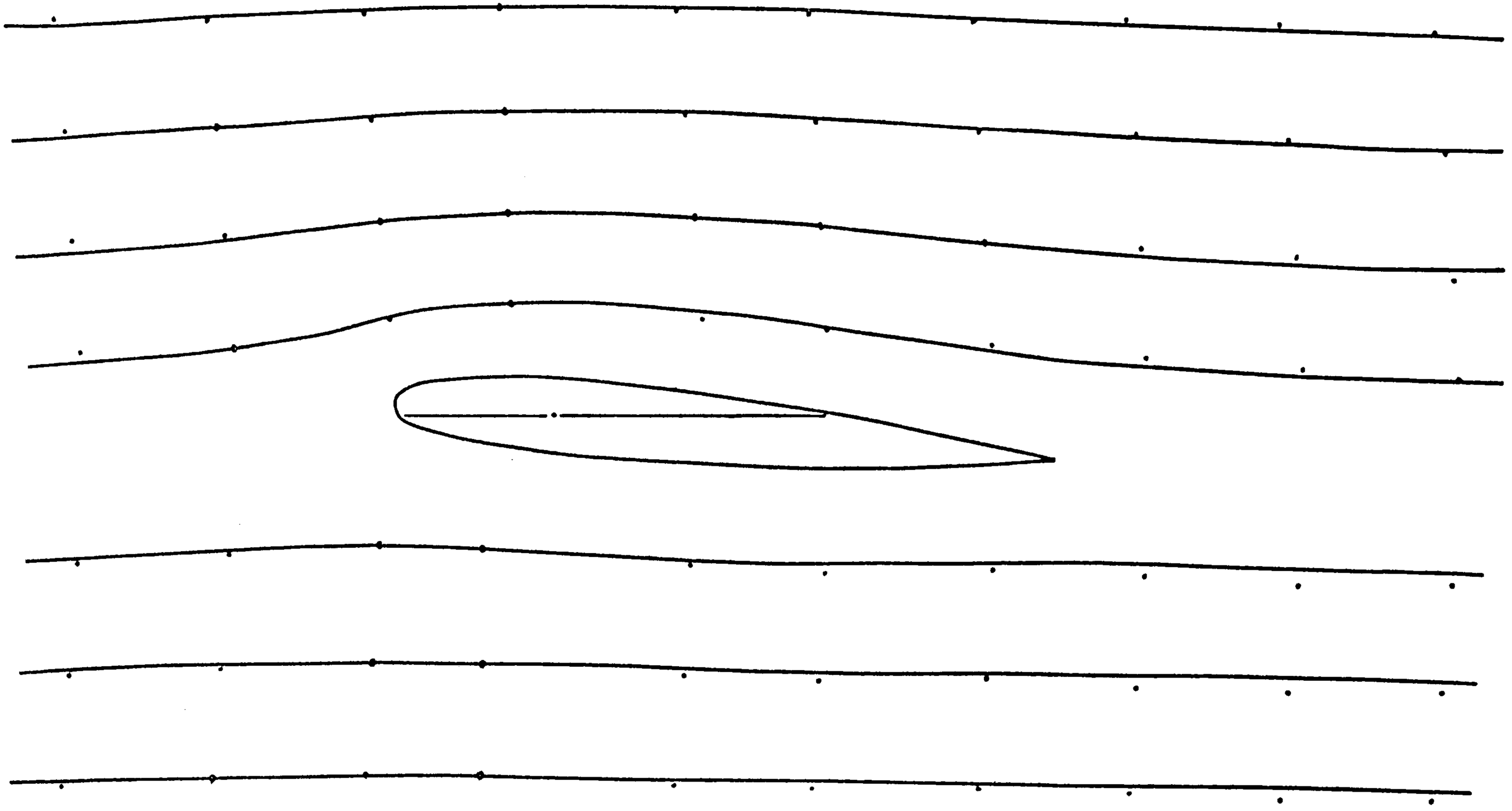

Figure 5.16 Streamline Tracing at 5^{o} Angle of Attack

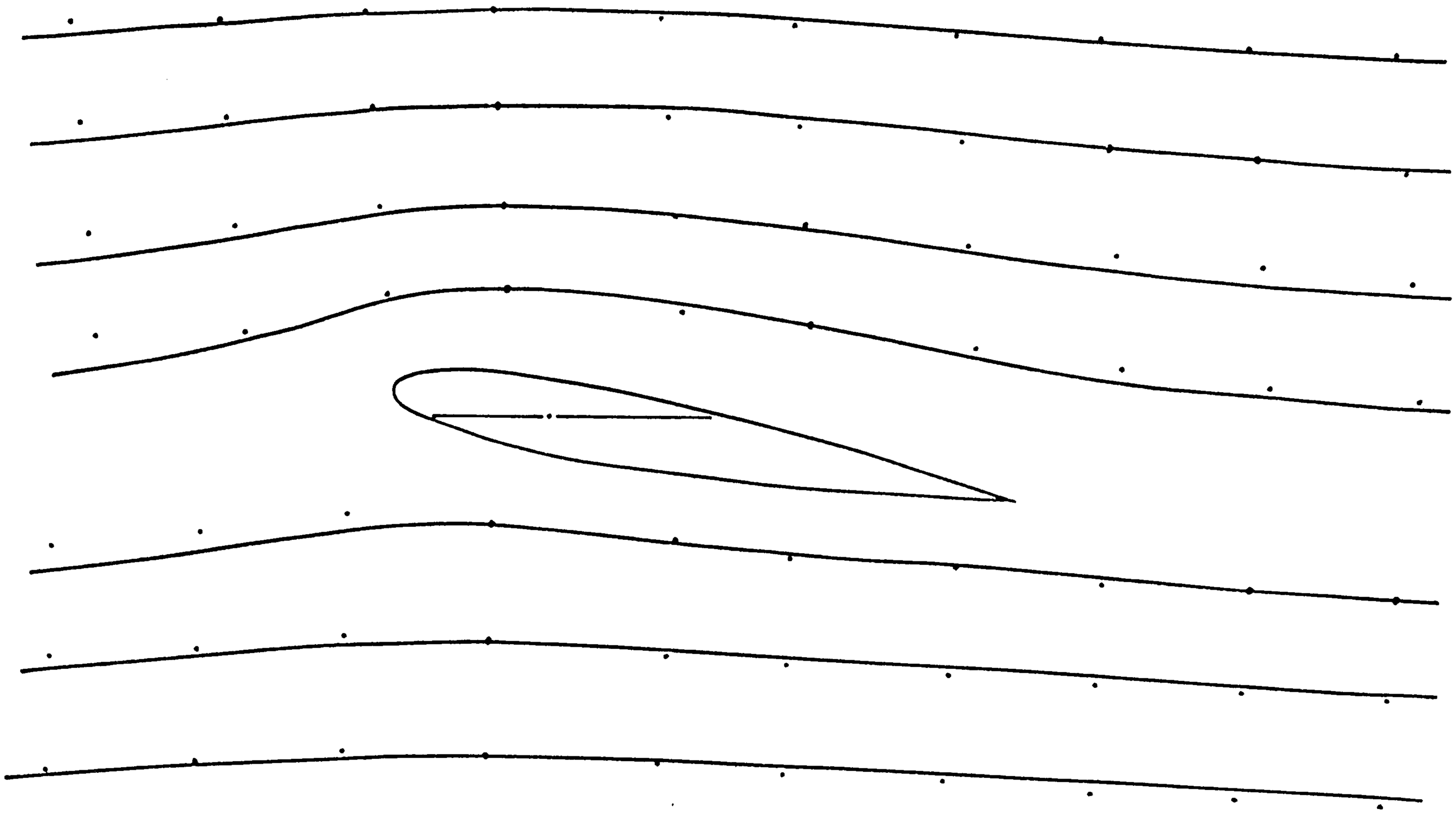

Figure 5.17 Streamline Tracing at 10^{o} Angle of Attack

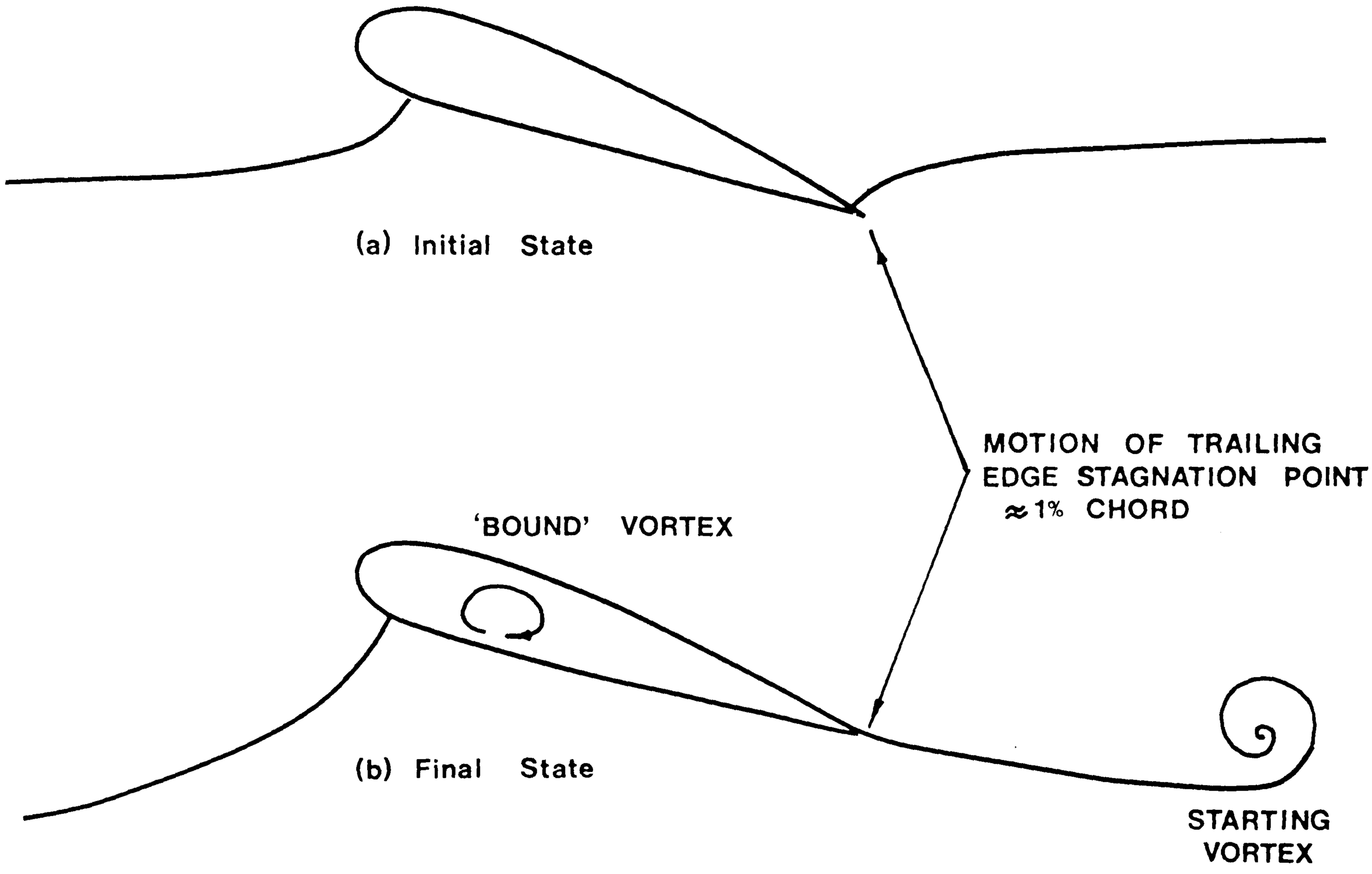

Figure 5.18 The Establishment of the Kutta–Joukowski Condition

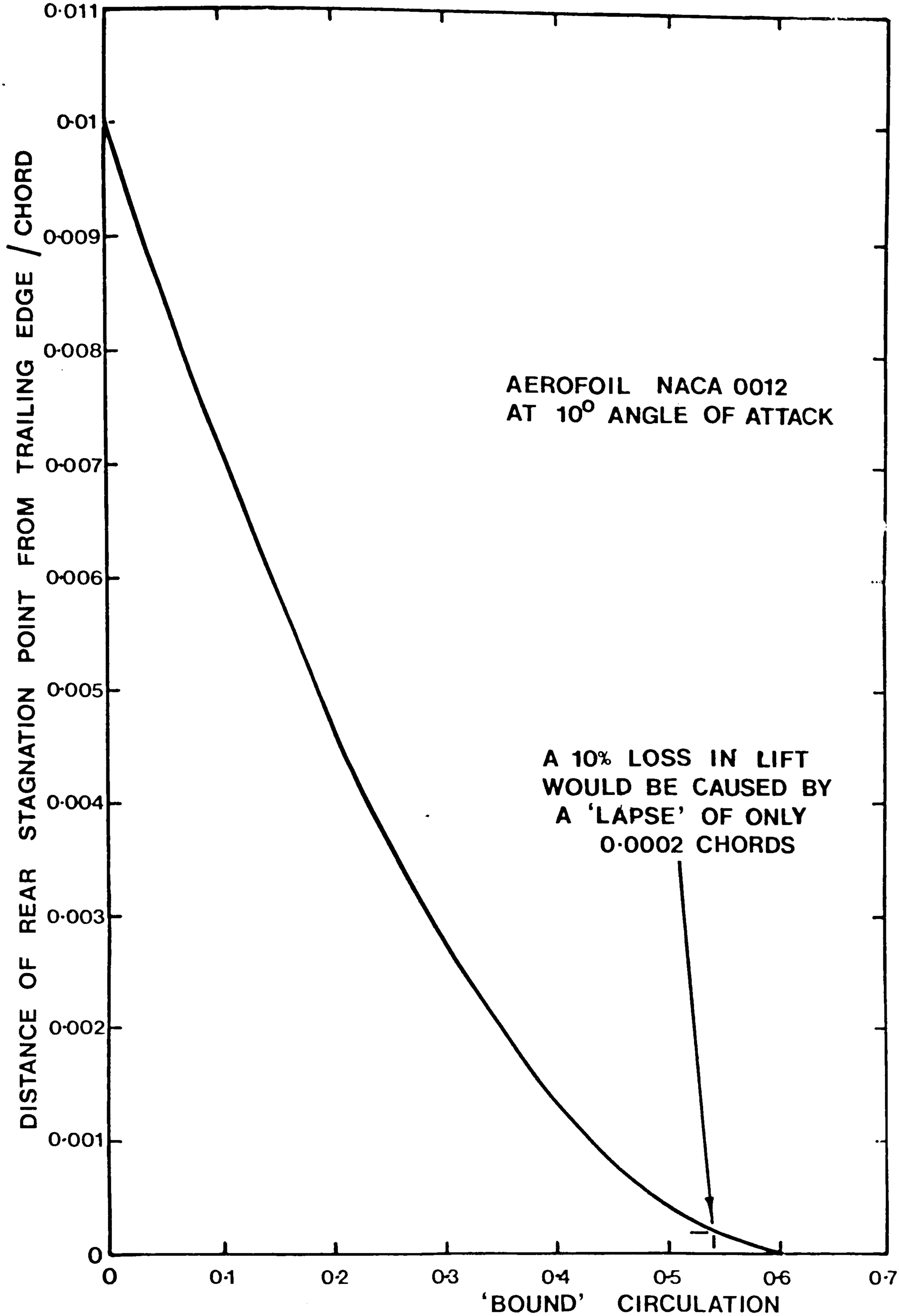

Figure 5.19 A Numerical Study of the Rear Stagnation Point

CHAPTER 6. THE BLUFF BODY COMPUTER PROGRAM

The themes of the boundary layer program and the Martensen Method will now be brought together to produce a computer program which can simulate flow separation from bluff bodies of arbitrary shape. When a body is instantaneously or impulsively started from rest, all the vorticity is on the surface of the body, and without the action of viscosity, that is where it would stay. However, the diffusion of vorticity to just a small distance away from the body introduces radical changes in the flow, so that vorticity may escape from the body by flow separation, and leave a residue of opposite vorticity near the body. In the case of an aerofoil, this residual vorticity produces the desired lift force.

The vorticity initially present on the body can be computed by the Martensen Method. The condition that there is no net circulation on the body is imposed, since if there is not zero total vorticity in any flow, then that flow would have infinite angular momentum! Before anything happens to this vorticity, there is no lift on the body, and the drag is zero or infinite depending upon whatever paradox one wishes to invent. The vorticity diffuses away from the body, which can of course be simulated by the random vortex method. At the trailing edge of an aerofoil, there would be a flow separation by the mechanism described in Chapter 4. If the angle

of attack is too high, there could also be a separation from the leading edge, in which case the aerofoil is said to be stalled. These phenomena can be simulated by the computer program described in this chapter.

The computer program has undergone considerable development, and its past history is outlined by Lewis and Porthouse[37]. Earlier models of flow separation were found to be inadequate, and even if they were successful, they would have been open to the objection of arbitrariness in the modelling. The model presented here makes some attempt to simulate the body's boundary layers without prejudging the course of events, so that it is left to the flow to establish itself. As the program has been developed, it has actually become shorter and simpler, which in the author's experience is rare among computer programs. Only the latest version of the program will be described.

A general description of the program is given in Section 6.1. In Section 6.2, the relation between vortex fluxes onto and off the contour and the pressure distribution is described in detail, since the obvious aim of this work is to predict lift and drag on bluff bodies. In a sense, Section 6.2 describes one half of the program. The other half, the free vortex dynamics, is mentioned briefly in Section 6.3.

6.1 GENERAL DESCRIPTION OF THE PROGRAM

Suppose that the flow has developed for some time. There is now a contour and a cloud of free vorticity around it (figure [6.1]). Perhaps by the random motion of diffusion, some of the vorticity has crossed the contour, lying inside it in the nominally solid body. It is the task of the part of the program which applies the Martensen Method to ensure that the surface speed on the contour is everywhere zero, which implies of course that there is no bound vorticity on the contour, and no free vorticity inside it.

For the moment, the contour is permitted to have some bound vorticity. All the vortices lying inside the contour are annihilated, but their strengths are added together and the bound vorticity of the contour is made equal to the sum. This will be seen to guarantee conservation of vorticity. The matrix operator from the Martensen Method is applied to the flow around the contour induced by all vortices outside the contour (we have just dealt summarily with vortices inside the contour). This gives the flow speed, u_i, at each pivotal point around the contour. If it should be found that there are places on the contour where the computed speed is not quite zero, then new vorticity must be placed in the flow (figure [6.2]), just as in the

boundary layer program. The strength of the new vorticity is given by

$$\gamma = u_i \Delta s_i \tag{6.1}$$

The total strength of all newly created vorticity will naturally be equal to the bound vorticity of the contour, so that upon the creation of this new vorticity, the bound vorticity of the contour is lost back to the flow, and becomes equal to zero again.

In effect, a vortex which drifts inside the contour when it is inappropriate will vanish briefly into the bound circulation of the contour, but then it will be recreated by the application of the matrix operator and 'bounced' back into the flow. To a distant observer, the response of the contour to a nearby vortex gives the same flow as if the vortex had already been absorbed by the contour, with the appropriate change to the bound circulation of the contour. The contour reacts to a nearby vortex as if there were a mirror image of the vortex with opposite rotation within the contour (figure [6.3]) and this vortex doublet is relatively imperceptible to the observer. When a vortex is annihilated its image is also destroyed (echoing the boundary layer program), but the bound circulation of the contour must be adjusted so the strength of the annihilated vortex is not forgotten. Hence the interaction of such vortices with the contour is a local phenomenon, no matter how strong the vortices

might be, and the principle of conservation of vorticity is always observed.

For the sake of consistency with the boundary layer program, the newly created vorticity is placed at a distance away from the contour equal to

$$\sqrt{4 \nu \, dt/3}$$

which is a variance-conserving estimate of the previous position of vorticity which is now inside the contour, and which has to be put back into the flow.

Again on the theme of consistency, the circulation around the contour induced by an external vortex should be equal to zero (figure [6.4]). For every vortex, the circulation around the contour induced by that vortex is calculated assuming for the moment that the vortex has positive unit strength. This gives the method of detecting vorticity inside the contour, since the circulation will then be more than one half. If it is less than one half, but not zero (it could also be negative), the vortex must be outside the contour, but sufficiently close to a pivotal point to induce a potentially absurd velocity there. The influence of the vortex on the nearest pivotal point is corrected to make the circulation equal to zero. This idea has been met already in the boundary layer program, and in the

streamline tracing program in a more complicated form involving fluxes as well. It is the 'trade secret' of this work.

Once the new vorticity has been created, all vorticity is free vorticity, and the flow develops over the remainder of the time step as a configuration of free vorticity, where the contour might as well be absent. The presence of the contour is re-asserted on the next time step, when more vorticity is exchanged with the flow to preserve the no-slip condition. The computer program thus falls into two logical halves (Table 6.1). The significance of the matrix operator half for the pressure distribution is described in the next section. Some remarks on the vortex dynamics half are made in Section 6.3.

6.2 VORTEX EXCHANGE AND THE PRESSURE DISTRIBUTION

The application of the Martensen Method matrix operator reconciles the distribution of vorticity in the flow with the presence of a solid body with a no-slip condition at its surface. Vorticity inside the contour is removed, and new vorticity is put into the flow to make the flow speed at the surface equal to zero. The total strength of the newly created vorticity is equal to the total strength of the annihilated vorticity, by the principle of conservation of vorticity. This principle can be deduced

from the Navier-Stokes equation written in an appropriate form for incompressible flow

$$\frac{\nabla p_o}{\rho} = (\underset{\sim}{U} - \nu\nabla) \times \underset{\sim}{\omega} - \frac{\partial \underset{\sim}{U}}{\partial t} \tag{6.2}$$

or, as in Chapter 2, using the expected value of the vortex transport velocity

$$\frac{\nabla p_o}{\rho} = E(\underset{\sim}{U}) \times \underset{\sim}{\omega} - \frac{\partial \underset{\sim}{U}}{\partial t} \tag{6.3}$$

If this equation is integrated around any closed contour, we should return to the value of stagnation pressure that we started with. This closure of the pressure distribution is normally stated in the form for an infinitesimal contour

curl(grad(any scalar)) = 0

It was shown in Chapter 2 that the stagnation pressure may be obtained from the distribution of the moving vorticity. It follows that in order to obtain the closure of the pressure distribution around a contour,

$$\sum_i \Delta p_{o_i} = 0 \tag{6.4}$$

we must respect the principle of conservation of vorticity. This can be

seen by integrating equation (6.3) around a contour, giving a result which is best expressed in words

$$\begin{array}{c}\text{rate of change of}\\ \text{circulation within}\\ \text{contour}\end{array} = \begin{array}{c}\text{flux of vorticity}\\ \text{across contour}\\ \text{boundary}\end{array} \qquad (6.5)$$

The closure of the pressure distribution has been historically difficult to ensure in the computer program, and remains a problem in the work of Stansby and Dixon.[14]

Since on the body there is no slip, the stagnation and static pressures are the same, and equation (6.3) reduces to the rule

$$\begin{array}{c}\text{pressure gradient}\\ \text{along contour}\end{array} = \begin{array}{c}\text{vortex flux}\\ \text{across contour}\end{array} \qquad (6.6)$$

There is vorticity flowing across the contour in both directions. When vorticity is discovered inside the contour, the point at which it crossed the surface is assumed to be the pivotal point nearest to the vortex, which can be found in the process of calculating the influence of the vortex on the contour. Initially, the pressure gradient is assumed to be zero. When a vortex crosses into the contour, it causes a 'blip' to the pressure gradient at the nearest pivotal point (figure [6.5]) which decrements the pressure gradient as

$$\frac{\Delta p'_{o_i}}{\rho} := \frac{\Delta p_{o_i}}{\rho} - \gamma/_{dt} \qquad (6.7)$$

If the contour now has some bound circulation, there is for the moment no closure of the pressure distribution. This will be rectified when new vorticity is created, incrementing each value of the pressure gradient again

$$\frac{\Delta p'_{o_i}}{\rho} := \frac{\Delta p_{o_i}}{\rho} + \gamma_i/_{dt} \tag{6.8}$$

Since the sum of the two generations of vorticity in equations (6.7) and (6.8) is the same, the closure of the pressure distribution is ensured. The computer program has ben made to publish accounts showing that vorticity is indeed being conserved, that is

$$\sum_j \gamma_j = 0 \tag{6.9}$$

where it is assumed that there is no initial circulation, and that equation (6.4) is also true. Conditions (6.4) and (6.9) are now satisfied on every time step within the accuracy of the computer.

In the present case where there is zero flow speed on the contour, the stagnation and static pressures are equal. Equations (6.7) and (6.8) are just another way of stating Lewis'[13] equation (18)

$$\frac{1}{\rho}\frac{dp}{ds} = \frac{d\gamma}{dt}$$

or the first compatibility condition of approximate methods in boundary layer theory.

From the pressure distribution it is possible to obtain the lift and form drag forces on the contour by integration

$$C_L = - \oint p \cos \theta \, ds$$

$$C_D = \oint p \sin \theta \, ds \qquad (6.10)$$

where it is apparent that the pressure has been expressed in absolute units. The skin friction drag, though possible to obtain in theory by the method applied to obtain the shear stress in the boundary layer in Chapter 3, has been ignored since though it is small compared to the form drag, it will be very 'noisy', and its value will not have any significance with such a crude representation of the boundary layer as that to be employed.

It has been necessary to develop this approach to the calculation of pressure distribution since the Blasius theorem is obviously inadequate. Consider a single moving vortex outside the contour. It is known that the stagnation pressure distribution of a moving vortex is a function of its velocity, and so the pressure on the contour should be a function of this velocity. The Blasius theorem does not contain this dependency, so it is restricted to stationary vortices. Besides this, the flow speed at the

surface is always zero in this computer program, so the pressure gradient at the surface arises not from the flow of fluid along the surface, but from the flow of vorticity across it.

It will be seen in practice that the pressure distributions obtained are very noisy, because relatively few vortices cross the contour on any one time step. However, since all the relations between pressure gradient and vortex flux are linear, it is permissible to integrate the vortex flux over many time steps to obtain an average pressure distribution. Computer programs have been written to do this, giving the user a choice of the number of time steps in a batch, and a choice of output such as pressure distributions at any one time, or the time varying lift and drag.

6.3 THE MOVEMENT OF FREE VORTICITY

After the creation of the new vorticity, there is in effect a cloud of free vorticity with an aerofoil-shaped 'hole' in it as in figure [6.6]. Vorticity near the boundary of the hole is travelling parallel to this boundary, so that for a short interval of time, the shape of the hole will be preserved. The programming necessary to describe the movement of free vorticity can thus be borrowed from the boundary layer program. One modification is that the method of displacing the vortex at random has been

changed to the simpler form of equation (2.22), so that the Central Limit Theorem is relied upon to give the correct distribution of vorticity after many displacements.

There is no need to deal with the interaction betweem free vorticity and the contour, since the contour effectively vanishes when new vorticity is put into the flow. It is only on the next time step that the presence of the body is re-asserted. The lack of interaction between contour and free vorticity, whether the contour is represented by surface vorticity (Lewis,[13] Porthouse and Lewis[38]) or by mirror images (Chorin[4]), simplifies the program and shortens the computing time needed to simulate a given flow. It does restrict the present method to bodies in uniform translation. Rotating bodies would require some new theoretical work.

The flow far downstream of the body can be represented by fewer vortices, due to resolution effects. The vortex combination algorithm from the boundary layer program has been included to do this, and it tolerates larger vortices at distances far away from the contour. We are really more interested in lift and drag due to the flow near the contour than in the wake downstream, though the appearance of the wake is a visual check on the method. This led Lewis and Porthouse[37] to reject an earlier model of flow separation on the grounds that the appearance of the wake from a stalling

aerofoil was unrealistic.

A word should be said about the results to be expected from the program. For an unstalled aerofoil, we would expect to see the starting vortex separate from the trailing edge, and then travel far downstream. Since the total vorticity in the flow is zero, vorticity of opposite rotation must be left behind in the vicinity of the aerofoil. This is often referred to as the 'bound vorticity' of the aerofoil, by analogy with the real bound vorticity of a rotating cylinder. From the present point of view this is a misnomer. There just happens to be vorticity in the boundary layers surrounding the aerofoil whose effect on the lift force is the same as if there were bound vorticity on the aerofoil itself. Except for the instantaneous time when the Martensen Method is being applied, there is no bound vorticity on the aerofoil itself in the computer program.

Most of the newly created vorticity is near the leading edge (figure [6.7]). When this vorticity travels towards the rear of the aerofoil, some of it should be re-absorbed by passing inside the contour and subsequent annihilation. The remaining vorticity leaves the body to form a viscous wake. At the trailing edge, the two streams of vorticity on either side are of opposite rotation but equal magnitude. This is the Kutta-Joukowski condition, which is this sense is also valid for bluff bodies and aerofoils

without a sharp trailing edge, since the time-averaged values of the two streams must be of the same magnitude.

When a computer program has been written, it is normal to test it for convergence. In principle, the program described here would converge to the solution of the Navier-Stokes equation in the limit of an infinite number of pivotal points on the body, infinitesimal time step, and so on. The Martensen Method program has been separately tested for convergence, and is trustworthy, but the vortex dynamics program is well outside the limits of convergence, and no existing computer would be adequate to test it, except perhaps at very low Reynolds numbers. At higher Reynolds numbers, another difficult question is how one would formulate a convergence criterion for two- or three-dimensional turbulent flow (remember that if one doubles the number of vortices to represent the flow in greater detail, there will then be a different sequence of random numbers, and thus a different outcome to the test, so each run of the computer is unrepeatable). For the moment, we must accept that 'the proof of the pudding is in the eating'. We will try the program and see how it predicts the performance of a stalling aerofoil.

TABLE 6.1 THE BLUFF BODY COMPUTER PROGRAM

(1) Set the bound circulation of the contour, Γ, equal to zero.

Set the flow speed distribution on the contour, U_i, equal to the local component of the mainstream flow. Set the pressure gradient distribution, Δp_i, equal to zero.

(2) Take each free vortex and evaluate the induced velocity distribution around the contour due to that particular vortex.

If this indicates that the vortex is inside the contour

then (a) Forget the induced velocity distribution just obtained.

(b) Add the strength of the vortex into the bound circulation of the contour

$$\Gamma := \Gamma + \gamma$$

(c) Decrement the pressure gradient at the point where the vortex crossed the contour

$$\Delta p_i := \Delta p_i - \frac{\gamma}{dt}$$

(d) Annihilate the vortex.

otherwise (e) Add the contribution of that vortex into the flow speed distribution, U_i, on the contour.

(3) Since it is known already that

$$\sum_i U_i \Delta s_i = 0$$

the last value of U given is a redundant piece of information.

Replace this with a circulation condition. Apply the matrix operator from the Martensen Method with the circulation equal to Γ

$$U'_i = L(U_i;\Gamma)$$

(4) Create a new vortex at each pivotal point on the contour with strength

$$\gamma = U'_i \Delta s_i$$

at a distance

$$\sqrt{4 \nu \, dt/3}$$

outside the contour.

(5) Increment the pressure gradient at each pivotal point by

$$\Delta p_i := \Delta p_i + \frac{U'_i \Delta s_i}{dt}$$

Calculate the pressure distribution, and hence the lift and drag on the body.

(6) Forget about the contour. Forget the value of Γ.

(7) Give every vortex a random displacement to represent diffusion.

(8) Compute the convection of each vortex by the Improved Euler Method.

(9) Combine nearby vortices by rules given in Table 3.2.

(10) Do whatever sampling is desired.

(11) Go back to step (1) for another time step.

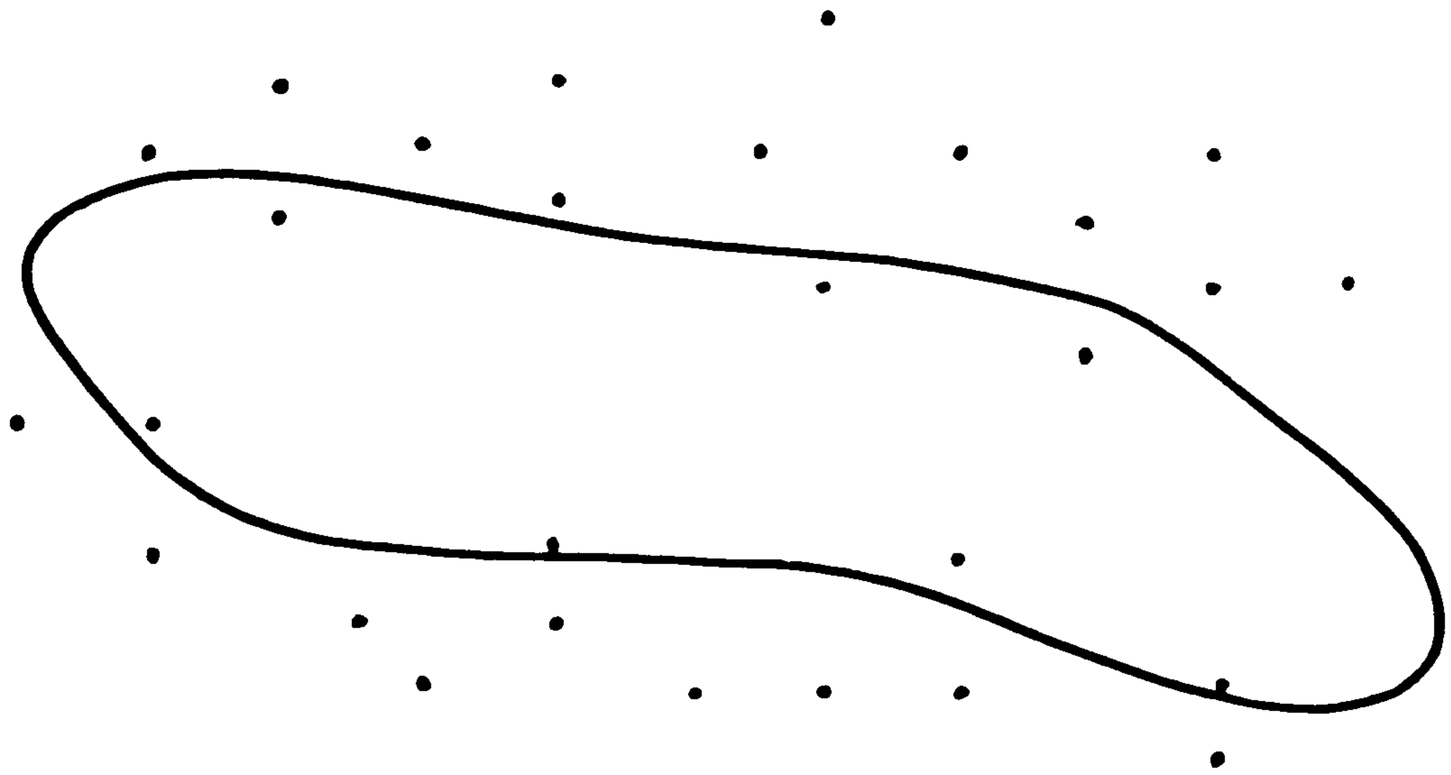

Figure 6.1 The Distribution of Vorticity near the Contour before the Application of the Martensen Method

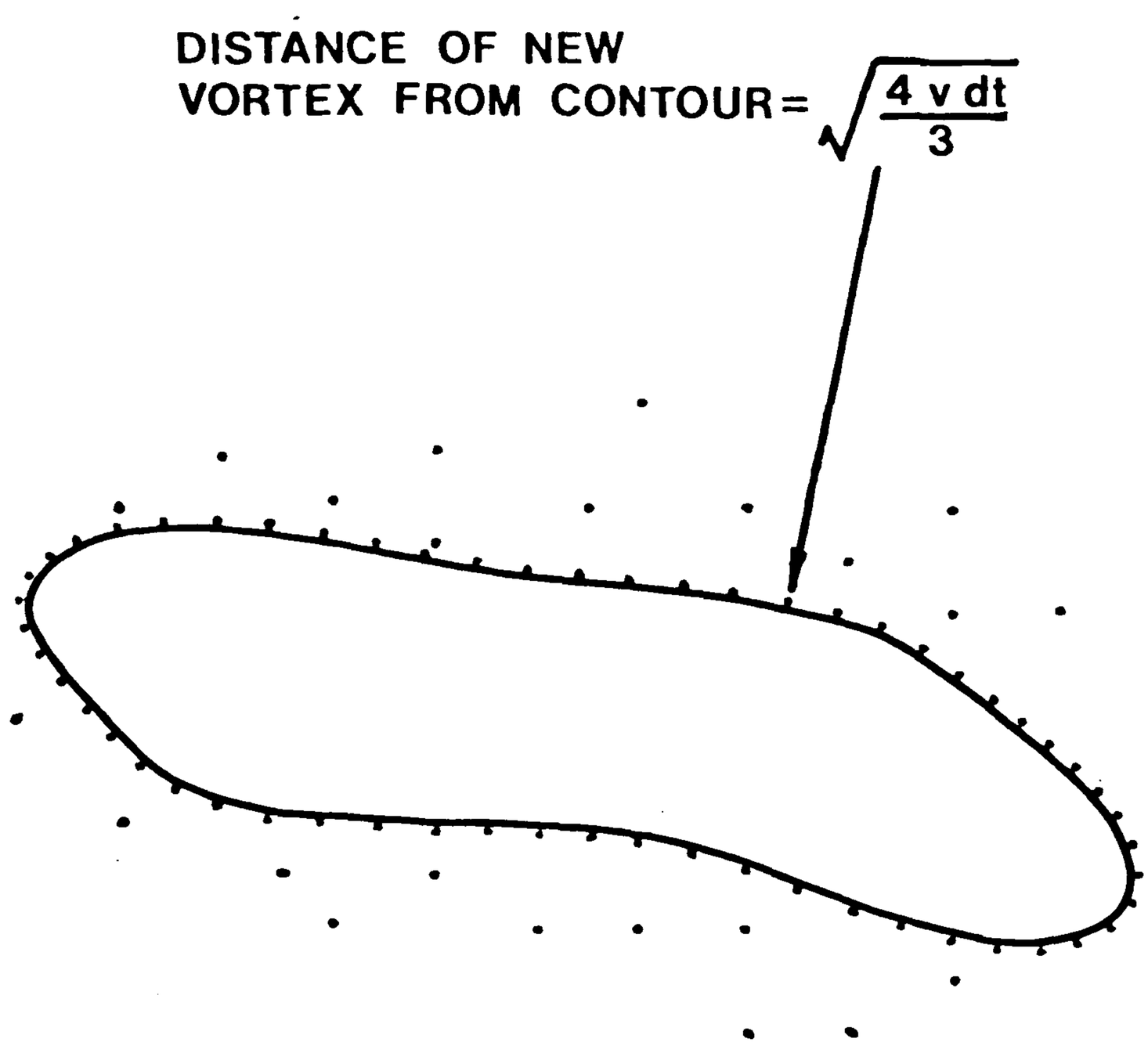

Figure 6.2 The Vorticity Distribution after the Martensen Method

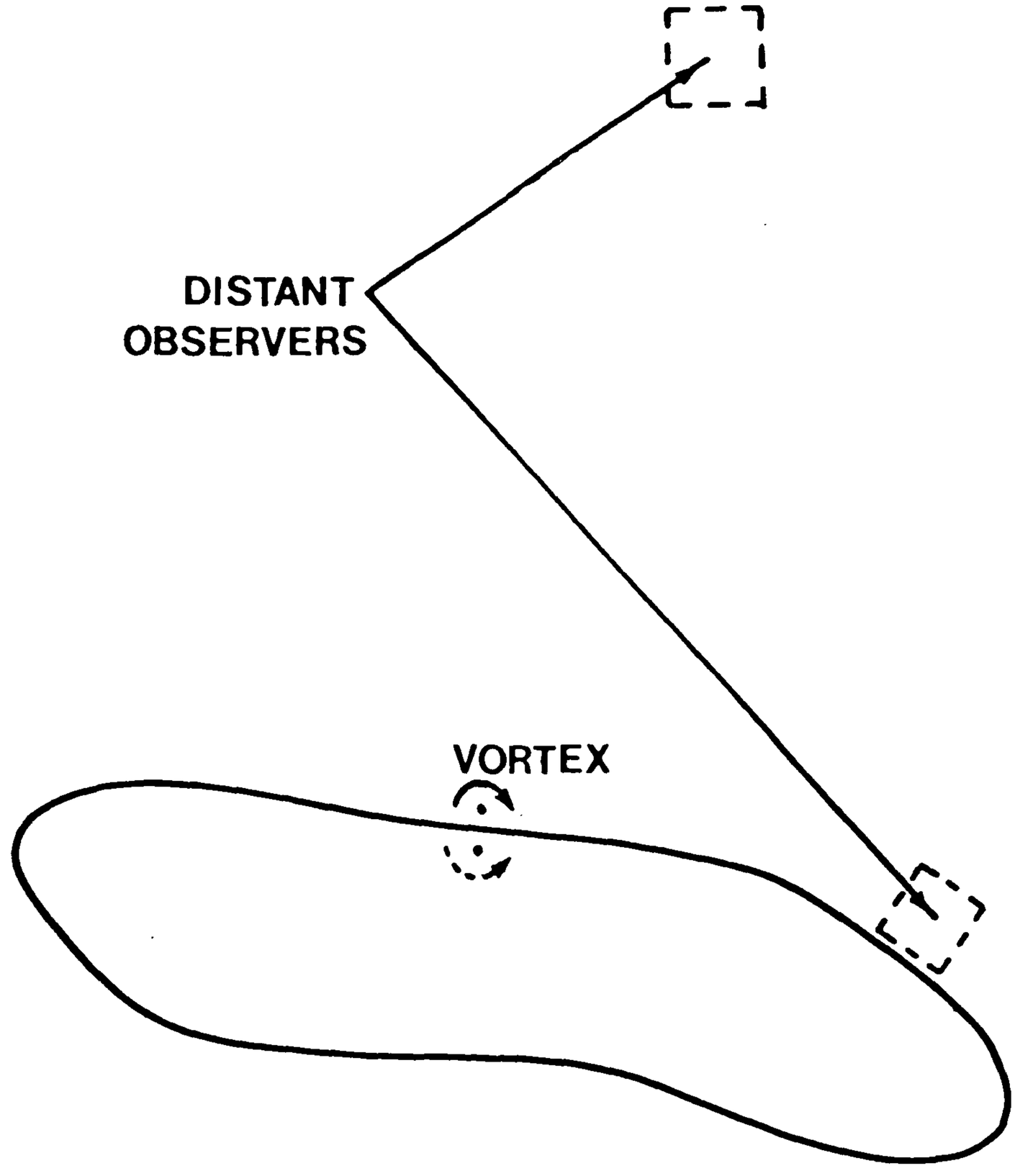

Figure 6.3 The Reaction of the Contour to a Nearby Vortex

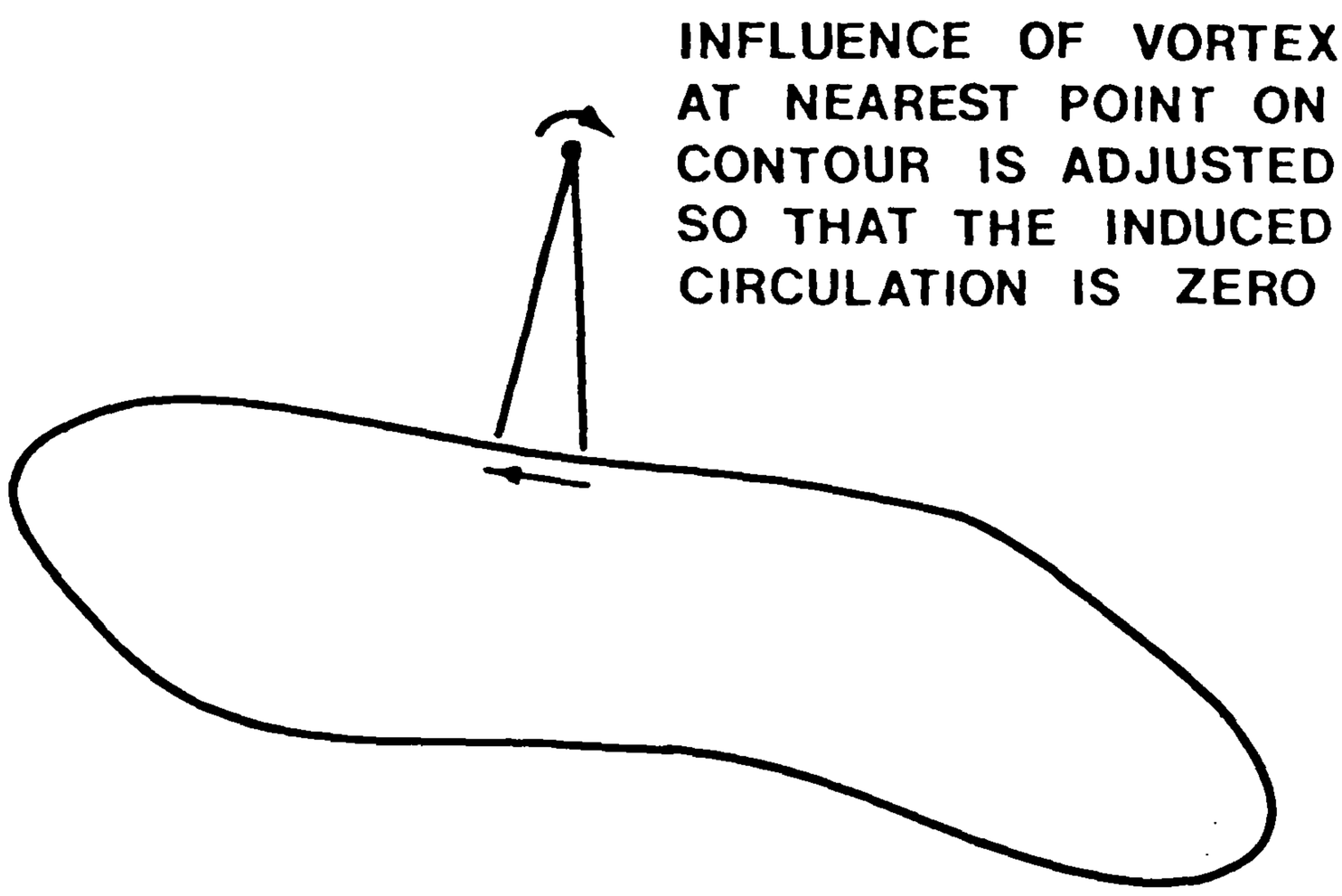

Figure 6.4 A Correction to Ensure Sensible Velocities on the Contour

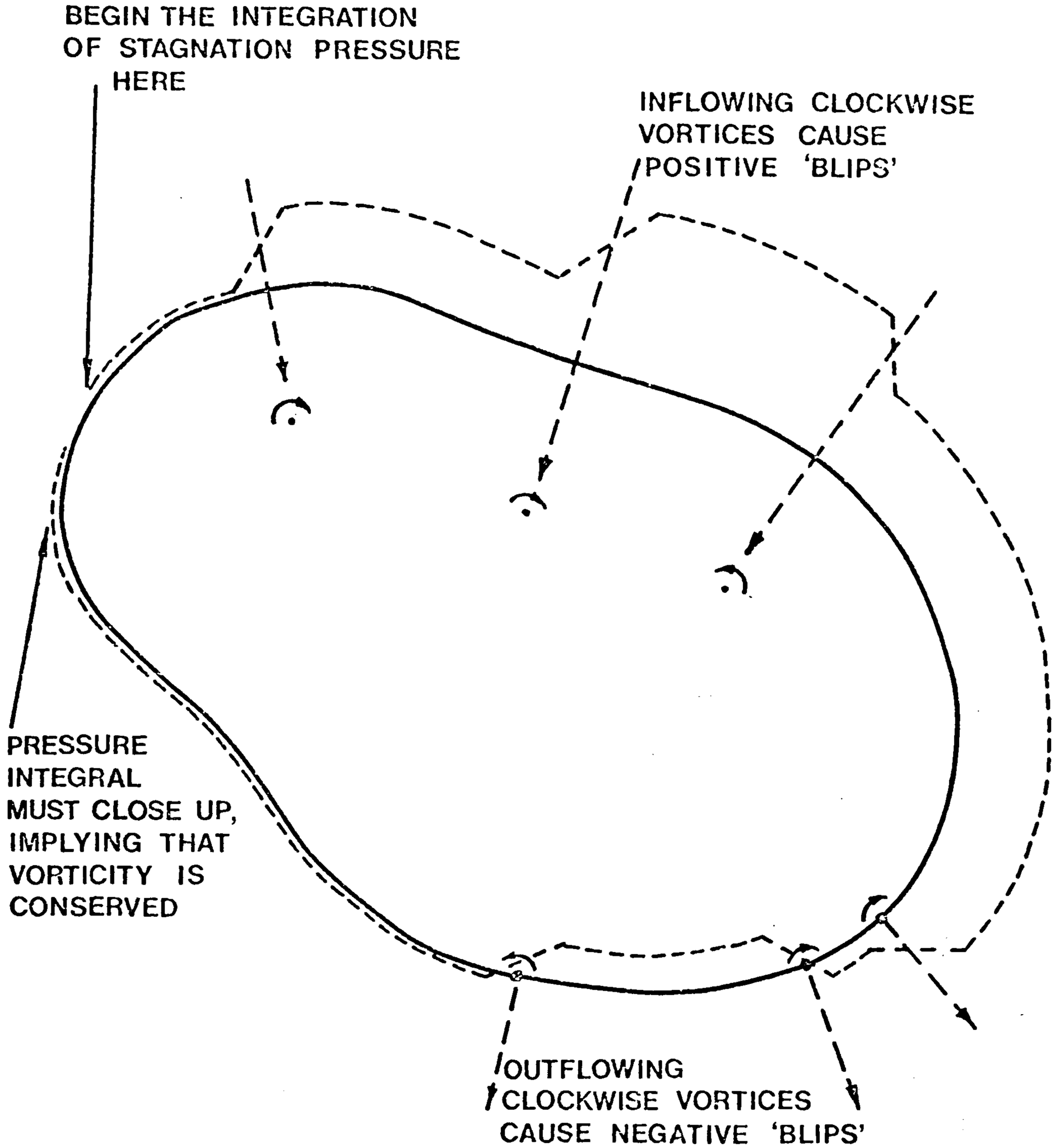

Figure 6.5 The Relation of Pressure to Vortex Flux

(a) Initial State

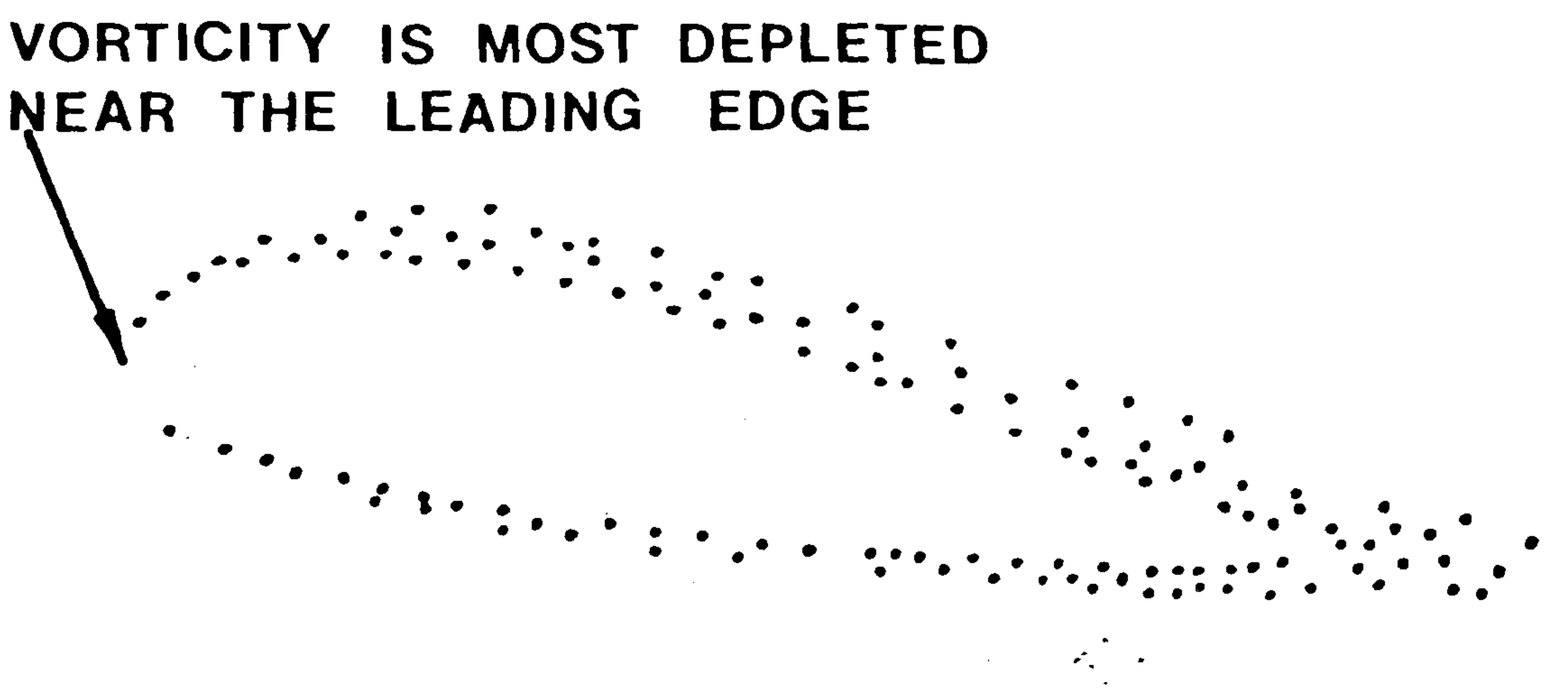

(b) State after Time dt

Figure 6.6 The Temporary Preservation of Contour Shape in a Configuration of Free Vorticity

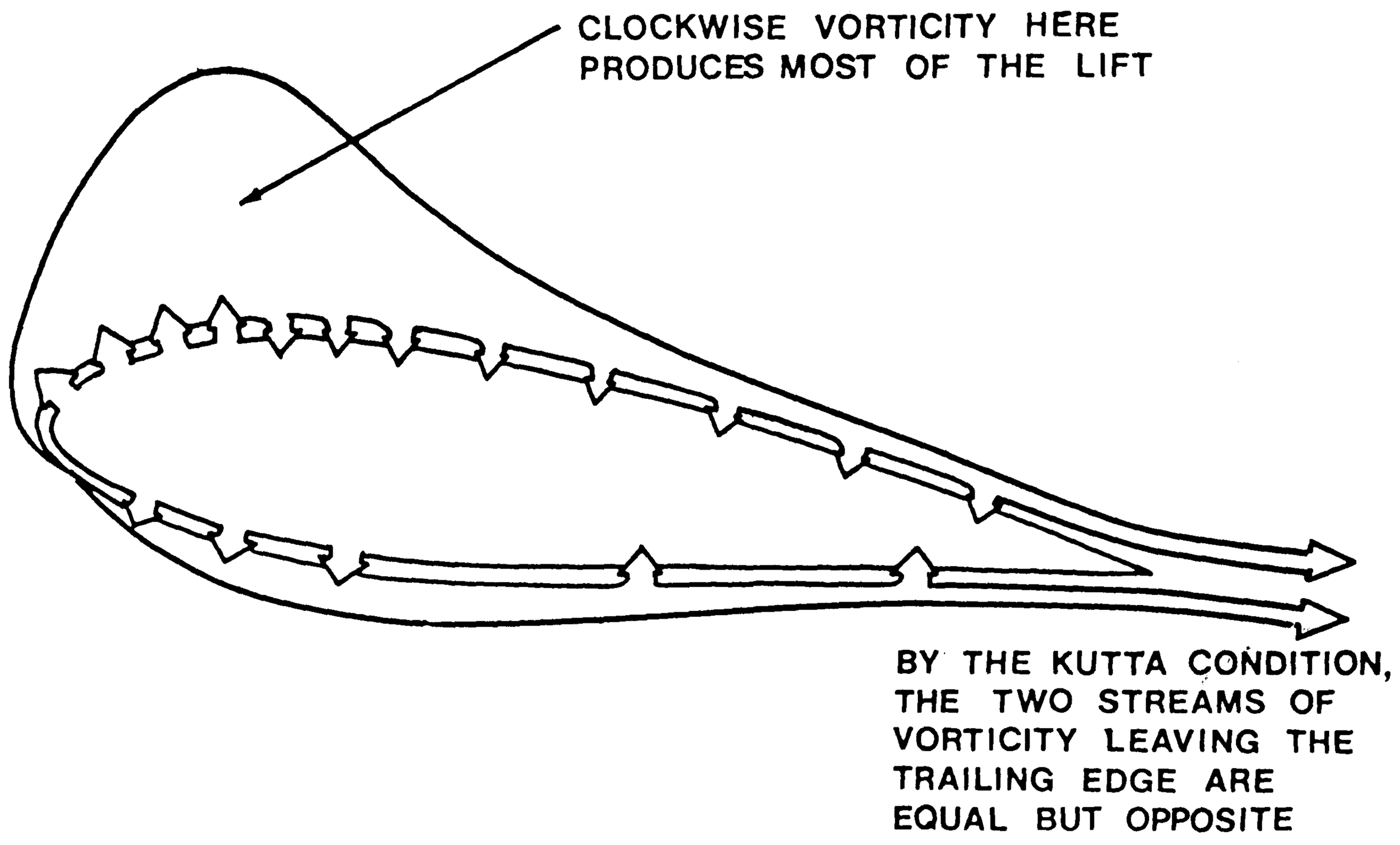

Figure 6.7 Vortex Fluxes around an Aerofoil

CHAPTER 7. TESTING THE BLUFF BODY COMPUTER PROGRAM

Two bluff bodies will be dealt with in this chapter. These are the aerofoil NACA 0012 at a range of angles of attack from zero to ninety degrees, and a circular cylinder. To the author's knowledge, this will be the first ever attempt to reconstruct the complete behaviour of an aerofoil at all angles of attack. The project to simulate the aerofoil took some eight months to complete in terms of the author's limited access to mainframe computing facilities. After this project, it was decided to change to a fast microcomputer, and the circular cylinder was simulated on this latter computer. One consequence of this is that still pictures of the flow are available for the aerofoil, but not for the cylinder. It is intended to connect the microcomputer to a video cassette recorder, and thus produce one of the first direct computer film generation facilities. This adoption of a new technology will take time.

7.1 AEROFOIL NACA 0012

It is convenient to begin by describing the experimental work. The same wind tunnel as in Chapter 5 was employed, and the pressure distribution measurements were extended up to ninety degrees, so the description of the apparatus and the possible errors remains the same. When the aerofoil is at

a high angle of attack, it is causing a significant blockage in the wind tunnel. Regarding the aerofoil as a flat plate with a very simple wake as in figure [7.1], it is evident that one can assume as a first approximation that the blockage is equal to half the drag coefficient, giving

$$C_{D_{apparent}} = \frac{C_{D_{real}}}{\left[1 - a\,\frac{C_{D_{real}}}{d}\right]^2} \qquad (7.1)$$

This permits us to deduce the blockage effect from the observed drag coefficient as the solution of a simple quadratic equation,

$$C_{D_{real}} = \frac{2\,C_{D_{apparent}}}{1 + a\,\frac{C_{D_{apparent}}}{d} + \sqrt{1 + 2a\,\frac{C_{D_{apparent}}}{d}}} \qquad (7.2)$$

and thus to correct the results obtained by a factor

$$C_{D_{real}} / C_{D_{apparent}}$$

It will be seen that this correction works remarkably well for so simple an approach.

The pressure distribution obtained at discrete points may be

interpolated, working in intrinsic co-ordinates around the aerofoil contour, to give the pressure at any point on the aerofoil. There were twenty three pressure tappings, giving forty six readings from which the pressure at five hundred points around the aerofoil was interpolated. The lift and drag coefficients could then be obtained by integration. This was done for 2.5 degree intervals at small angles of attack, at 1 degree intervals near the stall, and then at progressively larger intervals at higher angles of attack. The results obtained will be compared below with similar results from Critzos, Heyson and Boswinkle.[39]

Computer simulations of the aerofoil are shown in figures [7.2]-[7.6] for a range of angles of attack. The Reynolds number adopted was 100,000 and the time step was arbitrarily chosen to be one twentieth of the time taken by the mean flow to travel one aerofoil chord length. The aerofoil was represented by fifty pivotal points. At 5 degrees (figure [7.2]), we know that there will be no stall, but a starting vortex will be shed. The appearance of this starting vortex is indistinct in figure [7.2], but obvious as a transient at high angles of attack before the aerofoil stalls. The boundary layers in figure [7.2] are about ten times too thick at a nominal Reynolds number of 100,000, but this is only to be expected since too few vortices are being used to represent the boundary layer.

At 10 degrees (figure [7.3]), it is seen that the aerofoil does not immediately stall, but that there is some kind of flow separation. One has the impression that there is a laminar separation followed by a turbulent reattachment, but it cannot be claimed that the computer program is able to simulate the flow in such great detail.

At 15 degrees (figure [7.4]), there is an obvious separation from near the leading edge, so in contrast to the 10 degrees case, this may be regarded as true stalling. Despite the limited resolution, the mechanism of flow separation, the piling up of vorticity described in Chapter 4, is still operating. This is where we can be pleased at having chosen a phenomenological method of simulation based upon vortex dynamics. Though the computer program is operating well outside numerical convergence on any conventional criterion (rather like simulating a satellite's orbit with a time step longer than the orbital period), it is still producing credible results. There is a leading edge separation producing strong clockwise vortices. These induce backflow on the aerofoil, and this backflow is also prone to separation. As the clockwise vortices pass the trailing edge, strong anti-clockwise vortices are shed there in response. The two streams of clockwise and anti-clockwise vorticity are on average of the same magnitude, and for an aerofoil with a blunt trailing edge, no other meaning

but this can be attached to the 'Kutta condition'.

The simulations at 30 degrees (figure [7.5]) and 60 degrees (figure [7.6]) show a fully stalled aerofoil with an irregular vortex street downstream. All of the stalled simulations look similar to a high-speed cine film from which Goldstein[34] shows a few frames (Plate 9 of the Dover edition).

It would be desirable to convert all these simulations into films, but this is no easy matter. One feels that if computers cannot produce films of simulations of physical phenomena, then time spent on them without an end product is just a waste of human energy. Unfortunately, computer facilities for film generation are rare. A film has been made by the primitive method of repeatedly photographing the screen of a graphics terminal. This is an exhausting and expensive way to use a human being in the absence of mechanisation, and so means of generating video films by computer are under investigation.

A mass of information on surface pressure distributions has also been obtained. One could hardly show all this raw data, so instead space-averaged results are shown with variation in time in figures [7.7] and [7.8] averaged in batches of ten time steps to reduce noise, and time-averaged results with variations in space are shown in figures [7.9] -

[7.13]. Also shown in these latter figures are the experimental results. The experimental results have not been corrected for blockage, but even if they were so corrected, the conclusions would be the same. There are differences between simulation and experiment in the scale of the results, but if we were permitted to 'cheat' by a scale factor, the correspondence between simulation and experiment is very good for a fully stalled aerofoil. For an unstalled aerofoil, it is seen that with the limited resolution of the simulation, it is difficult to reproduce the peak pressure distribution near the leading edge.

Time- and space- averaged results are shown in figures [7.14]-[7.17]. Experimental results with and without blockage corrections are also shown, together with the results of Critzos,Heyson and Boswinkle. There is no flow blockage correction necessary for the unstalled results. The simulation and the experiments were all performed at different Reynolds numbers, but this need not alter our judgement of the performance of the computer simulation. Estimated errors of the prediction by computer simulation, due to the limited computing time available at each angle, are shown in each figure as a vertical line delimited by short horizontal bars.

For the unstalled aerofoil, the simulation underpredicts the lift coefficient. Since the lift coefficient is sensitive to a small region near

the leading edge, and to the Kutta condition being fully established, the prediction may still be regarded as good for a first attempt. The stalling angle appears to be overpredicted, due to the low number of vortices used. The drag coefficient obtained by integrating the experimental results is apparently negative for the unstalled aerofoil, merely illustrating the error to be expected from using just twenty three pressure tappings. This error would be serious if our interest were confined to unstalled flow, but in the present context it is negligible. The predicted drag coefficient does not show any discontinuity at the stall, which is again a matter of too few vortices.

For the stalled aerofoil, there is a maximum discrepancy of 40% in the predictions by simulation. The experimental tunnel blockage correction is seen to work well in terms of the resulting agreement with the results of Critzos, Heyson and Boswinkle. The general form of the characteristic has been adequately predicted by the computer simulation. Not too much significance is claimed for its shape around the stalling angle, but the results obtained are encouraging. For the sake of completeness, the total force on the aerofoil (figure [7.16]) and the direction of this force (figure [7.17]) are also shown. For a stalled aerofoil, the direction of this force is normal to the aerofoil chord to a first approximation. Thus

since the force direction may well be easy to predict by simulation, the magnitude of the force in figure [7.16] may be felt to be the most significant display of the results when an interest is taken in the performance of the computer program, though lift and drag are the force components of interest in considering the performance of the aerofoil as an exchanger of work.

7.2 THE CIRCULAR CYLINDER

A cylinder of 3.5 inches diameter was placed in the centre of the same 18 inch wind tunnel. There is just one pressure tapping on the cylinder, but the cylinder may be rotated so the mean pressure at any point may be measured. The cylinder also causes blockage of the tunnel, which was estimated in the same way as the aerofoil's blockage. Without the blockage correction, the measured drag coefficient was about 1.5 over the small range of Reynolds numbers taken (85,000 - 200,000), but with the correction it falls to 1.2, which is the value normally measured by other workers. Once again, a simple blockage correction is doing well. This drag coefficient was obtained by integration of the pressure distribution, which is easy for a circular cylinder. The transverse force coefficient, or lift coefficient, should on average be zero. It was found to be within 0.04 of

zero, and this may be interpreted as the experimental error to be expected.

The new microcomputer was run at a range of Reynolds numbers from 100 to 1,000,000. The circular cylinder was represented by forty eight pivotal points, and the time step was one twentieth of the time taken for the mean flow to travel the length of one cylinder diameter. As previously explained, this computer has no conventional plotting facility, but it is intended to make video films instead. A display of the flow on a computer terminal does indeed show that the initial separation is symmetric, but later an asymmetry develops leading to the expected vortex street.

The lift and drag forces were averaged in batches of ten time steps to remove noise, and their variation is shown in figures [7.18]-[7.22]. There is clearly a characteristic oscillation in the lift coefficient. Previously, Porthouse and Lewis[38] had also found a small oscillation in drag force at twice the frequency in their computer simulation. This is not observed here, but it is just what one would expect to happen.

This series of computer simulations was intended to find the Strouhal number fD/U as a function of Reynolds number. However, there is not enough regularity in the frequency over the time taken in the simulations for us to say that the Strouhal number can be measured to a value any better than the usual 0.2. The simulations should be run for much longer, and a Fourier

analysis performed if necessary, but this is beyond the practical limit of the computer. There is also the problem with Fourier analysis that there may be a basic frequency present, but with a random phase shift due to various transients such as that in figure [7.19] at time=14, and this will cause problems which will require plenty of computing time for their resolution. Just the same, it seems to be easy with this type of simulation to get the right Strouhal number, so this no longer becomes such a significant quantity in testing the computer program.

The time-averaged pressure distributions are shown in figures [7.23]-[7.27]. In figure [7.26] an experimental result is also given. At the lower Reynolds numbers, the pressure distributions all look much the same, save that there is normally an unsystematic asymmetry due to the relatively short times of each simulation, even though over this time the flow has travelled thirty cylinder diameters. At high Reynolds numbers, the pressure distribution is peculiarly flat near the leading part of the cylinder. This is probably due to lack of resolution once again, and seems to support the idea that an upper limit to the Reynolds number at present is 10,000, which Stansby and Dixon[14] propose. The comparison with experiment in figure [7.26] shows considerable discrepancy, though the trend is the same. This can only be attributed to the numerical method being executed with an insufficient

number of vortices.

The vortex-in-cell method has already been suggested as a remedy for this. It would be desirable to change to this method immediately, and repeat most of the computer simulations given so far, as well as to examine other shapes of bluff body. Lewis and Porthouse[37] also show the vortex street behind a wedge with a simpler model of flow separation. There has been no time to repeat this simulation with the latest model.

There are many other shapes of body to try, and the question is raised as to what constitutes a good test of the computer program. It is conceivable that some particular shape gives very good agreement in surface pressure distribution, which is relatively quick to confirm by experiment, but that the flow far from the body is different. Measurements of the flow field of non-trivial quantity would be necessary to test for this, but the mass of data obtained may be unmanageable. An alternative approach is to put several bodies in the flow, to attempt to predict the flow around all of them, and to see if the non-linear interactions between the bodies produce effects which are observed in practice.

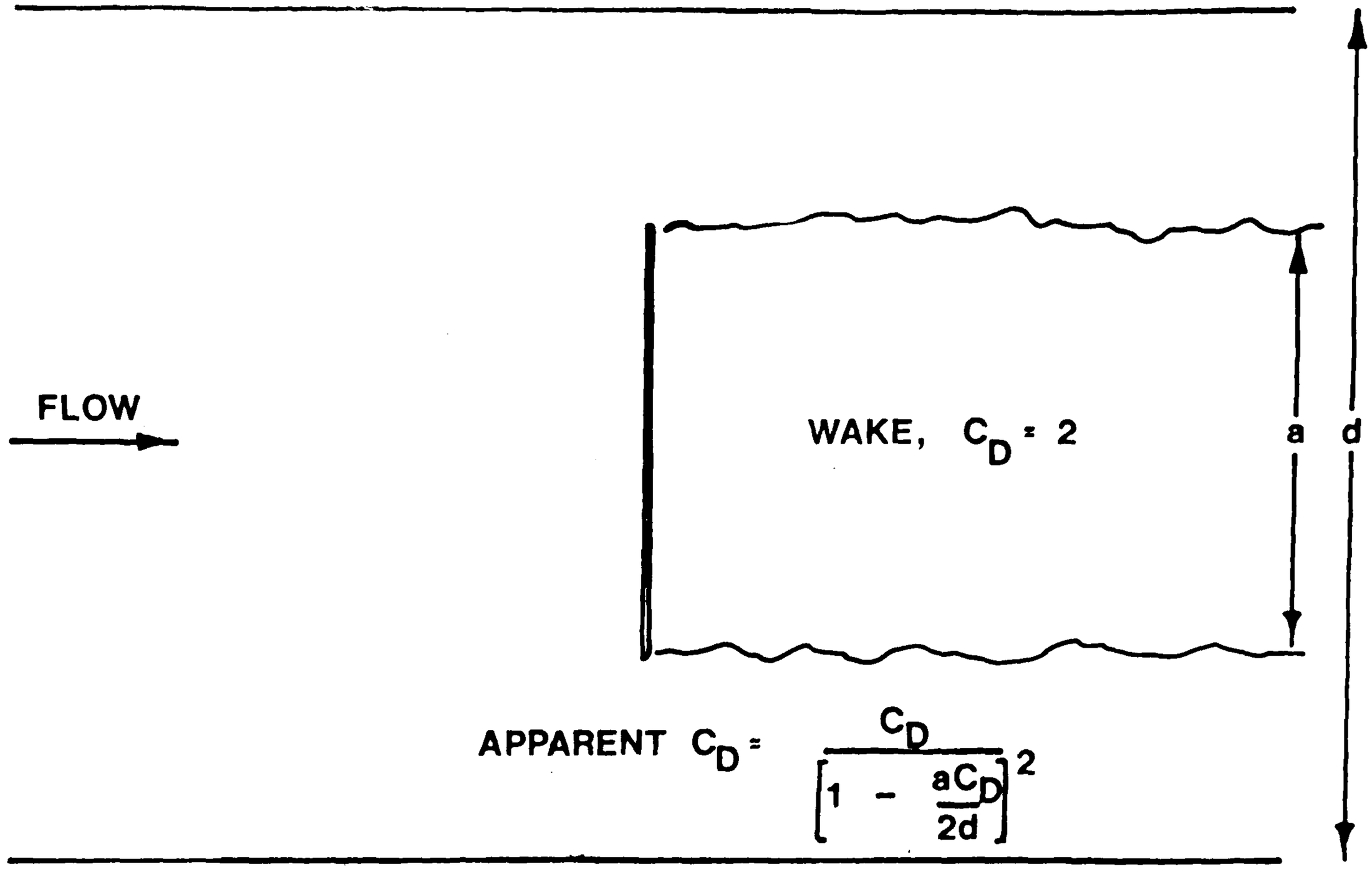

Figure 7.1 A Simple Model of Tunnel Blockage by a Flat Plate

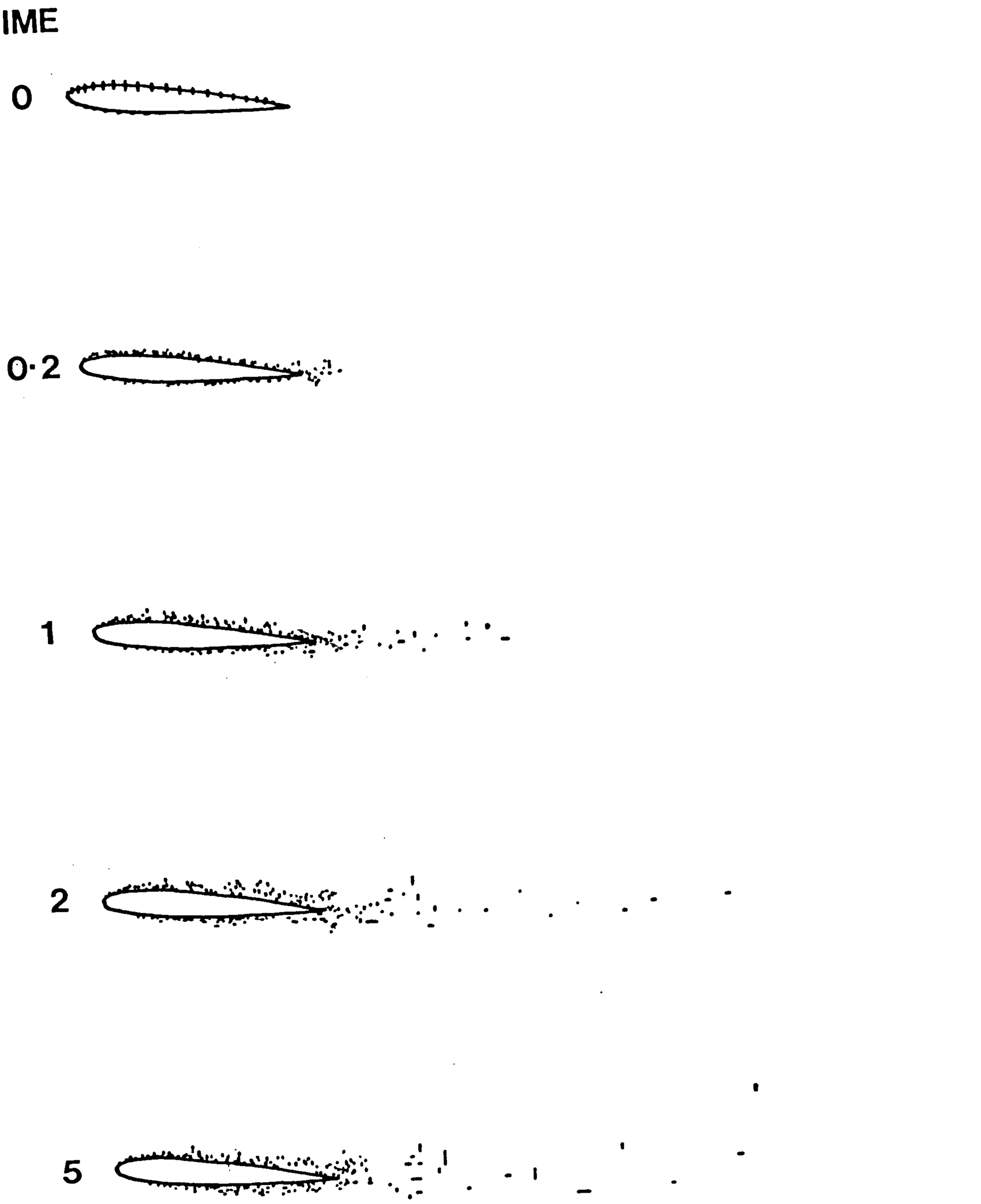

Figure 7.2 The Aerofoil at 5^{o}

Figure 7.3 At 10°

Figure 7.4 At 15°

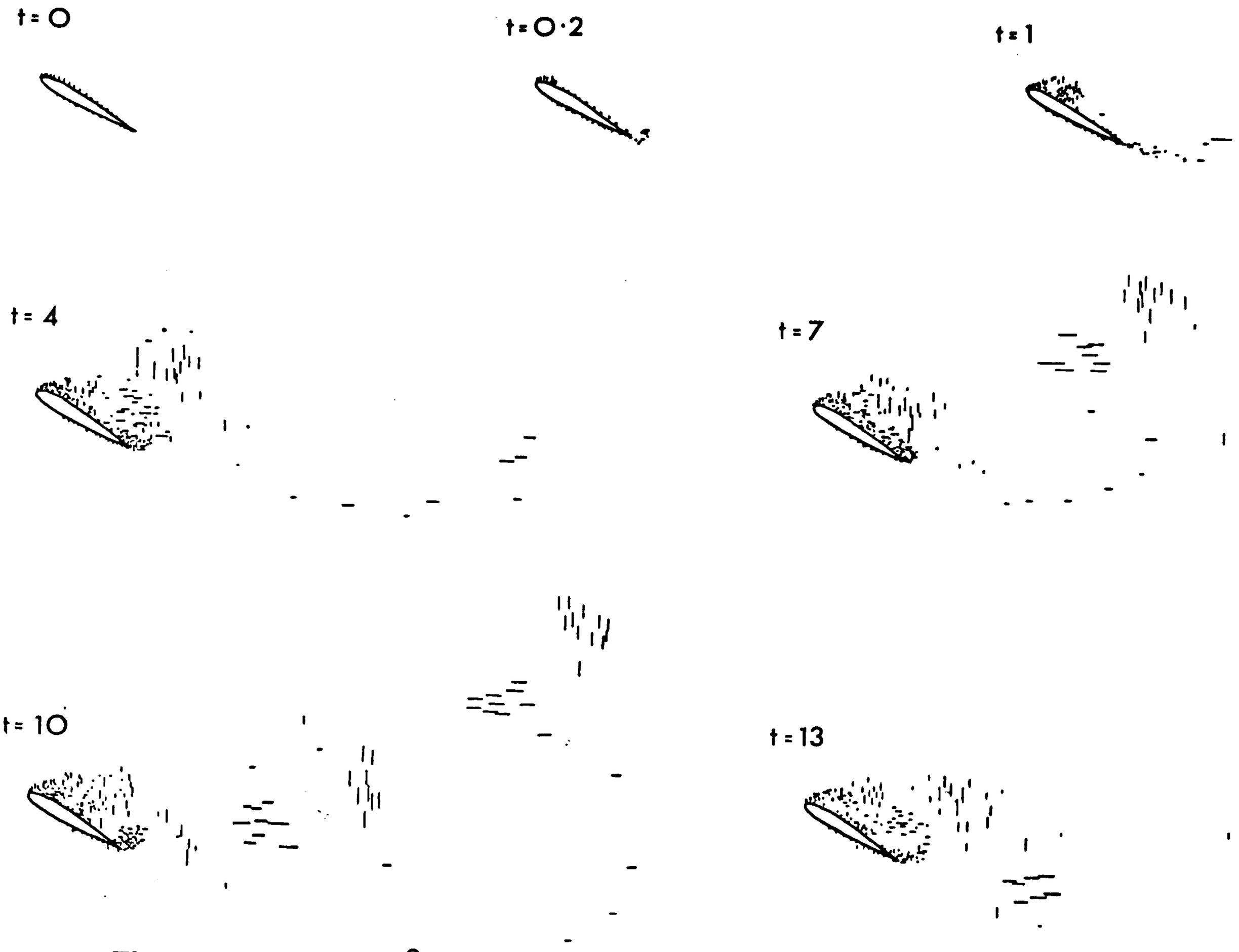

Figure 7.5 At 30°

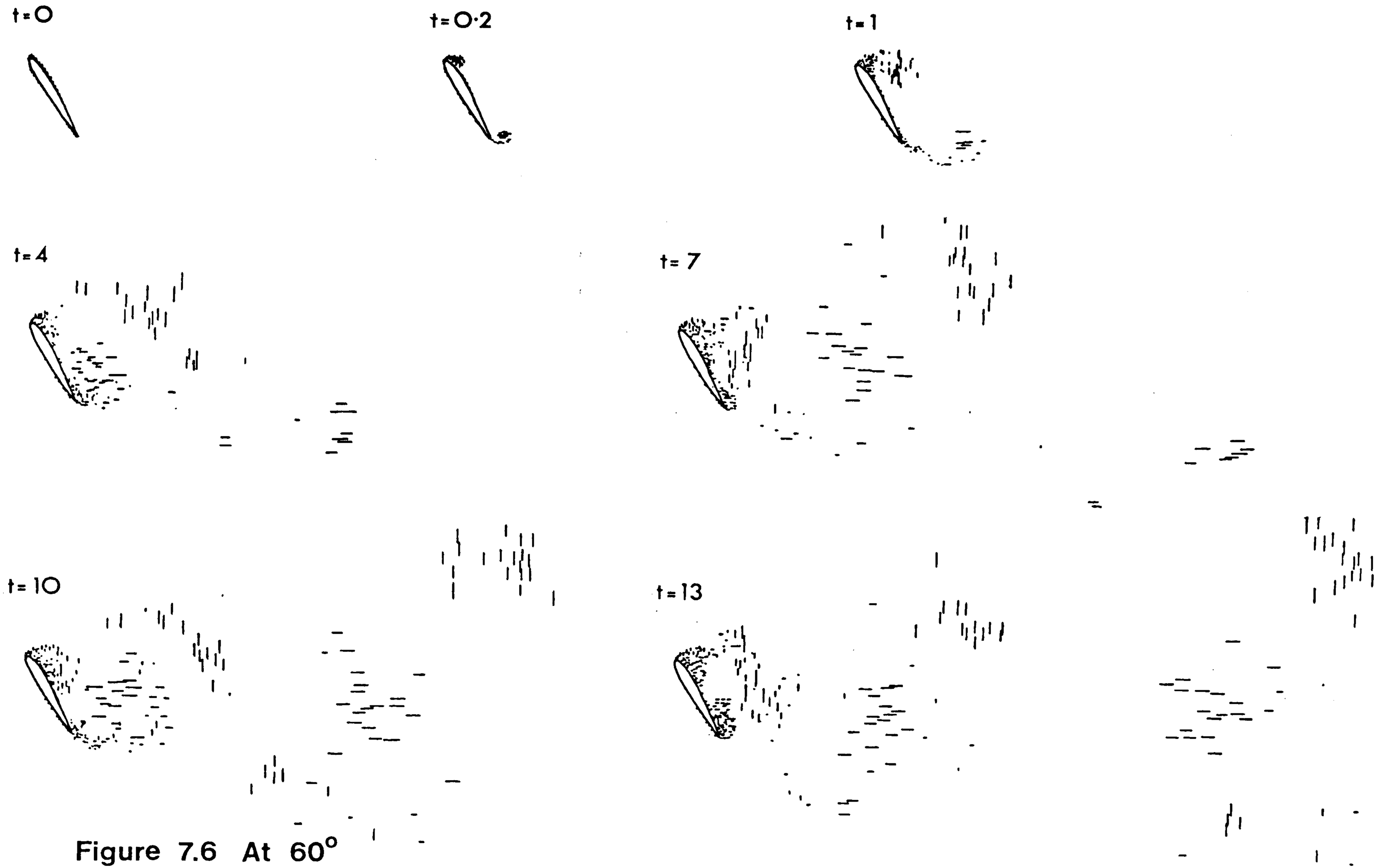

Figure 7.6 At 60°

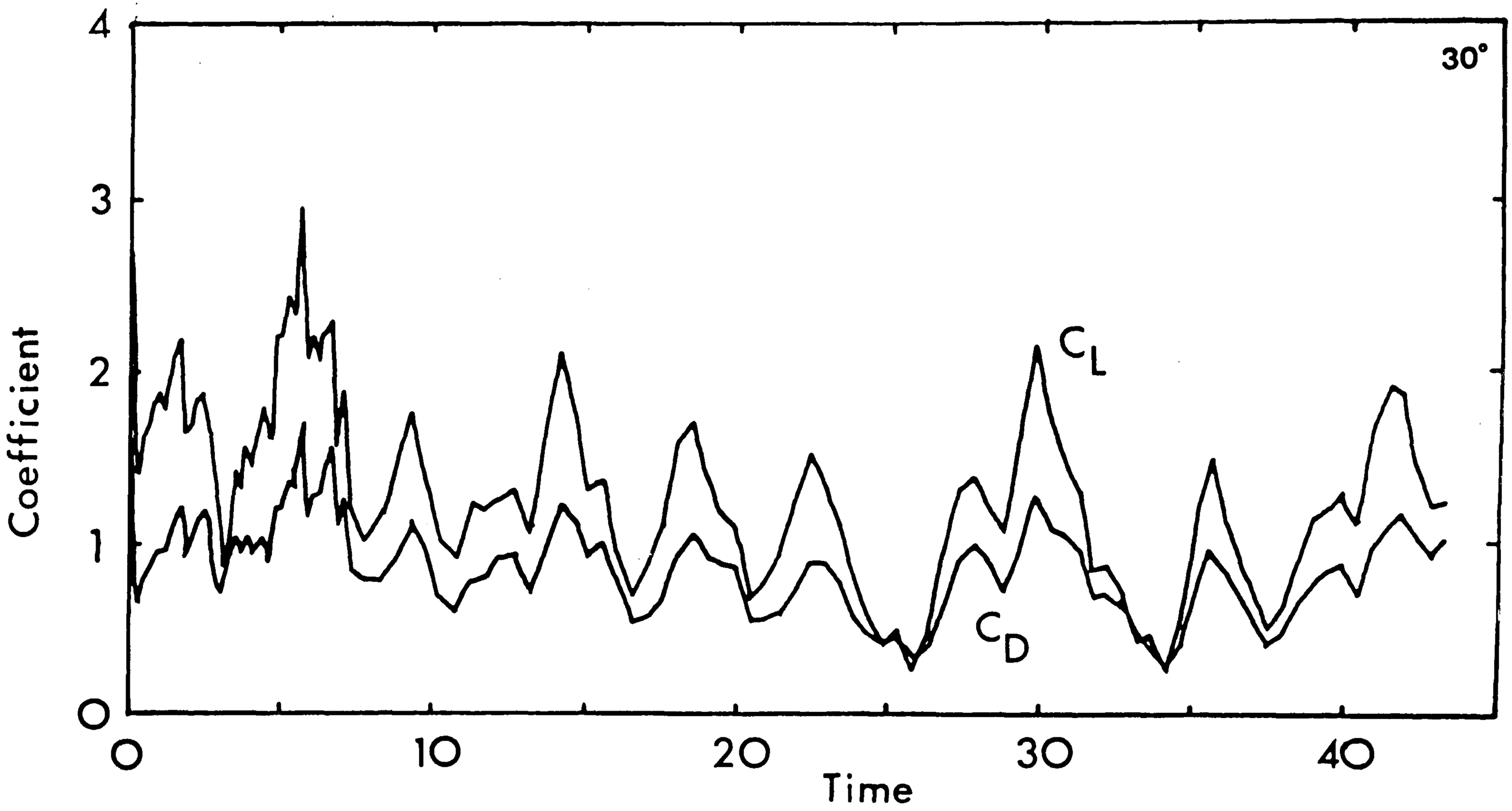

Figure 7.7 The Time Variation of Lift and Drag at 30° Angle of Attack

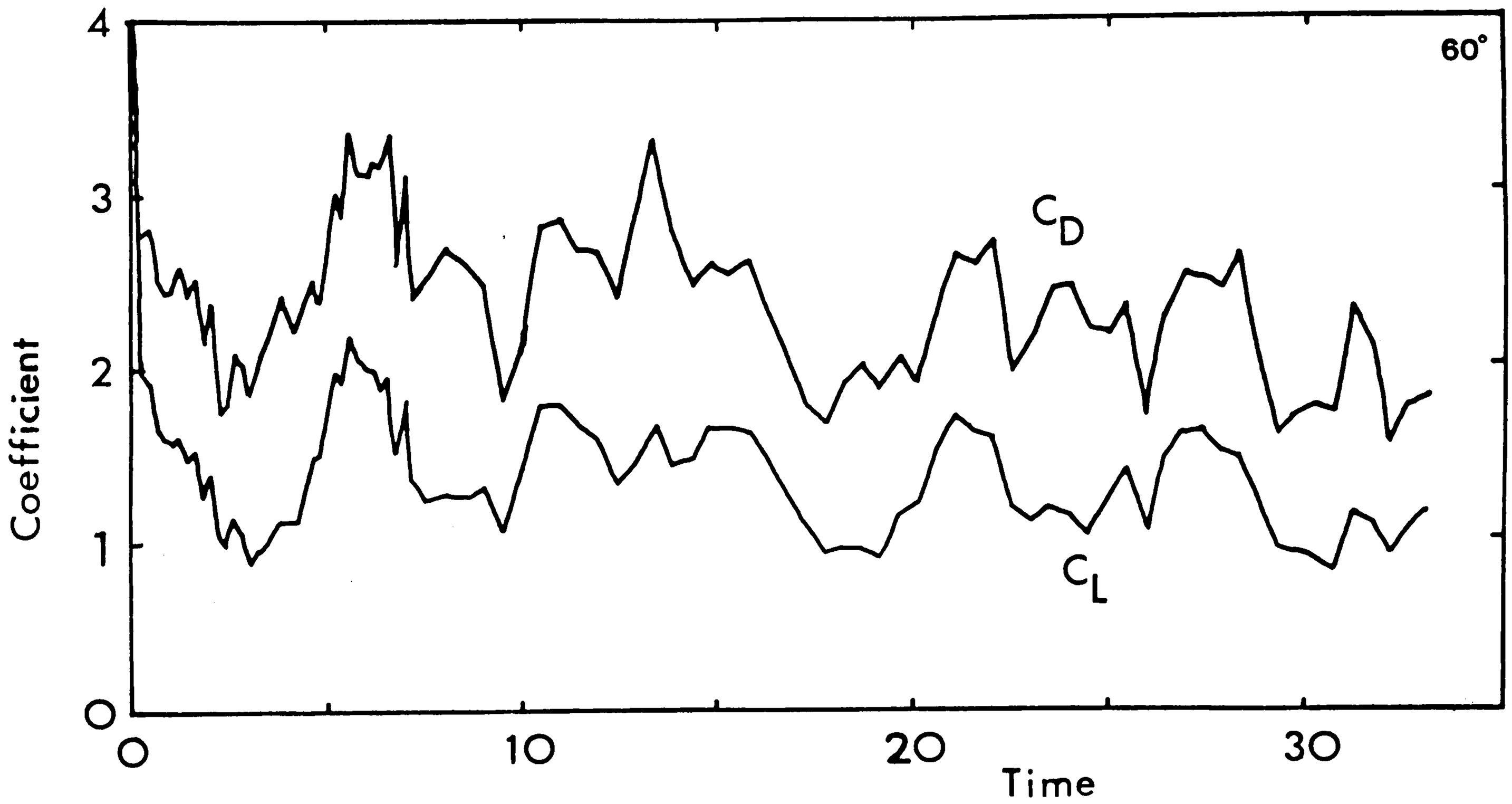

Figure 7.8 Lift and Drag at 60°

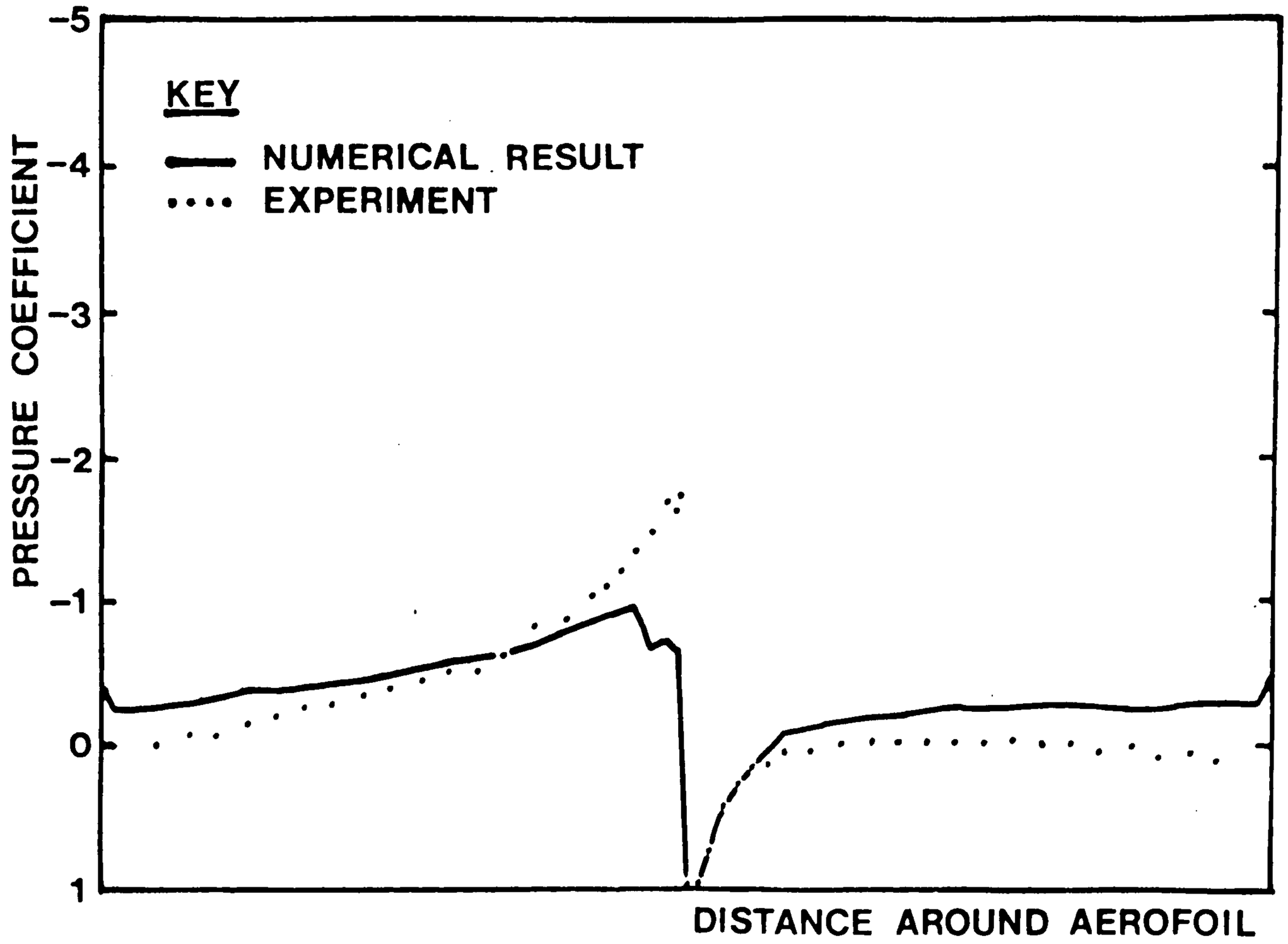

Figure 7.9 The Time-Averaged Surface Pressure Distribution at 5° Angle of Attack

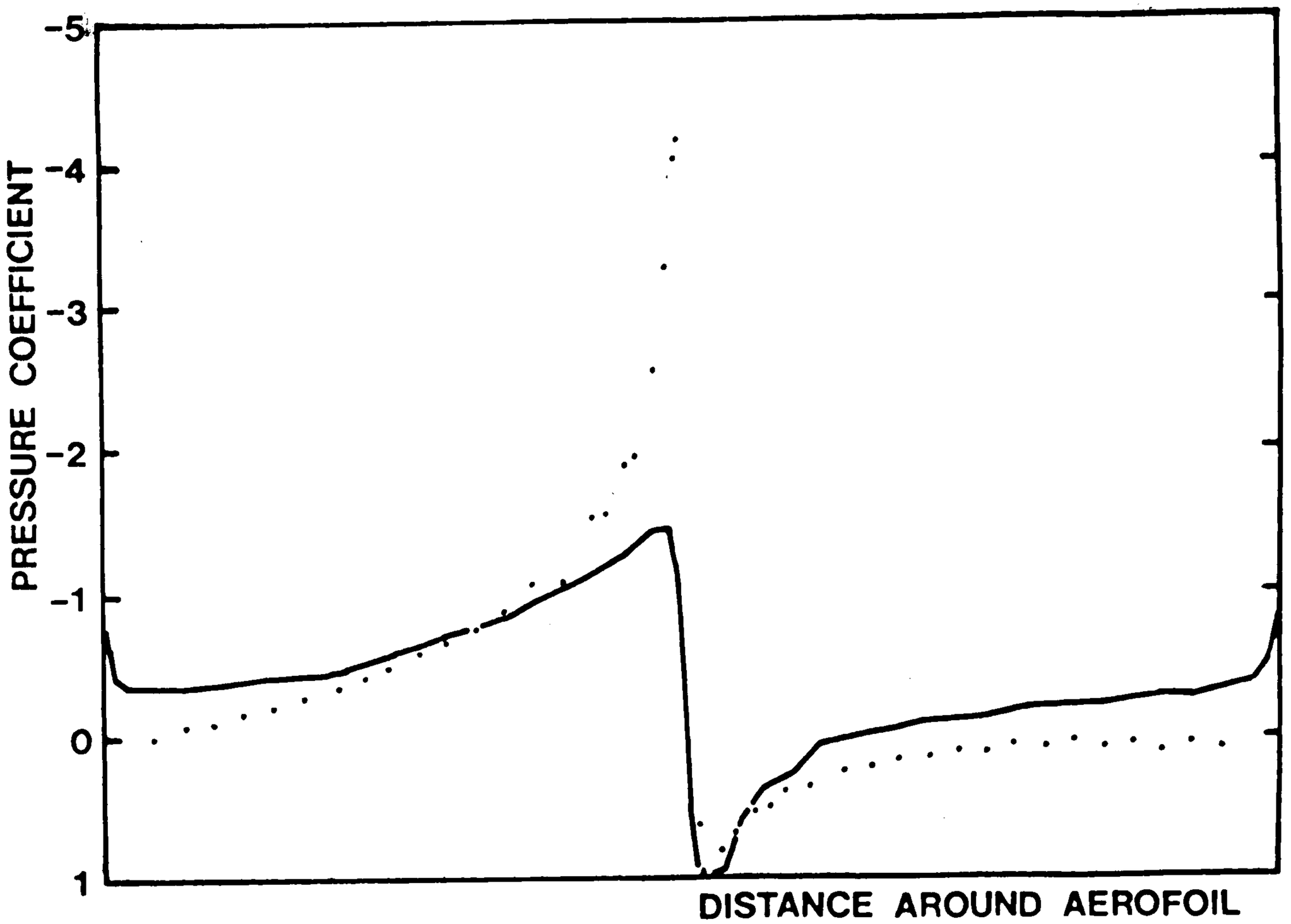

Figure 7.10 The Surface Pressure at 10°

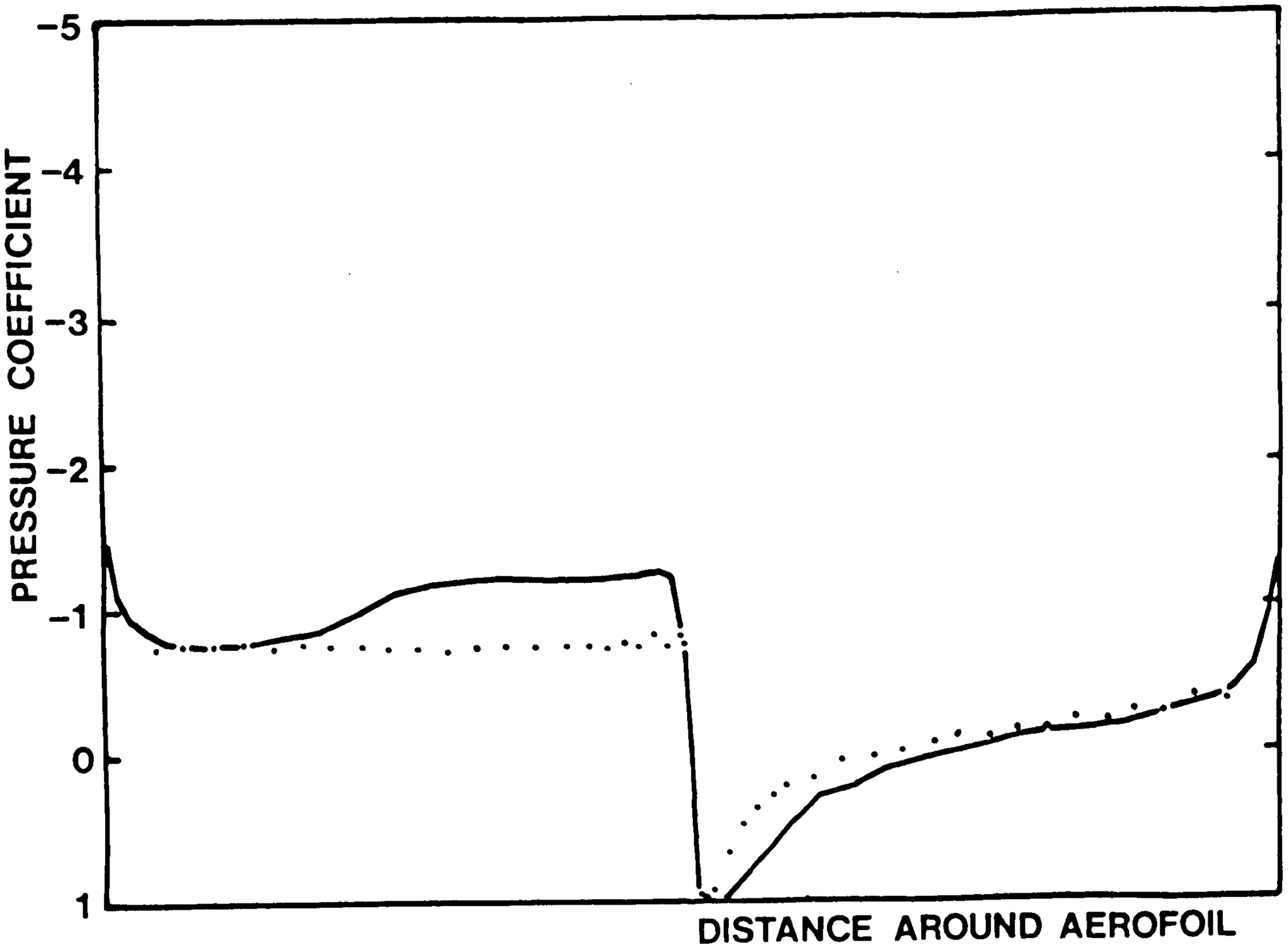

Figure 7.11 The Surface Pressure at 15°

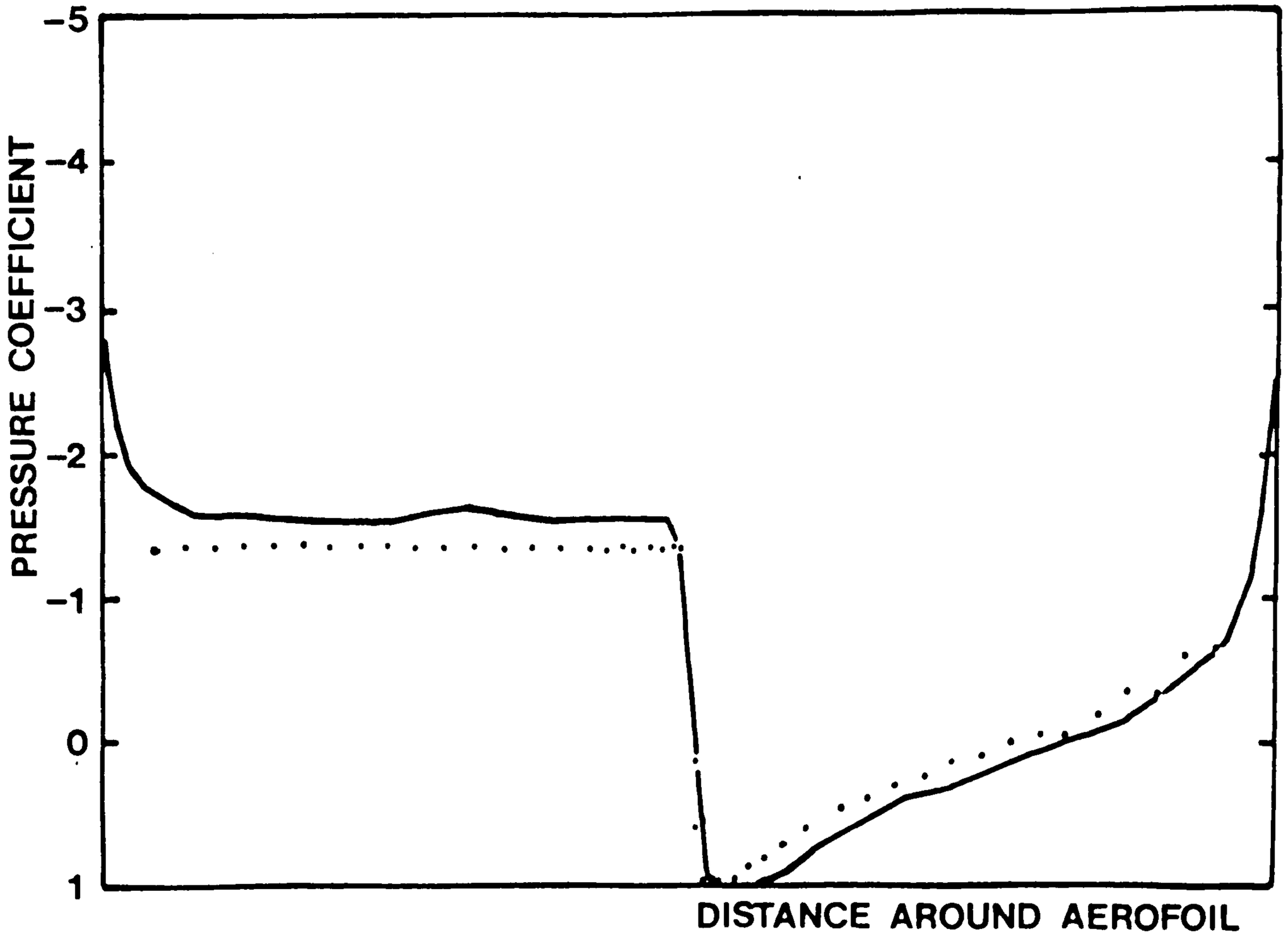

Figure 7.12 The Surface Pressure at 30°

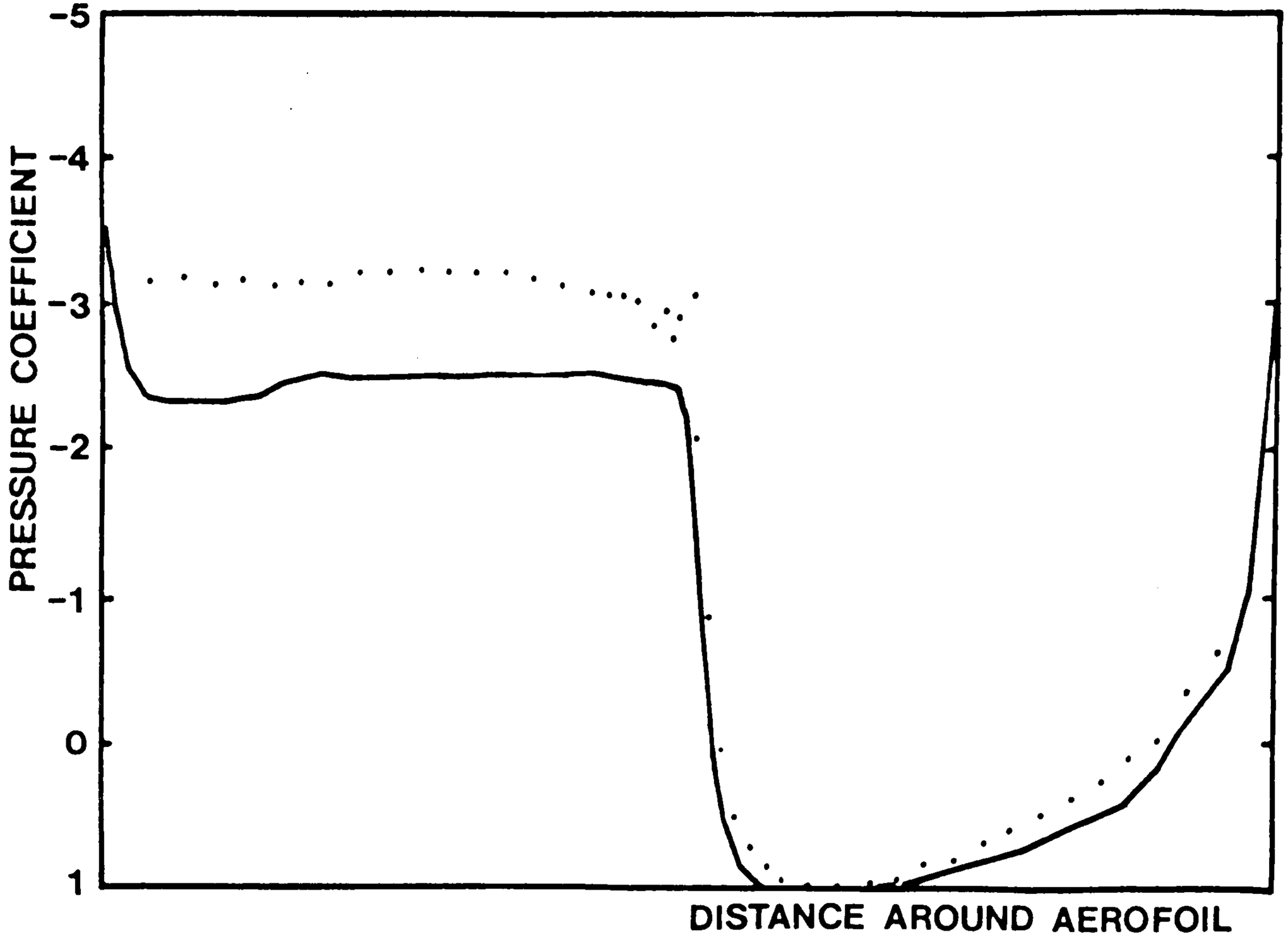

Figure 7.13 The Surface Pressure at 60°

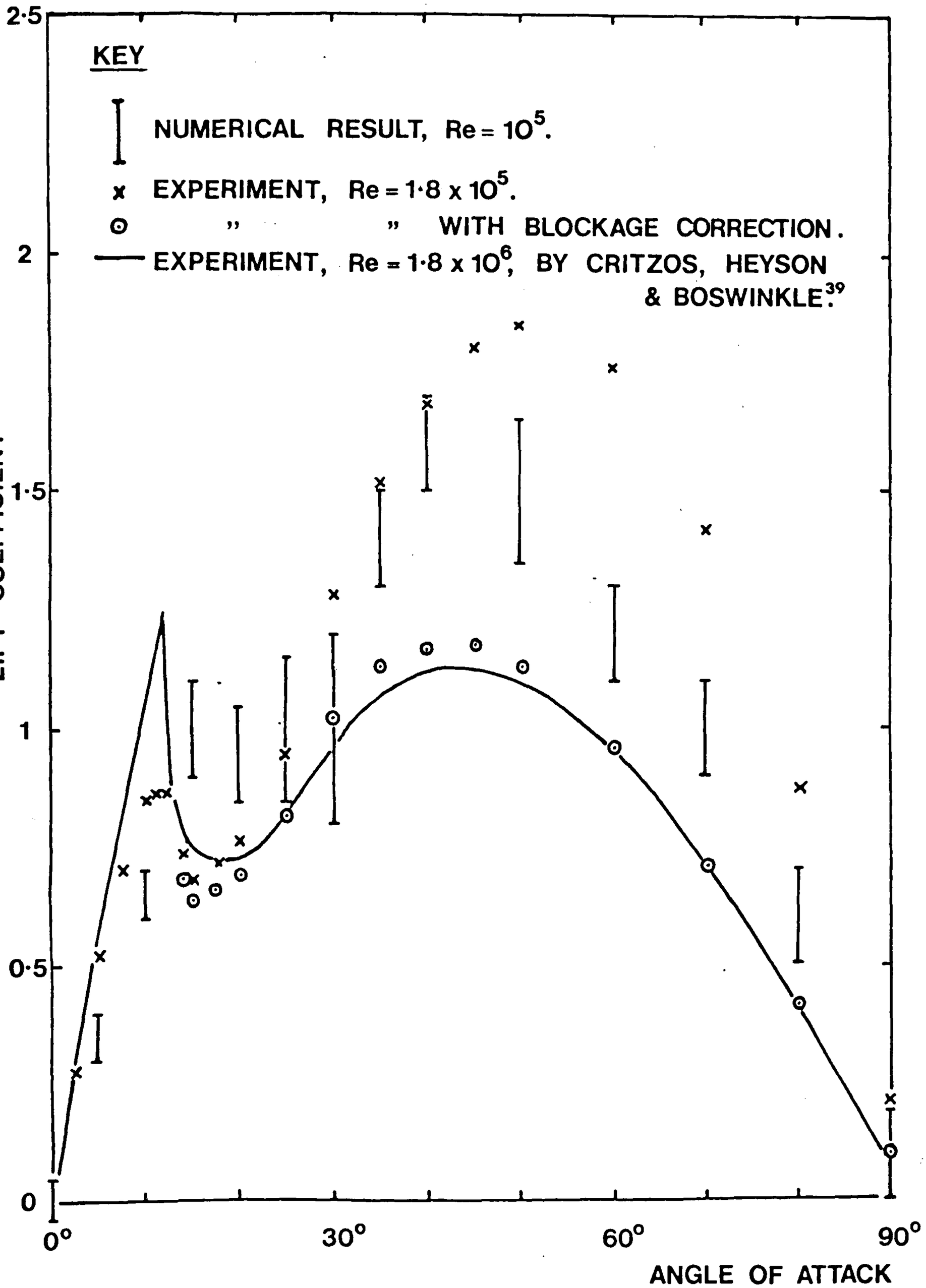

Figure 7.14 The Aerofoil Lift Characteristic

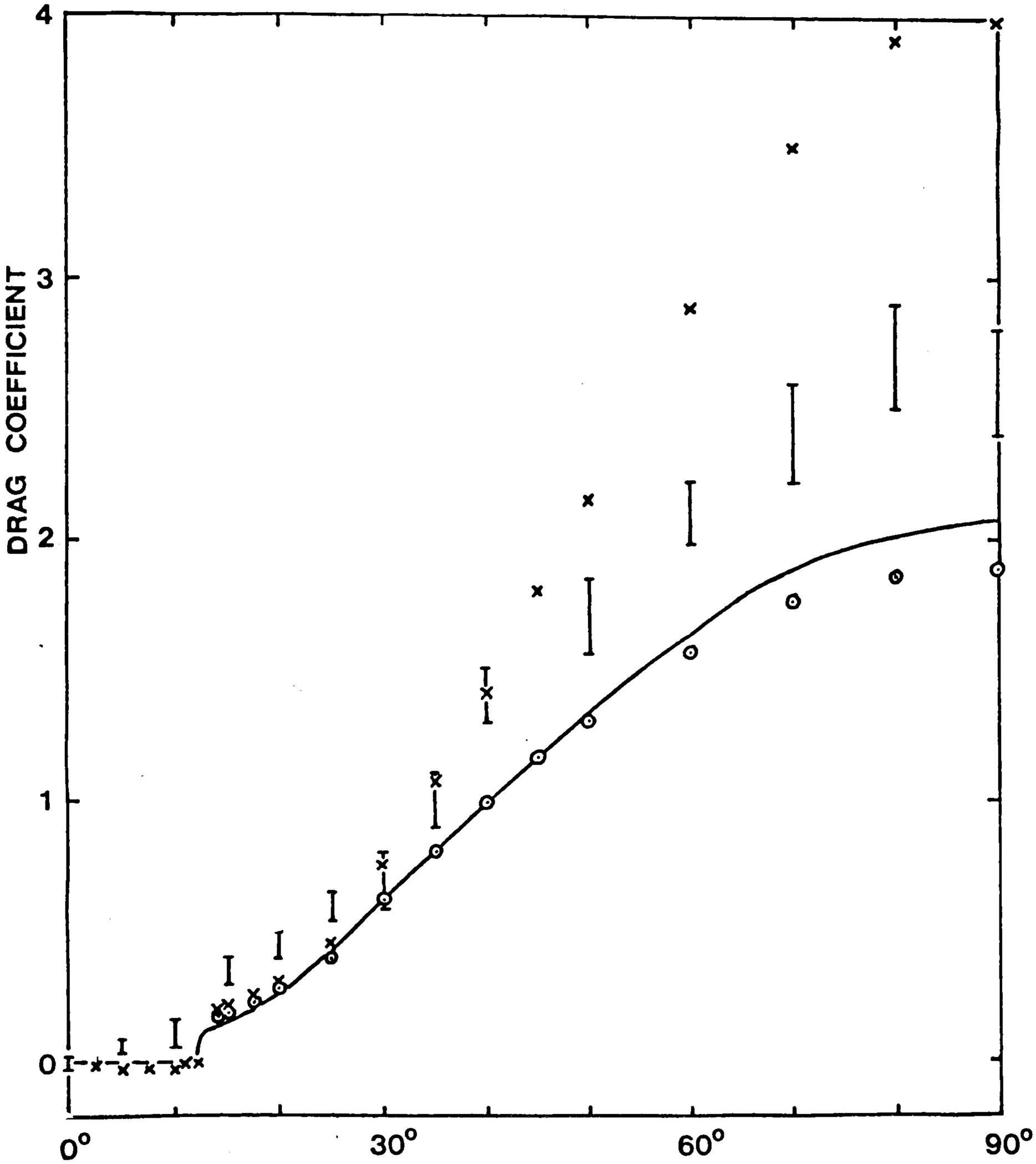

Figure 7.15 The Aerofoil Drag Characteristic

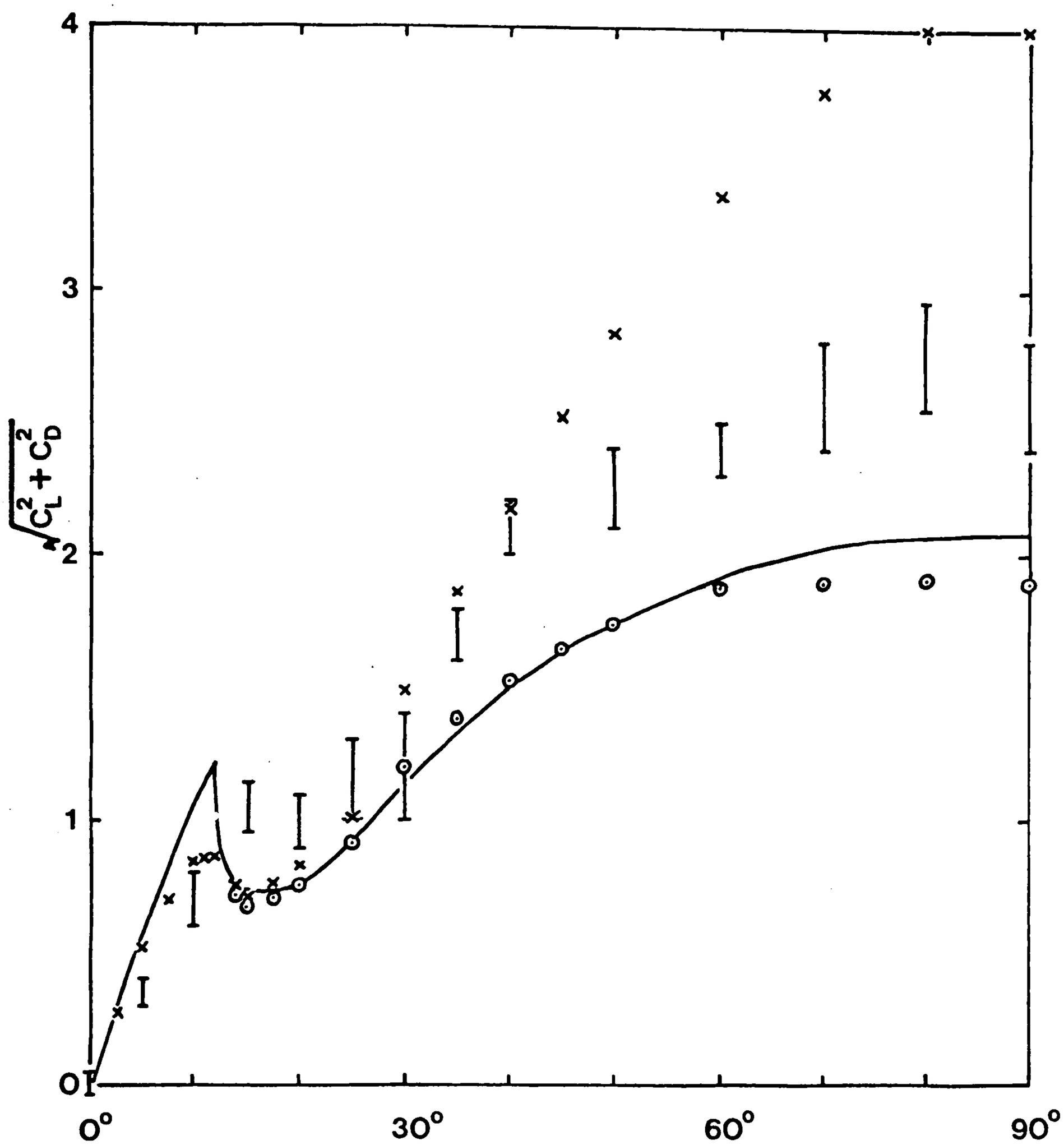

Figure 7.16 The Total Force on the Aerofoil

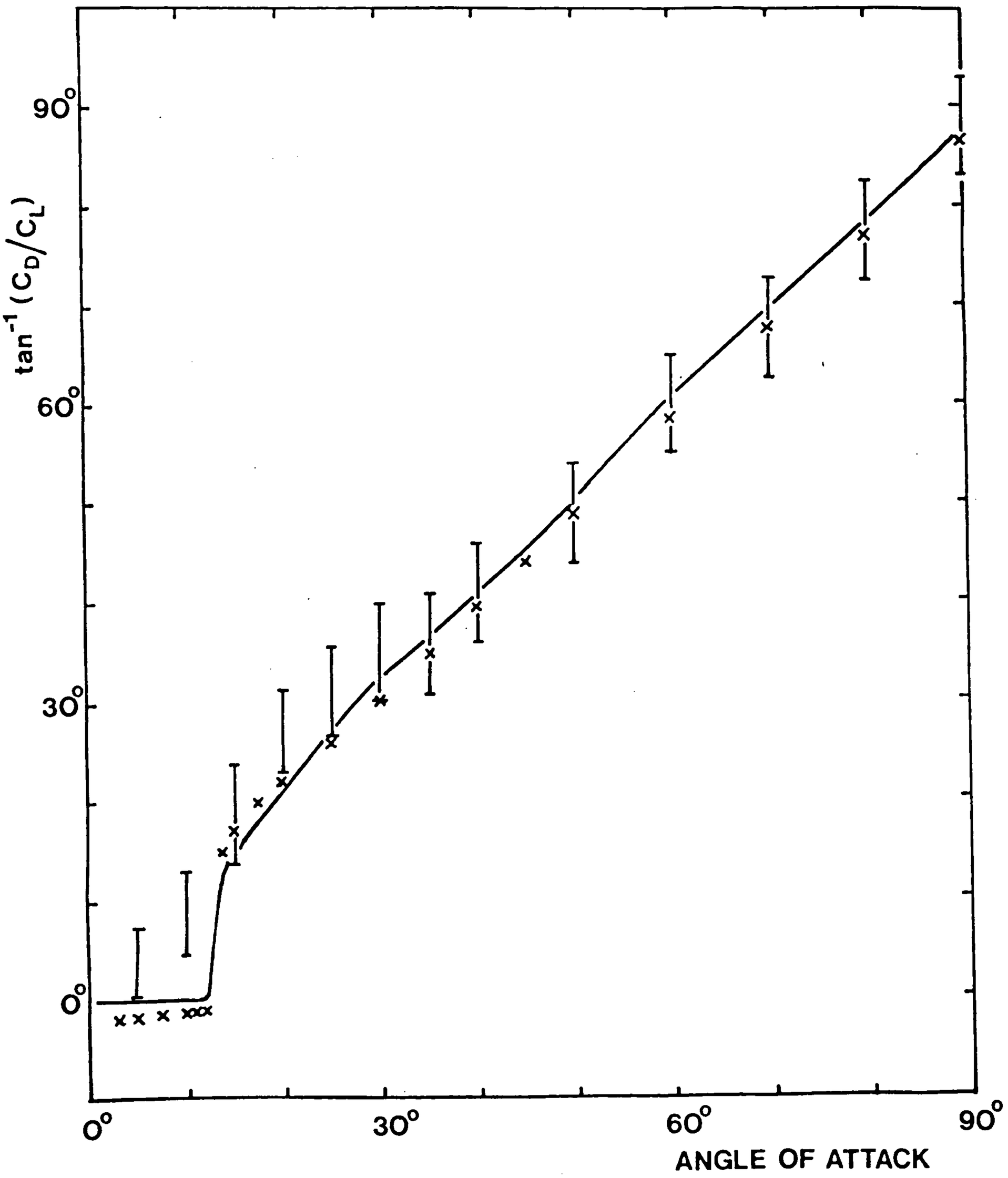

Figure 7.17 The Direction of the Force on the Aerofoil

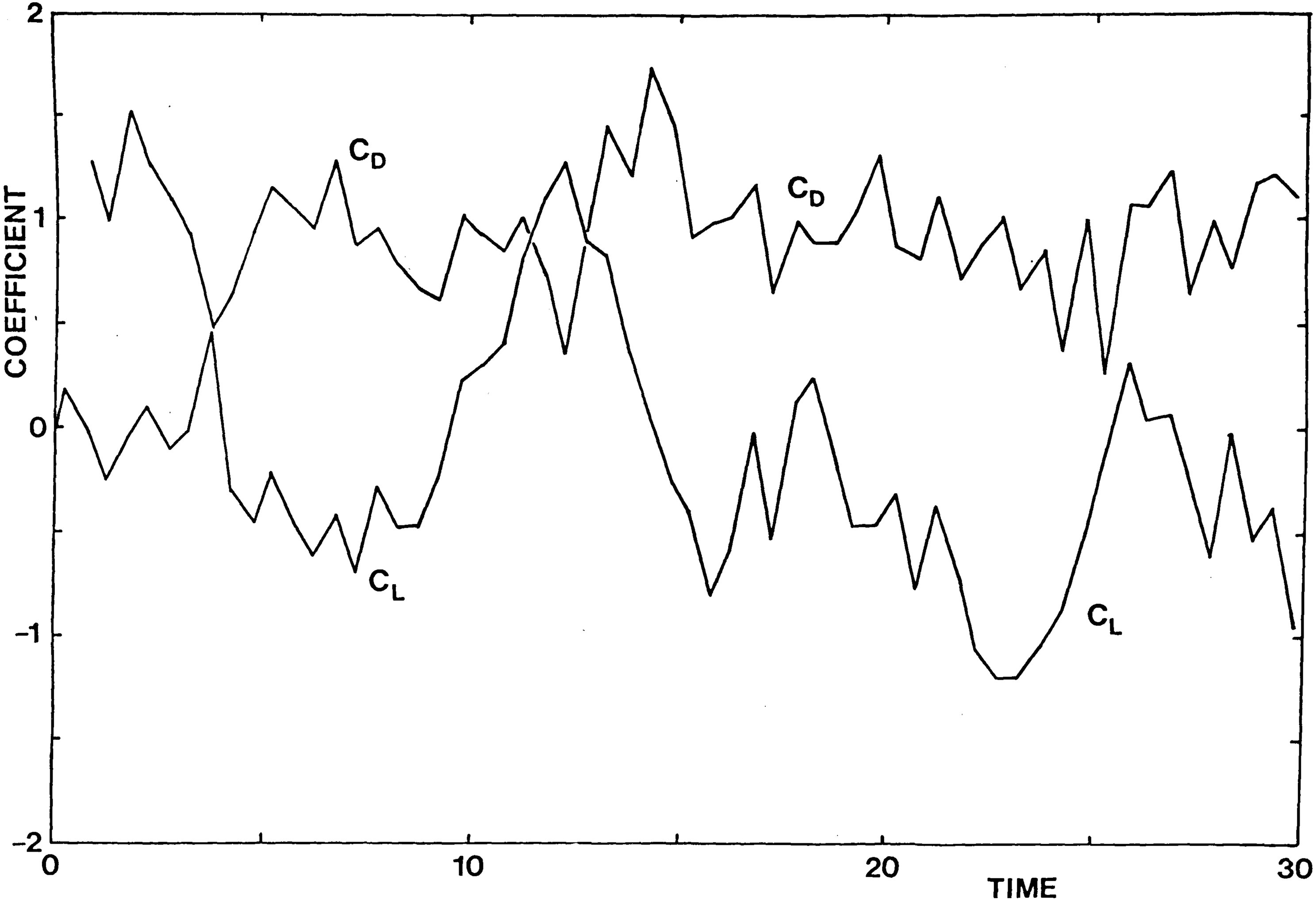

Figure 7.18 The Time Variation of Lift and Drag on a Circular Cylinder by Simulation at Re = 100

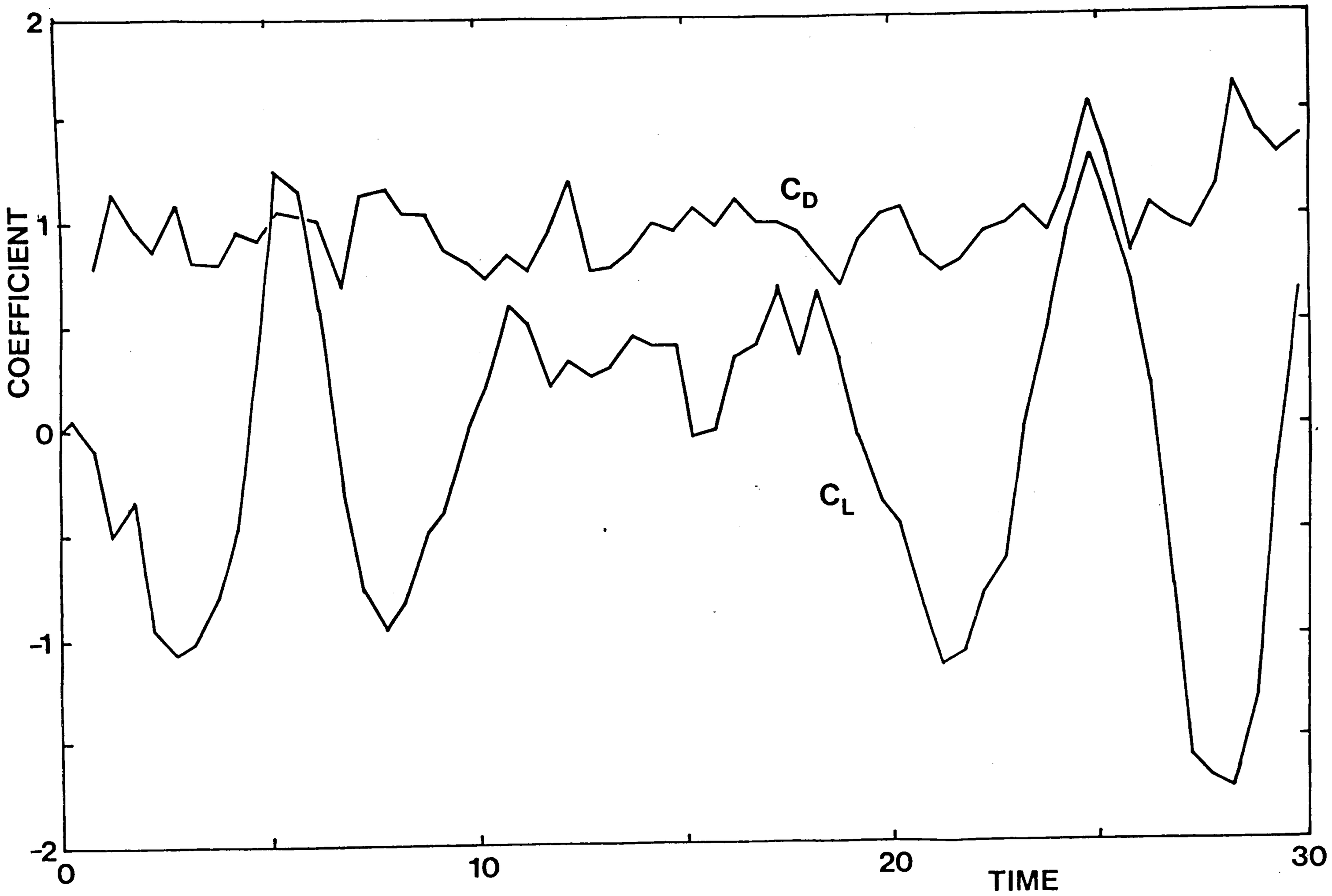

Figure 7.19 Lift and Drag at Re = 1,000

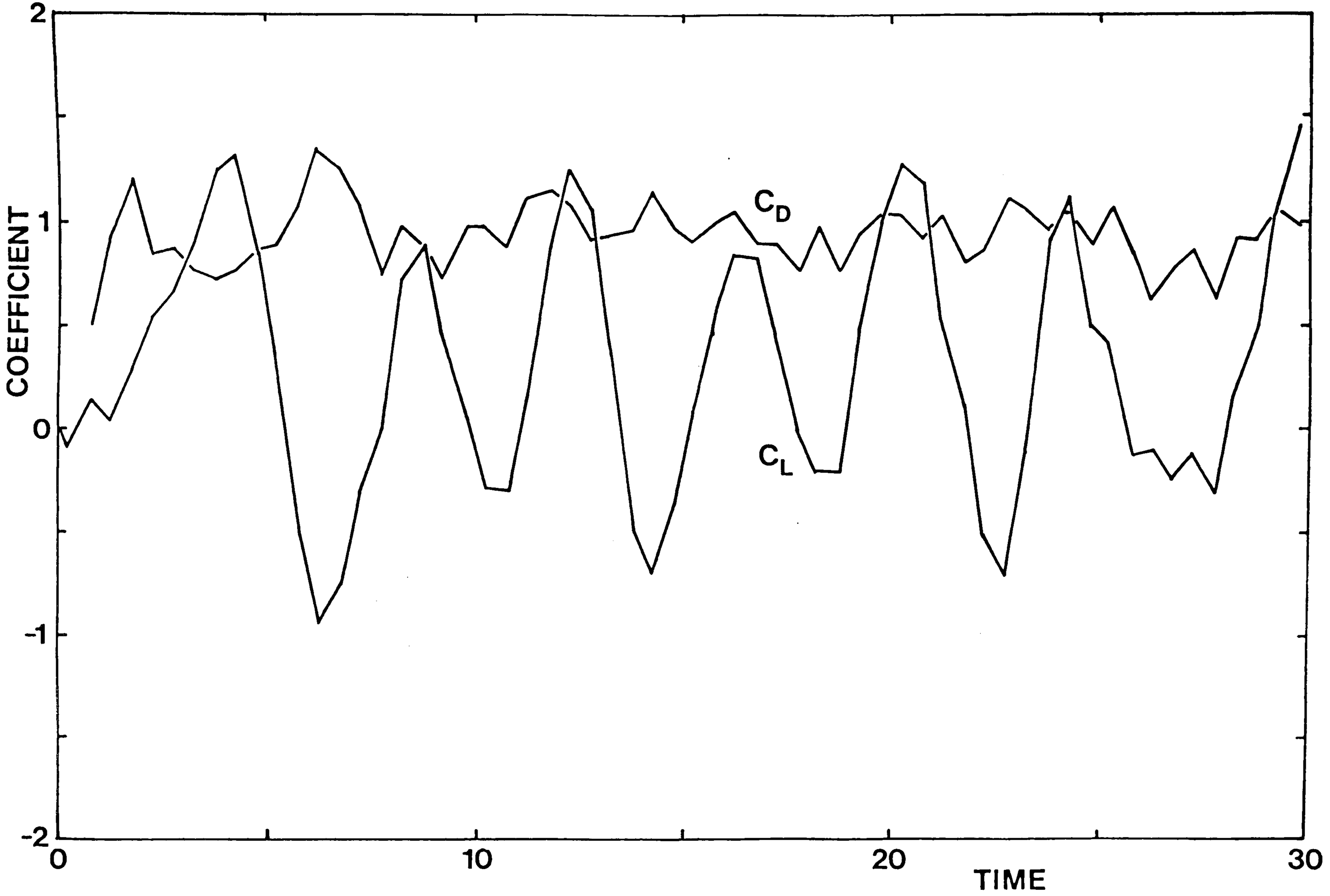

Figure 7.20 Lift and Drag at Re = 10,000

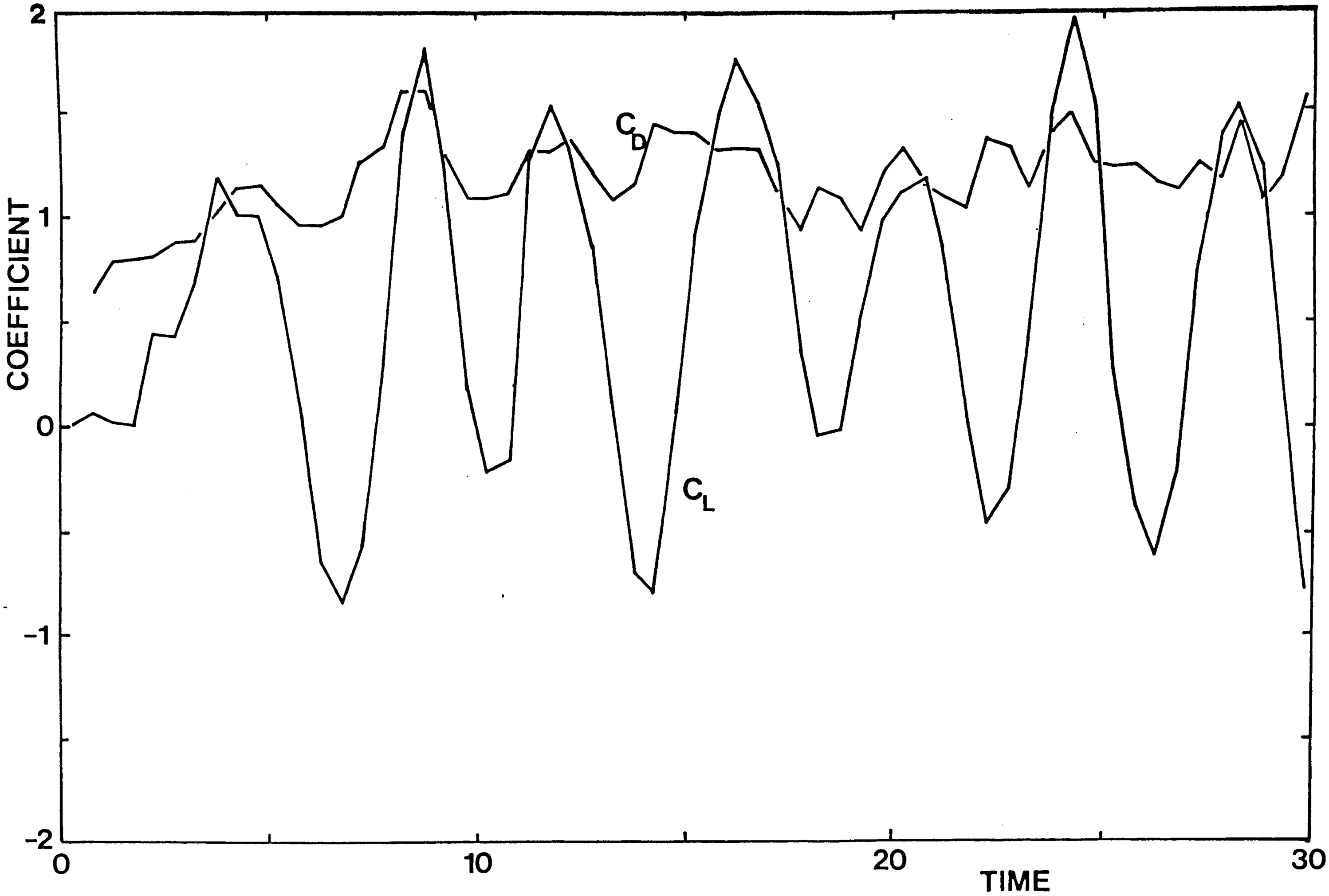

Figure 7.21 Lift and Drag at Re = 100,000

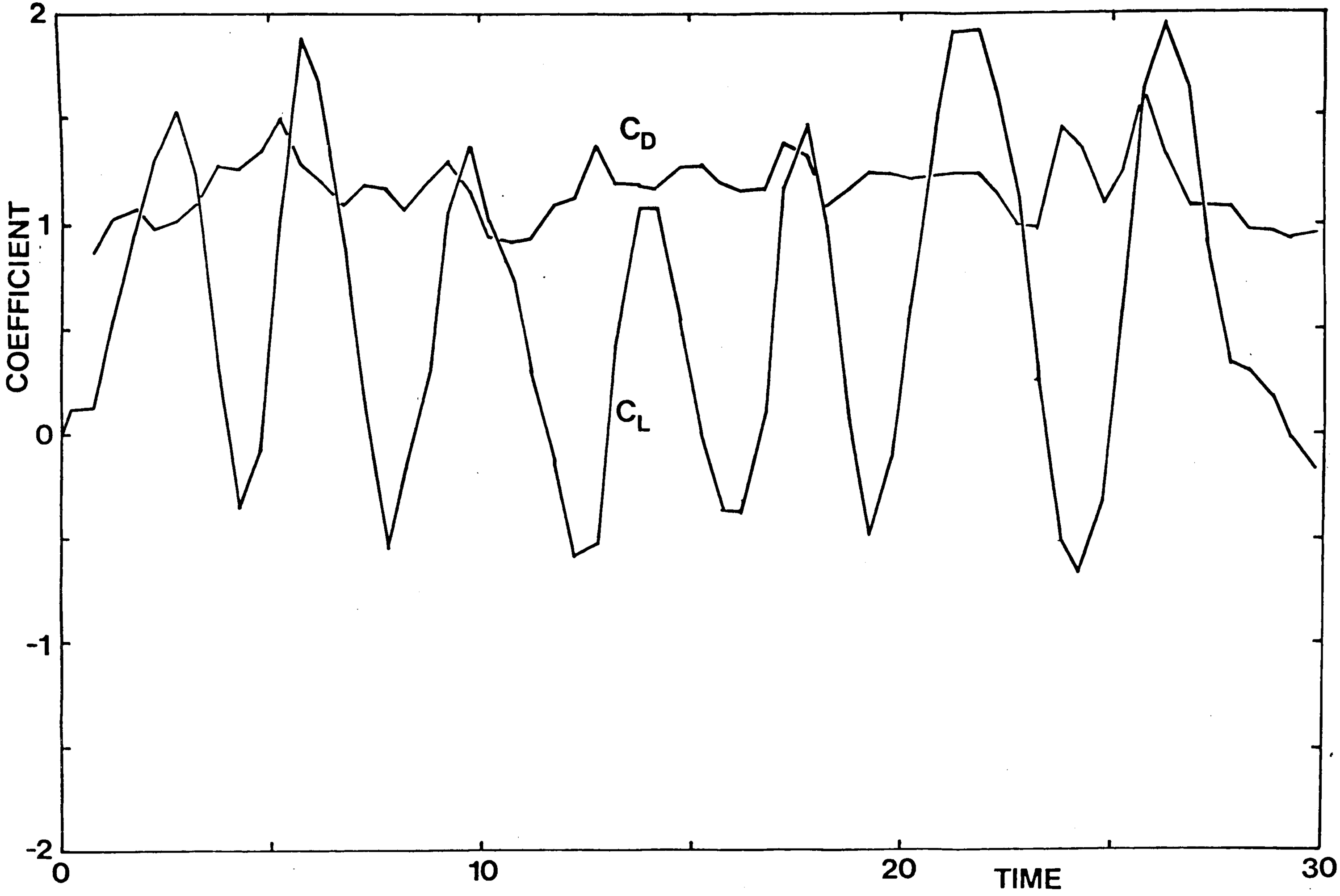

Figure 7.22 Lift and Drag at Re = 1,000,000

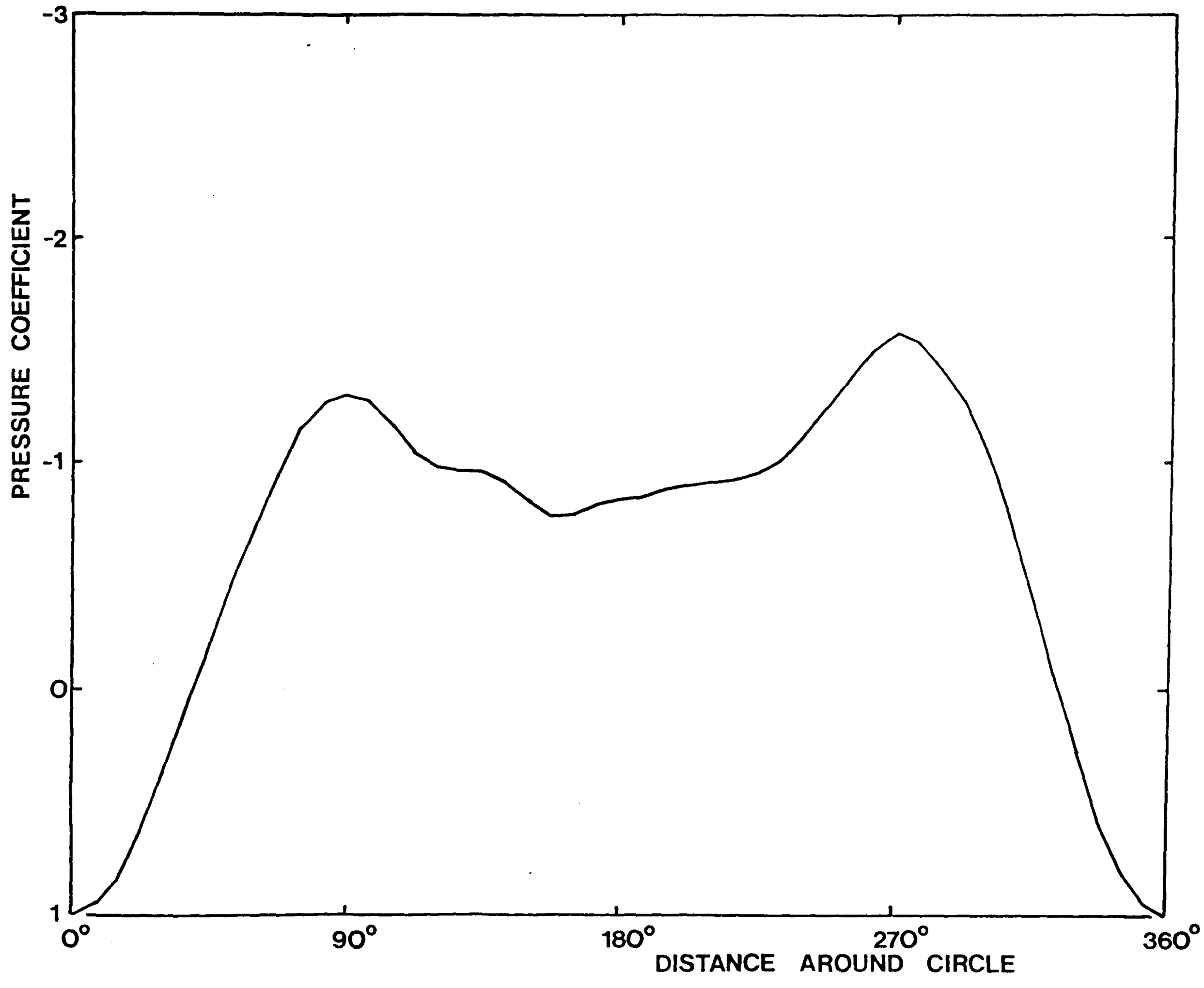

Figure 7.23 The Time-Averaged Surface Pressure Distribution at Re=100

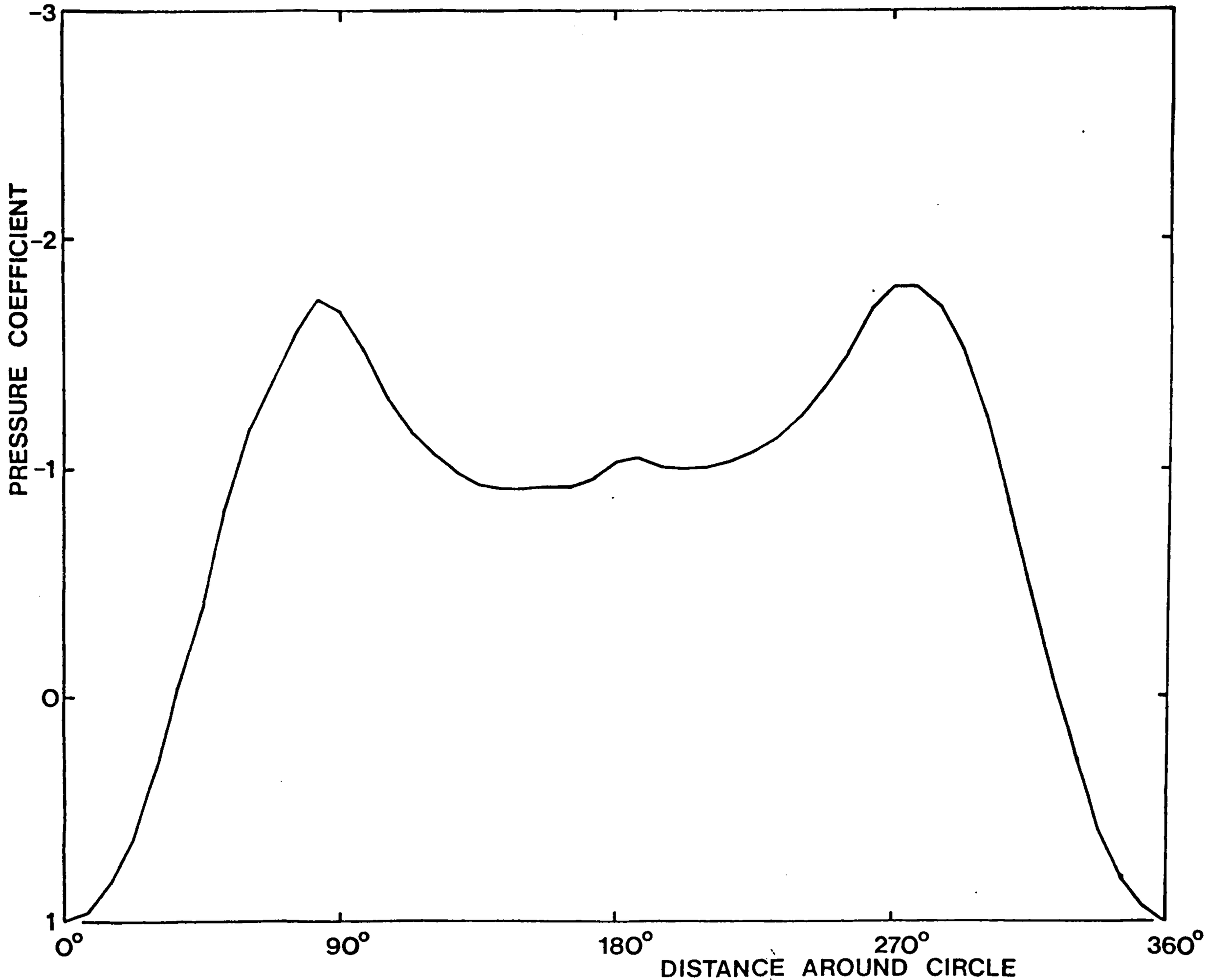

Figure 7.24 The Surface Pressure at Re = 1,000

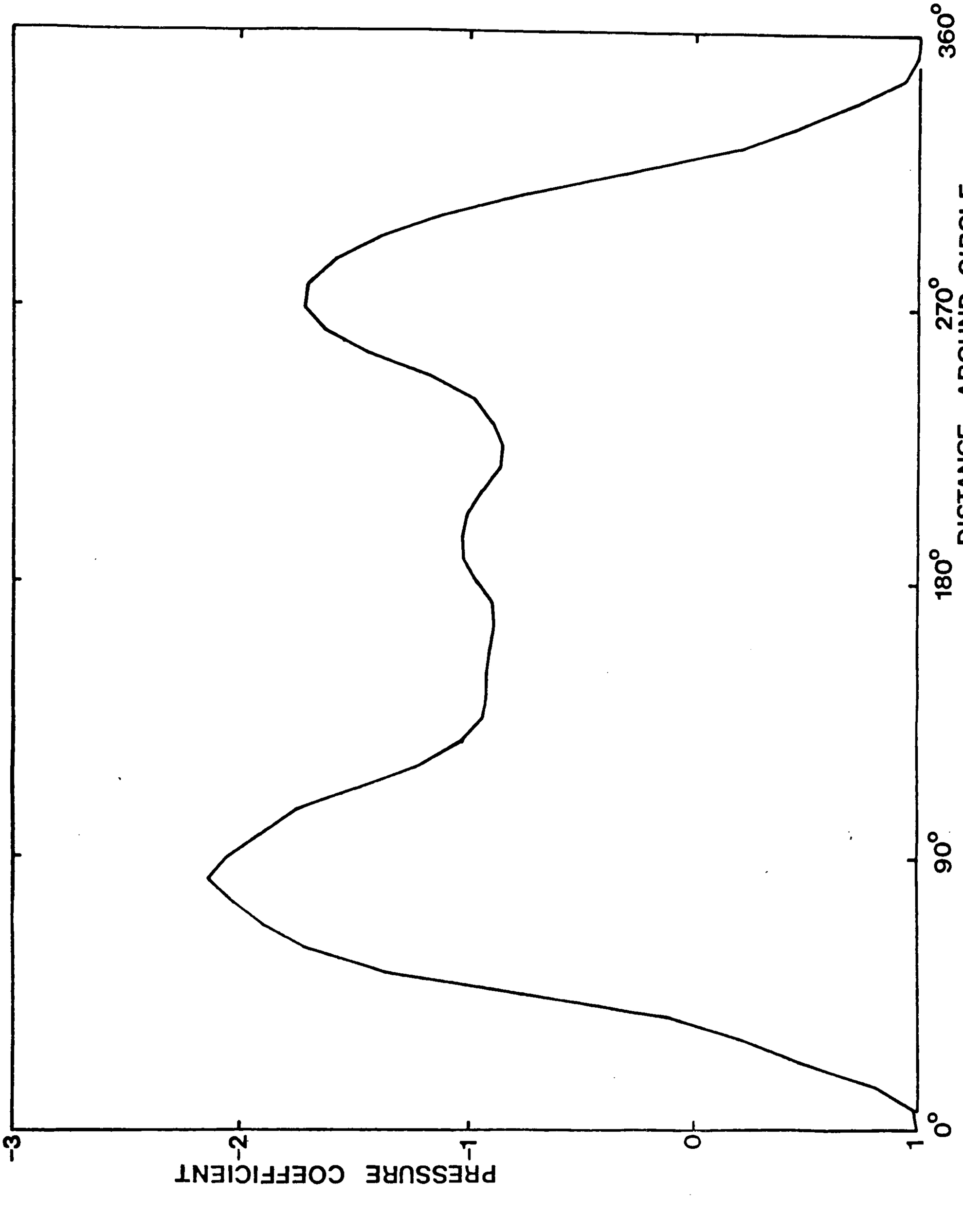

Figure 7.25 The Surface Pressure at Re=10,000

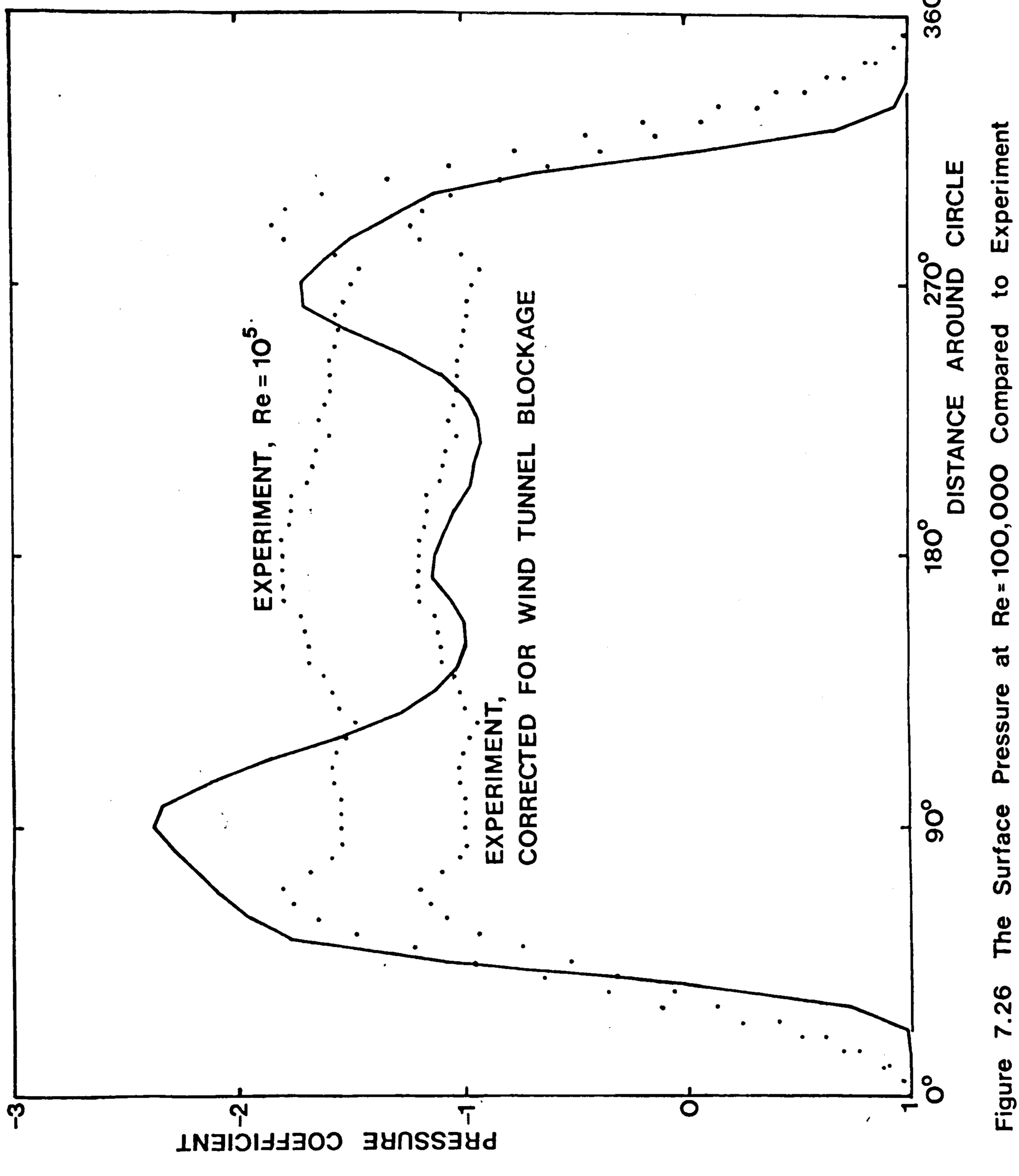

Figure 7.26 The Surface Pressure at Re = 100,000 Compared to Experiment

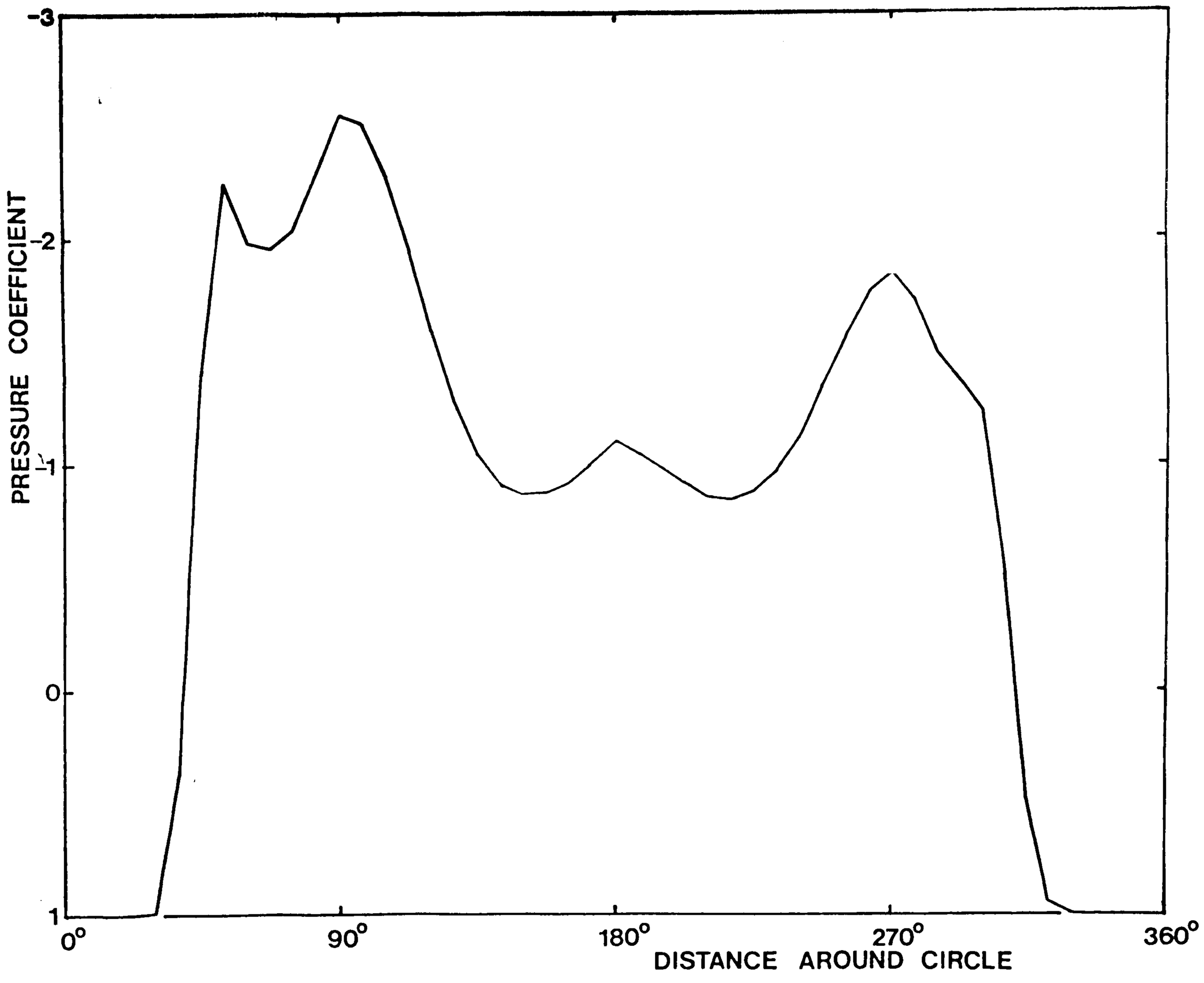

Figure 7.27 The Surface Pressure at Re = 1,000,000

CHAPTER 8. FLOW SEPARATION FROM MULTIPLE BODIES

It has been seen already that there is a shortage of computing power to do the simulations of flow separation, so it would seem excessively ambitious to consider separation from several bodies when the computing time is liable to increase as the square of the number of bodies. There is though one stall phenomenon which it is well worth trying to reproduce. When a compressor is taken to a high loading, it can do two things (Emmons,Pearson and Grant[40]; Huppert and Benser[41]; Stenning[42]). There may be large irregular oscillations in the flow through the compressor, known as surge, and an oscillating force of much higher frequency may appear on the compressor blades, indicating a type of stall which jumps from blade to blade which is known as rotating stall. Since surge is a function of the 'capacitance' of the system, related to the compressibility of the fluid, it cannot be simulated by the present method. It is as well to remember, though, that changes in the axial flow through a compressor propagate at the speed of sound, but as the inlet angle to a cascade fluctuates, it sheds vortex sheets to try to retain a Kutta condition, and these sheets travel at the speed of the fluid.

There was considerable effort to understand rotating stall beginning with the 1950s, but this effort has met the basic problem of intractibility

for any method but the one presented here. Even for the present method, there is an obvious difficulty that there are two very different length scales, one the thickness of the boundary layer, and the other the distance between the blades. The simulation that will be performed is necessarily crude. It will be seen how matters turn out, but before this, some general considerations on multiple bodies will be presented.

8.1 THE ANALYSIS OF MULTIPLE BODIES

It was remarked in Chapter 5 that the Martensen Method requires a supplementary condition. This is either a Kutta condition or a circulation condition. In the case of several bodies, each body will require its own supplementary condition. Each body could be given a Kutta condition before the matrix is inverted. Alternatively, each body could be given a circulation condition before the big matrix is inverted. After inversion, a Kutta condition could be introduced by solving a second small system of linear simultaneous equations which describe how each body can influence the Kutta condition on another body. This was the method used to test the computer program.

The circulation around each body was also corrected in a manner which must now seem familiar to the reader. The correction applied was adequate,

but not the most sophisticated correction that could be applied. We could correct the coupling coefficients between bodies so that the flux and circulation integrals around both contours were correct. This would be essential in the case of an aerofoil with a flap or slat, but it is not necessary otherwise.

For several bodies, each with a Kutta condition, the total lift should equal the total circulation, and the total drag should be zero. A Martensen Method can be executed, and the pressure distribution around each body obtained, giving, by integration, the forces on each body. These may be summed and the resulting comparison with the total force which should be obtained is a good check on the computer program. This has been tested for several geometries, and the results are satisfactory. Also, one can analyse a single aerofoil in cascade, and then two aerofoils at twice the pitch, and show that the results are the same. This also works properly.

When a cascade of aerofoils has an initial condition of no circulation, the flow outlet angle must be equal to the flow inlet angle (figure [8.1]). Each aerofoil then sheds a starting vortex, and when the starting vortices have been convected sufficiently far downstream, resolution effects make them look like a continuous vortex sheet. Between the aerofoil and the sheet the flow is deflected. It is this deflected angle which is normally

referred to as the outlet angle.

When the cascade is not stalled, it is customary to define yet another angle, the vector mean angle, by

$$\tan \alpha_m = 0.5 (\tan \alpha_1 + \tan \alpha_2) \qquad (8.1)$$

The component of the blade force parallel to the direction of the vector mean angle does not do any useful work on the flow, but merely increases its entropy, and for this reason it is referred to as the drag force. The other component of the blade force is exchanging work with the flow as desired, which may alternatively be interpreted in terms of the blade as a moving vortex as in Chapter 2.

When the cascade is stalled, a mean outlet flow angle may still be estimated in any given plane by counting the amount of vorticity upstream of this plane (figure [8.2]). Then let the amount of vorticity per blade pitch be Γ/t. The outlet angle is given by

$$\tan \alpha_2 = \tan \alpha_1 - \frac{\Gamma}{t\ U_{axial}} \qquad (8.2)$$

This outlet angle is something which must be left to the computer simulation to determine. Only the inlet angle can be prescribed.

8.2 AN ATTEMPT TO SIMULATE ROTATING STALL

The customary explanation of rotating stall, as given by Iura and Rannie,[43] is that a stalled blade represents a flow blockage which diverts the flow to either side of if. This decreases the angle of attack on the preceding blade (figure [8.3]), causing any stall present there to be suppressed, and increases the angle of attack on the following blade, promoting a stall. The newly promoted stall then diverts the flow in its turn, and so on. Many other explanations may be speculated upon. For example, a stalled blade produces a vortex street, which can lock on to the vortex street produced by another blade. Each blade then experiences an oscillating force, but the phase shift between the blades gives the appearance of a rotating stall. It is possible that no two-dimensional flow explanation will suffice, or that there are several different regimes of rotating stall. Since there is so little a priori knowledge, one can only try out the computer simulation and see.

Three blades is probably the minimum necessary to observe rotating stall, even though real compressors have something like ten times as many. For the computer simulation, these three blades have been cascaded in a pitch equal to three times the distance between blades. Thus this is like unwrapping a three-bladed rotor, where the flow around each blade is

independent. Each blade was represented by thirty two pivotal points, and in one time step the asymptotic inlet flow travelled a distance of one tenth of a blade chord.

The results for a high angle of attack will be shown first, even though rotating stall is normally observed as the first sign of stalling. At an angle of attack of 85 degrees (figure [8.4]), the three aerofoils begin by doing the same thing. Each sheds a trailing vortex, and then stalls at the leading edge. For a considerable time after this, the flow looks confused. Beginning at a time when the flow has travelled about twenty blade chords, a large vortex appears upstream of the blades (figure [8.5]) and persists for as long as the simulation is continued (figure [8.6]). The vortex loses vorticity through the blade passages, but is replenished as it passes each blade, and will presumably last forever. This is obviously a possible mechanism for 'deep' rotating stall.

Reducing the angle of attack to 80 degrees (figure [8.7]), a vortex of the same type may still be seen. This vortex does not last indefinitely. It was observed that the vortex occasionally vanished, and then another vortex appeared at an unpredictable position, to disappear some time later in its turn. The same mechanism is at work, but it may be a fault of the crudeness of the simulation that the vortex does not persist.

At 75 degrees angle of attack, there is no visual evidence of any type of rotating stall (figure [8.8]), although there does appear to be some flow separation behind the blades. It is likely that this case corresponds to a single aerofoil at about 10 degrees angle of attack, so the blades are not truly stalled.

This range of flows from 85 to 75 degrees seems, then, to bracket the range in which rotating stall is likely to occur. The mechanism of rotating stall, which is one positive conclusion to be drawn from this simulation, is that of the large vortex or soliton. The conclusion of engineering interest to be drawn from this is that it is worth the attempt to place a splitter plate just upstream of the rotor in order to disrupt the vortex when it collides with the plate.

For other cascade geometries there may be other modes of rotating stall. A point to note is that as a blade stalls it sheds large vortices which may then interact directly with the next blade, as observed by Stenning and Kriebel.[44] The standard flow blockage explanation of rotating stall only looks at the wake as if it were the same as the time-averaged wake of an isolated aerofoil, so if rotating stall is any kind of vortex phenomenon then the standard explanation is inadequate. Rotating stall is not likely to be amenable to any method but the vortex-based computer simulation given

here, because of its transient nature, its non-linearity, and the wide range of length scales.

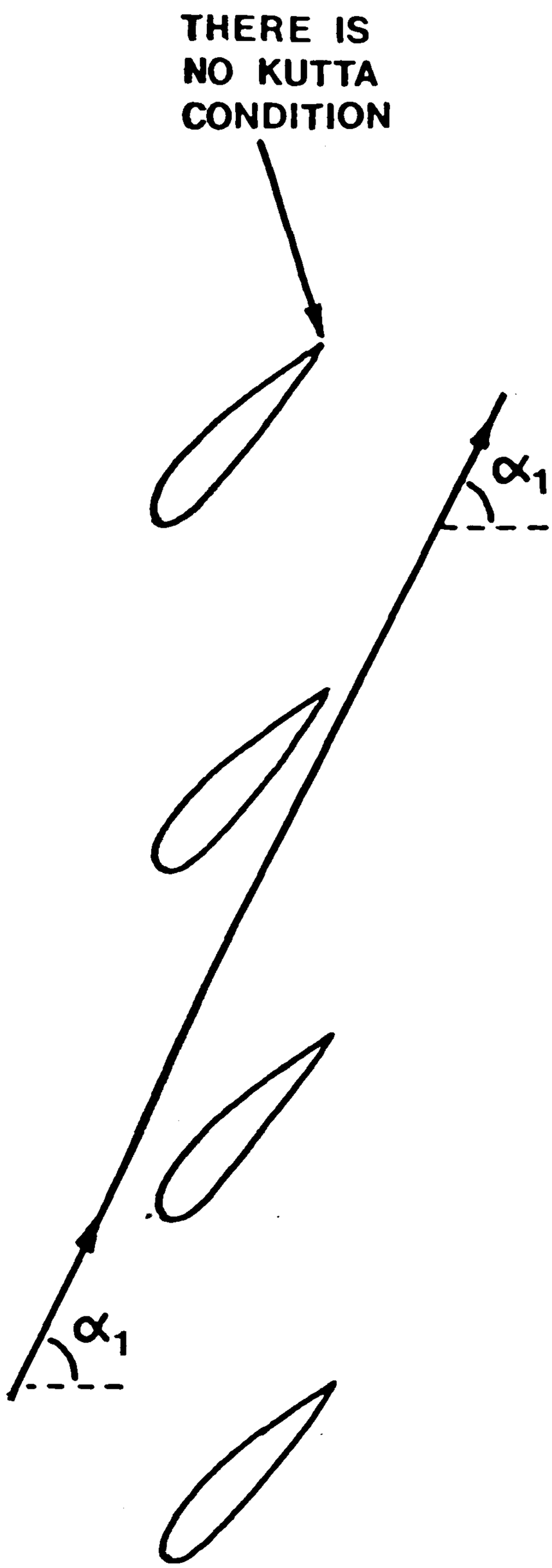

(a) Initial State

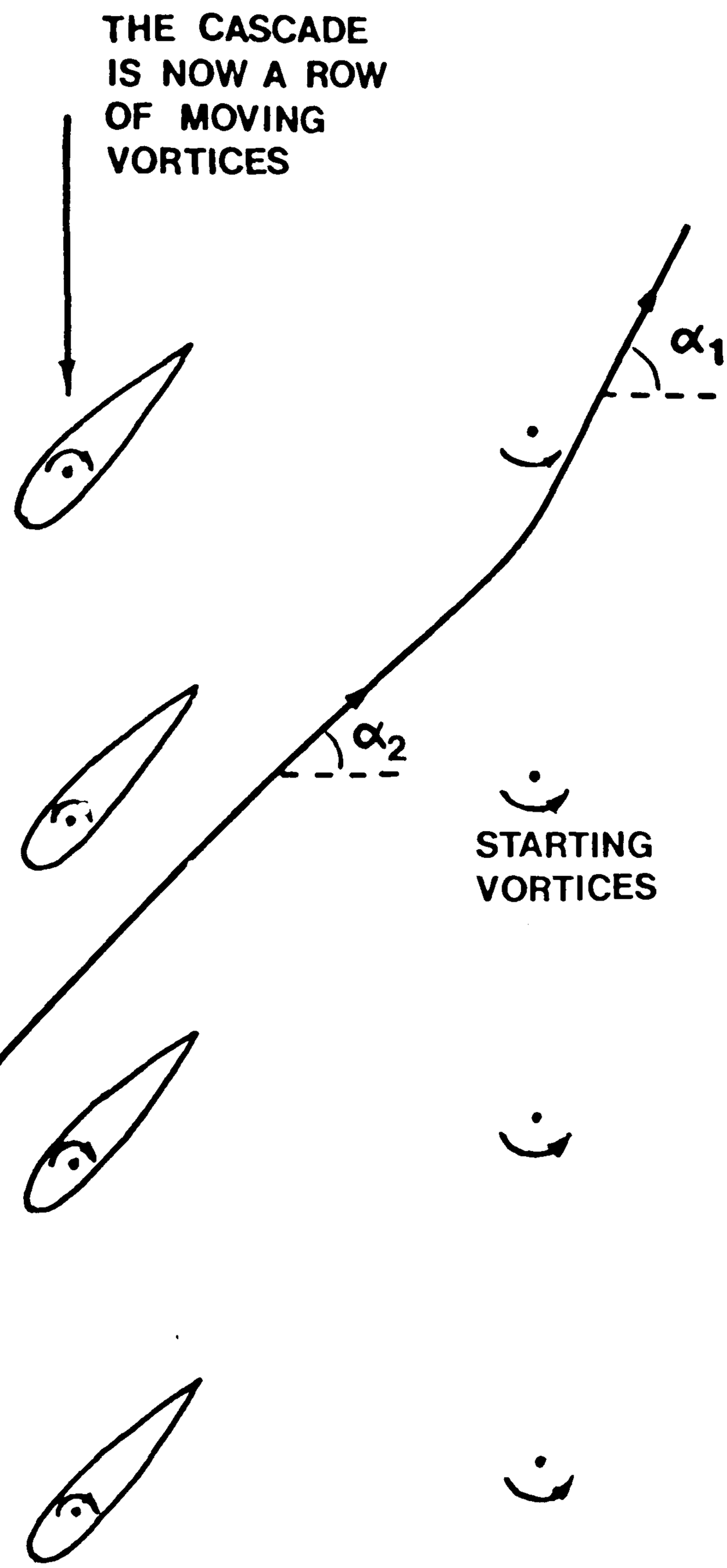

(b) Final State

Figure 8.1 The Establishment of the Flow through a Cascade

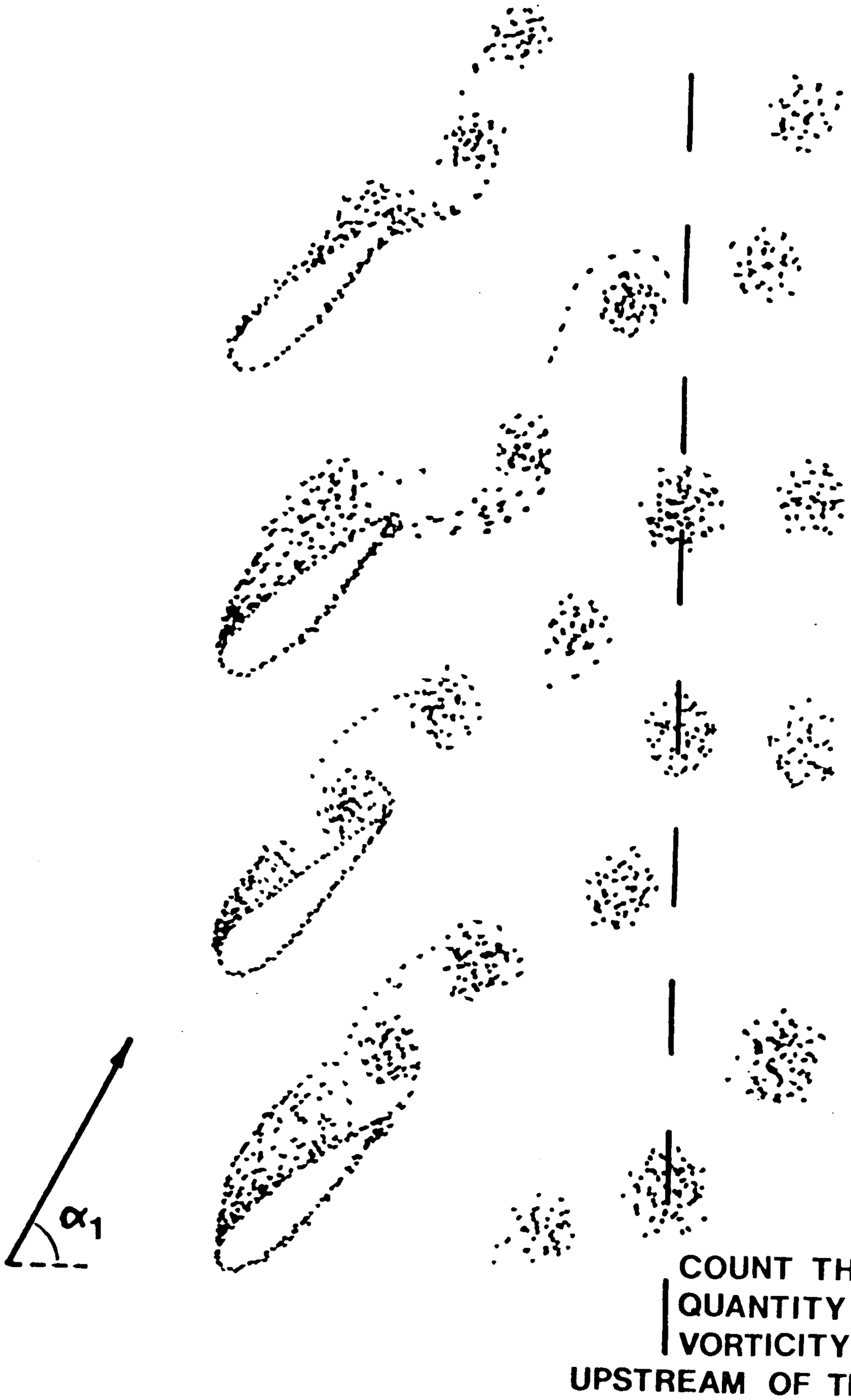

Figure 8.2 Determination of the Outlet Flow Angle

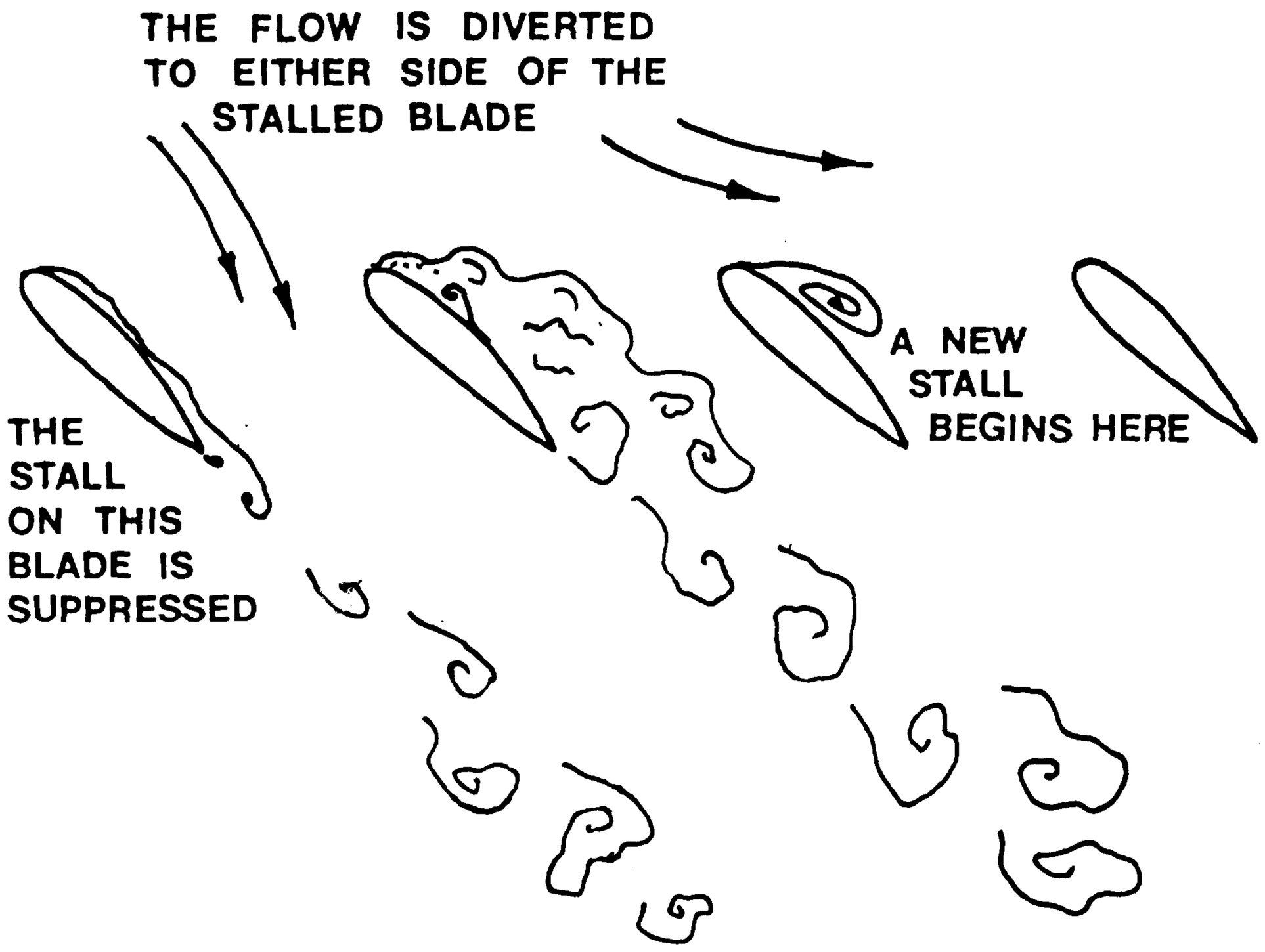

Figure 8.3 The Explanation of Rotating Stall as a Flow Blockage

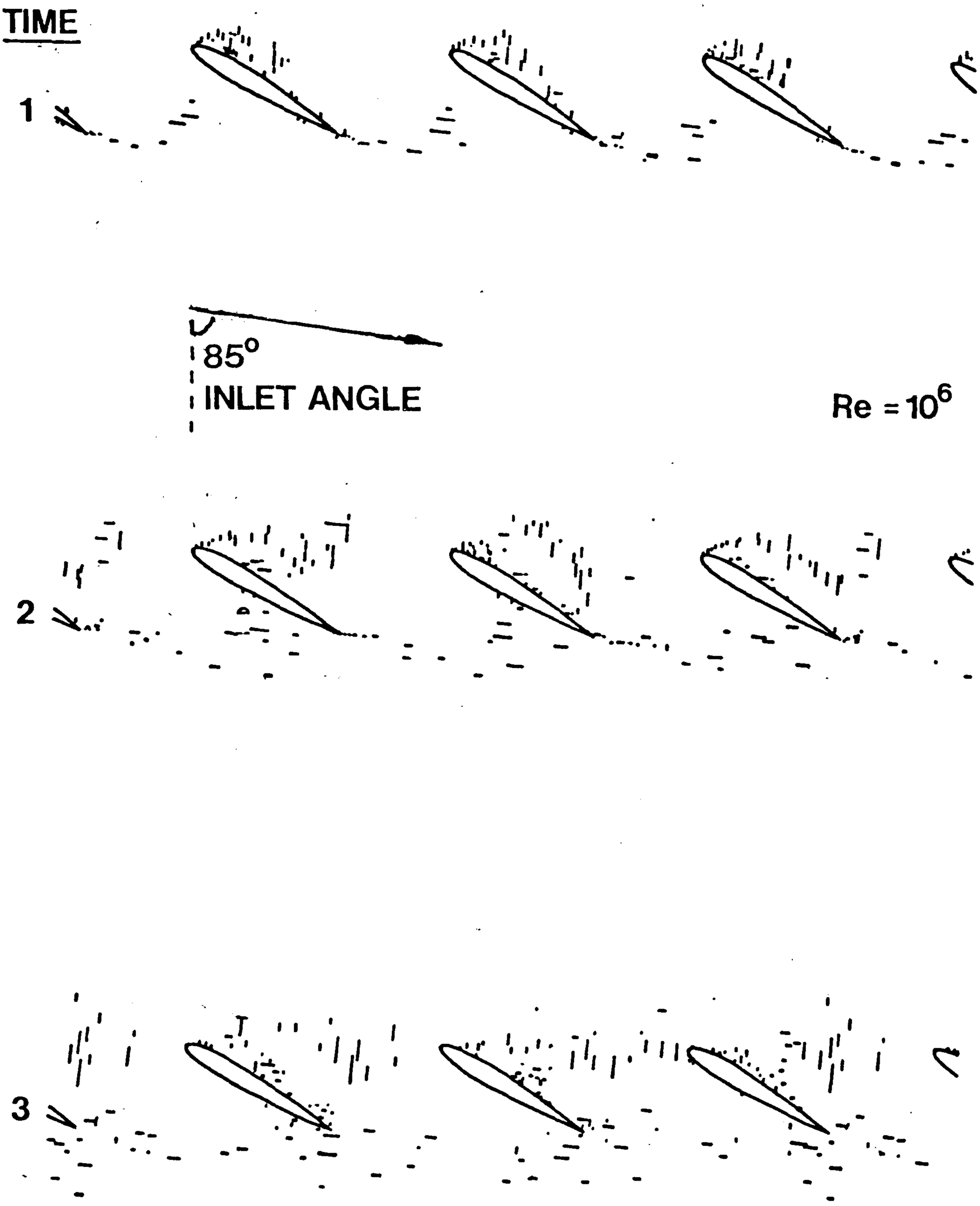

Figure 8.4 The Initial Development of the Stall of a Three-Blade Rotor

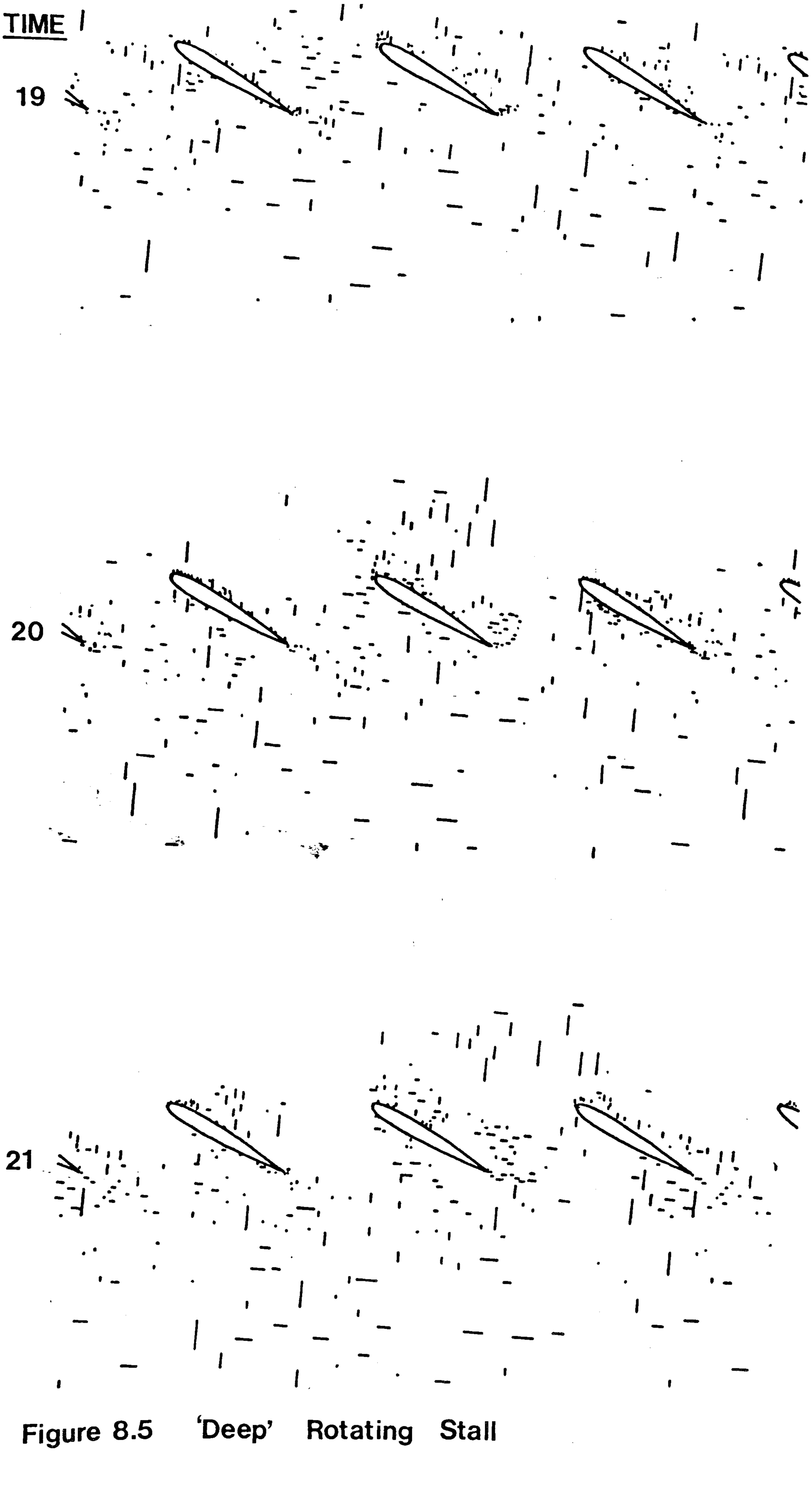

Figure 8.5 'Deep' Rotating Stall

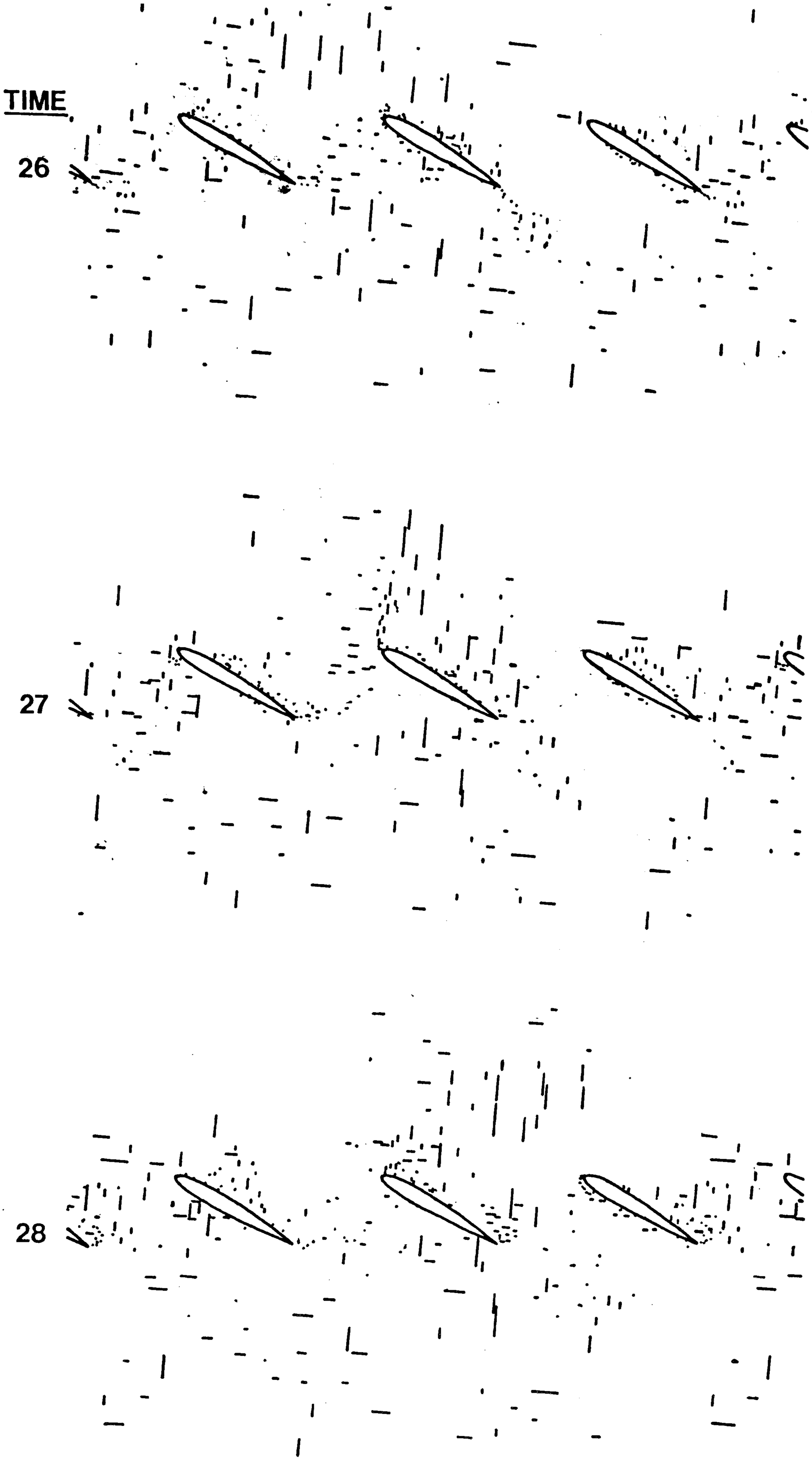

Figure 8.6 'Deep' Rotating Stall some time later

TIME

9

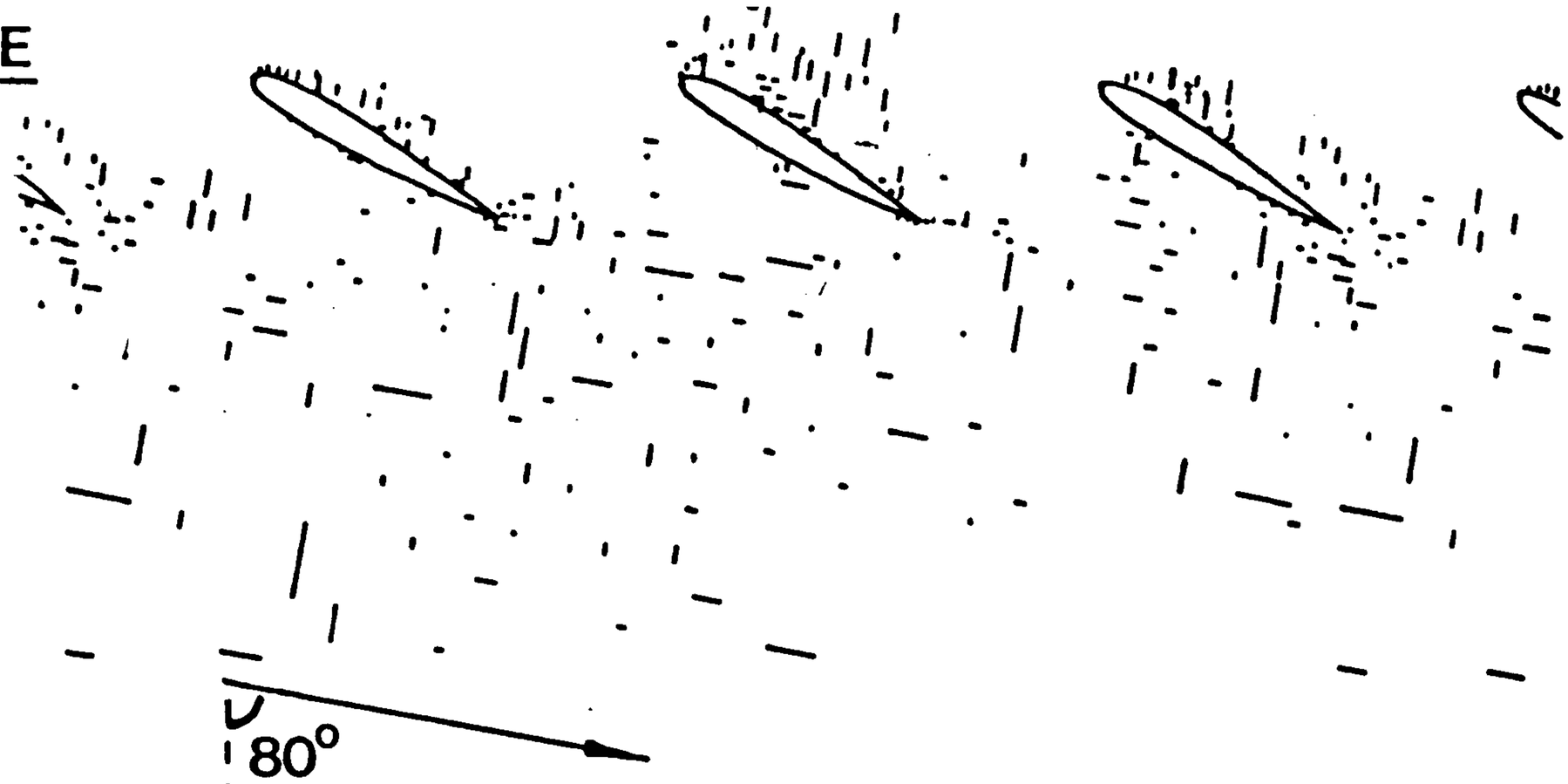

10

11

12

'Slow' Rotating Stall

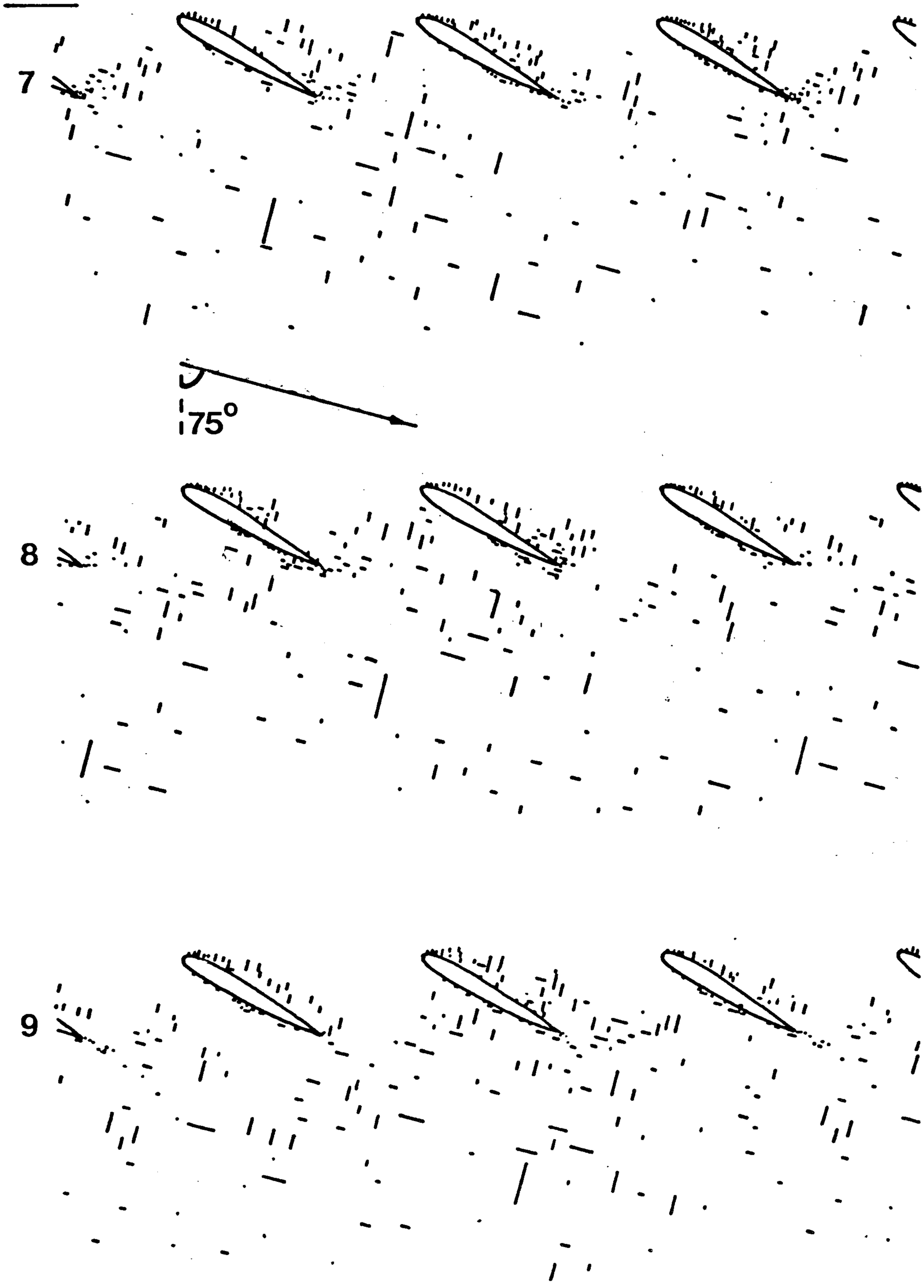

Figure 8.8 The Unstalled Rotor

CHAPTER 9. CONCLUSION

When the author began this work, computer simulation of vortex dynamics was hardly more than a curiosity. The nature of vortices as singularities posed formidable problems for the computer programmer, which are not solved just by adopting a vortex-in-cell method. Vortex methods have been developed here into a serious method for the large-scale prediction of fluid flows. All the theoretical problems have been solved for two-dimensional incompressible flow. The remaining problem is that of implementation, and as Stansby and Dixon[14] propose, the best implementation is of a vortex-in-cell method, where with thousands of vortices the error due to randomness alone is much reduced, so that at least laminar flows can be well simulated. The vortex-in-cell method is satisfactory in that it:

(a) Does not introduce numerical viscosity. There may be some second-order effects equivalent to viscosity, but a pointlike vortex does remain pointlike indefinitely.

(b) Does not introduce mysterious effects such as the 'diochotron' instability. At a first reading of Christiansen's[11] paper, the impression gained by the author was that this instability was an objection to the use of the method. A closer examination of the paper

shows that this is not so.

(c) Guarantees that the integral of flux and circulation around any closed path is correct due to the use of potentials. Note that in evaluating the circulation, we are evaluating subtended angle. It would be a gross error to imply that we could evaluate π, a transcendental number, by a finite algebraic process such as the direct evaluation of coupling coefficients. The use of potentials in the solution of Poisson's equation avoids this error.

(d) Is relativistically invariant. This is related to property (a).

These are all issues of quality control in computer simulation.

We will be forever hungry for computing power, but even so, the method works with relatively few vortices. To double the resolution of the flow, four times the number of vortices are needed, but it follows conversely that if fewer vortices are used, then there will not be too serious a deterioration in the results, so a good qualitative picture of the flow is often readily obtainable.

From the vortex dynamics, it has been shown how to calculate pressure distributions, and thus lift and drag. It is pleasant to note that in this respect, fluid mechanics is linear in the relation between pressure and

vortex flux, so that after all the complication of the Martensen Method and the vortex dynamics, something very simple remains to be done. Once it did not look so simple, but now we can do predictions of the forces in the flow around bluff bodies which are of engineering interest. One immediately thinks of the bridges, cooling towers, and oil rigs which have had problems with wind and sea forces. Prior analysis of these in a 'numerical wind tunnel' would have saved a good deal of grief at little cost. It is also a simple matter to allow a body to be non-rigid, so oscillating bodies can be dealt with. Bodies exhibiting a standard second order response to applied lift and drag forces would be reasonably insensitive to the noise produced by the random vortex method. The extra degrees of freedom of the body would greatly increase the computing time necessary to study the interaction between the characteristic frequencies of body and flow.

The results obtained from the numerical simulations are of mixed quality. The worst results, in the author's opinion, are of the critically decelerating boundary layer and the circular cylinder. The best results are the Blasius profile, the stalling aerofoil and rotating stall. Every one of these simulations is worthy of repetition with more computing time and a bigger computer.

One problem to note is it took eight months to compute the

characteristic of a stalling aerofoil. Does one dare to think that there might be a mistake in the writing of the computer program? On this timescale, it would be a terrible thought, which is why so much attention has been given to questions of quality control in the numerical method. The first computer programs were written in FORTRAN, hardly the most secure of computing languages. Later, programs on the microcomputer were written in PASCAL, which is designed so that as many mistakes as possible are detected by the compiler. The very last program written, to integrate experimental results for the stalling aerofoil, was written in MODULA-2, designed to be the successor to PASCAL. This is quite a change in software technique, but it is in the direction of greater security of computer programming, essential to minimise the number of errors made in undertaking large and long computer projects.

One type of error which may be made is in the formulation of the model. For example, the quantity

$$\sqrt{4\,\nu\,dt/3}$$

which appears as the distance of a newly created vortex outside the surface is dimensionally correct, but the reader may be able to prove either that the numeric factor is wrong, or that it is wrongly implemented in the computer program. Likewise, if one has a function of x and y correct for

x>0 and y>0, something can go wrong if either x<0 or y<0, particularly if a program has been modified several times to trap special cases. These errors, if made, can be insidiously difficult to detect. It should be just a matter of algebra, but proper algebraic computing languages (the 'abstract data type' languages such as SIMULA, ALGOL, MODULA-2 and ADA) are not widely available. It is not normal in publishing the results of research to suggest that one may have made a mistake. However, it is also not normal to have performed some 100,000,000,000 arithmetic operations, so it is worth pointing out that there is a heavy price to pay for even minor errors in terms of the doubt that is cast upon months of computing.

The eight month timescale must be reduced if any progress is to be made. On this timescale, it is difficult to repeat anything. With hindsight, there has been discoordination between theory and experiment in the way that the experiment has an aerofoil in a wind tunnel with a three-to-one ratio between tunnel height and aerofoil chord, while the simulation has an isolated aerofoil at a different Reynolds number. The simulation should be repeated with the experimental geometry at the correct Reynolds number. Furthermore, the simulation should be tried with shorter timesteps and more vortices to see how sensitive it is to these. In the normal course of research, one would just go back and do all these things, but on an eight-

month cycle, matters become much more difficult. Nevertheless, we would not be concluding that this would be a worthwhile activity if the method were not quite good so far.

So the future lies with the vortex-in-cell method. Rather than repeat the stalling aerofoil with the simpler method, one should proceed immediately to the better method. Then the boundary layer simulations can be attacked in greater force, and the stalling aerofoil characteristic refined. Many more cascade geometries should be examined in the simulation of rotating stall. Looking further ahead, it can be specified in theory how sources may be added to simulate compressibility. Three-dimensional flows are also likely to be much easier to simulate with a compressible flow method, since one abandons instantaneous action at a distance, and thus the complications of the Martensen' type of analysis can be dispensed with.

It is fascinating to see that a method developed to simulate incompressible flow has such a strong undercurrent of thermodynamic theory, so that we have, in choosing a Monte-Carlo method, stumbled upon the mechanism of process thermodynamics, at least for the requirements of computer simulation. Two-dimensional incompressible fluid mechanics may be described as the prototype of any big nonlinear system, so with the concrete example of vortex dynamics in mind, we can now generalise. These

generalisations will prove to be important when compressible flows are considered.

Suppose we have a universe full of Hamiltonian systems. We formulate a definition of entropy. For every Hamiltonian system in which this entropy is increasing, there is an equal probability of existence of a system in which entropy is decreasing. This remains true when one mixes a 'hot' system with a 'cold' system, or systems equivalent to gases of two different species. It will be found that with any definition of entropy, either one half of all Hamiltonian systems are decreasing in entropy, or Hamiltonian systems are isentropic.

This is known as Loschmidt's Paradox.[31] Another paradox, due to Zermelo, is that a Hamiltonian system must at some future time return somewhere near its original state, so the entropy must decrease as often as it increases. These well-known paradoxes remain unaltered when the Hamiltonian system is replaced by its corresponding quantum-mechanical system. The standard deterministic answer to them is that the timescale for a return to the original state is much longer than anything we can imagine, so it is quite possible to have a system which is microscopically reversible, but a macroscopic description of this system on ordinary timescales from ordinary initial conditions can validly use an irreversible equation such

as the diffusion equation. This diffusion equation will have a positive diffusion coefficient because that is appropriate to the type of system which we encounter in the present state of the universe.

The difficulty with these arguments is seen in computer simulation. We could just go ahead and simulate a hot gas mixing with a cold gas, where to avoid complication we will say that the gas is monatomic and does not emit or absorb electromagnetic radiation (a white body radiator). With a properly written computer program, every molecular encounter would be reversible, and so the whole process would presumably be 'adiabatic'. Yet we know that there is heat transfer between the two gases, increasing the entropy, although this appears microscopically as a collection of work transfers. The difficulty is that in computer simulation one does not know how to distinguish between adiabatic and non-adiabatic processes or between microscopic and macroscopic processes. Thus one has no idea of the scale upon which one stops using reversible mechanics and introduces a diffusion term, and there is nothing to fix the value of the Reynolds number. In the future we will have supercomputers able to do reversible simulations of systems with some 10^{26} particles, and these difficulties will become progressively more obvious. In the case of two-dimensional

vortex dynamics, the variance of the vortex distribution about the centre of vorticity is a constant for inviscid flow, and no transition from the microscopic to the macroscopic viewpoint will ever alter this fact. One can argue that the vortices represent the collective motion of another medium in which it is possible to use a diffusion equation to summarise the bulk movement of the medium, but this argument will be refuted by the existence of superfluidity, which will be described below. It is not obvious why a computer simulation of a fluid should represent anything but an inviscid superfluid.

Furthermore, to our computer program we could add a module which does the work of Maxwell's Demon, separating 'hot' and 'cold' molecules, where visibility of information between modules is restricted to experimentally observable quantities. It is not clear what would prevent this module from working and thus being able to drive a perpetual motion machine of the second kind if the dynamics are solely the dynamics of a Hamiltonian system. Note that this idea of restricting the visibility of computer generated information to make a computer simulation the perfect imitation of an experiment is best implemented in the programming language MODULA-2. A module is virtually an independent computer program, whose output is controllable so that another module can only have access to those variables

specified by the programmer. In proposing a Maxwell's Demon, we are effectively setting one computer program at war with another computer program. The Demon will win over a program based on deterministic dynamics, but if some randomness is admitted, the Demon will lose in the sense that it cannot then construct a perpetual motion machine.

All of these objections, the objections of Loschmidt and Zermelo, and of the author as a computer programmer, depend upon the idea that where a system has a number of possible states at one time, there is a one-to-one correspondence with the states which it may assume at another time. This one-to-one correspondence is established by the evolution of a Hamiltonian system. To do computer simulations of real thermodynamic systems, one must find a way to destroy the one-to-one correspondence, and there is an additional requirement that any method chosen must be symmetric in time since there is no common physical process which does not have a corresponding process running in reverse (of course, in this corresponding process one must also reverse all momenta, all magnetic fields and so on). The 'random vortex' method of Chorin[4] answers these requirements, and in fact we have just given a specification of what is meant by randomness, namely the destruction of the one-to-one correspondence.

It is instructive to consider the behaviour of liquid Helium, though the

argument will be restricted to two dimensions. Below a certain temperature, 2.172^{o} K, liquid Helium exhibits a phenomenon known as superfluidity, which means that the viscosity vanishes, and it is then known as Helium II. Bearing in mind the discussion of flow separation presented here, the best evidence that the viscosity of Helium II is strictly zero is given by its failure to exhibit flow separation. Thus a pitot tube linked to manometers to measure the difference between static and stagnation pressures fails to work because ordinarily the measurement of static pressure relies upon a flow separation somewhere in the system. Likewise, the electron fluid in a metal loses its 'viscosity' below a certain temperature, and the resulting phenomenon is known as superconductivity. A description of this type of behaviour which emphasises superfluidity and vortex dynamics is given by Putterman[45]. Most engineers will have heard of these phenomena, but will consider them to be exotic quantum mechanical effects.

In fact, it is non-superfluidity which is the 'exotic' quantum mechanical behaviour of a fluid. In a superfluid, the fluid is so cold that there is no energy available for transition to the higher energy levels predicted by quantum mechanics, and so in effect at the absolute zero of temperature quantum mechanics has been switched off. All the Helium atoms

are in their 'ground state', and there is no opportunity for any atom to jump to an 'excited state'. Nevertheless, Helium II can still support vortices, though one will find it difficult to create them. The effect of the vortices over time is to transform one ground state to another ground state without going through an excited state, and this has a very interesting consequence.

The Helium II itself cannot rotate, so the vortices are pointlike. The strength of the circulation of each point vortex is quantised. This implies that the vortices can move as a Hamiltonian system, and their macroscopic behaviour is adequately described by the convection equation. The quantum mechanics of the system is in a sense orthogonal to its Hamiltonian mechanics, since the knowledge that the strength of the vortices is quantised is irrelevant to predicting their behaviour as a Hamiltonian system. The relative scale of these two systems of mechanics usually has the quantum mechanics as a much smaller scale, but in superfluidity the quantum mechanics is the larger scale, and the microscopic behaviour of a superfluid is often Hamiltonian. Frequently, then, the analysis of superfluidity makes no distinction between microscopic and macroscopic scales of motion, and this is the problem which has been previously stated as a problem of any properly programmed computer simulation. Some new

principle must be incorporated into the simulation in order to represent dissipation.

There is no viscosity in Helium II, so viscosity in a liquid must be regarded as a quantum mechanical effect. If the Helium II is warmed up slightly, some of the Helium atoms jump to higher energy levels. Later, some atoms revert back to their minimum level, and other atoms are promoted to keep the total energy constant over long timescales. The effect of this is to shuffle vortices sideways, and with successive displacements of a point vortex being uncorrelated, the vortex is moving according to a Wiener[23] process. The macroscopic description of this will use a diffusion equation.

There is no theory which can predict when a given Helium atom will make a jump between energy levels, and quantum mechanics can only predict the probability per unit time of the jump occuring. If a deterministic theory emerged which could predict the time at which a jump occured, it would have one of two properties:

(a) In the style of MODULA-2, we could package the theory in a module to use in computer simulation. Some of the variables employed would be invisible outside the module. The objection to this is that the module would be indistinguishable from the pseudo-random number generator

already used. The apparent randomness which the module should simulate in, say, a prediction of radioactive decay would be achieved by setting the initial condition of the unobservable variables of a deterministic process. The same results could be achieved by a module whose initial state was known, but which used a random process, and this module would be much simpler to program.

(b) The theory would predict new effects which were visible outside the module just described. We could then program a second module which analysed the variables visible outside the first module, and so construct a Maxwell's Demon. Given that the visible variables are an encoding of the variables within the module, we are asserting our confidence in our ability to break any code. A theory complicated enough to produce an unbreakable code would be refuted by the application of Occam's Razor when compared to the alternative postulate of true randomness.

Such a theory is not likely to appear within the foreseeable future. This is currently good reason for regarding the jumps between energy levels as random, producing random displacements of vortices. The 'random vortex' method has now been shown to have some justification, if only on the principle of Occam's Razor, and one can generalise this to say that the

computer simulation of thermodynamics amounts to taking a Hamiltonian system and adding randomness.

In Helium II we see a separation between the concept of a Hamiltonian system and of a system in which entropy can increase by virtue of a changing distribution of the system components between energy levels, with diffusion as a side effect. The probability per unit time of a given transition between energy levels is related to Planck's constant. We do not specify the value of Planck's constant in the simulation of a Hamiltonian system, so the simulation does not include any quantum mechanical effects. The conclusion is that no Hamiltonian system can be responsible for an increase in entropy, and thus for diffusion, not even when timescales are short and the system is looked at from a macroscopic viewpoint.

This conclusion remains valid when the 'phase space' of the system is increased from two dimensions to the six dimensions of real systems. In the case of a dilute gas, the energy levels of a single molecule are so close together that they are barely distinguishable from a continuum. A single molecule colliding with another molecule can therefore change energy levels so easily that one might as well regard the outcome of the collision as purely random, though of course the collision may be perfectly elastic in the sense of conserving energy and momentum. There is then no correlation

between the trajectories of a single molecule on successive collisions, so it then describes a Wiener[23] process, and one can validly use a diffusion equation.

One has to have some method of simulating the quantum mechanical effect of apparently random jumps in energy levels, an extra degree of freedom which does not appear in the dynamic specification but which can dramatically alter the outcome of a simulation. This method will incorporate randomness in some appropriate fashion. Then for computer simulation the First Law of Thermodynamics can be expressed as

> It is possible to add randomness to a deterministic system in such a way as to preserve at least some of the invariants of the deterministic behaviour of the system.

The First Law is usually known as the conservation of energy, but it is not obvious why energy should be singled out when other invariants exist, such as momentum and angular momentum, and indeed the Special Theory of Relativity puts energy and momentum on an equal footing. It would be prosaic to amend the First Law to say that a system has invariants without saying what they are invariant to. This is remedied by the formulation of the First Law just given. It explains why one expresses the First Law as

$$\Delta U = Q - W$$

without making any distinction between various forms of heat or work transfer taken separately. Heat is the random motion of molecules, and work is their deterministic motion, and now heat and work transfers are distinguishable in computer programming. The attempt to program a Maxwell's Demon module will be defeated by the randomness of the system giving rise to an Uncertainty Principle as described in Chapter 2. When one measures the energy of a molecule, one will have to wait for some time for the randomness to be sufficiently averaged out, and by the time one has done this, the molecule will be somewhere else and it will be hopeless trying to pursue it. Alternatively, if one makes a measurement over a short time, it will be impossible to tell whether the molecule is hot or cold.

The addition of randomness will mean that on average, quantities such as energy, momentum and angular momentum are expected to be invariant. Thus all these quantities obey the First Law. On the other hand, the variance of a system of two-dimensional point vortices remains constant with respect to the centre of vorticity without randomness, but increases steadily in time with randomness, so here is an invariant which does not obey the First Law. One notices of course that quantities obeying the First Law are linear measures with respect to the randomness, and quantities not obeying it are

non-linear measures.

For computer simulation the Second Law of Thermodynamics becomes

The addition of random motion to a system at some given time always causes it to evolve in the direction of its most probable state.

This will be true whether one then goes forwards or backwards in time from the given time, making the addition of randomness reversible in the sense that one cannot use the observation of a thermodynamic system to assess whether time is running forwards or backwards in the artificial universe of a computer simulation. All one can say is that from the 'time zero' at which one encountered the simulation, subjective time always runs in the direction of increasing entropy. It is an open question whether this subjective time is an artefact of the computer simulation, or whether one can speculate that it corresponds to something objective like the relativistic proper time, on the argument that 'causality' and 'increase in entropy' are the same concept.

The entropy is a measure of the nearness to the most probable state of a system, and it is computed by counting the distribution of particles over quantum mechanical energy levels. An adequate substitute for the process of the redistribution of particles between energy levels is, in fluid

mechanics, the Brownian motion of vortices. For other Hamiltonian systems, one will have to find other explicit methods of entropy generation, and if one does not, then the computer will make up this deficiency through random errors associated with the finite representation of a quantity in the computer memory. These errors will be difficult to quantify, and so we come to the sting in the tail. It may be charged that the discussion given here is an unnecessary digression from the subject of fluid mechanics whose unity was stressed in the Introduction, so the basic problem will be restated. Define the Reynolds' Number as the timescale of entropy increase divided by the dynamic timescale. Whether one's interest is in the process thermodynamics of fluid mechanics, celestial mechanics, nuclear physics or plasma physics, one does not want a computer program to be labelled

Simulation at Unknown Reynolds' Number

ACKNOWLEDGEMENTS

The Author wishes to acknowledge the advice and guidance of his Supervisor, Professor R.I. Lewis, of the Department of Mechanical Engineering. The benefit of many hours of conversation with Doctors K.Y. Cheng and I. Potts must also be noted.

The Central Electricity Generating Board contributed to a CASE award, in collaboration with the Science Research Council, to fund the initial part of this work. Later, the Author was employed as a Research Associate under a grant to the University from the Science and Engineering Research Council.

This work involved many hours of computing on the Northern Universities Multiple Access Computer, and it is desired to thank the computing staff.

REFERENCES

1. Martensen, E., Die Barechnung der Druckverteilungen dicken gitterprofilen mit hilfe von Fredhomschen integral-gleichungen, Zweiter Art. Arch. Rat. Mech. Anal., 3, 235-237 (1959).

2. Charney, J.G., Fjortoft, R. and von Neumann, J., Numerical Integration of the Barotropic Vorticity Equation, Tellus, 2, 237-254 (1950).

3. Buneman, O., Time-Reversible Difference Procedures, J. Comp. Phys., 1, 517-535 (1967).

4. Chorin, A.J., Numerical Study of Slightly Viscous Flow, J. Fluid Mech., 57, 785-796 (1973).

5. Saffman, P.G., and Baker, G.R., Vortex Interactions, Ann. Rev. Fluid Mech., 11, 95-122 (1979).

6. Rosenhead, L., The formation of vortices from a surface of discontinuity, Proc. Roy. Soc., Series A, 134, 170-192 (1931).

7. Abernathy, F.H. and Kronauer, R.E., The formation of vortex streets, J. Fluid Mech., 13, 1-20 (1962).

8. Fromm, J., The time dependent flow of an incompressible viscous fluid, Methods in Computational Physics, 3, 345-382 (1964).

9. Salmon, R., Practical Use of Hamilton's Principle, J. Fluid Mech., 132, 431-444 (1983).

10. Gerrard, J.H., Numerical Computation of the Magnitude and Frequency of Lift on a Circular Cylinder, Phil. Trans. Roy. Soc., 261, 137-162 (1967).

11. Christiansen, J.P., Numerical Simulation of Hydrodynamics by the Method of Point Vortices, J. Comp. Phys., 13, 363-379 (1973).

12. Chorin, A.J., Vortex Sheet Approximation of Boundary Layers, J. Comp. Phys., 27, 428-442 (1978).

13. Lewis, R.I., Surface vorticity modelling of separated flows from two-dimensional bluff bodies of arbitrary shape, J. Mech. Eng. Sci., 23(1), 1-12 (1981).

14. Stansby, P.K. and Dixon, A.G., Simulation of flows around cylinders by a Lagrangian Vortex scheme, Applied Ocean Research, 5(3), 167-178 (1983).

15. Aref, H., Integrable, Chaotic and Turbulent Vortex Motion in Two-dimensional Flows, Ann. Rev. Fluid Mech., 15, 345-89 (1983).

16. Baker, G.R., Meiron, D.I. and Orszag, S.A., Vortex simulations of the Rayleigh-Taylor instability, Phys. Fluids, 23(8), 1485-1490 (1980).

17. Leonard, A., Simulation of Three-dimensional Separated Flows with Vortex Filaments, Proc. 5th Int. Conf. Num. Meth. Fluid Dyn., Springer, 280-284 (Berlin, 1976).

18. Wilkinson, D., A numerical solution of the analysis and design problems for the flow past one or more aerofoils or cascades, A.R.C. R & M No. 3545 (1968).

19. Einstein, A., Investigation on the theory of Brownian motion, Dover (1956).

20. Smoluchowski, Drei Vortrage uber Diffusion, Brownische Bewegung und Koagulation von Kolloidteilchen, Physik. Zeit., 17, 557-585 (1916).

21. Perrin, J., Atoms, Constable (London, 1916).

22. Batchelor, G.K., An introduction to fluid dynamics, Cambridge University Press (1967).

23. Wiener, N., Differential space, J. Math. Phys. Mass. Inst. Tech., 2, 131-174 (1923).

24. Milinazzo, F. and Saffman, P.G., The calculation of large Reynolds number two-dimensional flow using discrete vortices with random walk, J. Comp. Phys., 23, 380-392 (1977).

25. Fürth, R., Uber einige Beziehungen zwischen klassischer Statistik und Quantenmechanik, Zeitschrift fur Physik, 81, 143-162 (1933).

26. Prandtl, L., Essentials of fluid dynamics, Blackie and Son Ltd. (Glasgow, 1952).

27. Leonard, A., Turbulent Structures in Wall-bounded shear flows observed via three-dimensional numerical simulations, Lecture Notes in Physics, 136, Springer-Verlag (New York, 1981).

28. Duffey, R.B. and Porthouse, D.T.C., The Physics of Rewetting in Water Reactor Emergency Core Cooling, Nuclear Engineering and Design, 25(3), 379-394 (1973).

29. Deffenbaugh, F.D. and Marshall, F.J., Time Development of the Flow about an Impulsively Started Cylinder, AIAA Journal, 14(7), 908-913 (July 1976).

30. Schlichting, H., Boundary Layer Theory, McGraw-Hill (New York, 1960).

31. For a discussion of these paradoxes, see Woods, L.C., The Thermodynamics of Fluid Systems, Oxford Engineering Science Series (Oxford, 1975). The substance of Woods' argument is that a deterministic system can imitate diffusion.

32. Prandtl, L., and Tietjens, O.G., Applied hydro- and aerodynamics, Dover (New York, 1957).

33. Thwaites, B., Approximate calculation of the laminar boundary layer, Aeronaut. Quart., 1, 245 (1949).

34. Goldstein, S., Modern developments in fluid dynamics, Volumes I & II, Dover (New York, 1957).

35. Tanner, A.R.C. R & M, No. 1353 (1931).

36. Bryant, L.W. and Williams, D.H., An investigation of the flow of air around an aerofoil of infinite span, Proc. Roy. Soc., Series A, 225, 199-245 (1925).

37. Lewis, R.I. and Porthouse, D.T.C., A generalised numerical method for bluff body and stalling aerofoil flow, ASME 82-GT-70 (1982 Conference on Gas Turbines, Wembley, London).

38. Porthouse, D.T.C. and Lewis, R.I., Simulation of viscous diffusion for extension of the surface vorticity method to boundary layer and separated flows, J. Mech. Eng. Sci., 23(3), 157-167 (1981).

39. Critzos, C.C., Heyson, H.H. and Boswinkle R.W., Aerodynamic Characteristics of NACA 0012 Airfoil Section at Angles of Attack from 0^{o} to 180^{o}, NACA Technical Note 3361.

40. Emmons, H.W., Pearson, C.E. and Grant, H.P., Compressor Surge and Stall Propagation, Trans. ASME, 455-469 (1955).

41. Huppert, M.C. and Benser, W.A., Some Stall and Surge Phenomena in Axial-Flow Compressors, J. Aeronaut. Sci., 835-845 (1953).

42. Stenning, A.H., Rotating Stall and Surge, J. Fluids Eng., 102, 14-20 (1980).

43. Iura, T. and Rannie, W.D., Experimental Investigations of Propagating Stall in Axial-Flow Compressors, Trans. ASME, 463-471 (1954).

44. Stenning, A.H. and Kriebel, A.R., Stall Propagation in a Cascade of Airfoils, Trans. ASME, 777-790 (1958).

45. Putterman, S.J., Superfluid Hydrodynamics, North-Holland Publishing Company (Amsterdam, 1974).